



**Michigan
Technological
University**

Michigan Technological University
Digital Commons @ Michigan Tech

Dissertations, Master's Theses and Master's Reports

2022

Maximum likelihood estimator method to estimate flaw parameters for different glass types

Nabhajit Goswami

Michigan Technological University, ngoswami@mtu.edu

Copyright 2022 Nabhajit Goswami

Recommended Citation

Goswami, Nabhajit, "Maximum likelihood estimator method to estimate flaw parameters for different glass types", Open Access Dissertation, Michigan Technological University, 2022.

<https://doi.org/10.37099/mtu.dc.etr/1417>

Follow this and additional works at: <https://digitalcommons.mtu.edu/etr>



Part of the [Civil Engineering Commons](#), [Other Statistics and Probability Commons](#), [Probability Commons](#), and the [Statistical Methodology Commons](#)

MAXIMUM LIKELIHOOD ESTIMATOR METHOD TO ESTIMATE FLAW
PARAMETERS FOR DIFFERENT GLASS TYPES

By

Nabhajit Goswami

A DISSERTATION

Submitted in partial fulfillment of the requirements for the degree of

DOCTOR OF PHILOSOPHY

In Civil Engineering

MICHIGAN TECHNOLOGICAL UNIVERSITY

2022

© 2022 Nabhajit Goswami

This dissertation has been approved in partial fulfillment of the requirements for the Degree of DOCTOR OF PHILOSOPHY in Civil Engineering.

Department of Civil, Environmental, and Geospatial Engineering

Dissertation Advisor: *Dr. Stephen M. Morse*

Committee Member: *Dr. Daniel M. Dowden*

Committee Member: *Dr. Joshua A. Schultz*

Committee Member: *Dr. R. Andrew Swartz*

Committee Member: *Dr. Kui Zhang*

Department Chair: *Dr. Audra N. Morse*

Dedication

The dissertation is dedicated to all the glass nerds all around the world, who are constantly developing new techniques to make this world aesthetically a sexier place. To my mother, father, brother, and sister in-law who always believed in me even when I self doubted myself, pushed me forward when I slowed down, smiled and cried with me, and supported me through thick and thin. And finally to my ex girlfriend, Puja, who was with me every step from the moment I started my Ph.D. and whose unwavering believe in me made any hurdle/obstacle seem small.

Contents

List of Figures	xiii
List of Tables	xvii
Acknowledgments	xxv
Abstract	xxvii
1 Introduction	1
1.1 Glass failure prediction model	1
1.1.1 Material property of a brittle vs ductile material	1
1.1.2 The Weibull distribution	5
1.1.3 Factors affecting the strength of glass	5
1.1.4 Glass failure prediction model	8
1.1.5 Surface flaw parameter estimation	11
1.1.6 The maximum likelihood estimator method	18
1.2 Research Objective	19
1.3 Monolithic annealed glass plates	22
1.3.1 Published historical experimental test records	22

1.3.2	Minimum criterion for historical experimental data sets	24
1.3.2.1	Load time history	24
1.3.2.2	Specimen rectangular dimensions and boundary conditions	26
1.3.2.3	Specimen thickness	27
1.3.3	Equivalent failure load duration	29
1.3.4	Determination of 3-sec surface flaw parameters using MLE	32
1.4	Monolithic heat-treated glass plate	37
1.4.1	Heat-treated glass	37
1.4.2	GFPM modification for RCSS	38
1.4.3	Published historical experimental test records	40
1.4.4	Determination of representative sample RCSS	41
1.4.5	Determination of 3-sec surface flaw parameter using MLE	42
1.4.6	Comparison of experimental data CDFs to ASTM E1300 analytical method	45
1.5	Glass with holes	47
1.5.1	GFPM for holes	47
1.5.2	Published historical experimental test records	50
1.5.3	Determination of hole parameter for GFPM for holes using MLE	51
1.5.4	Modified GFPM for holes	52

1.5.5	Determination of hole parameters for the modified GFPM for holes	54
2	Estimation of Surface Flaw Parameters for Annealed glass using Maximum Likelihood Estimator	57
2.1	Introduction	58
2.2	Background	61
2.2.1	Glass Failure Prediction Model	61
2.2.2	Historical method to estimate of surface flaw parameters	64
2.3	Procedure to estimate surface flaw parameters for glass failure prediction model	66
2.4	Estimation of surface flaw parameters	69
2.4.1	Historical destructive testing	70
2.4.2	Information required to calculate equivalent failure loads	71
2.4.3	Strategies for Missing or incomplete data	71
2.4.4	60-sec equivalent failure loads	80
2.4.5	Estimation of 60-sec surface flaw parameters	83
2.4.6	3-sec EFL and surface flaw parameters	87
2.5	Discussion	92
2.5.1	Comparison of ASTM E1300 surface flaw parameter and MLE estimated surface flaw parameter for weathered in-service sample	92
2.5.2	Comparison of surface flaw parameters for new glass	94

2.6	Conclusion	96
3	Estimation of surface flaw parameters for heat treated glass using maximum likelihood estimator	99
3.1	Introduction	101
3.2	Background	103
3.2.1	Glass failure prediction model for annealed glass	103
3.2.2	Glass failure prediction model for heat-treated glass	106
3.2.3	Surface flaw parameter estimation	107
3.3	Methodology to estimate surface flaw parameters using the maximum likelihood estimator method for heat treated glass	110
3.3.1	Shape and scale parameter estimation	112
3.3.2	Estimation of the location parameter (RCSS)	114
3.4	Sample set and Analysis	115
3.4.1	Comparison of reported and recreated equivalent failure loads	117
3.4.2	3-sec equivalent failure load and surface flaw parameter estimation using MLE	123
3.5	Results and Discussion	127
3.5.1	Effect of RCSS on the strength of glass	128
3.5.2	Effect of RCSS on weathering of HT glass	129
3.5.3	Design example	133
3.6	Conclusion	139

4	Estimation of Flaw Parameters for Holes in Glass using Maximum Likelihood Estimator	141
4.1	Introduction	142
4.2	Glass failure prediction model	145
4.2.1	Glass failure prediction model for window glass	145
4.2.2	Glass failure prediction model for heat treated glass	148
4.2.3	Glass failure prediction model for edges and holes in tension	149
4.3	Procedure to estimate flaw parameters for glass failure prediction model for holes	152
4.3.1	Application of maximum likelihood estimator to glass with holes	153
4.3.2	Glass failure prediction model and parameter estimation for heat-treated glass with holes	158
4.4	Estimation of glass failure prediction model parameters for holes	161
4.4.1	Experimental failure data for glass specimen with a hole	161
4.4.2	Equivalent failure loads for glass specimens with a hole	162
4.4.3	Estimation of two parameter glass failure prediction model parameters for holes	164
4.4.4	Estimation of three parameter glass failure prediction model parameters for holes	169
4.5	Conclusion	175
5	Conclusion	179

References	183
A Failure Data and Load resistance table for annealed monolithic glass . . .	193
B Failure Data and load resistance table for heat-treated monolithic glass .	275
C Load resistance table for point supported glass	291

List of Figures

1.1	Stress vs strain curve for a) Ductile material b) Brittle material	3
1.2	(a) Surface flaws on glass [59] (b) Cross sectional view of glass	3
1.3	Stress concentration and sharpening of flaw due to applied tensile stress	4
1.4	(a) Water molecule interacting with the silica network (b) the chemical re- action between water molecule and silica network bond of glass [41], [26] (c) crack blunting phenomenon	6
1.5	Effect of load duration on glass strength [18]	7
1.6	Number of flaws in a a) small area b) large area of glass	7
1.7	Numerical model input and output	9
1.8	Numerical model output with i^{th} element	10
1.9	Flow chart for estimation of surface flaw parameters	11
1.10	A typical load time history	12
1.11	Load time histories of similar glass specimens	14
1.12	(a) A typical load time history converted to (b) a stress time history . . .	15
1.13	A Load time history and an equivalent 60- sec failure load	15
1.14	(a) Rank EFL (b) Theoretical CDF for a range of m_s and corresponding k_s	17

1.15	Flow chart to achieve goals for each research objective	22
1.16	Applied load TH and Idealized triangular TH	25
1.17	Dry Glaze (boundary condition)	27
1.18	Comparison of reported vs recreated p_b	28
1.19	Comparison of historical and recreated 60-sec EFL's for weathered sam- ples	31
1.20	60-sec MLE estimated vs historical surface flow parameters for in-service samples	32
1.21	A load time history and a 3-sec equivalent failure load	33
1.22	3-sec EFL vs CDF for in-service samples	35
1.23	3-sec EFL vs CDF for new samples	35
1.24	Comparison of ASTM E1300 surface flow parameter to historical in-service parameters	36
1.25	Tempering Procedure [48]	38
1.26	Stress distribution across the cross section of a glass	38
1.27	Representative RCSS of a HT sample	42
1.28	EFL_3 and CDF for HS and FT samples	43
1.29	Comparison of similar size glass to understand the effect of RCSS on the strength of glass	44
1.30	Comparison of similar sized in-service AN and HT glass samples	46
1.31	(a) Cutting glass to shape (b) Creating a hole	47

1.32 Comparison of MLE estimated flaw parameter vs flaw parameter estimated using the historically subjective method	53
1.33 3-sec EFL and fit for modified GFPM for holes	55
2.1 Dry Glaze (boundary condition)	72
2.2 Applied load TH and Idealized triangular TH	74
2.3 Comparison of historical and recreated 60-sec EFL's for weathered in-service samples	80
2.4 Comparison of historical and recreated 60-sec EFL's for new samples	82
2.5 60-sec MLE estimated vs historical surface flaw parameters for weathered in-service samples	84
2.6 60-sec MLE estimated vs historical surface flaw parameters for new samples	85
2.7 3-sec EFL vs CDF for weathered in-service samples	89
2.8 3-sec EFL vs CDF for new samples	89
2.9 Load resistance chart using MLE estimated surface flaw parameters from weathered samples	94
2.10 Load Resistance chart for different dimensions	96
3.1 Comparison of EFL_{Hist} and EFL_{Rec} for H1 and H2	119
3.2 Comparison of EFL_{Hist} and EFL_{Rec} for FT-01, FT-02, FT-03 and FT-04	122
3.3 EFL_3 and CDF for HS and FT samples	125
3.4 Comparison of H1, H1 and F2	126

3.5	Comparison of LR for different type of glass of same dimension	130
3.6	Load ratio vs RCSS of sample for glass sample with aspect ratio equal to 2	131
3.7	LR of weathered in-service AN and weathered in-service FT of similar dimension	133
3.8	Design CDF for different dimension	135
3.9	Design CDF for weathered FT glass	137
3.10	Relation between LR for HT and AN to RCSS for weathered samples	138
4.1	Specimen with holes	162
4.2	Variation of γ around the hole	165
4.3	Cumulative distribution fit of a 2P GFPM for holes vs EFL_{3s}	167
4.4	Cumulative distribution fit for $P3P_H$ vs EFL_{3s}	172
4.5	Difference in pb calculated using hole parameters with estimated RCSS and measured RCSS	174
4.6	Load Resistance chart for test specimen	176

List of Tables

1.1	Sample description of in-service glass sample set	23
1.2	Sample description of new glass sample set	24
1.3	Method to determine missing thickness	29
1.4	In-service and new glass 3-sec surface flaw parameters	34
1.5	Sample Description of HT samples	40
1.6	3-sec surface flaw parameters	43
1.7	Sample data for glass with holes	50
1.8	MLE estimated vs historically subjective method hole flaw parameters .	52
2.1	Summary of weathered in-service glass sample set	76
2.2	Summary of new glass sample set	79
2.3	weathered in-service and new glass 3-sec surface flaw parameters	88
2.4	Representative geometries for comparison	93
3.1	Sample Description	116
3.2	Parameters historically used to calculate equivalent failure load and surface flaw parameter	118
3.3	3-sec surface flaw parameters	124

3.4	Load corresponding to different p_b for different glass types but similar dimension	132
4.1	Measured specimen data	161
4.2	Failure load and stress and EFS and EFL for specimens	164
4.3	2 parameter hole estimates and statistical measures	165
4.4	3 parameter hole estimates and statistical measures	170
A.1	W01 - Loading time history, failure location, EFL_{60} and EFL_3	194
A.2	W02 - Loading time history, failure location, EFL_{60} and EFL_3	195
A.3	W03 - Loading time history, failure location, EFL_{60} and EFL_3	196
A.4	W04 - Loading time history, failure location, EFL_{60} and EFL_3	197
A.5	W05 - Loading time history, failure location, EFL_{60} and EFL_3	200
A.6	W06 - Loading time history, failure location, EFL_{60} and EFL_3	203
A.7	W07 - Loading time history, failure location, EFL_{60} and EFL_3	205
A.8	W08 - Loading time history, failure location, EFL_{60} and EFL_3	207
A.9	W09 - Loading time history, failure location, EFL_{60} and EFL_3	209
A.10	W10 - Loading time history, failure location, EFL_{60} and EFL_3	210
A.11	W11 - Loading time history, failure location, EFL_{60} and EFL_3	211
A.12	W12 - Loading time history, failure location, EFL_{60} and EFL_3	212
A.13	W13 - Loading time history, failure location, EFL_{60} and EFL_3	213
A.14	W14 - Loading time history, failure location, EFL_{60} and EFL_3	214
A.15	N01 - Loading time history, failure location, EFL_{60} and EFL_3	215

A.16 N02 - Loading time history, failure location, EFL_{60} and EFL_3	216
A.17 N03 - Loading time history, failure location, EFL_{60} and EFL_3	218
A.18 N04 - Loading time history, failure location, EFL_{60} and EFL_3	219
A.19 N05 - Loading time history, failure location, EFL_{60} and EFL_3	220
A.20 N06 - Loading time history, failure location, EFL_{60} and EFL_3	221
A.21 N07 - Loading time history, failure location, EFL_{60} and EFL_3	222
A.22 N08 - Loading time history, failure location, EFL_{60} and EFL_3	223
A.23 N09 - Loading time history, failure location, EFL_{60} and EFL_3	224
A.24 W01: 60-sec cumulative distribution table : reported vs recreated (Data related to Figure 2.5)	230
A.25 W02: 60-sec cumulative distribution table : reported vs recreated (Data related to Figure 2.5)	231
A.26 W03: 60-sec cumulative distribution table : reported vs recreated (Data related to Figure 2.5)	232
A.27 W04: 60-sec cumulative distribution table : reported vs recreated (Data related to Figure 2.5)	233
A.28 W05: 60-sec cumulative distribution table : reported vs recreated (Data related to Figure 2.5)	234
A.29 W06: 60-sec cumulative distribution table : reported vs recreated (Data related to Figure 2.5)	235

A.30 W07: 60-sec cumulative distribution table : reported vs recreated (Data related to Figure 2.5)	236
A.31 W08: 60-sec cumulative distribution table : reported vs recreated (Data related to Figure 2.5)	237
A.32 W09: 60-sec cumulative distribution table : reported vs recreated (Data related to Figure 2.5)	238
A.33 W10: 60-sec cumulative distribution table : reported vs recreated (Data related to Figure 2.5)	239
A.34 W11: 60-sec cumulative distribution table : reported vs recreated (Data related to Figure 2.5)	240
A.35 W12: 60-sec cumulative distribution table : reported vs recreated (Data related to Figure 2.5)	241
A.36 W13: 60-sec cumulative distribution table : reported vs recreated (Data related to Figure 2.5)	242
A.37 N01: 60-sec cumulative distribution table : reported vs recreated (Data related to Figure 2.6)	243
A.38 N02: 60-sec cumulative distribution table : reported vs recreated (Data related to Figure 2.6)	244
A.39 N03: 60-sec cumulative distribution table : reported vs recreated (Data related to Figure 2.6)	245

A.40 N04: 60-sec cumulative distribution table : reported vs recreated (Data related to Figure 2.6)	246
A.41 N05: 60-sec cumulative distribution table : reported vs recreated (Data related to Figure 2.6)	247
A.42 N06: 60-sec cumulative distribution table : reported vs recreated (Data related to Figure 2.6)	248
A.43 N07: 60-sec cumulative distribution table : reported vs recreated (Data related to Figure 2.6)	249
A.44 N08: 60-sec cumulative distribution table : reported vs recreated (Data related to Figure 2.6)	250
A.45 W01: 3-sec cumulative distribution table (Data related to Figure 2.7) . .	251
A.46 W02: 3-sec cumulative distribution table (Data related to Figure 2.7) . .	252
A.47 W03: 3-sec cumulative distribution table (Data related to Figure 2.7) . .	253
A.48 W04: 3-sec cumulative distribution table (Data related to Figure 2.7) . .	254
A.49 W05: 3-sec cumulative distribution table (Data related to Figure 2.7) . .	255
A.50 W06: 3-sec cumulative distribution table (Data related to Figure 2.7) . .	256
A.51 W07: 3-sec cumulative distribution table (Data related to Figure 2.7) . .	257
A.52 W08: 3-sec cumulative distribution table (Data related to Figure 2.7) . .	258
A.53 W09: 3-sec cumulative distribution table (Data related to Figure 2.7) . .	259
A.54 W10: 3-sec cumulative distribution table (Data related to Figure 2.7) . .	260
A.55 W11: 3-sec cumulative distribution table (Data related to Figure 2.7) . .	261

A.56 W12: 3-sec cumulative distribution table (Data related to Figure 2.7) . . .	262
A.57 W13: 3-sec cumulative distribution table (Data related to Figure 2.7) . . .	263
A.58 W14: 3-sec cumulative distribution table (Data related to Figure 2.7) . . .	264
A.59 N01: 3-sec cumulative distribution table (Data related to Figure 2.8) . . .	265
A.60 N02: 3-sec cumulative distribution table (Data related to Figure 2.8) . . .	266
A.61 N03: 3-sec cumulative distribution table (Data related to Figure 2.8) . . .	267
A.62 N04: 3-sec cumulative distribution table (Data related to Figure 2.8) . . .	268
A.63 N05: 3-sec cumulative distribution table (Data related to Figure 2.8) . . .	269
A.64 N06 3-sec cumulative distribution table (Data related to Figure 2.8) . . .	270
A.65 N07: 3-sec cumulative distribution table (Data related to Figure 2.8) . . .	271
A.66 N08: 3-sec cumulative distribution table (Data related to Figure 2.8) . . .	272
A.67 N09: 3-sec cumulative distribution table (Data related to Figure 2.8) . . .	273
B.1 H1 - Loading time history, failure location, EFL_{60} , and EFL_3	276
B.2 H2 - Loading time history, failure location, and EFL_3	277
B.3 F1 - Loading time history, failure location, EFL_{60} , and EFL_3	279
B.4 F2 - Loading time history, failure location, EFL_{60} , and EFL_3	281
B.5 F3 - Loading time history, failure location, and EFL_3	282
B.6 F4 - Loading time history, failure location, and EFL_3	283
B.7 H1: 3-sec cumulative distribution table (Data related to Figure 3.3) . . .	284
B.8 H2: 3-sec cumulative distribution table (Data related to Figure 3.3) . . .	285
B.9 F1: 3-sec cumulative distribution table (Data related to Figure 3.3) . . .	286

B.10 F2: 3-sec cumulative distribution table (Data related to Figure 3.3) . . .	287
B.11 F3: 3-sec cumulative distribution table (Data related to Figure 3.3) . . .	288
B.12 F4: 3-sec cumulative distribution table (Data related to Figure 3.3) . . .	289
C.1 Cumulative distribution table for 2P GFPM for holes (Data related to Figure 4.3)	292
C.2 Cumulative distribution table for $P3P_H$ for holes (Data related to Figure 4.4 and Figure 4.5)	293
C.3 Cumulative distribution table for test specimen with RCSS = 126 MPa (Data related to Figure 4.6)	294
C.4 Cumulative distribution table for test specimen with RCSS = 126 MPa (Data related to Figure 4.6)	295
C.5 Cumulative distribution table for test specimen with RCSS = 126 MPa (Data related to Figure 4.6)	296
C.6 Cumulative distribution table for test specimen with RCSS = 126 MPa (Data related to Figure 4.6)	297
C.7 Cumulative distribution table for test specimen with RCSS = 126 MPa (Data related to Figure 4.6)	298
C.8 Cumulative distribution table for test specimen with RCSS = 126 MPa (Data related to Figure 4.6)	299

Acknowledgments

I would like to acknowledge the following individuals for their contribution towards this research and dissertation:

1. Dr. Stephen M Morse for his unwavering support, continuous mentorship, and introducing new things over the past five years.
2. Dr. Joshua A. Schultz from Gonzaga University for providing the test data for the glass sample with holes, answering any questions I have and had for him, and always encouraging me to expand my research.
3. My committee members Dr. Daniel M Dowden and Dr. R. Andrew Swartz for always being present with a helping hand to answer any question I have for them and at the same time poke me with questions to keep me on my toes.
4. My committee member Dr. Kui Zhang, who has always been patient with me whenever I came to him with a crazy statistical problem and help me work through it with a smile on his face.
5. Department head Dr. Audra N Morse, for providing different opportunities to excel on a personal and professional level in the last five years
6. The Michigan Tech fraternity, that has provided a sense of family while being literally

on the opposite end of the globe.

7. My family, who has supported me from the very beginning, from the decision to pursue my higher studies in the United states, to moving to the upper peninsula to pursue my Ph.D., laughing and crying with me in my highs and lows.
8. My friends and peers in Michigan Tech that helped me to be the best version of myself, provided a helping hand every time I asked for a favor, or sticking with me especially when I was difficult to deal with.

Abstract

Glass is commonly used in architectural applications, such as windows and in-fill panels and structural applications, such as beams and staircases. Despite the popularity of structural glass use in buildings, an engineering design standard to determine the required component or member strength for design loads does not exist. Glass is a brittle material that lacks a well-defined yield or ultimate stress, unlike ductile materials. The traditional engineering methods used to design a ductile material cannot be used to design a glass component. Glass fails in tension primarily due to the presence of microscopic flaws present on the surface that acts as stress concentrators. Hence, to accurately estimate the strength of glass, the presence of surface flaws need to be addressed. The glass failure prediction model is a probabilistic model that addresses the microscopic flaws in the form of two parameters, along with other factors such as load duration, environmental conditions, glass component geometry, and boundary condition to determine the strength of glass. The flaw parameters associated with the glass failure prediction model describes the size, shape, and number of surface flaws present on the surface of the glass. Due to the microscopic nature and variability of the surface flaws, it is impractical to attempt to measure the flaw parameters directly. Instead, the flaw parameters are numerically estimated from experimental failure test data. However, there is no universally recognized method to select the best flaw parameters and this omission leads to subjective approaches inducing variability. Recognizing a lack of a standardized and repeatable method to estimate flaw parameters,

the universal, simple, and easy-to-use statistical tool, the maximum likelihood estimator method, is used in this work to estimate the surface flaw parameters for different glass failure prediction models such as glass failure prediction model for glass with holes, for annealed monolithic glass, and heat-treated monolithic glass. Published experimental data related to each model were collected and used to show the working principle of the maximum likelihood estimator method. Thus, the work herein removes variability associated with the historically subjective method and allows researchers to objectively and repeatably estimate flaw parameters for different glass failure prediction models consistently.

Chapter 1

Introduction

1.1 Glass failure prediction model

1.1.1 Material property of a brittle vs ductile material

Glass has become an increasingly popular choice for buildings facades and load bearing members in the last several decades due to its transparency, aesthetic appeal, and extensive range of geometric shapes and applications. Despite the popularity of structural glass use in buildings, an engineering design standard to determine the required component or member strength for design loads does not exist. The absence of a design standard for glass components is partially due to the rapid expansion of glass used in building beyond the traditional

infill panel for windows, among other issues.

Common materials used in a building such as steel and reinforced cement concrete, behavior ductile materials however glass is a brittle material. Figure 1.1 shows the stress-strain relationship of a ductile material (A36 steel) and a brittle material (glass). Ductile materials have a well-defined yield stress and an ultimate stress, σ_y and σ_u (Figure 1.1(a)), with a coefficient of variation (COV) for the rupture (failure) stress of than less than 6%. Hence, traditional engineering (allowable stress or partial load factor) design methods, based on the well-defined yield or ultimate stress, are sufficient to design ductile component of different geometries and loading applications. Conversely, brittle materials do not have a yield stress or an ultimate stress (Figure 1.1 (b)) and the COV for failure stress is approximately 20% (annealed float glass). Thus, traditional methods are not sufficient to design a glass component as these methods require a well-defined yield or ultimate stress value for the material.

The high variability in the failure stress of a brittle material is attributed to the presence of microscopic surface flaws on the glass that can result in a stress concentration. The surface flaws are of different shape, size, depth, orientation and randomly distributed over the surface of a brittle material (Figure 1.2(a)). The surface flaws are intrinsic to the surface of a brittle material because of the manufacturing process of the glass while additional flaws are created due to weathering and handling over the in-service period (Figure 1.2(b)). A critical surface flaw is the flaw that causes fracture [18] and its location is unknown prior

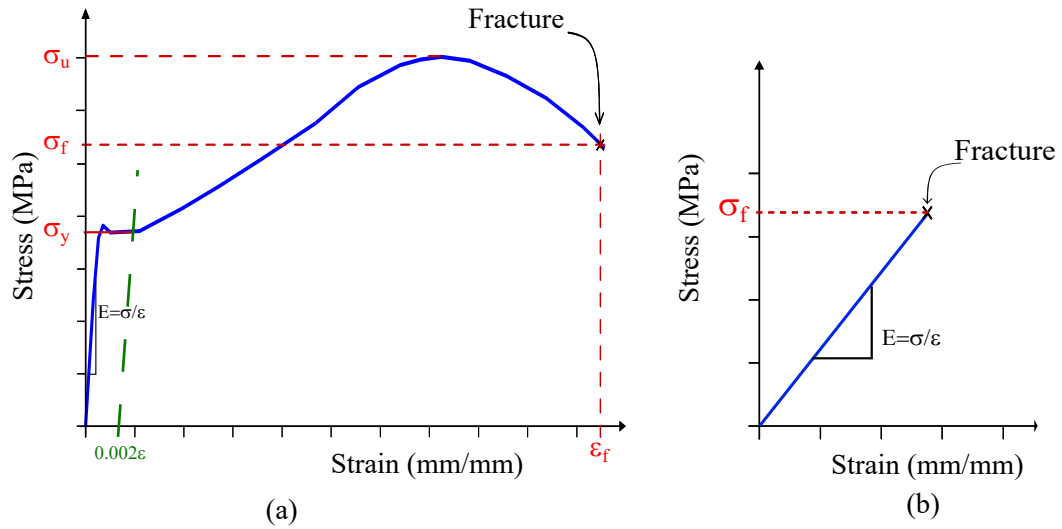


Figure 1.1: Stress vs strain curve for a) Ductile material b) Brittle material

to fracture as surface flaws are distributed across the surface and have varying orientation, shape, size and depth. Therefore, a probabilistic method is best suited to predict the strength of glass components rather than a traditional deterministic method based only on material strength (stress).

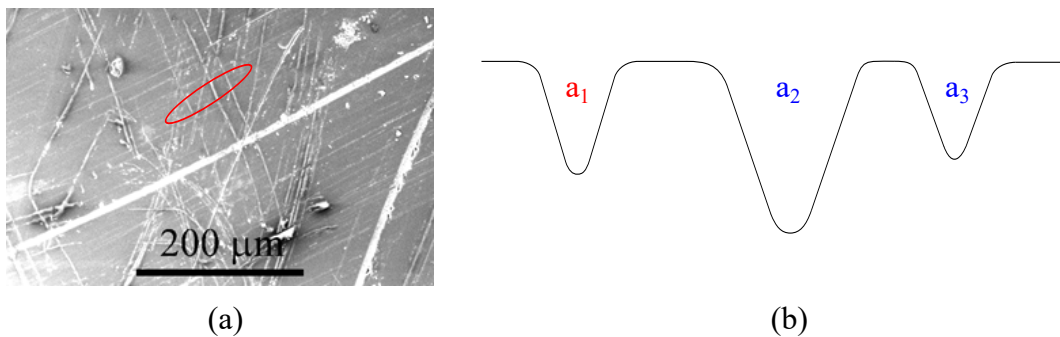


Figure 1.2: (a) Surface flaws on glass [59] (b) Cross sectional view of glass

Griffith [33] showed the presence of flaws on the surface create a stress concentration at the flaw tip (Figure 1.3). Inglis [35] put forward a mathematical expression to calculate

the stress at the tip of flaw as a function of the applied tensile stress on the surface and the radius of the flaw. Griffith, using 'the theorem of minimum energy', showed a rupture or scratch in the body causes a rise in potential energy due to the stress concentration. Thus, the deformed elastic body (from surface force) tries to be in the state of minimum potential energy by breaking the cohesive bonds that binds the silica molecules in glass. This phenomenon results in the sharpening of the flaw to the point when the fracture occurs. Thus, the strength of glass or any other brittle material is a function of the flaws present on the surface (orientation, shape, size and depth) and the tensile stress the flaws are subjected to.

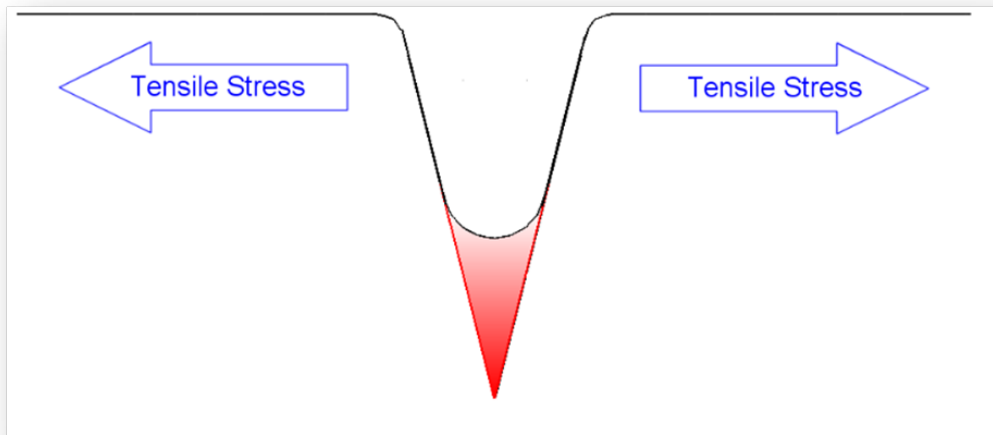


Figure 1.3: Stress concentration and sharpening of flaw due to applied tensile stress

1.1.2 The Weibull distribution

Weibull [64] based on the work of Griffith, introduced the well-known two-parameter Weibull distribution with a material function to predict the strength of brittle materials expressed as

$$F = 1 - e^{-\lambda \cdot \sigma^\beta} \quad (1.1)$$

where, λ is the shape parameter, β is related to scale parameter, and σ is the stress subjected on the surface of the brittle material. Weibull showed the Weibull distribution successfully predicted the strength of various brittle materials. Thus, the strength of glass, a brittle material, can theoretically be predicted using a Weibull distribution. However, the Weibull distribution parameters fitted to experimental test data from a particular geometry and loading condition fail to accurately predict the strength for alternate member geometries or boundary conditions. Thus numerous research project have been conducted to understand the factors affecting glass strength ([16], [24], [25], [23], [66], [56] [21]).

1.1.3 Factors affecting the strength of glass

Glass in the presence of water vapor can undergo a chemical reaction where the water molecules break the silica bond. In the absence of a tensile stress acting on the surface flaw the water vapor corrodes (increases the flaw tip radius) the flaw tip a phenomenon

commonly known as crack blunting (Figure 4) [24], [66].

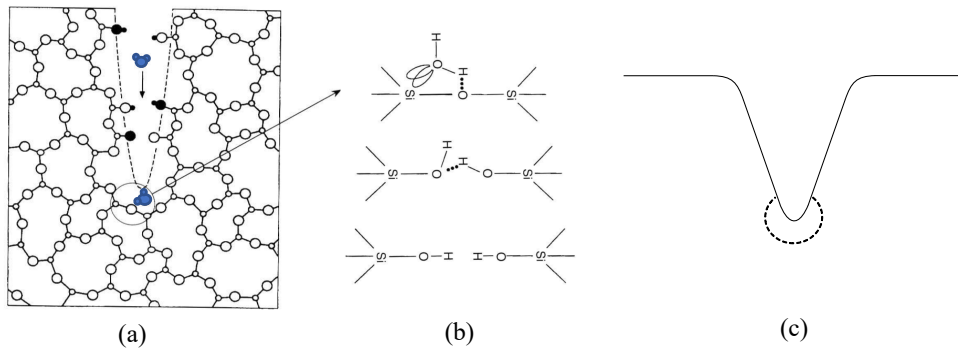


Figure 1.4: (a) Water molecule interacting with the silica network (b) the chemical reaction between water molecule and silica network bond of glass [41], [26] (c) crack blunting phenomenon

Preston [54], Baker and Preston [16], Shand [56] (1954) and Shand [57] showed the strength of glass decreases over time, a phenomenon termed as the static fatigue (Figure 1.5). Glass in the presence of water vapor and a tensile stress breaks the silica bond at a faster rate, compared to the presence of only water vapor. Hence, over time, a flaw that may not have been a critical flaw, due to the ‘corrosion’ effect and tensile stress may become the critical flaw. Charles [24], [25] showed the rate of corrosion for a flaw is a function of the temperature and tensile stress raised to the power of the static fatigue constant denoted as ‘n’ (experimentally approximated as 16).

Beason [18] recognized the orientation flaw capable to cause failure (the critical flaw) with respect to the maximum principal stress as affects the strength of glass. Beason [18] also showed as the area of glass increases, the number of flaws increases. Additionally, the

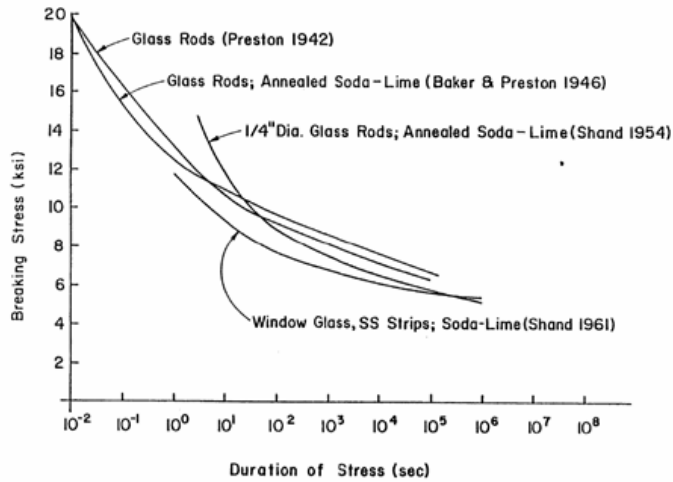


Figure 1.5: Effect of load duration on glass strength [18]

probability of a flaw oriented in the orientation of tensile stress increases for a glass with a bigger surface area. Hence, Beason [18] concluded that as the area of the glass increases, the strength of glass decreases (Figure 1.6).

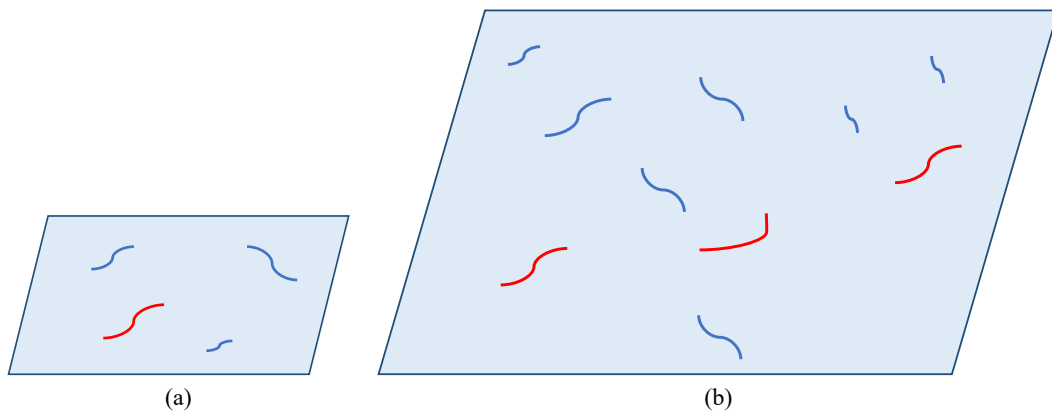


Figure 1.6: Number of flaws in a) small area b) large area of glass

To summarize, the strength of glass is dependent on the location, size, and orientation of microscopic flaws present on the glass surface, magnitude, and orientation of tensile stress at the glass surface, the duration of the load the glass is subjected to, and area of the glass.

Hence, to predict the strength of different geometries and boundary conditions of glass, it is desirable to have a material function that addresses all known factors affect glass strength.

1.1.4 Glass failure prediction model

Historically glass use in buildings was limited to infill panels for windows. Thus previous research on glass strength was primarily focused on 4-sided simply supported rectangular glass plates. Beason [18] advanced a modified material function for the two-parameter Weibull distribution addressing the additional factors affecting glass strength to calculate the probability of breakage (p_b) expressed as

$$p_b = 1 - e^{-B_s} \quad (1.2)$$

where, B_s is the modified strength (or risk) function denoted as the glass failure prediction model (GFPM) expressed as

$$B_s = k_s \cdot \int_0^y \cdot \int_0^x \left(c_{x,y} \cdot \left(\frac{t_d}{t_{par}} \right)^{1/n} \cdot \sigma_{max,x,y} \right)^{m_s} \cdot d_x \cdot d_y \quad (1.3)$$

where, k_s and m_s represent the size, shape, and number of surface flaws present on the surface of the glass, $\sigma_{max,x,y}$ denotes the maximum stress the location of glass is subjected to, $c_{x,y}$ denotes the biaxial correction ratio that takes into account the orientation of the stress, t_d denotes the load duration, t_{par} denotes the duration associated with the surface

flaw parameters, and ‘n’ denotes the static fatigue constant, equal to 16. Beason [18] used two parameters m_s and k_s in lieu of λ and β as the shape and scale parameter, to highlight these parameters are different from the classical Weibull distribution.

Although, the material property of glass (stress-strain) is elastic in nature, the geometry of the glass plate allows the glass to deflect well in excess of its thickness when a load is applied, thereby making the glass plate load-stress relationship non-linear. Hence, to model the stress distribution across the glass plate, a non-linear analysis is required. When the geometry (GEO) i.e., long dimension, short dimension, and thickness, boundary condition (BC), and the load (P) on the glass plate is modeled with a numerical model (NM), the model discretizes the glass plate into small elemental areas. For each of the discretized elemental area, the model calculates the magnitude of area, the maximum and the minimum principal stress associated with it. (Figure 1.7 and Figure 1.8)

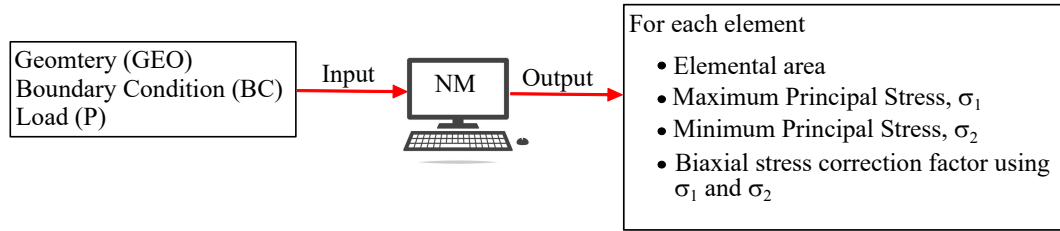


Figure 1.7: Numerical model input and output

Thus, the numerical form of the GFPM becomes

$$B_s = k_s \cdot \sum_{i=1}^{n_{elem}} \cdot \left(c_i \cdot \left(\frac{t_d}{t_{par}} \right)^{1/n} \cdot \sigma_{max,i} \right)^{m_s} \cdot A_i \quad (1.4)$$

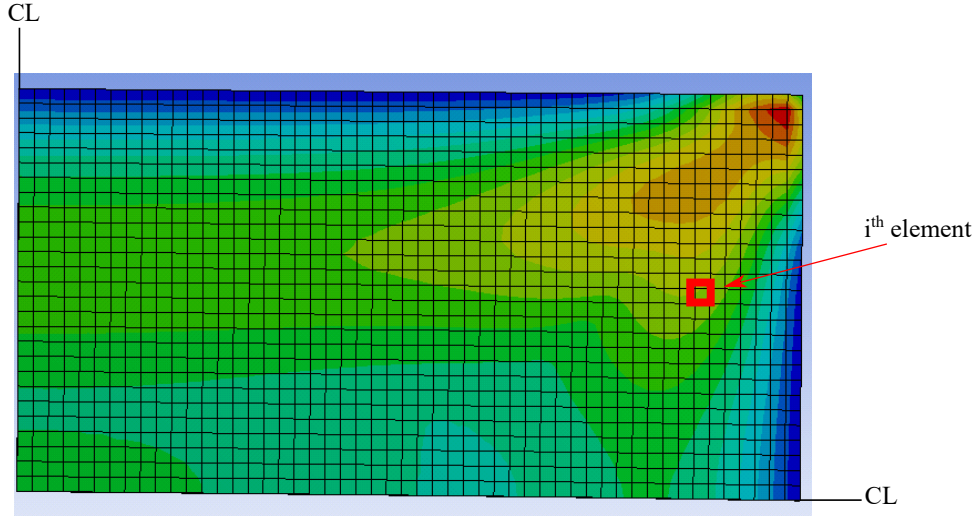


Figure 1.8: Numerical model output with i^{th} element

where, A_i denotes the area associated with the i^{th} element, $\sigma_{max,i}$ denotes the maximum principal stress of the i^{th} element, c_i denotes the biaxial stress correction factor for the i^{th} element and all other variables denotes the same as defined before. Apart from the ratio t_d/t_{par} , which can be a constant, the terms inside the summation are a function of the NM. Thus, the GFPM can be expressed as

$$B_s = k_s \cdot S_{m_s}(NM(GEO, BC, P), m_s) \quad (1.5)$$

where all the symbols denote the same as defined before.

1.1.5 Surface flaw parameter estimation

The two parameters associated with the GPFM are ostensibly describing the nature of surface flaws present, they are microscopic, randomly distributed and therefore it is impractical to attempt to measure them directly. Hence, the surface parameters are numerically estimated from experimental failure test data. The method to estimate surface flaw parameters is a three-step process as shown in Figure 1.9.

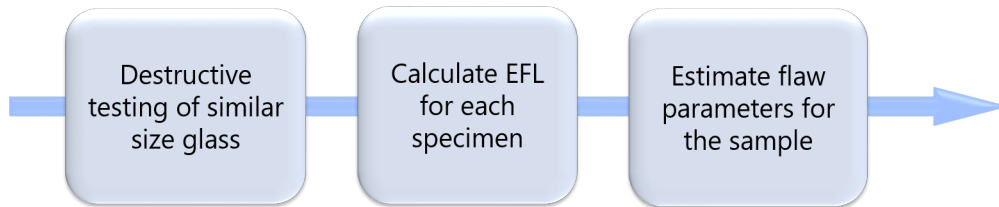


Figure 1.9: Flow chart for estimation of surface flaw parameters

The first step to estimate surface flaw parameters requires the destructive testing of similar sized glass. An appropriately sized test frame consistent with ASTM E997-15 [15] is used to dry glaze the specimens with neoprene gaskets providing a simply supported BC (unrestrained in-plane movement and rotation as the specimen edges). The test setup consists of a vacuum pump connected to an air receiver (tank), which in turn is connected by different sized valves to the frame (test chamber). Air is evacuated from the test chamber to the air receiver by opening the valves to create a pressure difference between the test chamber and the atmosphere. Manipulation of the valves controlling the air transfer can be used to produce a monotonically increasing uniform pressure until the specimen fractures. The

load-time history (LTH), failure load and time to failure is recorded for each specimen. A typical LTH, the failure load and failure time is shown in Figure 1.10.

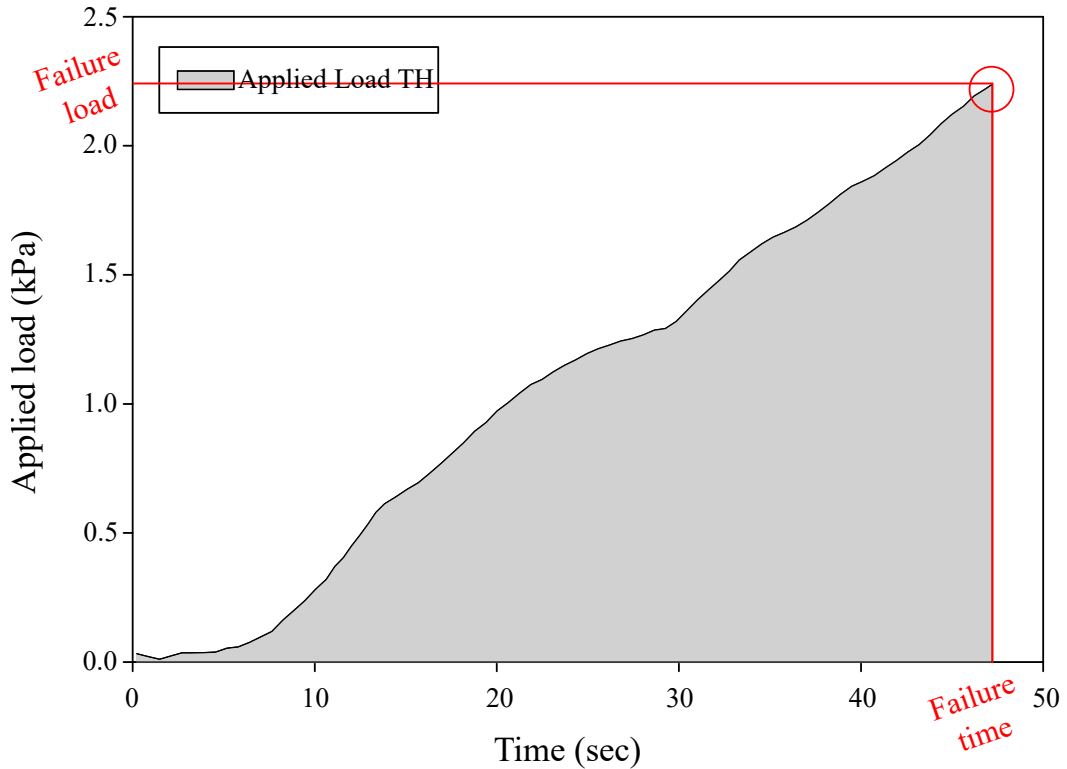


Figure 1.10: A typical load time history

Glass specimens loaded to failure fail at varying load magnitude and time due to the randomly distributed surface flaws (Figure 1.11), resulting in a unique LTH and fracture origin for each specimen. Before the LTHs can be used to estimate the surface flaw parameters, the temporal part of the LTH must be normalized to a common duration which constitutes the second step. Normalization of the failure load is achieved using an integration advanced

by Brown [21]. Brown [21] assumed the measure of damage of flaw over a time period is constant and expressed the measure of damage, K_f of a flaw to the time of failure, t_f as

$$K_f = \int_0^{t_f} \sigma(P(t))^n \cdot dt \quad (1.6)$$

where, $\sigma(P(t))$ denotes the stress the flaw is subjected to for a duration. Thus the stress σ_{t_d} required to fail the same flaw at some other time t_d is expressed as

$$\sigma_{t_d} = \left[\frac{\int_0^{t_f} \sigma(P(t))^n dt}{t_d} \right]^{\frac{1}{n}} \quad (1.7)$$

where all variables are same as defined before. Before 1995, ASCE 7-1993 ([6] defined the basic wind speed as the fastest-mile wind speed that translates to a 60-sec gust. Because infill glass panels were designed primary to resist wind loads, the time duration used to normalize the LTH was used as 60-sec. Hence, the 60-sec stress σ_{60} required to fail the same flaw is expressed as

$$\sigma_{60} = \left[\frac{\int_0^{t_f} \sigma(P(t))^n dt}{60} \right]^{\frac{1}{n}} \quad (1.8)$$

where, all variables are as defined before. The equation to normalize the LTH is a function of the stress at the location of failure, whereas the LTH records the load applied on the specimen at any time. Therefore, a conversion of LTH to stress time history (STH) at the fracture location is required. Figure 1.12 shows a typical LTH converted to a STH. The normalized stress σ_{60} is known as the 60-sec equivalent failure stress (EFS) and the load corresponding to the stress is known as 60-sec equivalent failure load (EFL). An applied

load time history and a normalized LTH (60-sec EFL) is shown in Figure 1.13.

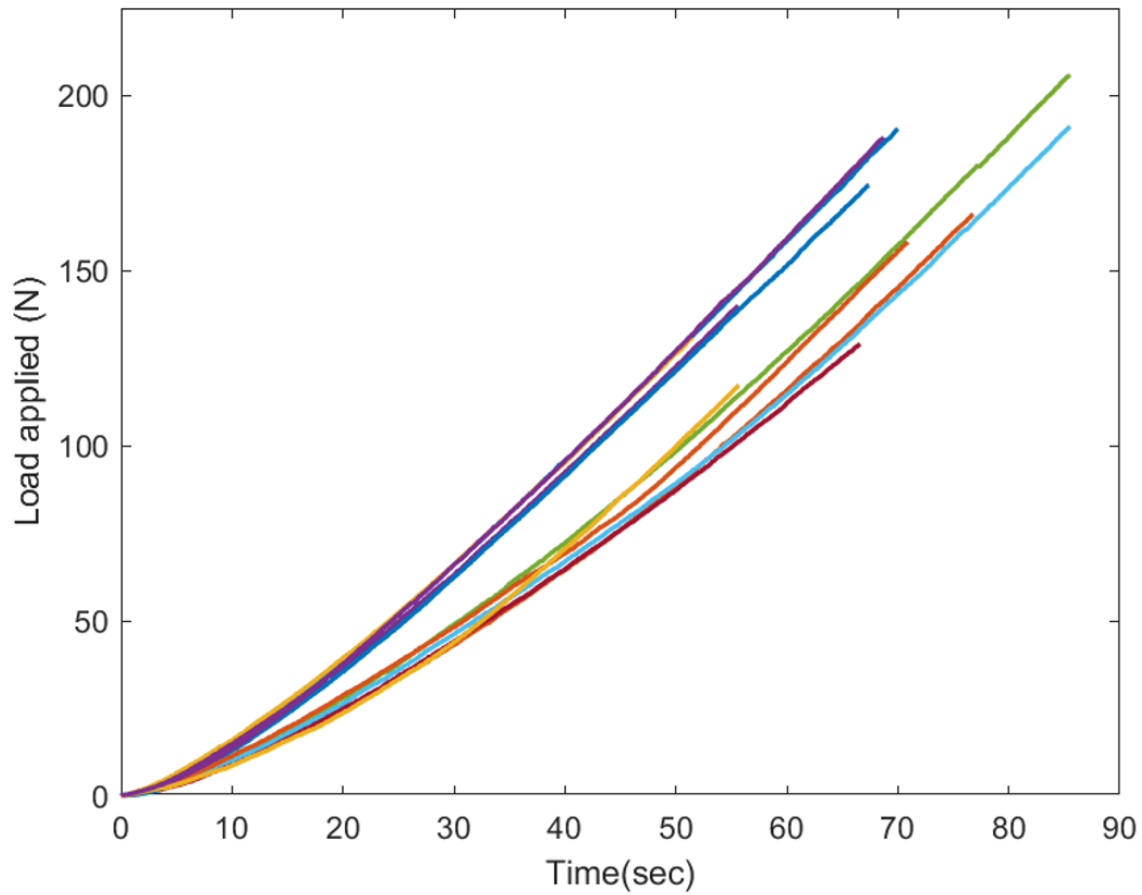


Figure 1.11: Load time histories of similar glass specimens

The resulting EFL values can then be used to estimate the surface flaw parameter of the sample (step 3). Historical estimation of surface flaw parameters includes the sorting the EFL values in ascending order and a median rank probability estimator, E_i , is assigned to each EFL according to Equation 1.9

$$E_i = \frac{i - 0.3}{n_{sam} + 0.4} \quad (1.9)$$

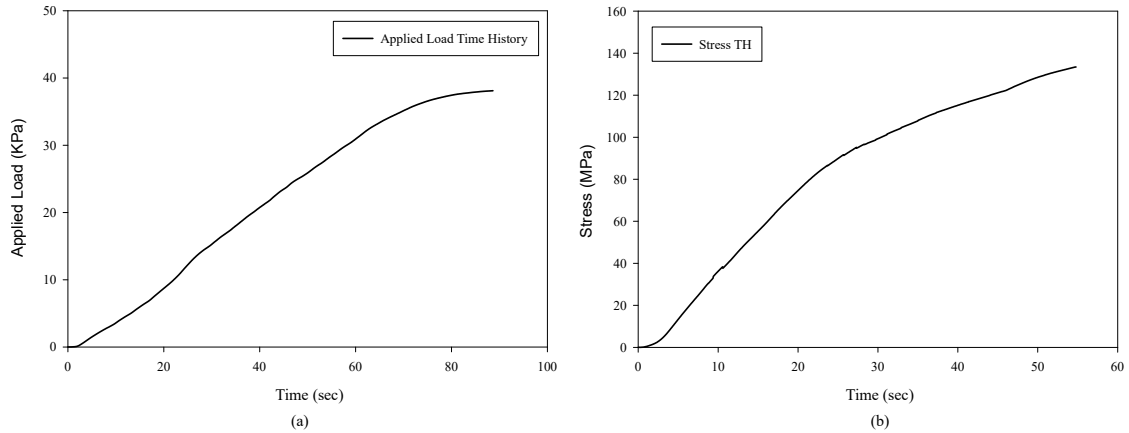


Figure 1.12: (a) A typical load time history converted to (b) a stress time history

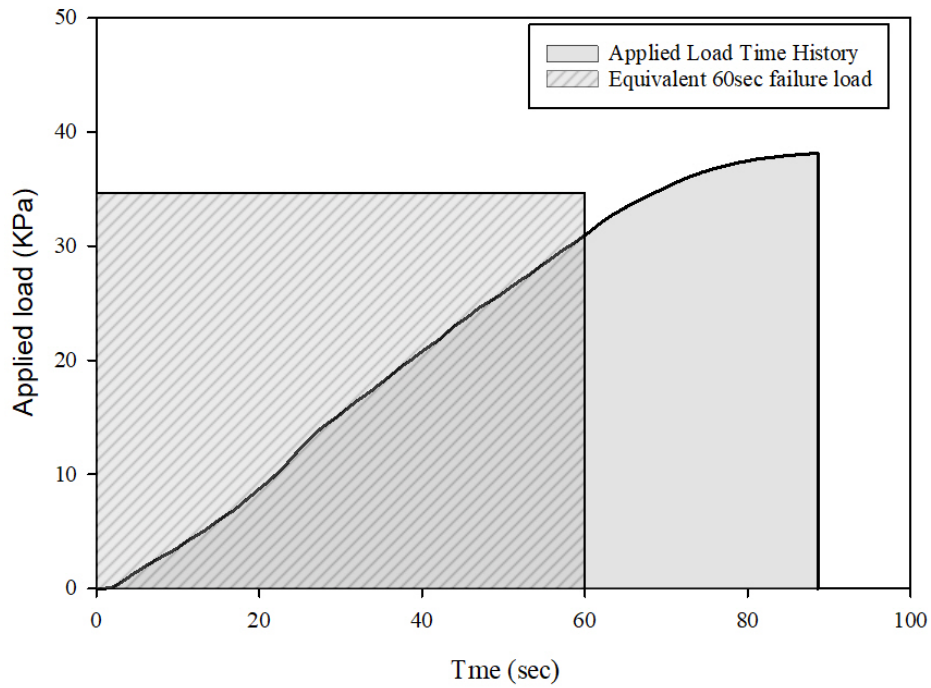
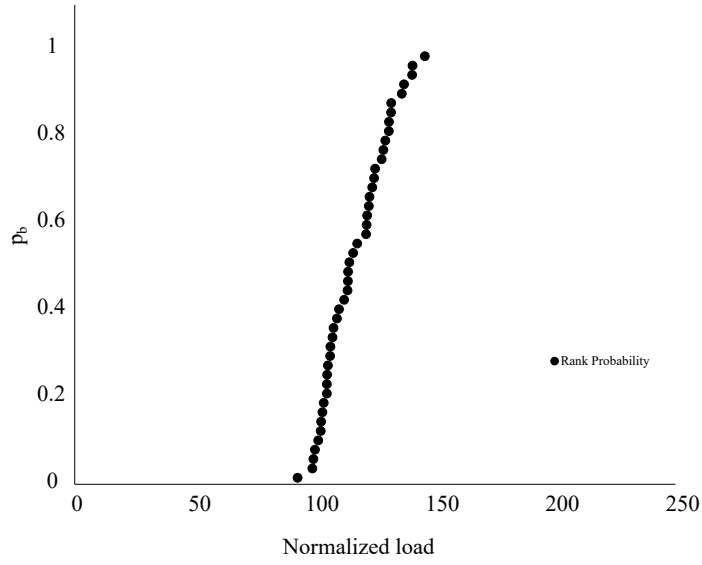


Figure 1.13: A Load time history and an equivalent 60- sec failure load

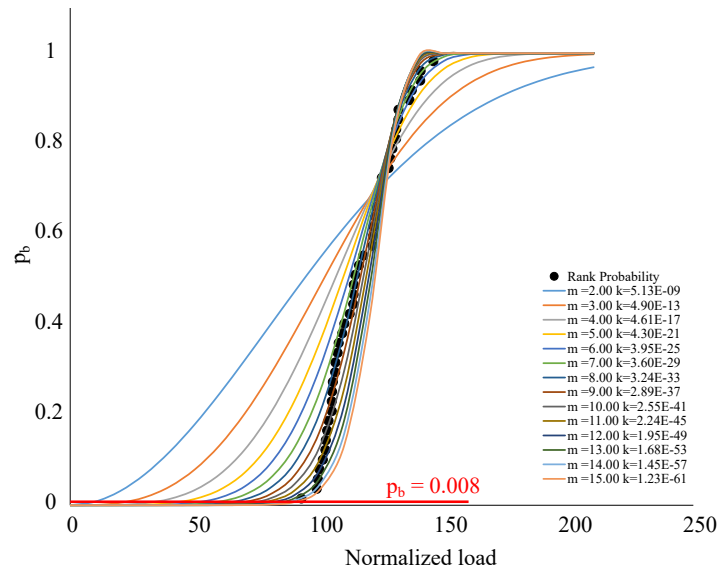
where, i denotes the rank of the EFL of specimen, and n_{sam} denotes the number of specimens in the sample. The EFL values are plotted in a graph (Figure 1.14 (a)) . A range of m_s , usually integers in published work, were guessed and corresponding values of k_s

were calculated by a method put forward by Beason [18]. For each set of surface flow parameters, corresponding theoretical fits, cumulative distribution functions (CDFs), were constructed and plotted against the EFL (Figure 1.14 (b)). The CDF with a mean, standard deviation, and COV that closely compared with the mean, standard deviation, and COV of the EFL was chosen as the pair of surface flow parameters that “best” describe the failure data. Often several parameter sets produced very similar mean, standard deviation, and COV, but a clear criterion for selecting which one that fit the “best” was not specified. Load corresponding to two p_b , 0.008 and 0.001, which are design probabilities for vertical and angled glazing respectively as described by ASTM E1300 [11] and AAMA [1], affects the decision making of choosing the “best” fit especially in cases when multiple fits produce the same statistical parameters. Because the p_b 0.008 is very close to 0 on a linear scaled axis (Figure 1.14 (b)), the CDF graphs will be drawn to a different scale for ease of comparison.

Many researchers in the past such as Abiassi [2], Kanabolo and Norville [39], Hsu [34], Sligar [58], Natividad et al. [47], Afolabi [3] used this method to estimate surface flow parameters for different samples tested. However, due to advancement in technology, Kanabolo and Norville [39], Hsu [34], Sligar [58], Natividad et al. [47], and Afolabi [3] used non-integer values for the flow parameter, m_s . Various statistical tools, such as the Kolmogorov–Smirnov (KS), the Anderson–Darling (AD) test, R-squared value, chi-squared test have been used in the past to assess the selection of the parameters. However, most of these statistical tests are only applicable for normally distributed data. The KS and the AD



(a)



(b)

Figure 1.14: (a) Rank EFL (b) Theoretical CDF for a range of m_s and corresponding k_s

test are performed to support the assumption that the data is drawn from a given probability distribution and are not tools for selecting flaw parameters. Although a chi-squared test is used to determine whether there is a statistically significant difference between the expected

and the observed frequencies, it was observed that multiple surface flow parameter sets justify the null hypothesis i.e., the expected and the observed frequencies are same. Hence, using any of these statistical tests to justify the selection of the surface flow parameter will not produce a single “best” set of parameters consistently. Therefore, a robust statistical method to consistently estimate surface flow parameters that removes the decision making is desirable.

1.1.6 The maximum likelihood estimator method

The maximum likelihood estimator (MLE) method is a robust, repeatable statistical method, used to estimate the parameters for any distribution type, including the Weibull distribution. For a Weibull distribution, the MLE method is used to estimate the scale and shape parameters by maximizing the likelihood function to provide a set of parameters that provide the highest probability compared to the observed outcomes. If the CDF of a statistical distribution is expressed as $F(x, \theta)$, where x is the random variable and θ denotes the parameter(s), the probability distribution or mass function $f(x, \theta)$ can be expressed by differentiating the CDF with respect to the random variable expressed as,

$$f(x, \theta) = \frac{d}{dx}F(x, \theta) \quad (1.10)$$

The likelihood function can be expressed as,

$$L(x, \theta) = \prod_{i=1}^{n_{sam}} f(x_i, \theta) \quad (1.11)$$

where all symbols are the same as defined before.

However, the CDF to describe the strength of glass, is expressed as

$$p_b = 1 - e^{-k_s \cdot S_{m_s}(NM(GEO, BC, EFL), m_s)} \quad (1.12)$$

To express the likelihood function for the strength function, the CDF must be expressed as the PDF, requiring the CDF to be differentiated with the respect of the random variable, which in this case is the EFL. However, a close form solution for the differentiation of the CDF for the strength of glass does not exist. Thus, the central difference numerical differentiation method is used in this research to differentiate the CDF with respect to the EFL.

1.2 Research Objective

The primary objective of the current work is to introduce a robust, consistent, standardized, and repeatable statistical method, the MLE method, to estimate flaw parameters. The primary objective is divided into three research objectives as follows:

1. ***Apply MLE method to estimate surface flaw parameters for annealed (AN) monolithic glass.*** To achieve the objective, the tasks are:

- a. Collected published historical experimental failure data for 4-sided simply supported monolithic AN glass plates (in-service and new)
- b. Curated published experimental data collection
- c. Created a minimum criterion required for experimental data with strategies to address missing or incomplete data
- d. Applied MLE to estimate the 3-sec surface flaw parameters for each sample.

2. ***Apply MLE method to estimate surface flaw parameters for heat-treated (HT) glass, and*** To achieve the objective, the tasks are:

- a. Collected published historical experimental data failure for 4-sided simply supported monolithic HT glass plates (in-service and new)
- b. Curated published experimental data collection
- c. Applied minimum criteria required for experimental data with strategies to address missing or incomplete data
- d. Applied MLE to estimate surface flaw parameters for the three-parameter GFPM HT sample
- e. Characterize the relationship between RCSS and weathering to load resistance.

3. *Apply MLE to estimate the flaw parameters for glass with holes* To achieve the objective, the tasks are:

- a. Collected published historical experimental failure data for glass with holes
- b. Applied MLE to estimate flaw parameters for the two-parameter GFPM for holes
- c. Extended the two-parameter GFPM for holes to a three-parameter GFPM for holes, and,
- d. Applied MLE to estimate surface flaw parameters for the three-parameter GFPM for holes.

Three journal articles are presented in Chapter 2, 3, and 4, addressing one research objective each. Each research objective is completed using the same set of steps illustrated with a flowchart (Figure 1.15). The first step consists of collecting historical published experimental failure data, followed by addressing missing or incomplete information required to analyze the collected data in second step. These two steps will provide a curated sample researchers can use for further analysis. The third step consists of calculating the EFL for each specimen in a sample using Equation 1.8, followed by using the MLE method to estimate surface flaw parameters for each sample.



Figure 1.15: Flow chart to achieve goals for each research objective

1.3 Monolithic annealed glass plates

1.3.1 Published historical experimental test records

Over the past four decades destructive uniform load tests have been performed on different shape, size, aspect ratio – the ratio of the long to short dimension of glass, and thickness to understand and establish the load resistance of simply supported monolithic AN glass plate. Table 1.1 and Table 1.2 presents a collection of experimental data for 14 in-service glass samples, and 9 new glass samples with relevant information (Task 1a). However, the published records of these tests are not consistently complete, and the methods used to select the corresponding GFPM surface parameters are not well documented.

Table 1.1
Sample description of in-service glass sample set

Sample Set	Number of specimen	Published Rectangular dimension Long x short x thickness mm x mm x mm (in. x in. x in.)	Measured thickness mm (in.)	Thickness Used mm (in.)	Load TH available
W01 ^a	20	724 x 724 x 6 (28 ¹ / ₂ x 28 ¹ / ₂ x 1/4)	5.56 ^f (0.219)	5.56 (0.219)	No
W02 ^a	20	1540 x 724 x 6 (60 ¹ / ₂ x 28 ¹ / ₂ x 1/4)	5.56 ^f (0.219)	5.56 (0.219)	No
W03 ^b	22	502 x 413 x 3 (19 ³ / ₄ x 16 ¹ / ₄ x 1/8)	3.05 ^f (0.120)	3.05 (0.120)	No
W04 ^b	111	921 x 356 x 3 (36 ¹ / ₄ x 14 x 1/8)	3.15 ^f (0.124)	3.15 (0.124)	No
W05 ^c	82	1730 x 502 x 6 (68 x 19 ³ / ₄ x 1/4)	5.84 ^f (0.230)	5.84 (0.230)	No
W06-I ^c	53	1730 x 502 x 6 (68 x 19 ³ / ₄ x 1/4)	5.54 ^f (0.218)	5.84* (0.230)	No
W07-I ^c	40	1730 x 502 x 6 (68 x 19 ³ / ₄ x 1/4)	5.82 ^f (0.229)	5.82 (0.229)	No
W08 ^c	66	1730 x 502 x 6 (68 x 19 ³ / ₄ x 1/4)	5.82 ^f (0.229)	5.82 (0.229)	No
W09 ^d	23	1490 x 654 x 6 (58 ³ / ₄ x 25 ³ / ₄ x 1/4)	-	5.97 [#] (0.235)	No
W10 ^d	12	1070 x 749 x 6 (42 x 29 ¹ / ₂ x 1/4)	-	5.87 [#] (0.231)	No
W11 ^d	11	940 x 749 x 6 (37 x 29 ¹ / ₂ x 1/4)	-	5.87 [#] (0.231)	No
W12 ^d	28	864 x 610 x 3 (34 x 24 x 1/8)	-	3.07 [#] (0.121)	No
W13 ^d	21	737 x 699 x 3 (29 x 27 ¹ / ₂ x 1/8)	-	3.10 [#] (0.122)	No
W14 ^e	18	2360 x 838 x 6 (93 x 33 x 1/4)	-	5.66 (0.223)	Yes

^a reported in Beason [18]; ^b reported in Abiassi [2]; ^c reported in Hsu [34]

^d reported in Sligar [58]; ^e unpublished; ^f reported in Norville and Minor [52]

[#]Thickness identified from reported surface flaw parameter using a trail and error method

* A different thickness from measured/reported thickness is used for calculations

Table 1.2
Sample description of new glass sample set

Sample Set	Number of specimen	Published Rectangular dimension Long x short x thickness mm x mm x mm (in. x in. x in.)	Measured/Used thickness mm (in.)	Load TH available
N01 ^a	23	502 x 413 x 3 (19-3/4 x 16-1/4 x 1/8)	2.97 ^d (0.117)	No
N02 ^b	53	1930 x 965 x 6 (76 x 38 x 1/4)	5.61 ^b (0.221)	No
N03 ^b	19	1676 x 838 x 6 (66 x 33 x 1/4)	5.93 ^b (0.233)	No
N04 ^b	16	2362 x 1181 x 6 (93 x 46-1/2 x 1/4)	6.13 ^b (0.242)	No
N05 ^b	19	1372 x 1372 x 6 (54 x 54 x 1/4)	5.62 ^b (0.221)	No
N06 ^b	18	1181 x 1181 x 6 (46-1/2 x 46-1/2 x 1/4)	6.00 ^b (0.236)	No
N07 ^b	12	1676 x 1676 x 6 (66 x 66 x 1/4)	5.66 ^b (0.223)	No
N08 ^b	15	2438x 1524 x 6 (96 x 60 x 1/4)	5.64 ^b (0.222)	No
N09 ^c	197	2438x 1524 x 6 (96 x 60 x 1/4)	5.81 ^c (0.229)	No

^a reported in Abiassi [2]; ^b reported in Kanabolo and Norville [38]

^c reported in Johar [36], Johar [37], ^d reported in Norville and Minor [52]

1.3.2 Minimum criterion for historical experimental data sets

1.3.2.1 Load time history

To establish a minimum criterion of required data from the experimental records, the normalization of the LTH was replicated and the EFL values were recreated and compared

to the published EFL values. The first step to calculate an EFL for a specimen is to convert the LTH to a STH. However, most of the samples collected did not report the LTH, instead failure load and time to failure were reported. Because the load applied was monotonically increasing with time at a uniform rate, an idealized triangular distribution for LTH was approximated using the reported failure load and failure time as shown in Figure 1.16. Only the upper portion of the LTH, (marked in red in Figure 1.16), contributes to the EFS calculation, as the lower portion does not change the sum. Hence, the triangular LTH approximation generally does not create significant error in calculating the ELS and consequently the EFL.

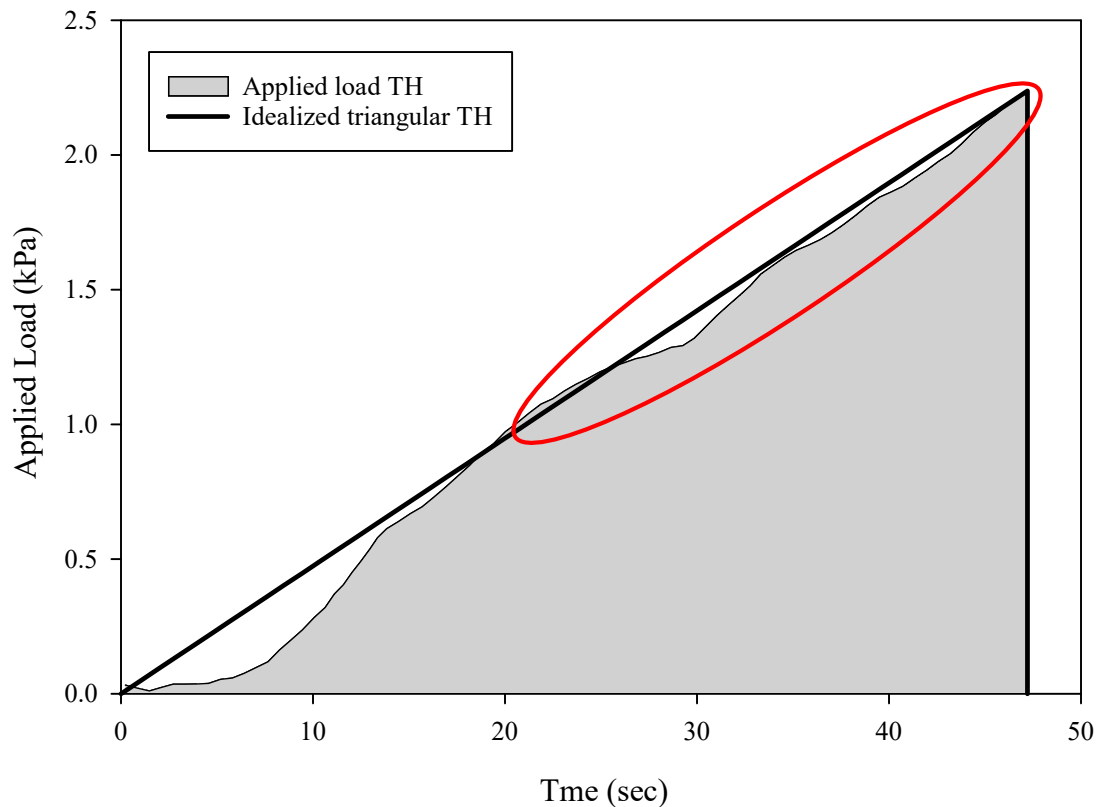


Figure 1.16: Applied load TH and Idealized triangular TH

1.3.2.2 Specimen rectangular dimensions and boundary conditions

The numerical model used to translate the LTH to a STH is sensitive to the specimen geometry and boundary condition. The boundary condition of the specimen is an artifact of the experimental setup. Although the experimental setup conforms to ASTM E997 [15], however the standard was first published in 1984. A few of the data collected not only preceded 1984, most published reports did not define the boundary condition used for stress analysis. According to ASTM E997 [15], the experimental setup requires the specimen to be dry glazed with neoprene gaskets of 6 mm x 6mm (1/4in. x 1/4in.) in size, allowed for in-plane slippage and rotation as shown in Figure 1.17. The glass specimen is to be centered with respect to the test frame, and specimens requires to be dry glazed all around with an overhang of 3 mm (1/8 in.) to prevent edge pullout due to large displacements during loading. Thus, the effective area of the plate stressed due to the uniform pressure will be the area between the neoprene gasket rather than the full surface area of the glass specimen. Because, most of the published data did not report the BC used to convert the LTH to STH, to be consistent the full rectangular dimension for each sample set was used in the procedure to calculate the surface flaw parameters.

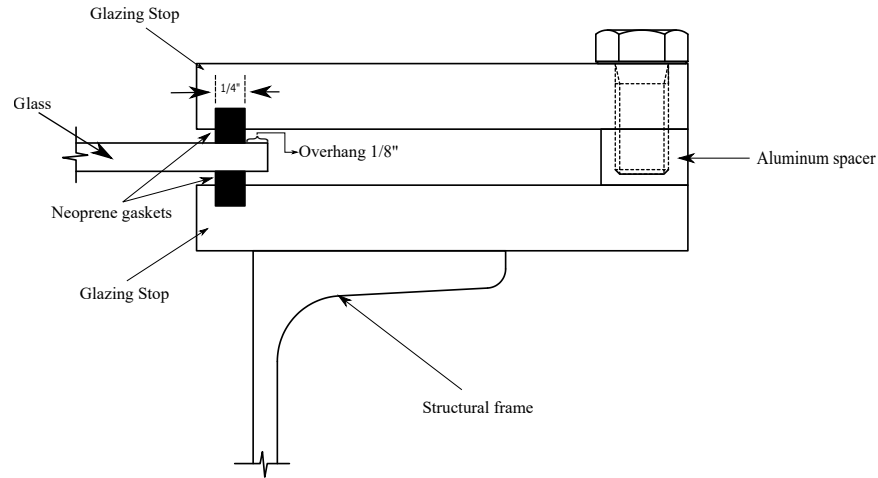


Figure 1.17: Dry Glaze (boundary condition)

1.3.2.3 Specimen thickness

In many of the historical published works, the mean thickness of the sample set was reported instead of the individual specimen thicknesses and a few samples neither reported individual thickness or mean thickness of the sample specimens (marked with # in Table 1.1). Hence, a representative thickness for the sample with missing thickness was required. An iterative method was used to find a representative thickness of the sample using the observed p_b for each EFL listed in the publication. An initial thickness was used with the reported failure data to calculate the EFL for each specimen followed by applying MLE to estimate the surface flaw parameters for the sample. The estimated surface flaw parameters were then used to calculate observed p_b for each EFL and compared to the historically reported observed p_b (Table 1.3). This method was repeated until a thickness was found

that matched the historically reported observed p_b . It is to be noted that the EFL calculated were different due to the assumptions such as an idealized triangular LTH, probable difference in boundary condition, using a mean thickness for each specimen instead of individual thickness, difference in numerical model, mesh size etc. Thus, the observed p_b for EFL values historically reported were calculated using the MLE estimated surface flaw parameters for the thickness chosen and compared (Figure 1.18). The x-axis on Figure 1.18 represents the EFL 60-sec (log scale) and the y-axis represents the probability of breakage, p_b ($\ln(\ln(1/(1-p_b)))$ scale). The representative thickness of the glass sample estimated was always greater than or equal to the minimum thickness, mentioned in ASTM 1300-16 [11]. These three strategies, namely the idealized LTH, BC, and representative thickness calculation were introduced for using incomplete data sets (Task 1.c).

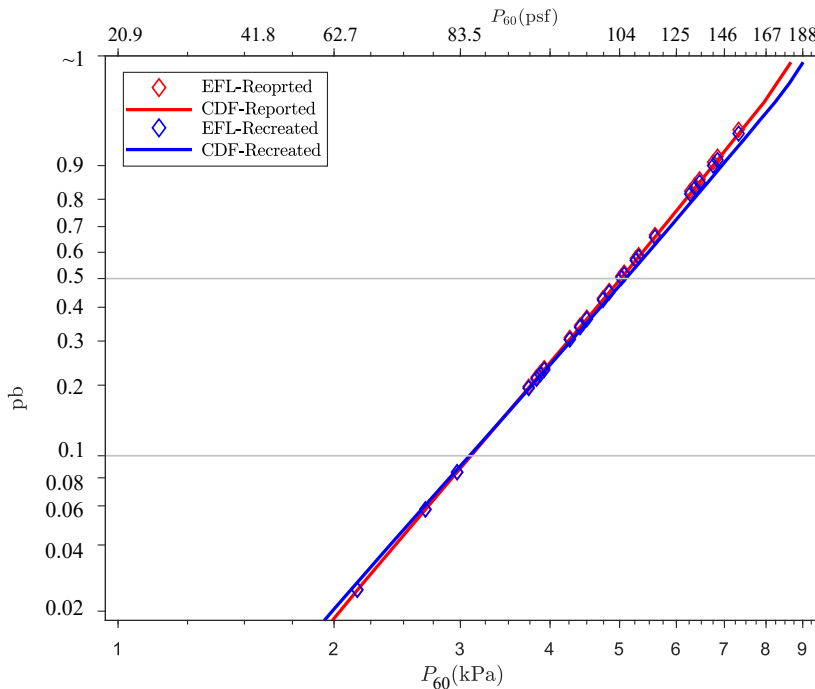


Figure 1.18: Comparison of reported vs recreated p_b

Table 1.3
Method to determine missing thickness

Load (psf)	Observed pb	Recreated observed pb for different thicknesses in mm (in.)			
		2.92 (0.115)	3.05 (0.120)	3.10 (0.122)	3.07 (0.121)
2.15 (45)	.0251	0.0304	0.0258	0.0242	0.0250
2.68 (56)	0.0577	0.0697	0.0597	0.0561	0.0579
2.97 (62)	0.0846	0.1018	0.0873	0.0823	0.0848
3.73 (78)	0.1972	0.2322	0.2001	0.1891	0.1945
3.83 (80)	0.2155	0.2533	0.2185	0.2065	0.2124
3.88 (81)	0.225	0.2642	0.2280	0.2156	0.2217
3.93 (82)	0.2347	0.2754	0.2378	0.2248	0.2312
4.26 (89)	0.3087	0.3602	0.3125	0.2960	0.3041
4.4 (92)	0.3433	0.3996	0.3476	0.3295	0.3384
4.5 (94)	0.3673	0.4267	0.3719	0.3527	0.3621
4.74 (99)	0.4296	0.4963	0.4352	0.4136	0.4242
4.84 (101)	0.4556	0.5247	0.4613	0.4388	0.4499
5.03 (105)	0.5086	0.5815	0.5144	0.4903	0.5022
5.08 (106)	0.522	0.5957	0.5278	0.5034	0.5154
5.27 (110)	0.5756	0.6514	0.5813	0.5557	0.5683
5.31 (111)	0.5889	0.6650	0.5946	0.5688	0.5815
5.6 (117)	0.6676	0.7430	0.6727	0.6461	0.6593
6.27 (131)	0.8271	0.8865	0.8298	0.8062	0.8180
6.37 (133)	0.8458	0.9016	0.8481	0.8255	0.8368
6.46 (135)	0.8633	0.9154	0.8652	0.8436	0.8544
6.75 (141)	0.9081	0.9485	0.9091	0.8911	0.9002
6.85 (143)	0.9206	0.9571	0.9213	0.9046	0.9131
7.33 (153)	0.9657	0.9850	0.9656	0.9553	0.9606

1.3.3 Equivalent failure load duration

During the inception of ASTM E1300 in 1989 [12], the design standard ASCE 7 [6] defined the basic wind speed as the fastest-mile wind speed that translated to a 60-sec gust. Because the primary load used to design a glass was wind load, hence, to be consistent with the ASCE 7 [6], ASTM E1300-1989 [12] also used a basic wind speed of 60-sec. Because

majority of the destructive testing of samples were performed before 1989, the EFL values calculated were for a reference time of 60-sec. Amongst the samples collected, 8 in-service (W01 through W08) and 8 new (N01 through N08) glass samples 60-sec EFL were reported in literature, referred to as EFL_{H60} . Therefore, EFL values for the 8 in-service and 8 new glass samples were recreated for a reference time of 60-sec, referred to as EFL_{Rec60} , and compared to EFL_{H60} . Comparison was carried out to understand the influence of strategies put forward to address missing or incomplete data in the calculation of EFL and if anomaly exists on the recorded data. For in-service samples, 94% of the specimen (389 specimen) EFL_{Rec60} had a difference of -5% to 5% of EFL_{H60} , of which a subset i.e. 83% (343 specimens) EFL_{Rec60} had a difference of -3% to 3%, while only 2 specimen had a difference of either more than 15% or less than -15% (Figure 1.19). Since the same method was used to calculate the EFL, the author believes, a difference of more than 15% or less than -15% was observed for the 2 specimens because of reporting error. A similar trend was observed for the new samples.

The EFL_{Rec60} was used to estimate the 60-sec surface flow parameters and compared to the historical 60-sec surface flow parameters. Because a numerical comparison of surface flow parameters is not meaningful, a graphical comparison is presented. The CDF created using historical surface flow parameters (showed in dash lines in Figure 1.20) is compared to the CDF created using MLE estimated surface flow parameters (showed in solid lines in Figure 1.20). A difference in reported vs MLE estimated surface flow parameters was expected because of the difference in historical and recreated EFL. The position of the

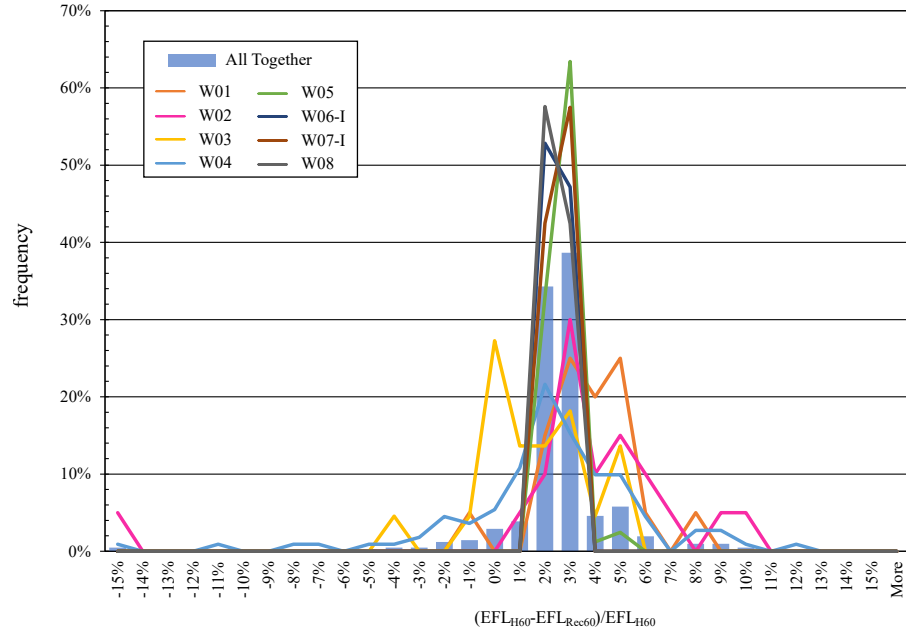


Figure 1.19: Comparison of historical and recreated 60-sec EFL's for weathered samples

CDF recreated using MLE estimated surface flow parameters was consistent with the CDF built using historically reported surface flow parameters. However, for some samples a difference in slope were observed. The MLE estimate surface flow parameters lay between -0.32 kPa (-7.75 psf) to 0.41 kPa (8.42 psf), when comparing the load at 0.008 p_b . A similar range was observed at 0.001 p_b , and a similar trend was observed for new samples.

In 1995, ASCE 7 [7] revised the basic wind speed to a 3 second gust speed. Thus, during the revision of ASTM E1300 in 1998, the basic wind speed to design glass was changed to a 3-sec gust, to be consistent with ASCE 7 [7]. Since then, 3-sec EFL values and consequently 3-sec surface flow parameters are desired. A 3-sec EFL calculation can be calculated using

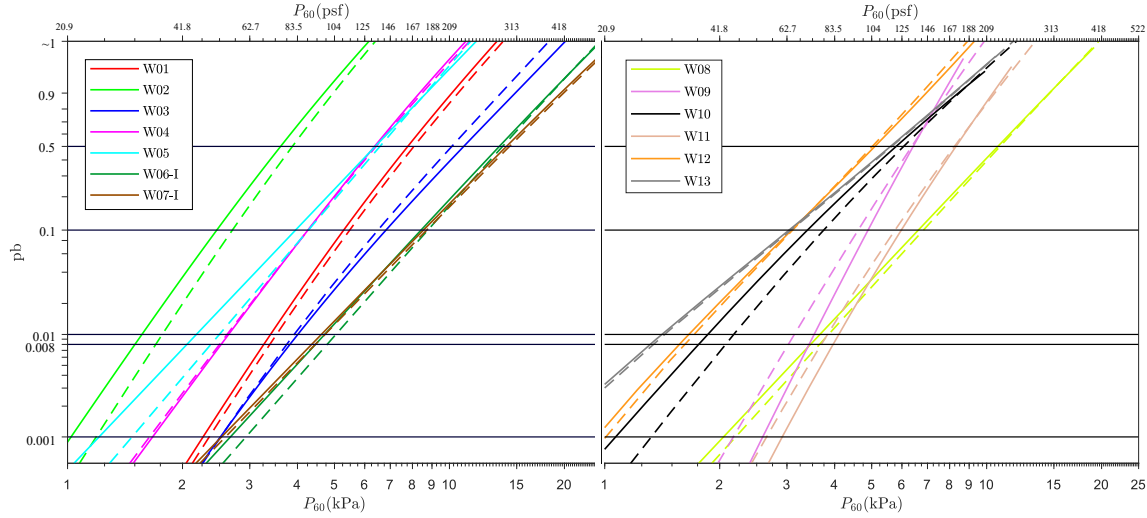


Figure 1.20: 60-sec MLE estimated vs historical surface flow parameters for in-service samples

Equation 1.7 with a t_d of 3-sec resulting in

$$\sigma_3 = \left[\frac{\int_0^{t_f} \sigma(P(t))^n dt}{3} \right]^{\frac{1}{n}} \quad (1.13)$$

where all symbols denote the same as defined before. An applied load time history and a 3-sec EFL is shown in Figure 1.21

1.3.4 Determination of 3-sec surface flow parameters using MLE

The 3-sec EFL values were calculated using Equation 1.13 for each specimen in a sample. The 3-sec EFL values for each sample were used to calculate the surface flow parameters for the sample using MLE. The MLE maximized the likelihood function that is defined using the PDF. Because the PDF of the GFPM is a function of a numerical model, a close

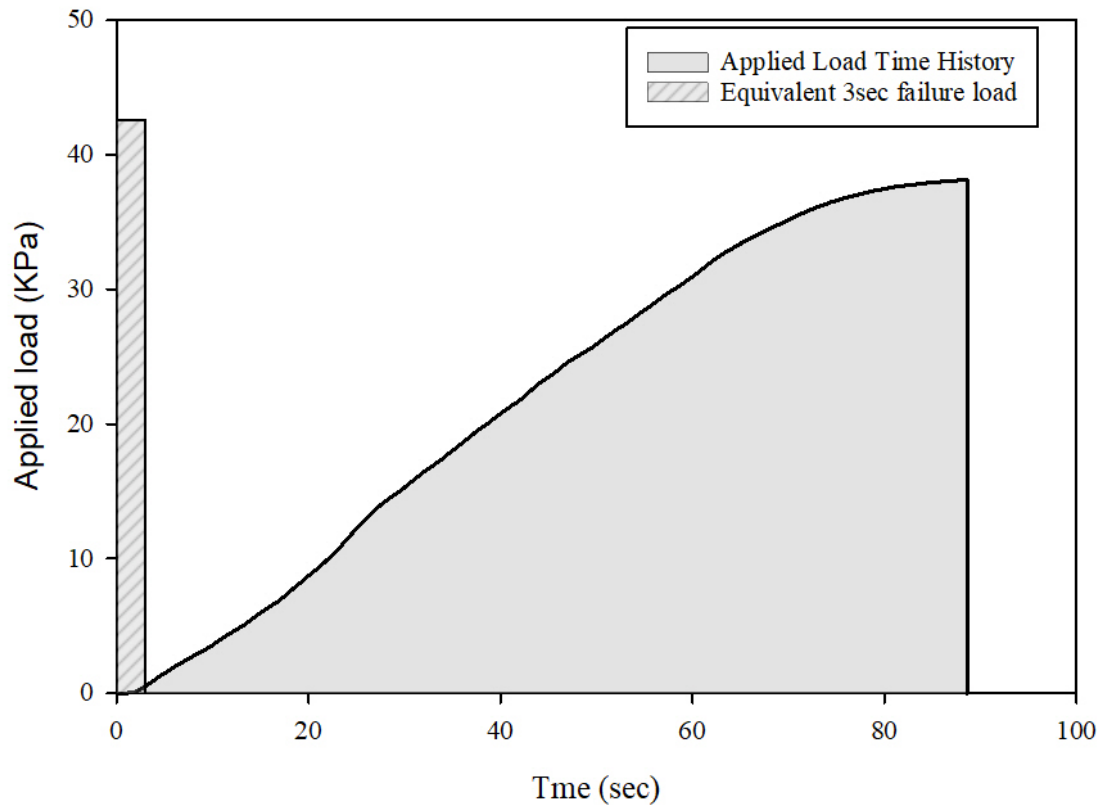


Figure 1.21: A load time history and a 3-sec equivalent failure load

form solution doesn't exist. Therefore, a numerical differentiation is used while defining the PDF. Because, a numerical model is associated, independent numerical analysis are required for each EFL. The MLE method uses the results from each numerical model for individual EFL to calculate the surface flow parameters, m_s and k_s . The likelihood function when maximized for m_s produces an equation that is only a function of m_s . A numerical solution does not exist for the equation, therefore a root finding algorithm can be used to determine the surface flow parameter, m_s . The other surface flow parameter, k_s , is dependent on the m_s and can be calculated with relative ease. Equations for the MLE method to estimate the surface flow parameters are provided in Chapter 2. A list of 3-sec surface flow

parameters estimated using MLE is provided for for each sample in Table 1.4 (Task 1.d).

Figure 1.22 and Figure 1.23 present the 3-sec EFL, and the corresponding CDF created using the MLE estimated surface flow parameters for in service and new glass respectively.

Table 1.4
In-service and new glass 3-sec surface flow parameters

Weathered			New		
Sample set	m_s	$\frac{k_s}{mm^{(2 \cdot m_s - 2)} \cdot N^{-m_s}}$ $\left(\frac{in.^{(2 \cdot m_s - 2)} \cdot lbf^{-m_s}}{mm^{(2 \cdot m_s - 2)} \cdot N^{-m_s}} \right)$	Sample set	m_s	$\frac{k_s}{m^{(2 \cdot m_s - 2)} \cdot N^{-m_s}}$ $\left(\frac{in.^{(2 \cdot m_s - 2)} \cdot lbf^{-m_s}}{m^{(2 \cdot m_s - 2)} \cdot N^{-m_s}} \right)$
W01	5.74	7.06E-15 (1.75E-24)	N01	7.84	2.78E-20 (2.03E-34)
W02	5.42	1.87E-14 (2.34E-23)	N02	6.78	3.08E-18 (4.39E-30)
W03	5.61	3.25E-15 (1.60E-24)	N03	8.48	1.43E-21 (4.42E-37)
W04	5.12	2.51E-14 (1.41E-22)	N04	8.34	1.80E-20 (1.10E-35)
W05	3.92	4.49E-12 (9.52E-18)	N05	9.14	5.51E-22 (6.22E-39)
W06-I	4.07	1.36E-13 (1.40E-19)	N06	9.92	3.49E-24 (7.97E-43)
W07-I	3.86	2.66E-13 (7.77E-19)	N07	9.58	1.27E-22 (1.60E-40)
W08	3.97	5.00E-13 (8.65E-19)	N08	8.87	9.81E-21 (4.18E-37)
W09	7.66	9.43E-19 (1.67E-32)	N09	5.82	1.19E-16 (2.00E-26)
W10	4.47	4.38E-13 (6.25E-20)			
W11	7.74	1.41E-18 (1.73E-32)			
W12	5.76	1.91E-15 (4.33E-25)			
W13	3.81	2.30E-12 (8.66E-18)			
W14	7.20	2.06E-18 (3.70E-31)			

The primary standard in the United States to determine the required thickness for simply supported glass plates used for infill windows panels, ASTM E1300 [11], has been used for the past three decades, the statistical basis of the GFPM surface flow parameters used in ASTM E1300 [11] has not been well understood by the engineering and architectural community. Therefore, using an arbitrary geometry, CDFs are created to illustrate the

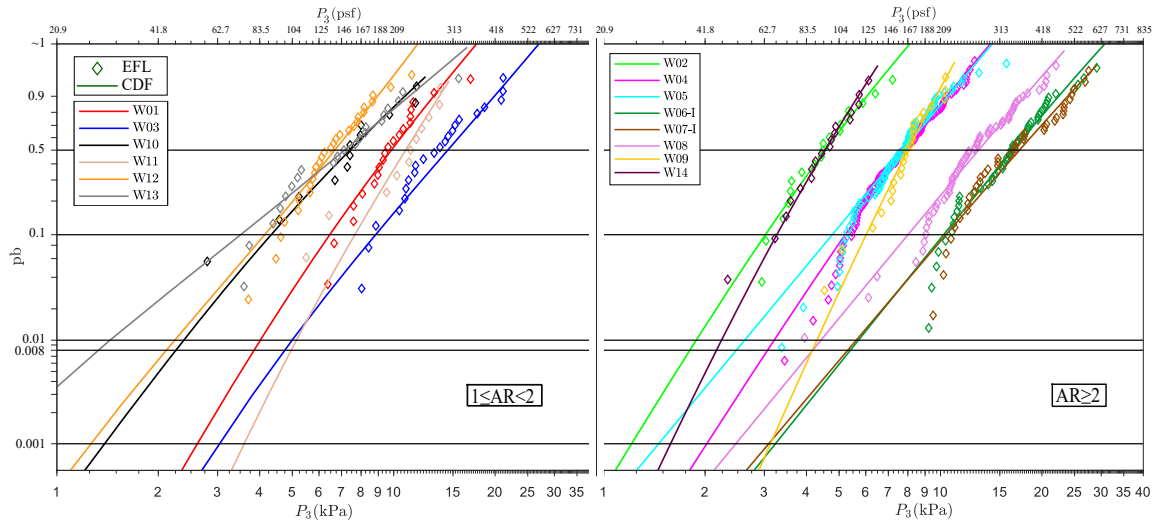


Figure 1.22: 3-sec EFL vs CDF for in-service samples

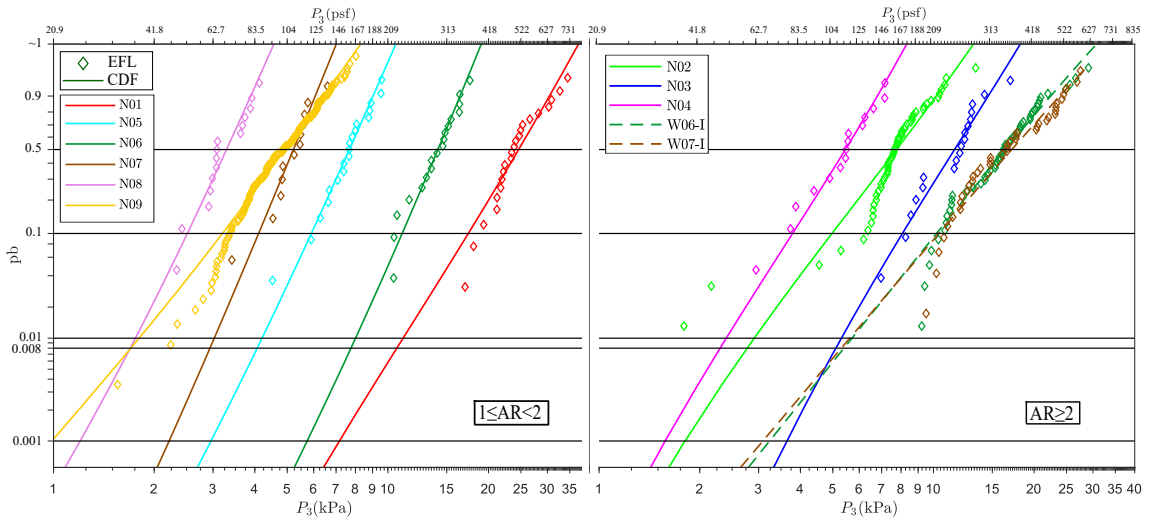


Figure 1.23: 3-sec EFL vs CDF for new samples

comparison of the historical in-service sample GFPM surface parameters to the current GFPM parameters used in ASTM E1300 (Figure 1.24). The CDF created using the surface flow parameter from W05 was the weakest, while the CDF created using the surface flow parameter from W14 was the strongest, and the CDF created using W09 had reasonable agreement to the ASTM E1300 [11]. ASTM E1300 [11] surface flow parameters over

predicted the load corresponding to 0.008 because it is reasonable to assume in-service samples were likely removed from the buildings due to unacceptable damage incurred from a storm event.

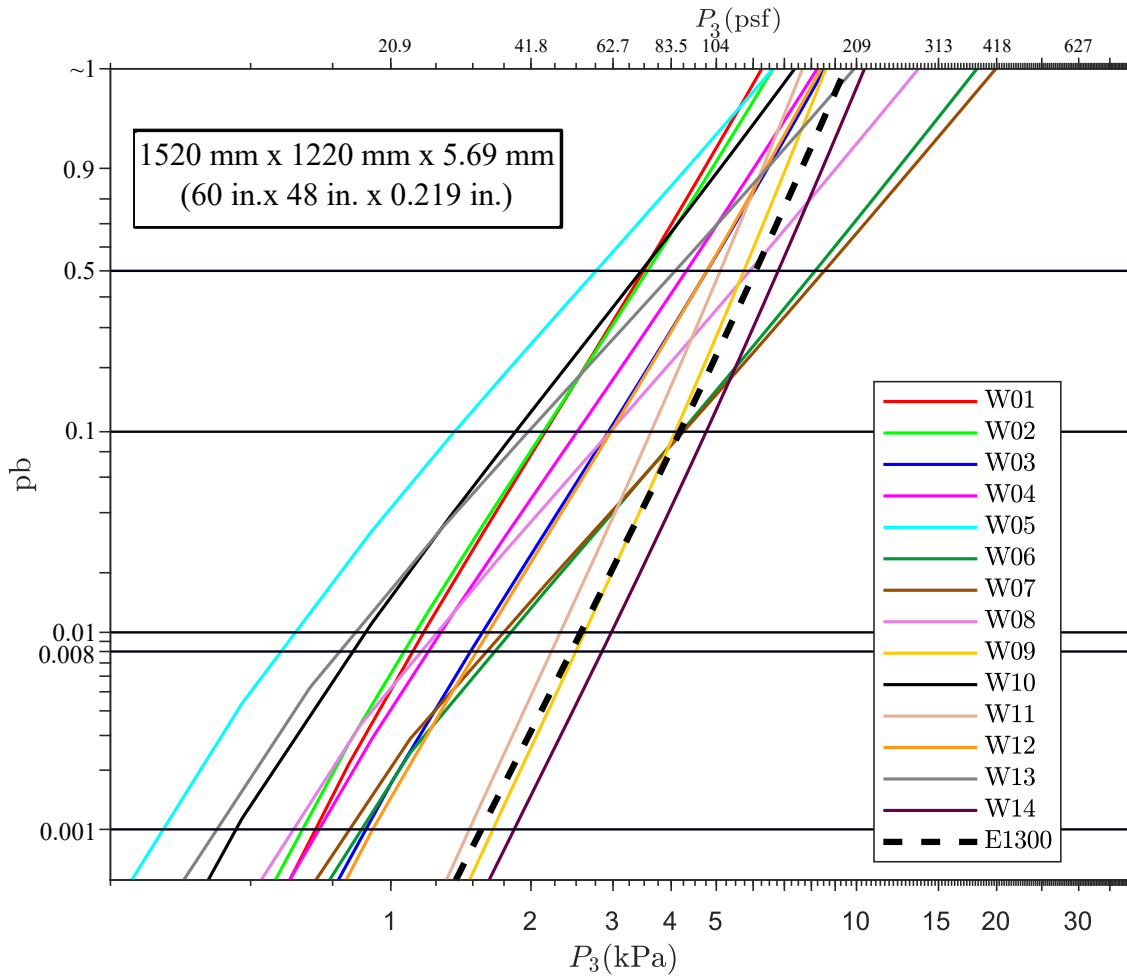


Figure 1.24: Comparison of ASTM E1300 surface flaw parameter to historical in-service parameters

Chapter 2 presents the first article ready to be submitted to the ASCE Journal of Architecture Engineering titled “Estimation of Surface Flaw Parameters for Annealed glass using Maximum Likelihood Estimator” addressing research objective 1 and pertinent information

are provided in Appendix A.

1.4 Monolithic heat-treated glass plate

1.4.1 Heat-treated glass

The process of producing HT glass is by heating AN float glass to near its softening point and then rapidly cooling the glass in a process known as quenching (Figure 1.25). The quenching of the heated AN glass causes the outer surface to cool down while the inner surface is still molten, creating a temperature difference across the cross section of the glass. As the glass cools down, a compressive stress also known as the residual compressive surface stress (RCSS) will be introduced to the outer surface, while the inner surface will be in tension (Figure 1.26). Depending on the value of RCSS, HT samples are classified into two categories, a heat strengthened (HS) glass and a fully tempered (FT) glass. If the RCSS in the glass sample is between 24 MPa (3500 psi) to 52 MPa (7500 psi), the glass is classified as HS glass, and if the RCSS of the glass is above 69 MPa (10000 psi) or if the RCSS at the edge is above 67 MPa (9700 psi), the glass is classified as FT glass.

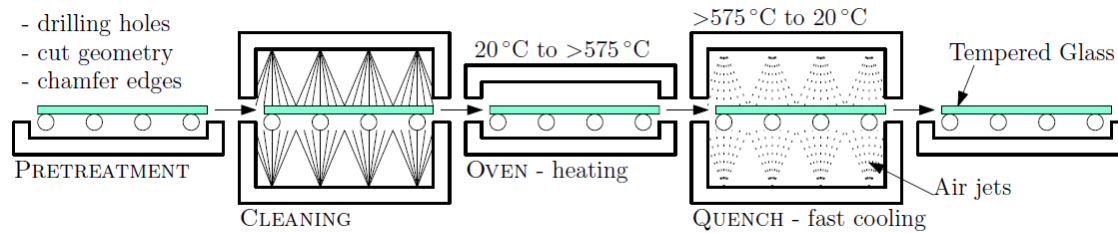


Figure 1.25: Tempering Procedure [48]



Figure 1.26: Stress distribution across the cross section of a glass

1.4.2 GFPM modification for RCSS

Because the surface of the HT glass is in a compressive stress state, the flaws present on the surface are also in compression. However, to initiate fracture, the surface flaws on glass must be in tension to allow for the flaw tip radius to sharpen and create a stress concentration sufficient to initiate fracture [44]. Thus, a load large enough to induce a tensile stress that exceeds the RCSS of the glass must be applied before the flaws are in tension. On the other hand, if the applied load produces a stress that is less than the RCSS

of the sample, the flaws on the surface of the glass will not be in tension, and hence glass will not fracture in other words the glass can hold this load indefinitely. Hence, the RCSS of a HT specimen act as a location parameter because the p_b of a HT glass below the RCSS is zero. Norville et al. [50] and Morse and Norville [44] put forward a modified GFPM (MGFPM) by introducing the RCSS of HT specimen as the third or location parameter and mathematically presented the material function of the MGFPM as

$$B_s = k_s \cdot \sum_{i=1}^{n_{elem}} \cdot \left(c_i \cdot \left(\frac{t_d}{t_{par}} \right)^{1/n} \cdot (\sigma_{max,i} - RCSS) \right)^{m_s} \cdot A_i \quad (1.14)$$

Since, the MGFPM represents the sample, the RCSS in Equation 1.14 denotes the RCSS value that best represents the sample. Similarly, Bergers et al. [19] and Afolabi et al. [3] recognized for HT glass, the measure of damage, k_f of a flaw to the time of failure, t_f should be measured only after the stress the flaw is subjected for a duration surpasses the RCSS of the sample. Thus, for a HT specimen, the stress σ_{t_d} required for the same flaw to fail for a different time duration, t_d can be equated as

$$\sigma_{t_d} = \left[\frac{\int_0^{t_f} (\sigma(P(t))_{RCSS})^n dt}{t_d} \right]^{\frac{1}{n}} + RCSS \quad (1.15)$$

thereby changing the EFL calculation for a HT specimen. Since, the EFL calculation represents individual specimen, the RCSS in Equation 1.15 denotes the individual minimum measured RCSS of the specimen in question.

1.4.3 Published historical experimental test records

Over the past four decades, destructive uniform load tests have been performed only on six HT samples of different shape, size, aspect ratio to understand and establish the load resistance of simply supported monolithic HT glass plates. Table 1.5 presents a collection of experimental data for 6 new and in-service HT glass samples with relevant information (Task 2.a). Similar to the previous chapter, the published records of these tests are not consistently complete, and the methods used to select the corresponding GFPM surface parameters are not well documented. This article provides a curated collection of historical destructive uniform test data of new, and in-service simply supported rectangular HT glass plates samples and strategies introduced previously for missing or incomplete data were applied to the collected data sets (Task 2.b and 2.c respectively).

Table 1.5
Sample Description of HT samples

Sample	# Specimens	Rectangular Dimension mm x mm (in. x in.)	Measured Thickness mm (in.)	RCSS measured	LTH
H1 ^{a,e}	20	1930 x 965 (76 x 38)	5.66 (0.223)	Yes ^f	No
H2 ^b	26	1930 x 965 (76 x 38)	5.61 (0.221)	Yes* ^f	Yes
F1 ^c	26	1680 x 1680 (66 x 66)	5.66 (0.223)	Yes ^g	Yes
F2 ^{a,e}	20	1930 x 965 (76 x 38)	5.64 (0.222)	Yes ^g	No
F3 ^d	14	1520 x 737 (60 x 29)	5.87 (0.231)	Yes ^{f,h}	Yes
F4 ^d	16	2360 x 838 (93 x 33)	5.72 (0.225)	Yes ^{f,h}	Yes

^a reported in [20]; ^b reported in [19], ^c reported in [50]

^d reported in [3]; ^e reported in [51]

* only mean RCSS of sample was reported in [19]

stress measuring device used: ^f GASP, ^g DSR, and ^h SCALP

1.4.4 Determination of representative sample RCSS

The 3-sec EFL values were calculated using Equation 1.15 for each specimen in a sample. The 3-sec EFL values for each sample were used to calculate the surface flow parameters for the sample using MLE. However, the two surface flow parameters for a HT sample are dependent on the RCSS value. Therefore, it is important to determine (estimate) the RCSS value to best represent the sample. After the RCSS is estimated, a similar procedure as described in §1.3.4 can be used to estimate the surface flow parameters. The procedure to estimate the best representative RCSS of the sample is an iterative process. An initial value of RCSS, usually the minimum of the measured RCSS of the sample is chosen and surface flow parameters are estimated using MLE for the chosen RCSS. Observed p_b for each EFL is calculated using the chosen RCSS and the individual specimen RCSS using the MLE estimated surface flow parameter. The difference of the observed p_b using the chosen and individual RCSS for each EFL is calculated and plotted in Figure 1.27 (the red horizontal bars). The average of the difference of observed p_b for the sample is calculated and plotted (the red horizontal line) in Figure 1.27. It was observed that, the minimum of the measured RCSS of the sample underestimated the observed p_b , while the maximum of the measured RCSS of the sample overestimated the observed p_b (the blue horizontal line in Figure 1.27). The mean of the measured RCSS of the sample neutralized the effect to some extent. Hence, a RCSS that nearly produces the average of the difference of observed p_b equal to zero is desired, referred to as the base RCSS.

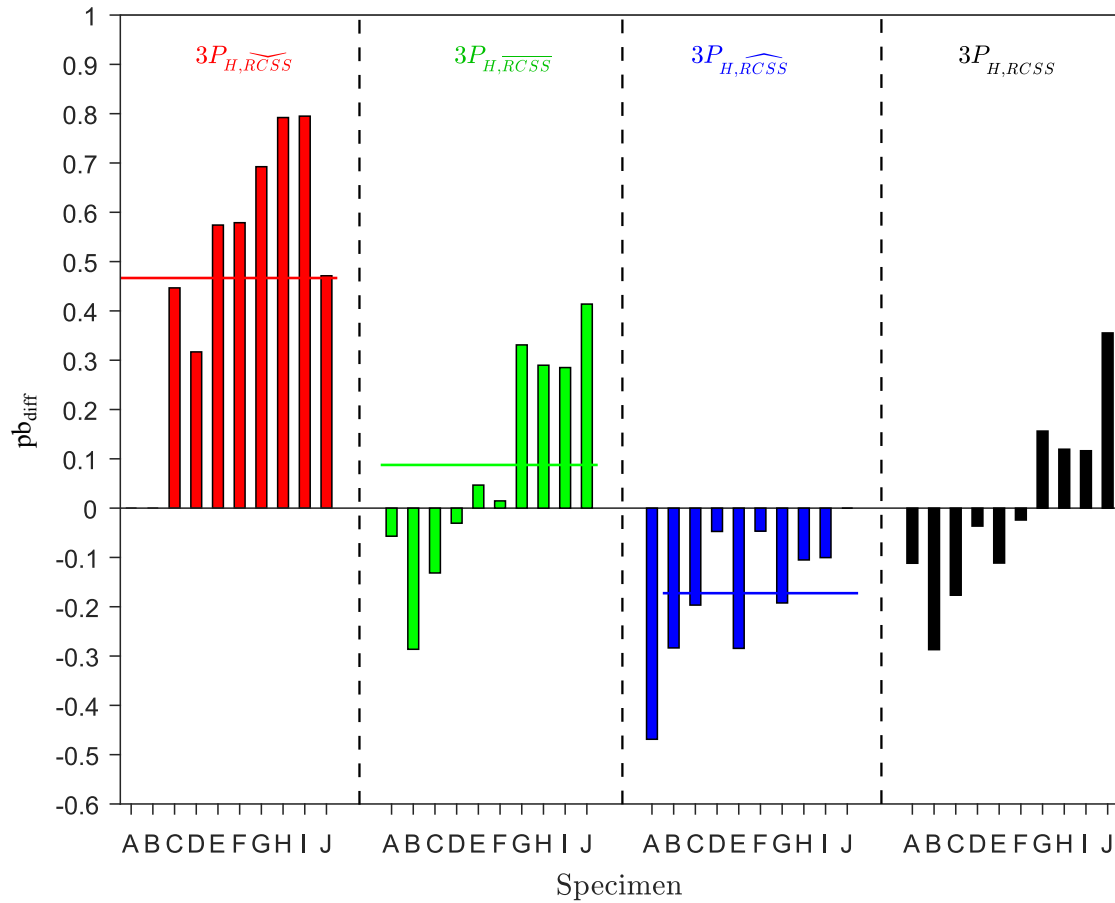


Figure 1.27: Representative RCSS of a HT sample

1.4.5 Determination of 3-sec surface flow parameter using MLE

The base RCSS for each sample was calculated using the procedure describes in §1.4.4 and used to estimate the 3-sec surface flow parameters estimated using MLE (Task 2.d). Equations for the MLE method to estimate the surface flow parameters are provided in Chapter 3. Figure 1.28 shows the 3-sec EFL, and the corresponding CDF created using the MLE estimated surface flow parameters listed in Table 1.6.

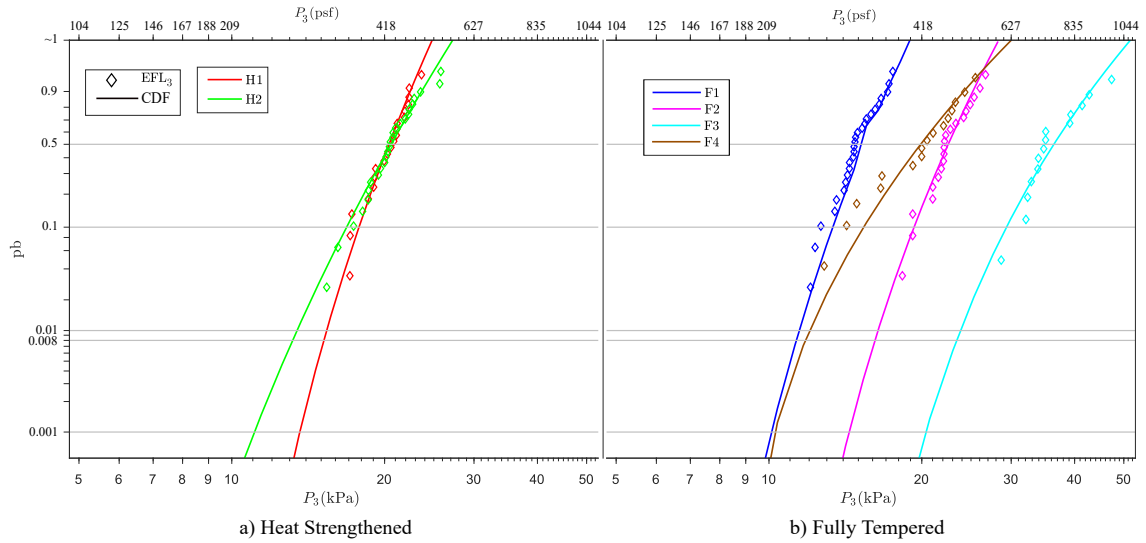


Figure 1.28: EFL_3 and CDF for HS and FT samples

Table 1.6
3-sec surface flow parameters

Sample	RCSS MPa (psi)	3-sec Surface flow parameter	
		m_s	k_s $m^{(2 \cdot m_s - 2)} \cdot N^{-m_s}$ $(in. \cdot (2 \cdot m_s - 2)) \cdot lbf^{-m_s}$
HS-01	64.3 (9317)	7.22	1.52E-18 (2.43E-31)
HS-02	42.5 (6160)	6.77	1.08E-18 (1.62E-30)
FT-01	76.7 (11119)	6.79	3.21E-18 (4.45E-30)
FT-02	68.4 (9921)	6.25	5.11E-17 (1.02E-27)
FT-03	82.4 (11943)	3.82	2.28E-12 (8.16E-18)
FT-04	84.7 (12278)	3.25	2.33E-11 (1.42E-15)

Three of the 6 samples collected were of similar size and different RCSS, namely H1, H2 and F2. Hence, CDF of the samples were compared to understand the effect of RCSS on the strength of glass (Task 2.e) in Figure 1.29. The RCSS acts as a location or a shift parameter therefore, with increase in RCSS, the CDF should shift to the right and vice-versa. For the three samples, the base RCSS of H1 was 64.3 MPa (9317 psi), 42.5 MPa (6160 psi) for H2, and 68.4MPa (9921 psi) for F2. Comparing the load corresponding to 0.008 p_b , the

load increased with increase in RCSS i.e., H2 weakest, followed by H1 and F2. However, a change in slope in H2 from H1 and F2 was observed, and the author believes either the test procedures were different, or some other factors may have been in place the author is unaware of.

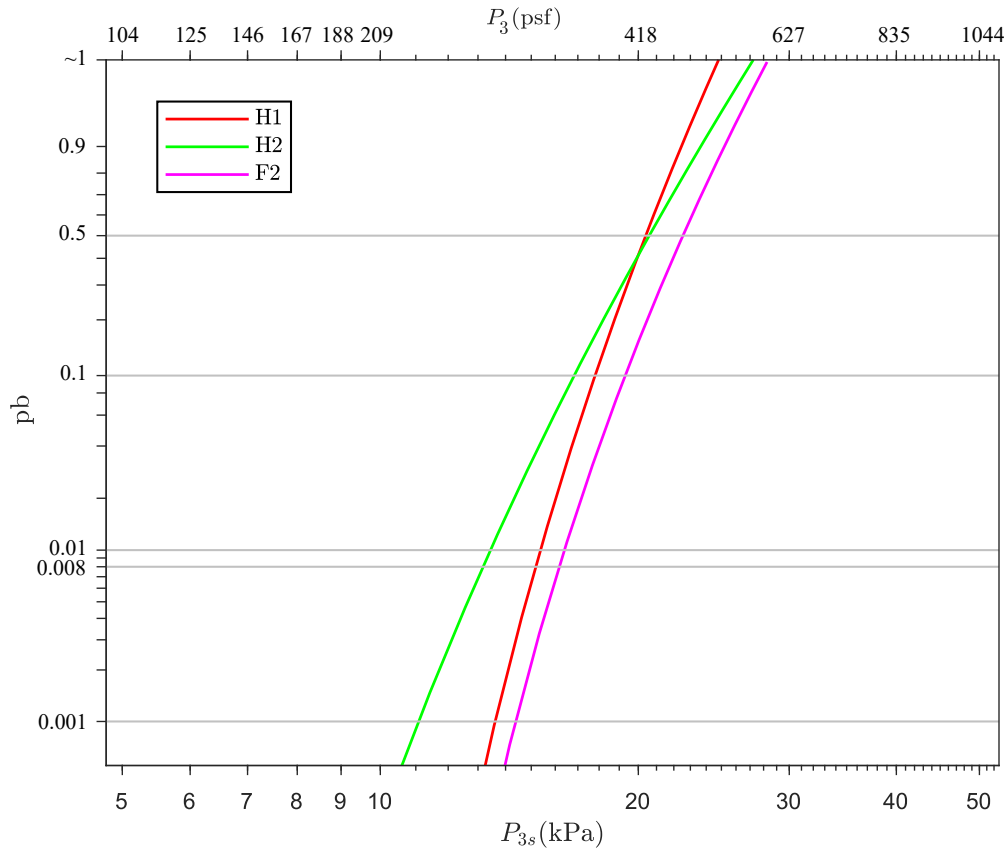


Figure 1.29: Comparison of similar size glass to understand the effect of RCSS on the strength of glass

1.4.6 Comparison of experimental data CDFs to ASTM E1300 analytical method

Although, ASTM E1300-16 [11] has been expanded to include the design of HT glass samples using the modified GFPM, the procedure uses the same set of surface flaw parameter to design a HT glass component as used to design a AN glass component. ASTM E1300-16 [11] fails to mention a reason for using the same set of surface flaw parameters to design HT glass. The author believes the same set of surface flaw parameters is used because it is assumed that there is no mechanical material difference between a HT and AN glass, therefore a HT sample weathers like an AN sample. Hence, the CDF for similar size in-service AN glass samples are compared to similar size in-service HT glass samples to better understand the effect of RCSS on weathering (Task 2.e) in Figure 1.30. Sample W02 from §1.3.1 and F3 are of similar size, while W14 from §1.3.1 and F4 are of similar size. The individual CDF are shown in solid lines for the FT samples, and in dash lines for the AN samples. To understand if AN and HT samples weather similarly, either the AN CDF can be compared to HT CDF but for a zero RCSS, or the HT CDF can be compared to the AN CDF but with the RCSS of the FT specimen. The work herein compared the HT CDF to the AN CDF with the RCSS of the FT specimen. The additional CDF was created using MGFPM and the surface flaw parameters from the weathered sample while using the RCSS of the FT sample denoted by the dash dot lines.

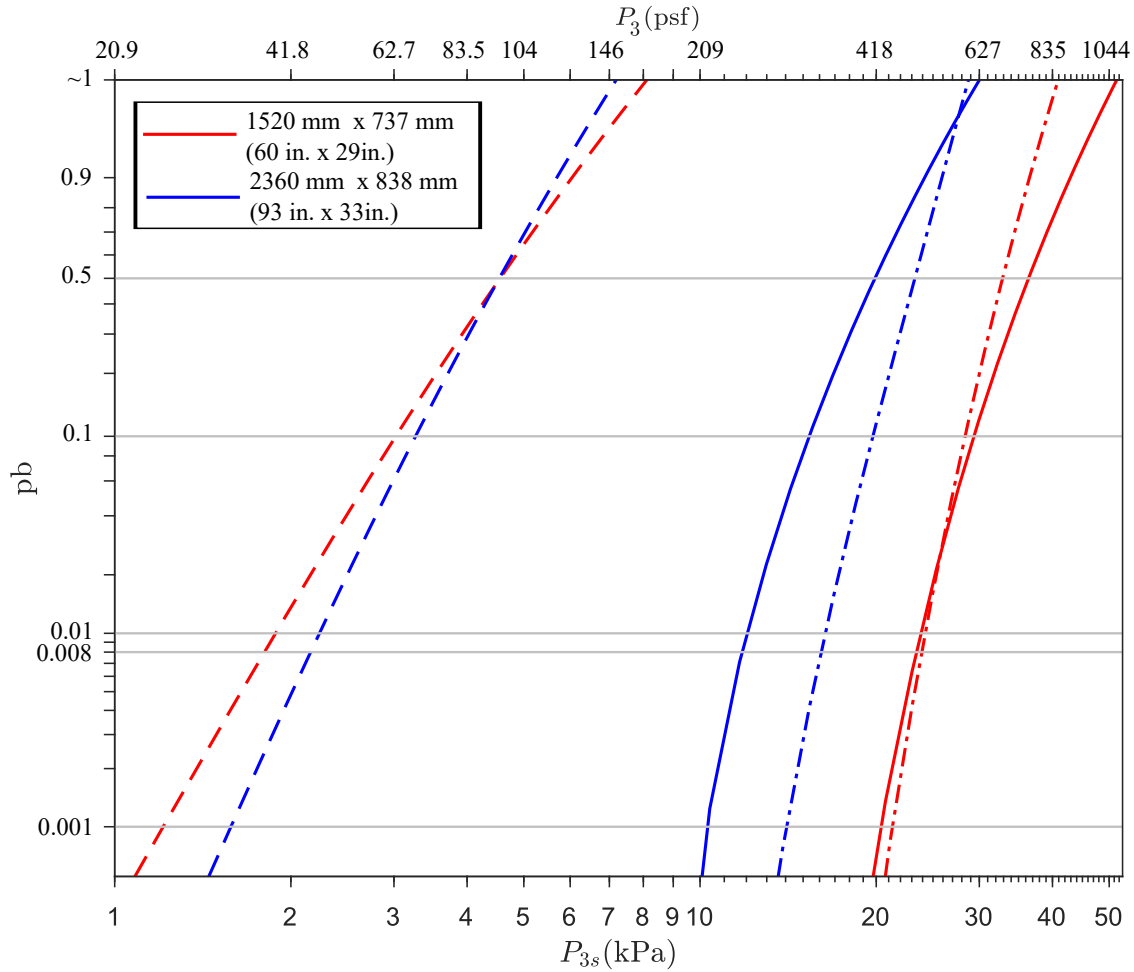


Figure 1.30: Comparison of similar sized in-service AN and HT glass samples

Surface flaw parameters from W02 estimated the load corresponding 0.008 p_b for the F3 geometry and RCSS with a difference of only 2.11%, whereas surface flaw parameters from W14 overestimated by 36.5%, for the F4 geometry and RCSS. A clear trend was not observed as to whether AN and HT samples weather similarly.

Chapter 3 presents the second article ready to be submitted to the Glass Structures & Engineering titled “Estimation of surface flaw parameters for heat treated glass using maximum

likelihood estimator” addressing research objective 2 and pertinent information are provided in Appendix B.

1.5 Glass with holes

1.5.1 GFPM for holes

In the modern era, many commonly used glass components including fins, awnings, and high-end atrium facades are connected to the structure with hardware anchors that pass-through holes in the glass component. The method to create a hole is similar to the method to cut the glass to the required size, i.e., additional flaws are created with a scoring tool or with a water-jet followed by propagating the flaw to either cut the glass to the required size or create the hole (Figure 1.31). Thus, holes can be considered as a specialized edge. ASTM E1300-16 [11] only provides a procedure to determine the strength of a rectangular



(a)



(b)

Figure 1.31: (a) Cutting glass to shape (b) Creating a hole

glass component also known as infill panels, or lite, continuously simply supported along two or more edges. The ASTM E1300-16 [11] does not address glass with holes. However, while designing glass with holes Table X7 in the annex of ASTM E1300-16 [11] is frequently referenced. Table X7 lists allowable stress intended for the design of non-rectangular glass shapes and alternate support conditions. It is not meant for glass with holes.

Walker and Muir [62] while investigating louver glass recognized both edges and the surface were stressed to the same magnitude. Flaws on the edges are different in geometry (shape, size, depth) and distribution compared to the flaws present on the surface of the glass because of the additional flaws created from the scoring process. Realizing this, Walker and Muir extended Beason's GFPM to include the effect of both edges (B_E) in addition to the surface (B_S) to calculate the p_b of louvre glass expressed as

$$B_{Louver} = B_s + 2 \cdot B_E \quad (1.16)$$

where, B_{Louver} denotes the material function of the louvre glass. The material function for the surface essentially remained the same as described by Beason [18], while the risk function for the edge was expressed as a function of the stress the edge is subjected to across the length of the edge, expressed as

$$B_E = k_{el} \cdot \sum_{i=1}^{n_{elem}} (\sigma_{max,i})^{m_{el}} \cdot L_i \quad (1.17)$$

where, k_{el} and m_{el} represents the size, shape, and number of flaws present on the edge of the glass, L_i denotes the length associated with the i_{th} element, $\sigma_{max,i}$ denotes the maximum principal stress at the i^{th} element. The biaxial correction factor, c_i , for the edge is equal to 1 as edges are stressed uniaxially.

The presence of the holes and the subsequent anchors result in significantly different stress distributions and surface flaws in and around the holes than addressed by the GFPM for plates. Thus, a new material function or GFPM for holes that addresses the flaws and the stress distribution around the hole is required. Schultz et. al. [55] and Yew et. al. [68], recognized that holes are specialized edges while determining the load resistance of point-supported glass components and put forward a material function for holes also referred to as the GFPM for holes expressed as

$$B_H = k_H \cdot \sum_{i=1}^{n_{elem}} (\sigma_{max,i})^{m_H} \cdot L_i \quad (1.18)$$

where, k_H and m_H represents the size, shape, and number of flaws present on the hole of the glass, L_i denotes the length associated with the i_{th} element around the hole, $\sigma_{max,i}$ denotes the maximum principal stress at the i^{th} element.

1.5.2 Published historical experimental test records

The work herein collected data for 4-point destructive testing of FT glass samples with a hole in the center (Task 3.a) listed in Table 1.7. The LTH for each specimen were recorded by Cervanka [22] and available. The long dimension, short dimension, thickness, diameter of the hole and the RCSS measurement are measured and provided in Table 1.7.

Table 1.7
Sample data for glass with holes

Specimen	Thickness, (t) (mm)	Width, (b) (mm)	Hole diameter, (d) (mm)	RCSS (MPa)
4H1	12.4	205	36.3	104
4H2	12.5	203	36.3	130
4H3	12.6	204	36.3	122
4H4	12.6	204	36.3	138
4H5	12.5	203	36.3	130
4H6	12.6	204	36.3	116
4H7	12.3	204	36.3	116
4H8	12.6	204	36.3	130
4H9	12.3	202	36.3	104
4H10	12.3	204	36.3	122

1.5.3 Determination of hole parameter for GFPM for holes using MLE

The 3-sec EFL values are calculated using Equation 1.13 and used to estimate the hole flow parameters using the MLE method (Task 3.b) and compared to the hole flow parameters estimated using the historically subjective approach. Equations for the MLE method to estimate the hole flow parameters are provided in Chapter 4. The MLE estimated hole flow parameters and hole flow parameters estimated using the historically subjective approach by Schultz et al. [55] is listed in Table 1.8. Because a numerical comparison of the MLE estimated flow parameter and the parameters estimated using the historically subjective approach is not meaningful, a graphical comparison is provided (Figure 1.32). In Figure 1.32, the dot represents the rank probabilities of the EFL, the dash line represents the CDF built using the historically subjective approach flow parameters, whereas the solid line represents the CDF built using the MLE estimated flow parameters. The lowest EFL is found to be an outlier according to ASTM E178-21 [14], but ASTM E178-21 [14] also mentions an outlier can be due to the inherent variability in the data and should be retained and processed if found to be true. Because there was no report of preexisting damage or issues during the load test for specimen, the observation is considered as a valid observation. The load at 0.001 and 0.008 p_b calculated for the CDF built using MLE estimated surface flow parameter is 12.6 % and 8.74 % higher compared to the CDF built using the

historically subjective approach flaw parameters, respectively. It is observed that the MLE estimated flaw parameters are not as sensitive to the lower EFL. The load corresponding to the allowable stress mentioned in Table X7 of ASTM E1300-16 [11] is also plotted in the graph with a dashed black line. For the specimen geometry, the maximum allowable stress around the hole should be limited to 73.0 MPa (10600 psi) which corresponds to a 5.1 kN (1150 lbf). Thus, at 0.008 p_b , the load from ASTM E1300-16 [11] underestimated the strength by almost 50%.

Table 1.8
MLE estimated vs historically subjective method hole flaw parameters

	m_H	$\frac{k_H}{mm^{(2m_H-1)}N^{-m_H}}$
Schultz et al. [55]	15.25	5.06 E-37
MLE hole parameters	20.2	1.23 E-48

1.5.4 Modified GFPM for holes

All the specimen for the glass with holes were FT, hence, the GFPM for holes can be extended to include the RCSS as the location parameter. The same principle as described for HT glass samples in §1.4.2 is applicable for FT glass with holes. Thus, the GFPM for holes is modified consistent with the modification to the MGFPM advanced by Morse and Norville [44] for HT plates (Task 3.c). The modified GFPM for holes is expressed as

$$B_H = k_H \cdot \sum_{i=1}^{n_{elem}} (\sigma_{max,i} - RCSS)^{m_H} \cdot L_i \quad (1.19)$$

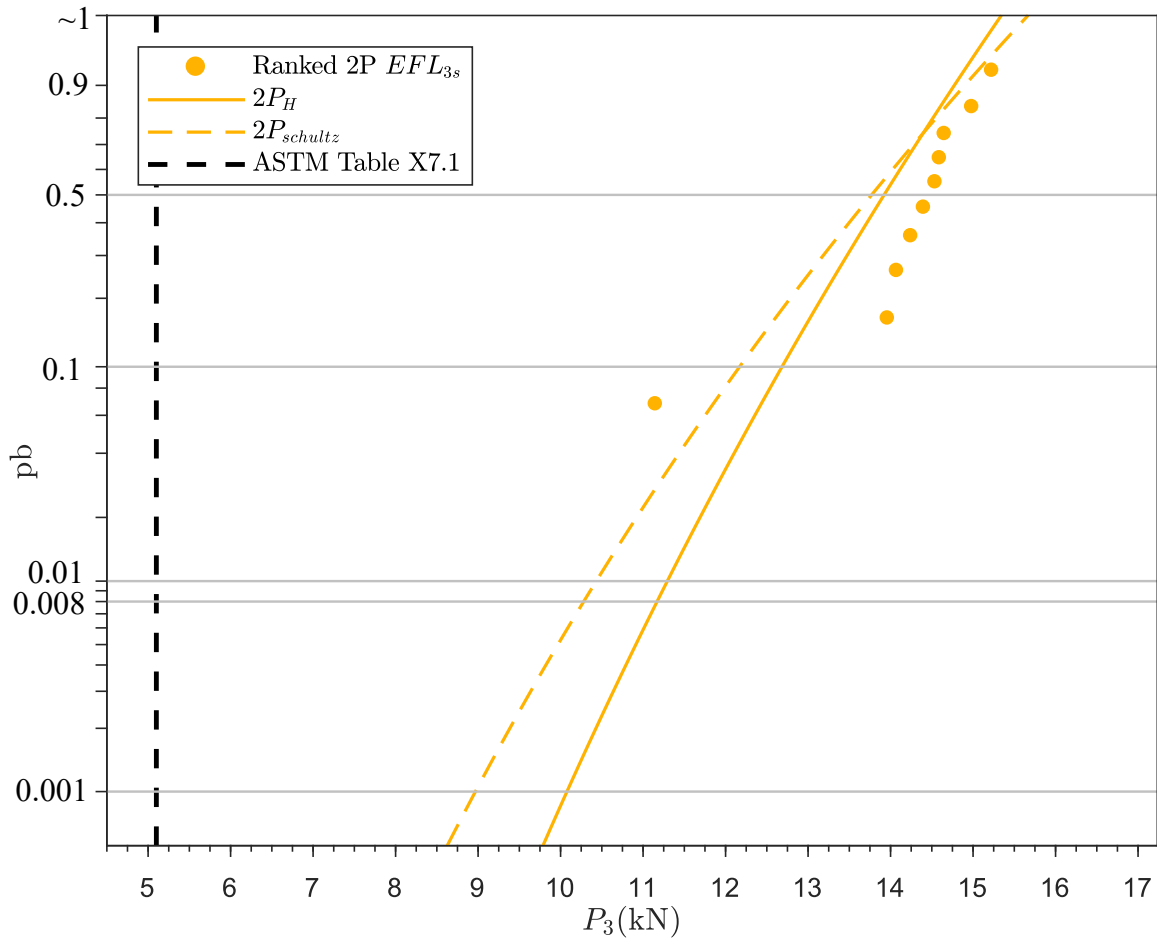


Figure 1.32: Comparison of MLE estimated flaw parameter vs flaw parameter estimated using the historically subjective method

where, all symbols denote the same as defined before. Since, the MGFPM fro holes represents the sample, the RCSS in Equation 1.19 denotes the RCSS value that best represents the sample. The 3-sec EFL values are calculated using Equation 1.15. Since, the EFL calculation represents individual specimen, the RCSS in Equation 1.15 denotes the individual minimum measured RCSS of the specimen in question.

1.5.5 Determination of hole parameters for the modified GFPM for holes

The hole flow parameters k_H and m_H in the modified GFPM for holes are dependent on the RCSS chosen. Thus, it is important to estimate the RCSS value to best represent the sample. The iterative procedure to estimate the best representative RCSS of the sample introduced in §1.4.4 is used to estimate the base RCSS. The base RCSS was used to estimate the 3-sec surface flow parameters estimated using MLE (Task 3.d). Equations for the MLE method to estimate the hole flow parameters for the modified GFPM for holes are also provided in Chapter 4. For the sample, a base of RCSS of 126 MPa was estimated and corresponding hole parameters m_H and k_H were estimated as 6.65 and $4.60\text{E-}14 \text{ mm}^{(2m_H-1)} \text{ N}^{-m_H}$, respectively, using MLE (Task 3.d). Figure 1.33 presents EFL calculated for the GFPM for holes and for the modified GFPM for holes. Figure 1.33 also presents the corresponding CDF created using the MLE estimated hole flow parameters for the GFPM for holes and the modified GFPM for holes.

Both the GFPM for holes and the modified GFPM for holes can be used to predict the strength of glass with holes. However, the GFPM fails to address the RCSS of the sample. Thus, to design the a glass with hole with the GFPM for hole, a modification is suggested to address the effect of RCSS.

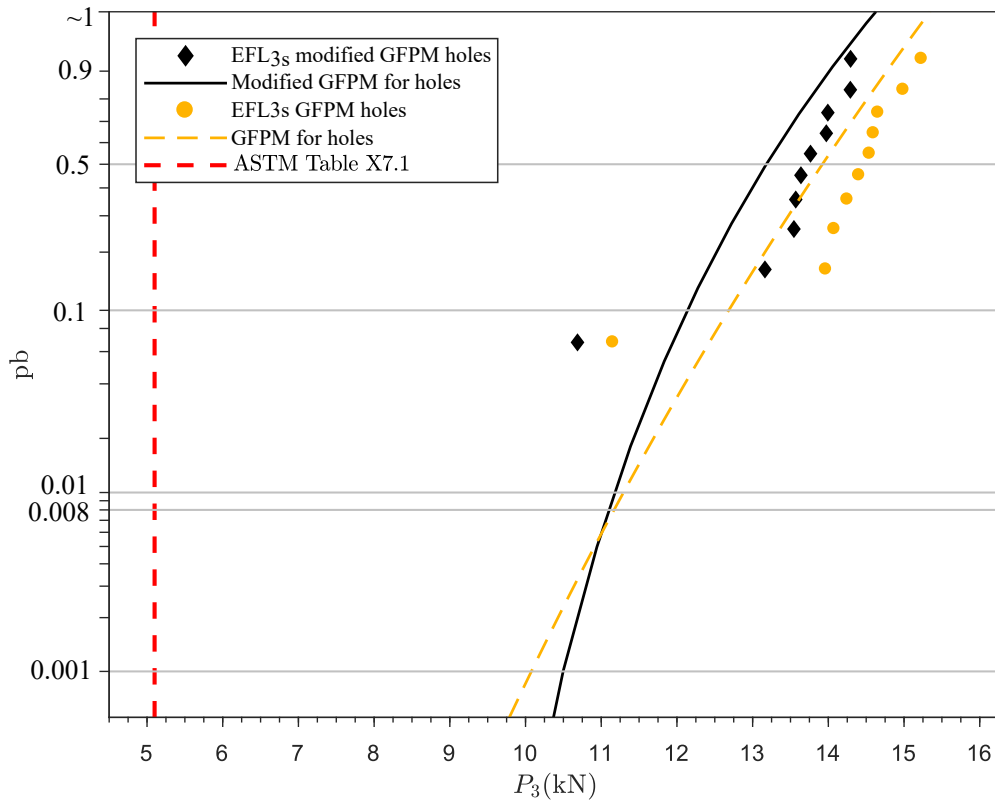


Figure 1.33: 3-sec EFL and fit for modified GFPM for holes

Chapter 4 presents the third article submitted to the Glass Structures & Engineering titled “Estimation of Flaw Parameters for Holes in Glass using Maximum Likelihood Estimator” addressing research objective 3 and pertinent information are provided in Appendix C.

Chapter 2

Estimation of Surface Flaw Parameters for Annealed glass using Maximum Likelihood Estimator

Over the past four decades, surface flaw parameters for the two-parameter glass failure prediction model were estimated based on statistical measures and researcher's interpretation of the failure data rather than an objective and a repeatable method. A robust statistical method, the maximum likelihood estimator method, is advanced in this work, tailored to the two-parameter glass failure prediction model for rectangular glass plates to objectively and repeatably estimate the surface flaw parameters. The surface flaw parameters represents the number, type, depth, and orientation of microscopic flaws present on the surface of the

glass, therefore it is impractical to physically measure them. Instead they are deduced from destructive testing of identical dimensions of glass plates monotonically loaded to failure. Historical failure test data consisting of in-service and new annealed monolithic glass specimens are collected and used to illustrate the working principle of the maximum likelihood estimator method. However, the collected published experimental data are not consistently complete, therefore several critical requirements and strategies were advanced for using incomplete data sets. Current design standards are based on 3-sec basic wind load, hence surface flaw parameters based on 3-sec time duration are reported. Several example designs are used to illustrate the comparison of the historical sample GFPM surface parameters to the current GFPM parameters used in ASTM E1300, the standard in the United States used to determine the load resistance of a glass component.

2.1 Introduction

Glass is a standard construction material used primarily for windows and facades. The use of glass as a building material requires engineers and designers to calculate the strength or load resistance (LR) of a glass component with a degree of confidence before use. Due to the brittle nature of glass, a well defined ultimate stress for glass is absent, thus to design a glass component, the allowable maximum stress design method cannot be used with a high degree of confidence. Glass fails primarily due to the presence of microscopic flaws present on the surface of the glass. Flaws are inherent to a glass surface because of manufacturing

process, and handling and cutting of glass. Since flaws on the glass surface are microscopic in nature and impractical to measure, the location and orientation of the critical flaw, i.e. the flaw that initiates failure is not known until failure occurs. The absence of a ultimate stress for glass combined with the unknown location of critical flaw causing failure necessitates a probabilistic approach to calculate the LR of glass.

The standard to determine the load resistance of a glass in building, ASTM E1300-16 [11], provides a probabilistic procedure, the glass failure prediction model (GFPM) developed by Beason [18], to determine the LR of a rectangular glass infill panel (lite) continuously supported along two or more edges. The GFPM is based on the well known probabilistic distribution function for brittle material, the Weibull distribution [64]. The GFPM that takes into account the number, severity, and orientation of microscopic flaws on the glass surface, the geometry of the glass component, the duration of the load applied, the stress the glass component is subjected to due to the applied load and orientation of the stress, and environmental exposure to calculate the probability of breakage (p_b) for the glass component.

The GFPM uses two surface flaw parameters, m_s and k_s , to represent the number, severity, and orientation of the microscopic surface flaws present on a glass surface. The surface flaw parameters are independent of aspect ratio (AR), surface area, and failure load duration [18]. Because the surface flaw parameters are impractical to measure, they are estimated

based on destructive testing of multiple specimens with the same geometry. The independent nature of the surface flaw parameters makes it possible to use the estimated surface flaw parameters to design a glass component of different dimension (AR and area), loading condition and boundary conditions. Hence it is essential to accurately estimate the surface flaw parameters. Historically, surface flaw parameters were selected/estimated based on the researcher's interpretation of failure data, rather than an objective and a repeatable procedure, thus introducing undesirable variations, especially when historical data is recreated.

The current work advances a robust statistical method, the maximum likelihood estimator (MLE), tailored to the GFPM for plates to estimate the surface flaw parameters for annealed (AN) monolithic glass, providing a consistent, objective, and repeatable method. To the authors knowledge, a body of work with all failure testing data tested for weathered in-service and new AN monolithic glass does not exist currently. Published historical failure data and associated surface flaw parameters for weathered in-service and new AN monolithic glass was collected for this work and presented for reference. Since most historical test data precedes 1995, and edition of ASCE 7-95 [7] wind load provisions were based on a fastest-mile wind speed, that corresponds to a 60-sec load duration, 60-sec surface flaw parameters were estimated. The current edition of ASCE 7-16 [5] wind load provision is based on 3-sec wind speeds, thus 3-sec surface flaw parameters for all the historical failure data collected were estimated using MLE and presented here.

2.2 Background

2.2.1 Glass Failure Prediction Model

Glass, a brittle material, does not have a well-defined yield stress point, unlike other construction materials, hence, the extremely popular maximum allowable stress design is inefficient to calculate the strength of a glass component. Glass fails primarily due to randomly oriented flaws intrinsic to the glass surface because of the manufacturing process and/or handling of glass [33]. Tensile stress applied to the glass component causes stress concentration at the flaw tip leading to a change in the flaw depth and/or radius that causes the glass to fail. Thus to reliably calculate the LR of a glass plate, the randomly distributed surface flaws must be addressed. As the location, shape, size, and orientation of the surface flaw that may initiate fracture are unknown, a probabilistic method is used to calculate the LR of a glass component. The well-known statistical distribution, the Weibull distribution, was put forward to predict the failure of a brittle material [64]. The two-parameter Weibull distribution (2PWD) is based on the principle of weakest link theory, and the cumulative distribution function (CDF) is mathematically expressed as

$$P_b = 1 - e^{-\lambda \cdot t^\beta} \quad (2.1)$$

where P_b denotes the probability of breakage, λ (> 0) denotes a parameter that is related to the scale parameter, and β (> 0) denotes the shape parameter, 't' is the independent random variable. Although the distribution function can predict the failure of brittle materials, it does not consider all known factors that affect the LR of glass. Hence, a modified distribution function was desired that included all the factors that affect the LR of glass.

Beason [18] related the probability of breakage to a material risk function, B_s , that included all the factors that affect the LR of glass and expressed it as

$$P_b = 1 - e^{-B_s} \quad (2.2)$$

The material risk function, known as the GFPM, was expanded on the work of Brown [21] and required a numerical model (NM) expressed as

$$B_s = k_s \cdot S_{m_s}(NM(GEO, BC, P), m_s) \quad (2.3)$$

where S_{m_s} denotes the equivalent area, and k_s and m_s are analogous to λ and β , referred to as the surface flaw parameters. The equivalent area uses the plate geometry (GEO), boundary conditions (BC), and a load (P) in a numerical model to calculate the maximum and minimum principal stresses (σ_1 and σ_2 respectively) for each nodal area, 'A'. A biaxial correction factor (c) is calculated using σ_1 and σ_2 for each nodal area to take into account

the orientation of the stress. The equivalent area is expressed as,

$$S_{m_s}(NM(GEO, BC, P), m_s) = \sum_{j=1}^N \left[\left\{ c_j \cdot \sigma_{1,j} \cdot \left(\frac{t_d}{t_{par}} \right)^{\frac{1}{n}} \right\}^{m_s} \cdot A_j \right] \quad (2.4)$$

where ‘j’ denotes the nodal area, t_d denotes the load duration, and t_{par} denotes the time duration for which the surface flaw parameters were estimated, N denotes the number of nodes, and ‘n’ is the static fatigue constant while all other variables are the same as defined previously. Charles [24] experimented on soda-lime glass rods and estimated ‘n’'s value as 16. Abiassi [2] and Kanabolo and Norville [38] experimentally verified the value of ‘n’ equal to 16 can be used for both weathered in-service and new glass plates, respectively. Because the material risk function was modified to incorporate a numerical model including the factors affecting glass strength, the distribution does not follow a classical two-parameter Weibull distribution.

The material property of glass (stress vs strain) is elastic in nature. However, the geometry of the glass plate allows the glass to deflect well in excess of its thickness when a load is applied, thereby making the glass plate geometrically non-linear [18]. The geometrical non-linearity necessitates a numerical model that considers the non-linear deflection behavior of glass lites. Beason [18] used a finite element model (FEM) while other researchers used a finite-difference model (FDM) developed by Wang [63] to calculate σ_1 and σ_2 for each nodal area, A_j [2], [38], [46], [4]. Morse [43] presented an example to illustrate the

calculation for A_j , σ_1 , σ_2 , and c_j using the FDM developed by Wang [63] for a rectangular monolithic AN glass. Yew et al. [67] developed a non-linear four-node quadrilateral finite-element model that has shown a good agreement to the FDM developed by Wang [63] for AN monolithic glass. The authors used the non-linear four-node quadrilateral finite-element model developed by Yew et al. [67] for all calculations.

2.2.2 Historical method to estimate of surface flaw parameters

The surface flaw parameters (m_s and k_s) are estimated from destructive tests of multiple specimens with the same geometry. Glass of similar dimension loaded to failure fails at different location because the location and orientation of the critical surface flaw that initiates fracture is not unknown until failure occurs. Thus, destructive testing of similar size glass specimens results in varying failure load-time histories (LTH), generally with different magnitudes of load at fracture and different locations of fracture. Hence, to estimate the surface flaw parameters, the recorded LTH's are normalized to a common reference time with the help of recorded fracture locations. Brown [21] put forward an integration to normalize failure data expressed as

$$EFS_{t_{ref}} = \left[\frac{\int_0^{t_f} (\sigma_{1,(x,y)}(t))^n \cdot dt}{t_{ref}} \right]^{\frac{1}{n}} \quad (2.5)$$

Where $\sigma_{1,(x,y)}$ denotes the corresponding stress-time history at the fracture location (x,y) known as the fracture origin maximum principal tensile stress (FOMPTS), t_f denotes the time to failure, n denoted the static fatigue constant, equal to 16, t_{ref} denotes the reference time i.e. either 60-sec or 3-sec, and $EFS_{t_{ref}}$ is the equivalent reference time failure stress. Stress-time history corresponding to load TH's are calculated using the non-linear four-node quadrilateral finite-element model developed by Yew et al. [67]. The load corresponding to $EFS_{t_{ref}}$ is known as the equivalent failure load ($EFL_{t,ref}$).

Historical estimation of surface flaw parameters, m_s , and k_s was a long iterative process. For a range of m_s , corresponding values of k_s were calculated by a method put forward by Beason [18]. The method included the calculation of equivalent area S_m for each EFL in a sample set expressed as

$$S_{m_s}(NM(GEO,BC,EFL),m_s)_i = \sum_{j=1}^N [(c_{j,i} \cdot \sigma_{1,j,i})^{m_s} \cdot A_{j,i}] \quad (2.6)$$

where all symbols are the same as expressed in Eqn. 2.3 and Eqn. 2.4 . Equivalent areas were calculated for each EFL in the sample for the range of m_s and the surface parameter k_s corresponding to each m_s was calculated as

$$k_s = \frac{N_{spec}}{\sum_{i=1}^{N_{spec}} S_{m_s}(NM(GEO,BC,EFL),m_s)_i} \quad (2.7)$$

where N_{spec} denotes the number of specimens in the sample. Statistical measures such

as the mean, standard deviation, and coefficient of variation (COV) for theoretical CDF's, constructed using each surface flaw pair of trial estimates using Eqn.2.2 and Eqn.2.3 were calculated and compared to EFL statistical measures. The trial surface parameters with the best agreement between EFL and the theoretical CDF were chosen to describe the failure data.

The method to choose the best parameters is based on the researcher's interpretation of the data. In the event when multiple trial estimates produce almost the same statistical parameters a method does not appear in the published literature to select the surface parameters to best describe the failure data. The MLE method eliminates the construction of many theoretical CDFs for all trial estimates and removes all the uncertainties in comparing the statistical measures by providing a consistent and objective method that can be repeated consistently.

2.3 Procedure to estimate surface flaw parameters for glass failure prediction model

The variability in the historical method to estimate flaw parameters requires a consistent, repeatable, and transparent method to estimate surface flaw parameters. Among different methods to estimate distribution parameters for commonly used distributions in a consistent

and repeatable manner, the maximum likelihood estimator (MLE) method is often used because of its simplicity and universality. Pisano and Carfagni [53] and Goswami et al. [32] showed the MLE method could be applied to the GFPM for Ring-on-Ring test data and GFPM for holes respectively, suggesting it can be applied to GFPM for rectangular plates. Goswami et al. [32] illustrated in detail the method to determine the flaw parameters corresponding to GFPM for holes. The flaw parameters for holes were estimated by maximizing the likelihood function for GFPM for holes, and a similar methodology is used for GFPM for rectangular plates. The CDF referred to as the probability of breakage for rectangular glass plates is expressed as

$$P_b = F(EFL, m_s, k_s) = 1 - \exp\{-k_s \cdot S_{m_s}(NM(GEO, BC, EFL), m_s)\} \quad (2.8)$$

where, all symbols denote the same as previously defined. The likelihood function is defined as the product of the probability distribution function (PDF) expressed as

$$L(EFL, m_s, k_s) = \prod_{i=1}^{N_{spec}} \left[k_s \cdot \frac{d}{d(EFL)} (S_{m_s}(NM(GEO, BC, EFL), m_s)_i) \cdot \exp(-k_s \cdot S_{m_s}(NM(GEO, BC, EFL), m_s)_i) \right] \quad (2.9)$$

Because it is easier to maximize a summation form compared to a product form, Eqn. 2.9 can be translated to a summation form by taking the natural logarithm expressed in Eqn.

2.10 as

$$\begin{aligned} \ln(L(EFL, m_s, k_s)) &= \sum_{i=1}^{N_{spec}} \left[\ln(k_s) - k_s \cdot S_{m_s}(NM(GEO, BC, EFL), m_s)_i \right. \\ &\quad \left. + \ln \left(\frac{d}{d(EFL)} (S_{m_s}(NM(GEO, BC, EFL), m_s)_i) \right) \right] \end{aligned} \quad (2.10)$$

where all symbols are same as previously defined. The scale parameter, k_s , is estimated by equating the term obtained from differentiating the natural logarithm of the likelihood equation (Eqn. 2.10) with respect to k_s to zero. Since $S_{m_s}(NM(GEO, BC, EFL), m_s)_i$ is not a function of k_s , rearranging the term the scale parameter k_s becomes

$$k_s = \frac{N_{spec}}{\sum_{i=1}^{N_{spec}} S_{m_s}(NM(GEO, BC, EFL), m_s)_i} \quad (2.11)$$

Similarly, to estimate the shape parameter, m_s the term obtained from differentiating the natural logarithm of the likelihood equation (Eqn. 2.10) with respect to m_s is set to zero resulting in

$$\begin{aligned} \frac{d}{dm_s} \ln(L(EFL, m_s, k_s)) &= \sum_{i=1}^{N_{spec}} \left[\frac{d}{dm_s} \ln \left(\frac{d}{d(EFL)} S_{m_s}(NM(GEO, BC, EFL), m_s)_i \right) \right. \\ &\quad \left. - k_s \cdot \frac{d}{dm_s} S_{m_s}(NM(GEO, BC, EFL), m_s)_i \right] \end{aligned} \quad (2.12)$$

Substituting Eqn. 2.11 to Eqn. 2.12 and equating to zero, the only unknown variable is the parameter m_s expressed as

$$\sum_{i=1}^{N_{spec}} \left[\frac{d}{dm_s} \ln \left(\frac{d}{d(EFL)} S_{m_s}(NM(GEO, BC, EFL), m_s)_i \right) - \frac{N_{spec}}{\sum_{i=1}^{N_{spec}} S_{m_s}(NM(GEO, BC, EFL), m_s)_i} \cdot \frac{d}{dm_s} S_{m_s}(NM(GEO, BC, EFL), m_s)_i \right] = 0 \quad (2.13)$$

Since analytical solutions of the differentiation in Eqn. 2.13 are not available, numerical integration using the central difference method is used with a root finding algorithm to estimate the surface flow parameter m_s . Corresponding surface flow parameter k_s is calculated by substituting the value of m_s from Eqn. 2.13 to Eqn. 2.11.

2.4 Estimation of surface flow parameters

Data from historical destructive testing of weathered in-service and new glass samples were collected to illustrate the use and repeatably of the proposed MLE method for estimating surface flow parameters. Data for 23 monolithic AN sample sets (14 weathered in-service, 9 new) with various rectangular dimensions and thicknesses were identified in the published literature with the addition of one previously unpublished weathered in-service sample set. The quality and type of data published for each of the historical samples set varied, requiring estimation or assumed values for the missing or incomplete data required to calculate

the equivalent failure loads needed for estimating surface flaw parameter. Several strategies were developed and employed to ensure each historical sample set is analyzed in a uniform manner when required sample set information was unknown.

2.4.1 Historical destructive testing

The test frame and procedure used for each historical sample set were consistent with ASTM E997 [15]. Using an appropriately sized test frame the specimens were dry glazed with neoprene gaskets that allowed for in-plane slippage and rotation. The neoprene gaskets were typically inset approximately 3 mm (1/8 in.) from the edge of the specimen to ensure large center of glass displacements do not result in edge pullout. Once a specimen is glazed into the test frame, a pressure differential is created by evacuating air from the test frame producing a monotonically increasing uniform pressure until the specimen fractures. The load-time history up to fracture and fracture origin location was recorded for each specimen. The thickness of each specimen was measured and recorded prior to glazing in the test frame.

2.4.2 Information required to calculate equivalent failure loads

Glass specimens in a sample fracture at varying combinations of load magnitude, fracture origin and time resulting in unique LTH for each. Thus, the temporal part is normalized by calculating the equivalent failure stress and load using Eqn. 2.5. The LTH is converted to a stress-time history (STH) with a numerical model that requires the rectangular dimension, the thickness, and the boundary condition of the glass lite. Glass does not fail at the location of the single largest maximum principal tensile stress (SLMPTS) but at different locations due to the presence of microscopic flaws. Natividad et al. [46] compared the maximum principal tensile stresses at the fracture origins (FOMPTS) and reported the FOMPTS were lower compared to SLMPTS. Thus, the location of fracture origin are necessary to account for the effect of flaws on the load resistance of glass.

2.4.3 Strategies for Missing or incomplete data

Data collected from literature mostly failed to report individual thickness of the specimen, the location of the boundary condition, and individual load-time history for specimen. Hence, strategies employed in the event of missing information are described herein.

Thickness - The stresses calculated for a glass lite are dependent on the thickness of the

lite. Thus individual thickness for each specimen were measured before destructive testing and are used herein for calculation of EFS and EFL, whereas if individual thicknesses are not listed, the mean thickness of the sample is used. Samples where neither individual thicknesses of specimens or the mean thickness of the sample was listed, a thickness was estimated from the reported observed p_b calculated using estimated surface flaw parameters. The thickness of the glass estimated was always greater than or equal to the minimum thickness, mentioned in ASTM 1300-16 [11].

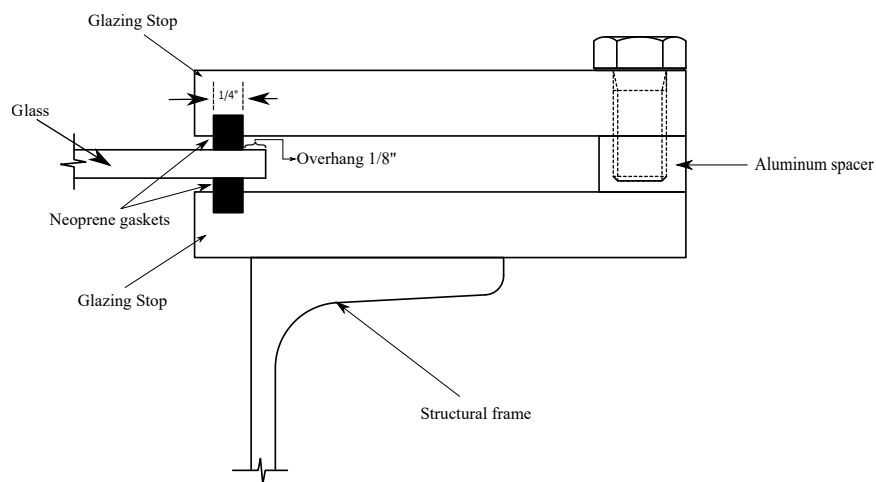


Figure 2.1: Dry Glaze (boundary condition)

Boundary condition - The dry glazing in the pressure chamber is done to laterally support the specimen with neoprene gaskets as shown in Fig 2.1. The neoprene gasket used was generally $6.35\text{mm} \times 6.35\text{mm}$ ($1/4\text{ in.} \times 1/4\text{ in.}$) cross section and kept in place by machining grooves in the glazing stop, all around the specimen. The glass specimen is centered within the glazing system and usually has a overhang of 3.18 mm ($1/8\text{ in.}$) to prevent edge pullout due to large displacement. Thus, the effective area of the plate in stress due to

the differential pressure is the area between the neoprene gasket rather than the full surface area of the glass specimen. Most published data have not reported the boundary condition and thus to be consistent, the full surface area for each sample is used. A bigger area leads to a conservative value for the strength of glass.

Load time history- For samples where failure LTH were provided in published literature, the failure LTHs were used for the EFS and EFL calculations. For samples where LTH was not provided, an idealized triangular distribution was approximated using the reported failure load and failure time as shown in Figure 2.2. The EFS calculation is achieved via Equation 2.5, using a numerical integration of the time related stress raised to the power of 16. As the time related stress raised to the power of 16 is added up, it is observed that only the upper portion of the LTH, marked in red in Figure 2.2, accounts for the EFS calculation, whereas the lower portion does not change the sum. Thus, when assuming a triangular distribution does not overlay well in the beginning of the test, but it overlays in the upper portion of the LTH that accounts for the EFS calculation.

With the strategies for missing information explained, the details for each sample set including the information present are as follows.

Sample sets W01 and W02 originated from Lubbock, TX, and were removed after damage during an extreme storm event in the late 1970s after approximately 20 years in service. Both samples consisted of 20 MO lites with nominal dimensions of W01 as 724 mm × 724 mm × 6 mm (28¹/₂ in. × 28¹/₂ in. × 1/4 in.) and W02 as 1540 mm × 724 mm × 6 mm

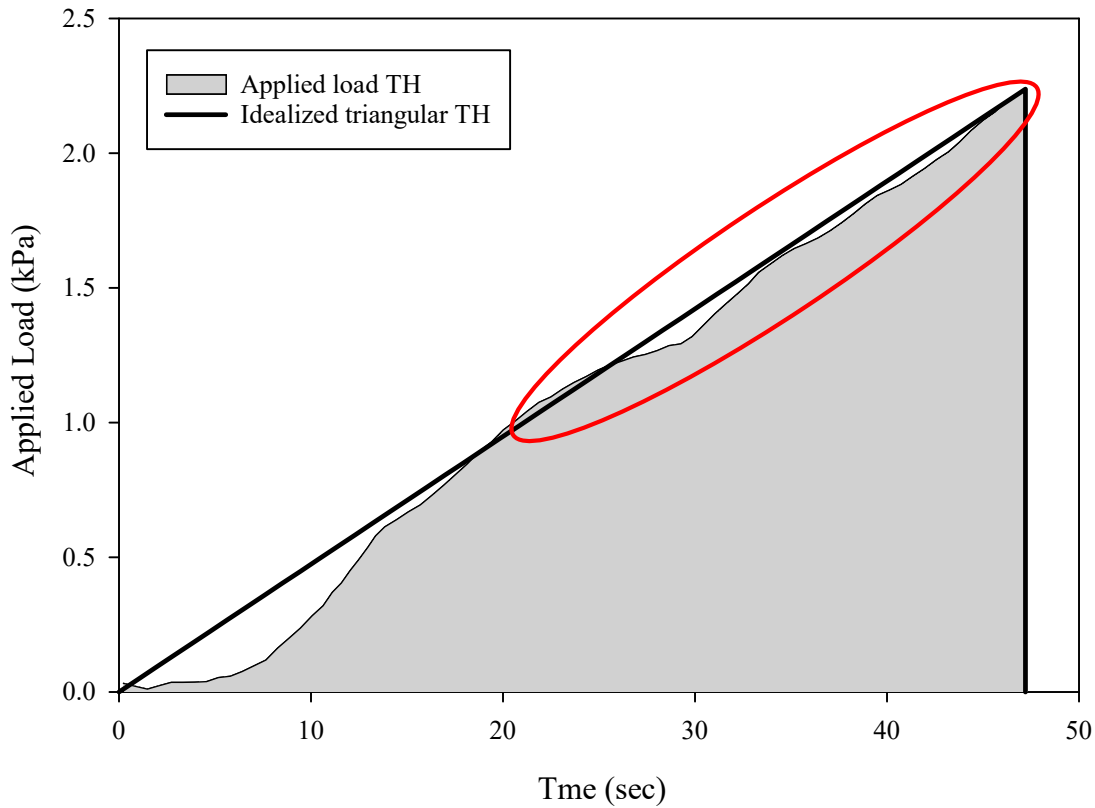


Figure 2.2: Applied load TH and Idealized triangular TH

($60\frac{1}{2}$ in. \times $28\frac{1}{2}$ in. \times $\frac{1}{4}$ in.). Sample W01 was cut from Sample W02 to size in the lab before testing. Loading TH's were not reported but failure time, failure load, and location of failure were recorded and reported by Beason [18]. The mean thickness of the sample was reported by Norville and Minor [52] but individual thicknesses were not reported.

Sample set W03 originated from Dallas, TX, and was removed in the year 1981 after approximately 20 years in-service. The set consisted of 22 rectangular MO lites with nominal dimensions of 502 mm \times 413 mm \times 3 mm ($19\frac{3}{4}$ in. \times $16\frac{1}{4}$ in. \times $\frac{1}{8}$ in.). Loading TH's were not reported but failure time, failure load, and location to failure were recorded and

reported in Abiassi [2]. The mean thickness of the sample was reported by Norville and Minor [52] but individual thicknesses were not reported.

Sample set W04 originated from Anton, TX, and was removed in the year 1980 after approximately 25 years in-service. The set W04 consisted of 111 rectangular monolithic lites with nominal dimensions of 921 mm × 356 mm × 3 mm (36¹/₄ in. × 14 × in. 1/₈ in.). Specimen from sample W04 was loaded at three different loading rates to evaluate if the value of static fatigue constant ($n = 16$) can be used for weathered in-service AN glass. Loading TH's were not reported but failure time, failure load, and location of failure were recorded and reported in Abiassi [2]. The mean thickness of the sample was reported by Norville and Minor [52] but individual thicknesses were not reported.

Sample sets W05, W06-I, W07-I, and W08 originated from Oklahoma City, OK, and were removed in the mid-1980s after approximately 8 years of in-service. The four samples consisted of glass lites that were separated from insulating glass (IG) units with a nominal size of 1750 mm × 502 mm × 6 mm (68 in. × 19³/₄ in. × 1/₄ in.). Sample W05 consisted of the outer glass lites, with the surface facing the environment placed in tension during testing, while W06 consisted of the same glass lite but the coated surface facing the airspace in tension during testing. Sample W07 consisted of the inner glass lite with the uncoated surface facing the airspace in tension during testing, while S08 consisted of the same glass lite but the indoor surface placed in tension. As the surfaces facing the airspace were not exposed to environmental conditions and had minimal to no handling, the surfaces facing

Table 2.1
Summary of weathered in-service glass sample set

Sample Set	Number of specimen	Published Rectangular dimension Long x short x thickness mm x mm x mm (in. x in. x in.)	Measured thickness mm (in.)	Thickness Used mm (in.)	Load TH available
W01 ^a	20	724 x 724 x 6 (28 ¹ / ₂ x 28 ¹ / ₂ x 1/4)	5.56 ^f (0.219)	5.56 (0.219)	No
W02 ^a	20	1540 x 724 x 6 (60 ¹ / ₂ x 28 ¹ / ₂ x 1/4)	5.56 ^f (0.219)	5.56 (0.219)	No
W03 ^b	22	502 x 413 x 3 (19 ³ / ₄ x 16 ¹ / ₄ x 1/8)	3.05 ^f (0.120)	3.05 (0.120)	No
W04 ^b	111	921 x 356 x 3 (36 ¹ / ₄ x 14 x 1/8)	3.15 ^f (0.124)	3.15 (0.124)	No
W05 ^c	82	1730 x 502 x 6 (68 x 19 ³ / ₄ x 1/4)	5.84 ^f (0.230)	5.84 (0.230)	No
W06-I ^c	53	1730 x 502 x 6 (68 x 19 ³ / ₄ x 1/4)	5.54 ^f (0.218)	5.84* (0.230)	No
W07-I ^c	40	1730 x 502 x 6 (68 x 19 ³ / ₄ x 1/4)	5.82 ^f (0.229)	5.82 (0.229)	No
W08 ^c	66	1730 x 502 x 6 (68 x 19 ³ / ₄ x 1/4)	5.82 ^f (0.229)	5.82 (0.229)	No
W09 ^d	23	1490 x 654 x 6 (58 ³ / ₄ x 25 ³ / ₄ x 1/4)	-	5.97 [#] (0.235)	No
W10 ^d	12	1070 x 749 x 6 (42 x 29 ¹ / ₂ x 1 ¹ / ₄)	-	5.87 [#] (0.231)	No
W11 ^d	11	940 x 749 x 6 (37 x 29 ¹ / ₂ x 1/4)	-	5.87 [#] (0.231)	No
W12 ^d	28	864 x 610 x 3 (34 x 24 x 1/8)	-	3.07 [#] (0.121)	No
W13 ^d	21	737 x 699 x 3 (29 x 27 ¹ / ₂ x 1/8)	-	3.10 [#] (0.122)	No
W14 ^e	18	2360 x 838 x 6 (93 x 33 x 1/4)	-	5.66 (0.223)	Yes

^a reported in Beason [18]; ^b reported in Abiassi [2]; ^c reported in Hsu [34]

^d reported in Sligar [58]; ^e unpublished; ^f reported in Norville and Minor [52]

[#]Thickness identified from reported surface flaw parameter using a trail and error method

* A different thickness from measured/reported thickness is used for calculations

the air spaces can be considered as new glass and hence an additional identification 'I' was added to differentiate between weathered in-service glass and the surfaces facing the airspace. Loading TH's were not reported but failure time, failure load, and location to

failure were recorded and reported in Hsu [34]. The mean thickness of the sample was reported by Norville and Minor [52] but individual thicknesses were not reported. Norville and Minor [52] reported the mean thickness of sample W06-I as 5.54 mm (0.218 in.), but since sample W05 and W06-I were essentially the same lite, the difference in thickness is considered as publishing error. Sample W07-I and W08 were the same lite hence the same thickness was seen. Thus, for sample W06-I, 5.84 mm (0.230 in.) thickness was used for calculations.

Samples W09, W10, and W11 originated from Lackland Air Force Base, and W12 and W13 originated from Kelly Air Force Base. Both sample sets were removed in the year 1988 after approximately 20 years of in-service. Sample W09, W10, and W11 were rectangular monolithic lites with varying nominal dimensions. Samples W12 and W13 consisted of the separated lites of double insulating glass units with different nominal rectangular dimensions. Loading TH's were not reported but failure time, failure load, and location to failure were recorded and reported in Sligar [58]. Individual and mean thicknesses for the five samples were not reported in Sligar [58] but the observed p_b calculated for EFL_{60} calculated using surface flaw parameters for each sample were reported. A mean thickness for each sample was back calculated using a root finding algorithm using the the observed p_b and the reported surface flaw parameters.

Sample W14 originated from San Antonio, Texas and were removed after approximately 20 years of in-service as floor to ceiling glazing systems. The samples were separated from

a IG unit consisting of a 6mm (1/4 in.) MO AN glass lite facing the exterior and a 6 mm (1/4 in.) MO fully tempered (FT) glass lite facing the interior of the building. The nominal dimensions of W14 was 2360 mm × 838 mm × 6 mm (93 in. × 33 in. × 1/4 in.). Sample W14 tests were conducted at the Wiss, Janney, Elstner Associates, Inc. Deerpark (WJE), IL, test lab and failure data was not reported previously. The loading TH for each sample was recorded and available for the sample. The number of specimens in each sample, nominal dimensions, measured mean thickness, loading rate for each sample, and years in service for weathered in-service samples are summarized in Table 2.1.

Sample sets N01 consisted of 23 new lites with nominal dimensions of 502 mm × 413 mm × 3 mm (19³/₄ in. × 16¹/₄ in. × 1/8 in.). Loading TH's were not reported but failure time, failure load, and location of failure were recorded and reported by Abiassi [2]. Individual thicknesses were not reported but the mean thickness of the sample was reported by Norville and Minor [52].

Sample set N02 consisted of 53 new lites with nominal dimensions of 1930 mm × 965 mm × 6 mm (76 in. × 38 in. × 1/4 in.). Specimen from sample N02 was loaded at three different loading rates to evaluate if the value of static fatigue constant ($n = 16$) can be used for new AN glass. Loading TH's were not reported but failure time, failure load, mean thickness of the sample, and location of failure were recorded and reported by Kanabolo and Norville [38].

Sample sets N03, N04, N05, N06, N07, and N08 consisted of 19, 16, 19, 18 12, and 15

Table 2.2
Summary of new glass sample set

Sample Set	Number of specimen	Published Rectangular dimension Long x short x thickness mm x mm x mm (in. x in. x in.)	Measured/Used thickness mm (in.)	Load TH available
N01 ^a	23	502 x 413 x 3 (19-3/4 x 16-1/4 x 1/8)	2.97 ^d (0.117)	No
N02 ^b	53	1930 x 965 x 6 (76 x 38 x 1/4)	5.61 ^b (0.221)	No
N03 ^b	19	1676 x 838 x 6 (66 x 33 x 1/4)	5.93 ^b (0.233)	No
N04 ^b	16	2362 x 1181 x 6 (93 x 46-1/2 x 1/4)	6.13 ^b (0.242)	No
N05 ^b	19	1372 x 1372 x 6 (54 x 54 x 1/4)	5.62 ^b (0.221)	No
N06 ^b	18	1181 x 1181 x 6 (46-1/2 x 46-1/2 x 1/4)	6.00 ^b (0.236)	No
N07 ^b	12	1676 x 1676 x 6 (66 x 66 x 1/4)	5.66 ^b (0.223)	No
N08 ^b	15	2438 x 1524 x 6 (96 x 60 x 1/4)	5.64 ^b (0.222)	No
N09 ^c	197	2438 x 1524 x 6 (96 x 60 x 1/4)	5.81 ^c (0.229)	No

^a reported in Abiassi [2]; ^b reported in Kanabolo and Norville [38]

^c reported in Johar [36], Johar [37], ^d reported in Norville and Minor [52]

specimens respectively. The nominal dimensions of the sample are 1680 mm × 838 mm × 6 mm (66 in. × 33 in. × 1/4 in.) for N03, 2360 mm × 1180 mm × 6 mm (93 in. × 46 1/2 in. × 1/4 in.) for N04, 1370 mm × 1370 mm × 6 mm (54 in. × 54 in. × 1/4 in.) for N05, 1180 mm × 1180 mm × 6 mm (46 1/2 in. × 46 1/2 in. × 1/4 in.) for N06, 1680 mm × 1680 mm × 6 mm (66 in. × 66 in. × 1/4 in.) for N07, and 2440 mm × 1520 mm × 6 mm (96 in. × 60 in. × 1/4 in.) for N08. Loading TH's were not reported but failure time, failure load, mean thickness for each sample and location of failure were recorded and reported by Kanabolo and Norville [38].

Sample set N09 consisted of 197 specimens of nominal dimensions 2440 mm × 1520 mm × 6 mm (96 in. × 60 in. × 1/4 in.). The sample-set was loaded at 8 different loading rates to relate the LR of windows to short, sharp, and peak gusts. Loading TH's were not reported but failure time, failure load, measured individual thickness and location of failure were recorded and reported by Johar [36] [37]. Surface flaw parameters were not calculated for the sample set N09 by Johar [36] [37]. The number of specimens in each sample, nominal dimensions, measured thickness, and loading rate for each new sample are summarized in Table 2.2.

2.4.4 60-sec equivalent failure loads

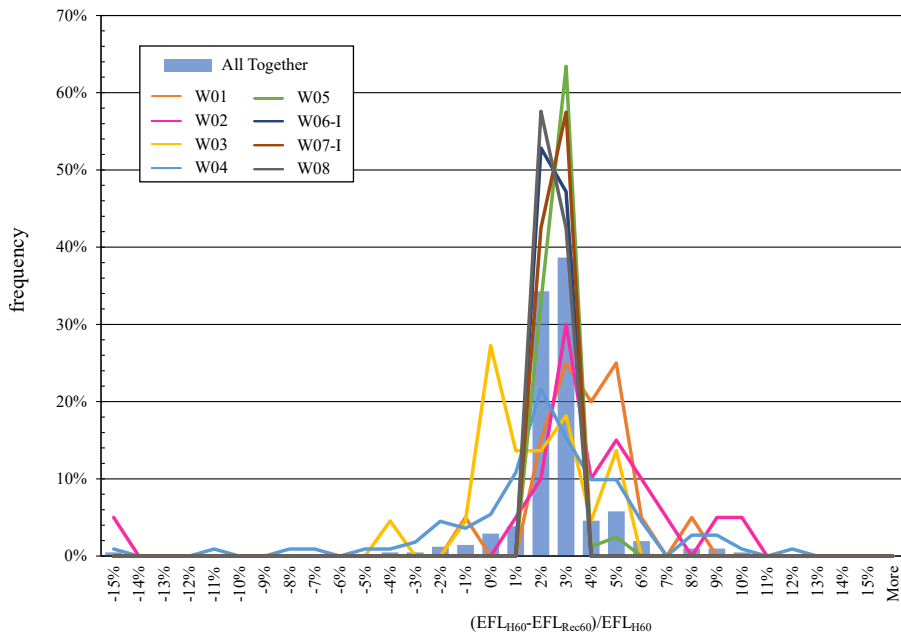


Figure 2.3: Comparison of historical and recreated 60-sec EFL's for weathered in-service samples

Glass specimens of the same size loaded monotonically, fail at different time duration and load magnitudes necessitating a normalization of the LTH to a reference time before flaw parameter are estimated. Historically, 60-sec was used as the reference time used to normalize the failure data because experiments preceded 1995, and the design standard ASCE7-95 [7] provisions were based on a fastest-mile wind speed, that corresponds to a 60-sec load duration. For the weathered in-service samples, EFL values calculated for a reference time of 60-sec were published for 8 weathered (W01 through W08) and 8 new samples (N01 through N08), referred to as EFL_{H60} . Hence for a reference time of 60-sec, EFL values were recreated, referred to as EFL_{Rec60} , to check if approximation of an idealized triangular load-time distribution, or the location of boundary condition, or using mean thickness instead of individual thickness has an effect on the calculation of EFL and if an anomaly exists on the recorded data. Percent differences between EFL_{H60} and EFL_{Rec60} for both weathered in-service and new samples were calculated and histogram of the percent differences were plotted in Figure 2.3 and Figure 2.4, respectively. The histogram in Figure 2.3 and Figure 2.4 represents the frequency distribution of percent differences between EFL_{H60} and EFL_{Rec60} for the total number of specimens, while the lines represents the frequency distribution of individual sample. For the weathered in-service samples, 94% of the specimen (389 specimen) percent difference lay between -5% to 5%, of which 83% (343 specimens) percent difference lay between -3% to 3%. Similarly, for the new sample, 84% of the specimen (147 specimen) percent difference lay between -5% to 5%. For samples N01, N06 and N08, a larger spread of the percent differences between EFL_{H60}

and EFL_{Rec60} was observed. Sample N01 spread of percent difference was attributed to a coarse mesh for converting LTH to STH for EFL calculation, and for sample N06 and N08 the small number of specimens in the sample was attributed for the large spread. The author believes, a large number of specimen for the new sample set will show a similar spread to that of the weathered in-service samples. Since majority of the EFL_{Rec60} lay between -5% to 5% of the EFL_{H60} , it was concluded that the strategies assumed for missing information such as idealized triangular distribution of failure load vs time, mean thickness, different mesh sizes and different boundary conditions although has some effect on EFL calculation, but the effect was deemed negligible.

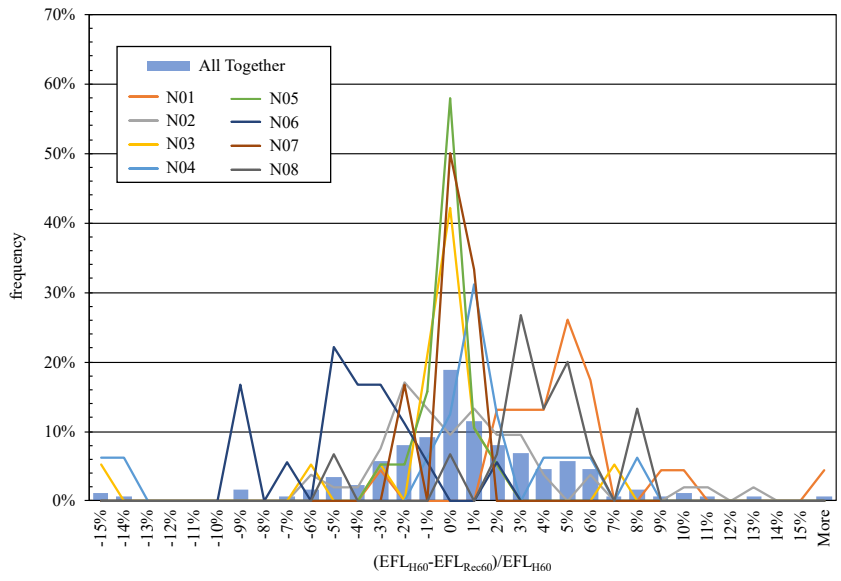


Figure 2.4: Comparison of historical and recreated 60-sec EFL's for new samples

Two specimen out of the 414 weathered in-service specimens, specimen 4 of sample W02

and specimen 91 of sample W04, had a percent difference of -15% or more. Three specimens out of the 175 new specimens, specimen 21 of sample N01, specimen 11 of sample N03, and 1 of sample N04, had a percent difference of 15% or more. Since the same method and same assumptions were used while calculating EFL, the author believes, a difference of more than 15% or less than -15% was observed for the 5 specimens because of reporting error. For example, specimen 4 of sample W02, the reported failure load and time to failure was 9.43 kPa (197 psf) and 42 sec, respectively. However, for the load rate, the load applied for 42 sec would result a constant pressure of about 4.64 kPa (97 psf). Thus, the reported load of 9.43 kPa(197 psf) was considered to be a error during publishing or recording the data. Thus, the 5 specimens were not used for estimation of surface flaw parameters.

2.4.5 Estimation of 60-sec surface flaw parameters

The EFL_{Rec60} 's were used to estimate 60-sec surface flaw parameters using the MLE method for both weathered in-service and new samples, by solving Eqn. 2.11 and Eqn. 2.11 and compared to the reported 60-sec surface flaw parameters. A graphical comparison of the historical and MLE estimated 60-sec surface flaw parameters is presented in Figure 2.5 and Figure 2.6 for weathered in-service and new sample, respectively since a numerical comparison is not meaningful. The plot presents CDFs created using historical and MLE estimated surface flaw parameters, denoted as CDF_{Hist} and CDF_{Rec} , respectively.

The CDFs were created using Eqn. 2.2, Eqn. 2.3, and the non-linear four-node quadrilateral finite-element model developed by Yew et al. [67] as the numerical model. The x-axis on the graph represents the 60-sec uniform load, P_{60} (log scale) and the y-axis represents the probability of breakage, p_b ($\ln(\ln(1/(1-(p_b \text{ or } E_i))))$ scale). The solid line in both the graph represents the CDF_{Rec} while the dash line represents the CDF_{Hist} .

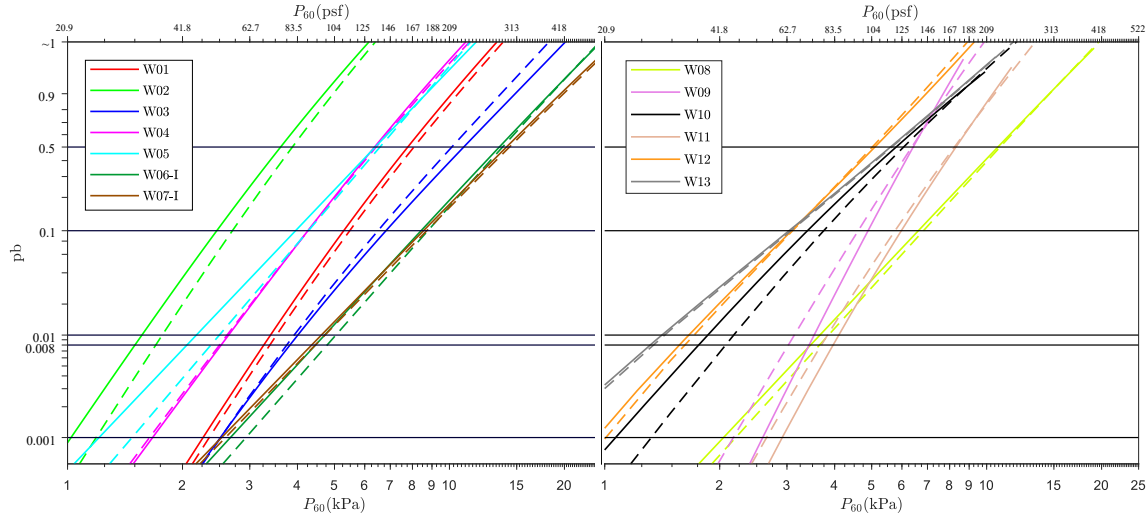


Figure 2.5: 60-sec MLE estimated vs historical surface flow parameters for weathered in-service samples

A difference in the historically reported and MLE estimated 60-sec surface flow parameters was expected because of the difference in EFL_{H60} and EFL_{Rec60} , evident in both Figure 2.5 and Figure 2.6. The difference is attributed to the method historically used to estimate surface flow parameters. Historically, the value m_s was limited to a whole number or to the first decimal place, whereas the MLE method does not have those limitations thus estimating the value of m_s to multiple decimal places. Furthermore, the CDF_{Hist} is recreated using the surface flow parameters listed in the literature and using the non-linear four-node

quadrilateral finite-element model developed by Yew et al. [67] as the numerical model. Although the non-linear four-node quadrilateral finite-element model developed by Yew et al. [67] showed reasonable agreement to the FDM method developed by Wang [63] that was used by researchers as the numerical model, small variations are expected while recreating the CDF due to boundary conditions and mesh sizes.

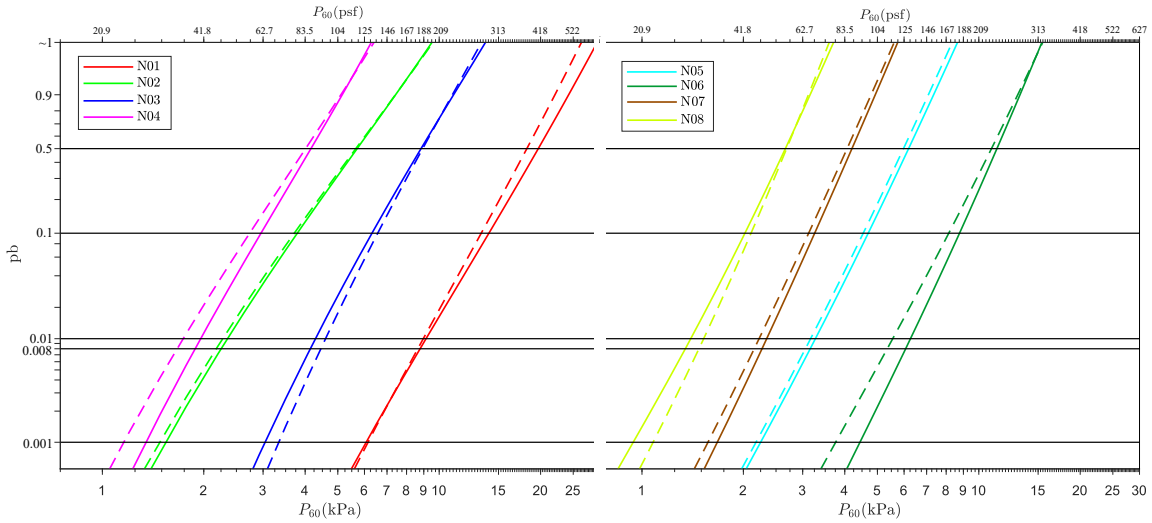


Figure 2.6: 60-sec MLE estimated vs historical surface flow parameters for new samples

In both the figures (Figure 2.5 and Figure 2.6), it was observed that the position of the CDF_{Rec} was consistent with the position of CDF_{Hist} but for some samples a difference in slope were observed. In Figure 2.5, the slope for W01, W03, W04, W06, W07, W08, W11, W12, and W13 CDF_{Rec} has a reasonable agreement to CDF_{Hist} , while W02, W05, W09, and W10 were seen to have different slopes to CDF_{Hist} . For W02, a specimen was not used to estimate the surface flow parameters and the removal of the specimen was assumed to have an effect on the CDF. Although a specimen from W04 was not used for

parameter estimation, W04 CDF_{Rec} had a similar slope to W04 CDF_{Hist} . This was observed because W04 had a large number of specimens compared to W02. For W09, and W10, EFL_{H60} were not listed by Sligar [58] and hence, whether the difference of slope in CDF was due to difference in EFL_{H60} or other reason can not be ascertained. For W05, the EFL_{H60} and EFL_{Rec60} were similar and yet the MLE method estimated a different slope, whereas for W06-I, W07-I and W08, samples from the same test setup, the CDF_{Rec} and the CDF_{Hist} slopes were similar. As the MLE method estimate surface flaw parameters in an objective, consistent and repeatable manner, the author believes that the historical surface flaw parameter estimated might have been influenced by the researchers interpretation of the failure data.

Load corresponding to different pb_s are compared to check if the surface flaw parameter historically reported and estimated using MLE method had a reasonable agreement. ASTM E1300-94 [13]) defined LR as a uniform lateral load corresponding to a p_b equal to 0.008 for a 60-sec load duration. Additionally, American Architectural Manufacturers Association [1] recommends a LR corresponding to a p_b equal to 0.001 for overhead sloped glazing. Hence, load corresponding to 0.001 and 0.008 p_b are compared. The maximum difference in LR at 0.001 p_b when compared between historically reported and MLE estimated surface flaw parameter for weathered in-service and new sample was calculated as be 0.42 kPa (8.79 psf) and 0.69 kPa (14.3 psf), respectively. A similar comparison at 0.008 p_b resulted in a maximum difference of 0.41 kPa (8.42 psf) and 0.73 kPa (15.1 psf) for weathered in-service and new sample, respectively.

Differences in reported surface flow parameter and surface flow parameter estimated using MLE were expected because of factors such as different numerical models used for stress calculation, different mesh size (historical mesh usually coarse), different boundary conditions among others. Due to the difference in historically reported and MLE estimated surface flow parameters, load corresponding to 0.001 and 0.008 p_b were expected, but the differences were not extreme. The MLE method removes the uncertainty associated with the judgement of the researcher and provides a consistent and reliable method to estimate the surface flow parameters and showed reasonable agreement to historically reported 60-sec surface flow parameters.

2.4.6 3-sec EFL and surface flow parameters

Because, the MLE estimated 60-sec surface flow parameters had a reasonable agreement to the historical surface flow parameter, MLE method was used to estimate 3-sec surface flow parameters. A 3-sec surface flow parameters are estimated because current design standards, ASCE7-16 [5]) defines basic wind speed as a 3-sec gust speed. The loading TH's were used to calculate EFL_{3s} using the non-linear four-node quadrilateral finite-element model by Yew et al. [67] for both weathered in-service and new samples using Equation 2.5 with t_{ref} as 3-sec. The EFL_{3s} were used to estimate surface flow parameters, by solving Eqn.2.11 and Eqn.2.11 and listed in Table 2.3.

Table 2.3
weathered in-service and new glass 3-sec surface flaw parameters

In-service			New		
Sample set	m_s	k_s $mm^{(2 \cdot m_s - 2)} \cdot N^{-m_s}$ $(in.^{(2 \cdot m_s - 2)} \cdot lbf^{-m_s})$	Sample set	m_s	k_s $m^{(2 \cdot m_s - 2)} \cdot N^{-m_s}$ $(in.^{(2 \cdot m_s - 2)} \cdot lbf^{-m_s})$
W01	5.74	7.06E-15 (1.75E-24)	N01	7.84	2.78E-20 (2.03E-34)
W02	5.42	1.87E-14 (2.34E-23)	N02	6.78	3.08E-18 (4.39E-30)
W03	5.61	3.25E-15 (1.60E-24)	N03	8.48	1.43E-21 (4.42E-37)
W04	5.12	2.51E-14 (1.41E-22)	N04	8.34	1.80E-20 (1.10E-35)
W05	3.92	4.49E-12 (9.52E-18)	N05	9.14	5.51E-22 (6.22E-39)
W06-I	4.07	1.36E-13 (1.40E-19)	N06	9.92	3.49E-24 (7.97E-43)
W07-I	3.86	2.66E-13 (7.77E-19)	N07	9.58	1.27E-22 (1.60E-40)
W08	3.97	5.00E-13 (8.65E-19)	N08	8.87	9.81E-21 (4.18E-37)
W09	7.66	9.43E-19 (1.67E-32)	N09	5.82	1.19E-16 (2.00E-26)
W10	4.47	4.38E-13 (6.25E-20)			
W11	7.74	1.41E-18 (1.73E-32)			
W12	5.76	1.91E-15 (4.33E-25)			
W13	3.81	2.30E-12 (8.66E-18)			
W14	7.20	2.06E-18 (3.70E-31)			

A graphical representation of the EFL_{3s} and the corresponding CDF_3 based on the AR of the glass for both weathered in-service and new samples are presented in Figure 2.7 and Figure 2.8, respectively. The EFL_{3s} for each sample were ranked in ascending order ($i = 1$ to n_{sam}) and median rank probability estimators, E_i , were assigned to each EFL_{3s} according to Equation 2.14 ([28]; [27]).

$$E_i = \frac{i - 0.3}{n_{sam} + 0.4} \quad (2.14)$$

where, i = rank of the EFL of specimen, and n_{sam} is the number of specimen in the sample. The x-axis in both the figures plots the 3-sec uniform load, (P_{3s}) in a log scale, and the probability of breakage, p_b and median rank probability (E_i) on the y-axis in a $\ln(\ln(1/(1-p_b(orE_i))))$ scale. The marker in both the figure represents the EFL_{3s} for a sample, while the solid lines

represent the corresponding CDF_3 .

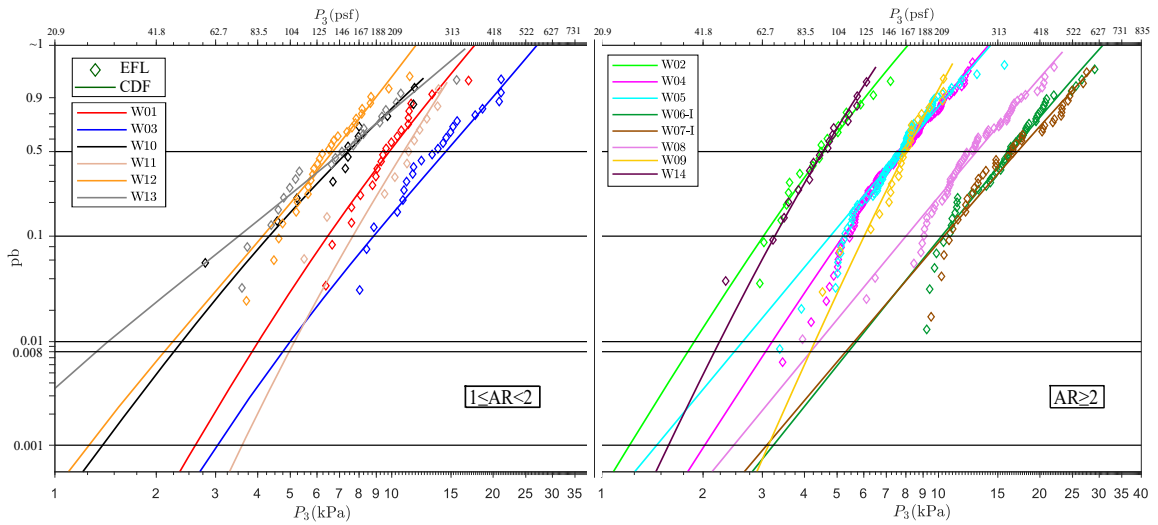


Figure 2.7: 3-sec EFL vs CDF for weathered in-service samples

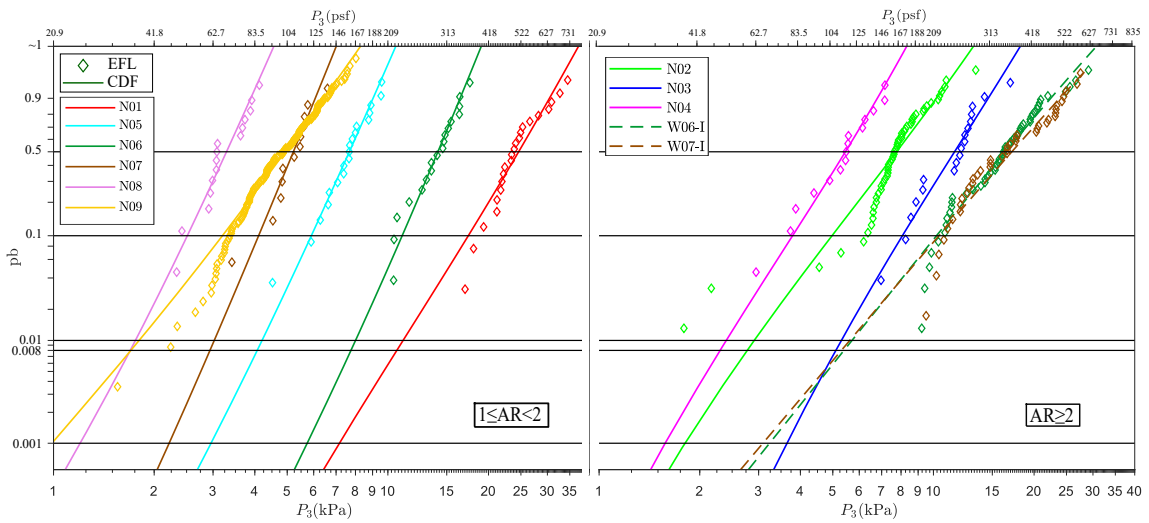


Figure 2.8: 3-sec EFL vs CDF for new samples

The weathered in-service samples were grouped into two groups with AR between 1 and 2, and samples with AR larger than 2 and presented in Figure 2.7. In both groups, a difference in position of the CDF_3 was observed because exposure to environmental conditions and handling were different for each sample. Samples with AR between 1 and 2 had different

surface area and AR and a clear trend was not observed for the samples. Samples W01, W03, and W12 had similar slopes. For W01 and W12, the surface areas of the samples were same whereas the AR was different, while sample W03 differed in surface area and AR compared to W01 and W12. Sample W03 had the smallest surface area amongst all the sample with AR between 1 and 2, and thus had the largest LR. Samples W12 and W13 were both 2.92 mm (1/8 in.) thick, and thus had the weakest LR. Among 5.56 mm (1/4 in.) thick glass, sample W10 had the largest area, and was the weakest.

Similarly for the group with AR larger than 2 a clear trend was not observed. Sample W05, W06-I, W07-I, W08 all had the same AR and area, and slopes of CDF_3 for each were similar. Sample W05 was the outer lite of the IG glass unit and thus was subjected to wind, abrasion and humidity, while sample W08 was the lite facing the interior of the building, and thus was subjected to handling but exposure to environmental conditions were limited. Thus, the LR of W05 was the weakest of the four samples followed by W08. Since samples W06-I and W07-I were the interior surface of the IG glass unit, there was no exposure to environmental conditions and handling, hence the LR for the two samples were similar and largest of the four samples. Amongst all the samples from the group with AR larger than 2, sample W04 had the smallest area, and thus had the largest L, albeit W06-I and W07-I. Sample W14 had the largest area and thus should had the weakest LR amongst the other samples, but the same was not observed. Sample W02 was the weakest amongst the samples in the group and since the was sample was storm damaged the author believes is the trend.

Similar to the weathered in-service samples, the new samples were grouped into two groups with respect to the AR i.e. samples with AR between 1 and 2 and AR greater than 2. For the group with AR between 1 and 2, samples N05, N06, N07, and N08 had similar slopes while sample N01 and N09 showed a different trend. Sample N01 had the lowest area and thus had the largest LR in the group. Although sample N08 and N09 were similar in size and AR, the slope of the corresponding CDF_3 were different. Sample N08 and N09 had different thickness (5.63mm to 5.81mm, respectively) and were tested at different locations (United states and Canada, respectively) and thus a dependency of the slope on thickness or different manufacture cannot be ascertained.

For the samples with AR between 2 and 3, sample N02, N03 and N04 had similar AR but different surface area. Samples N03 and N04 had similar slopes while sample N02 did not show a similar trend. Sample W06-I and W07-I are also included in this graph as both the samples had no exposure to environmental conditions and minimal handling, thus can be considered as new glass. Among the five samples, W06-I and W07-I had the smallest surface area, and thus their respective LR were strongest. Among sample N02, N03, and N04, sample N03 had the smallest surface area and thus had the strongest LR of the three, whereas sample N04 had the largest area and weakest LR amongst the five sample. Since the AR and the surface area of the samples varied, a practical comparison of the estimated surface flaw can be made by choosing a representative geometry and using the estimated surface flaw parameters from different samples to create LR for the chosen geometry.

2.5 Discussion

2.5.1 Comparison of ASTM E1300 surface flaw parameter and MLE estimated surface flaw parameter for weathered in-service sample

ASTM E1300-16 [11] uses m_s as 7 and k_s as $2.86 \times 10^{-17} N^{-7}mm^{12}$ ($1.365 \times 10^{-29} in^{12}lb f^{-7}$) for a 60-sec duration to design a glass component. Since current design standards are based on 3-sec basic wind speed, an equivalent 3-sec duration surface flaw parameters are presented for ease of comparison. The shape parameter m_s equal to 7 does not change while the the scale parameter k_s changes to $7.70 \times 10^{-18} N^{-7}m^{12}$ ($3.68 \times 10^{-30} in^{12}lb f^{-7}$). The surface flaw parameter values were agreed upon by the committee based on available historical experimental data of weathered in-service annealed glass and expert engineering judgment. However, the standard does not specifically reference the historical experimental data used for parameter estimation, resulting in a lack of transparency on how the surface flaw parameters were chosen. The work herein collected all available historical data for weathered in-service annealed glass samples tested to failure, it necessitates a comparison with ASTM E1300-16 [11]) LR charts. Since a numerical comparison of the MLE estimated surface flaw parameters of weathered in-service samples to the surface flaw parameter used in ASTM E1300-16 [11] is not meaningful, hence estimated surface

flaw parameters are compared by comparing LR charts for a representative geometry. Two representative geometries of different AR and surface area, listed in Table 2.4 are used to compare the estimated surface flaw parameters listed in Table 2.3 and surface flaw parameter used in ASTM E1300-16 [11].

Table 2.4
Representative geometries for comparison

Minimum Thickness mm (in.)	Long Dimension mm (in.)	Short Dimension mm (in.)	Area m^2 (sq. ft.)	AR
5.56 (0.219)	1520 (60)	1220 (48)	1.86(20.0)	1.25
5.56 (0.219)	1830 (72)	813 (32)	1.49 (16.0)	2.25

Figure 2.9 represent the LR for glass dimensions 1520 mm × 1220 mm (60 in. × 48 in.) and 1830 mm × 813 mm (72 in. × 32 in.) respectively. For both the dimension, the LR created using the surface flaw parameter from W05 was the weakest, while the LR creates using the surface flaw parameter from W14 was the strongest, for design pbs. LR created using W09 had reasonable agreement to the ASTM E1300-16 [11] LR chart for both the dimensions. Load corresponding to 0.001 and 0.008 pb for both the glass specimen designed were found to be greater for ASTM E1300-16 [11] surface flaw parameters except when designed using W14 surface flaw parameters. Sample W01 and W02 were documented as having exposure to an extreme wind event, however it is reasonable to assume the other samples were likely removed from the buildings due to unacceptable damage incurred from a storm event. Thus, the LR values are generally lower compared to ASTM E1300-16 [11] because these samples are damaged more than regular in-service glass windows addressed

in E1300. Surface flow parameters estimated from W06-I and W07-I were in service for almost 8 years but had limited handling and little to no environmental exposure as they were facing the air space in the IG unit. The LR charts using W06-I and W07-I were expected to be closer to if not stronger than the ASTM E1300-16 [11] LR chart, but at 0.001 and 0.008 pb, the corresponding loads are weaker. The trend is unexpected and the authors do not have enough evidence to explain the trend.

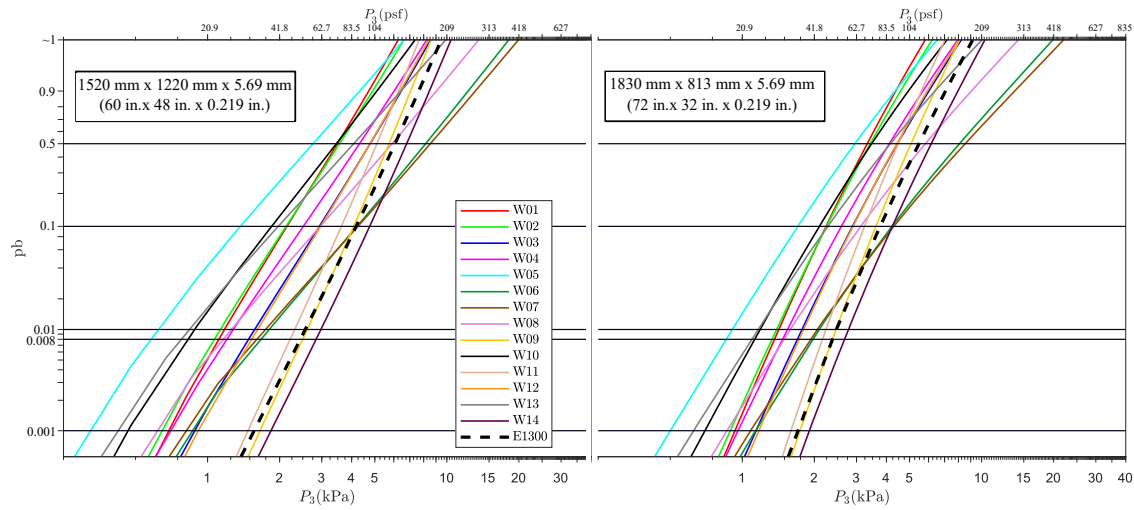


Figure 2.9: Load resistance chart using MLE estimated surface flow parameters from weathered samples

2.5.2 Comparison of surface flow parameters for new glass

The ASTM E1300-16 [11] doesn't list flow parameters to design new glass lites, but the 60-sec surface flow parameters determined by Abiassi [2] for new glass, m_s as 9 and k_s as $1.33 \times 10^{-21} N^{-9}m^{16}$ ($3.02 \times 10^{-38} in^{16}lb^{-9}$) is commonly used to design a new glass. As current design standards are based on 3-sec basic wind speed, the corresponding

3-sec surface flaw parameter for the new glass is calculated as m_s equals to 9 and k_s equals to $2.46 \times 10^{-22} N^{-9}m^{16}$ ($5.60 \times 10^{-39} in^{16}lb f^{-9}$). As a numerical comparison of the MLE estimated surface flaw parameters for new glass and parameter used to design a new glass is not meaningful, surface flaw parameters are compared by comparing LR charts for a representative geometry. Similar to the weathered in-service glass, two representative geometries of different AR and surface area, listed in Table 2.4 are used to compare the estimated surface flaw parameters for new glass listed in Table 2.3 to the surface flaw parameter used to design a new glass. Since surface flaw parameters estimated from W06-I and W07-I faced the airspace and were not exposed to environmental conditions with minimal to no handling, they were considered as new glass, surface flaw parameters estimated from W06-I and W07-I were compared with the new samples. Figure 2.10 represent the LR for glass dimensions 1520 mm \times 1220 mm (60 in. \times 48 in.) and 1830 mm \times 813 mm (72 in. \times 32 in.) respectively. For both the dimension, the LR created using the surface flaw parameter from W06-I and W07-I were the weakest, while the LR creates using the surface flaw parameter from N06 was the strongest. The LR charts created using surface flaw parameter from W06-I and W07-I were weakest because they have been in use for almost 8 years. The effect of time dependency on glass strength is observed with this two samples. Load corresponding to 0.001 and 0.008 probability of breakage for both the glass specimen designed were found to be overestimated by surface flaw parameters commonly used to design a new glass. Based on this data, the author recommends that surface flaw parameter estimated from either N01, N02, N04, or N07 should be used to design new

glass.

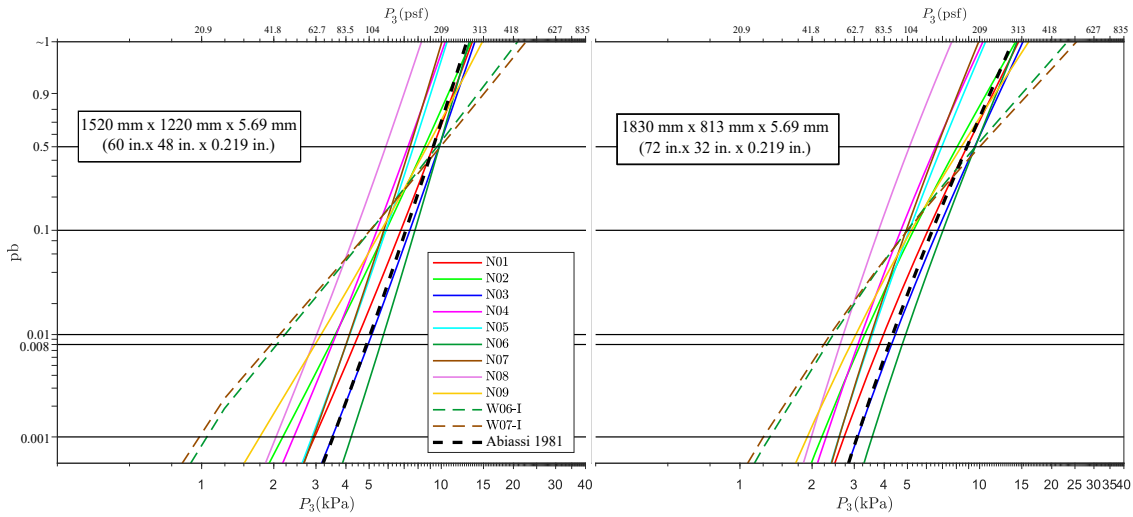


Figure 2.10: Load Resistance chart for different dimensions

2.6 Conclusion

A rigorous statistical method, the maximum likelihood estimator (MLE) method is presented in this work, to estimate surface flaw parameters tailored to the glass failure prediction model for annealed monolithic glass. The MLE method provides a repeatable and objective method while eliminating variability associated with the historical method which was based on the interpretation of the data according to the researcher. Historical published failure data for both weathered in-service and new glass annealed glass samples were collected and was used to illustrate the MLE method to estimate surface flaw parameters. The work presented herein is first of its kind that uses a single numerical model to estimate

the surface flaw parameter thereby removing all variability associated with different numerical model including boundary conditions and mesh size. The surface flaw estimated using MLE were used to create load resistance charts for two annealed glass lite of different aspect ratio and area and compared to the ASTM E1300-16 load resistance charts. The ASTM E1300-16 load resistance corresponding to 0.008 probability of breakage appear to over estimate the LR of weathered in-service glass sample sets. However, as some of the historical sample sets included specimens exposed to an extreme event prior to their removal, their LR's should be lower than regular in-service conditions. Additionally, since the inception of ASTM E1300 in 1989, there has not been a verified failure of a glass window due to a design wind event. Thus the authors believe the ASTM E1300-16 surface parameters are adequate for design. A similar comparison was made for surface flaw parameters estimated for new glass and it was found the surface flaw parameters used to design a new glass usually overestimated the LR.

Chapter 3

Estimation of surface flaw parameters for heat treated glass using maximum likelihood estimator

Currently a robust repeatable statistical method to estimate the surface flaw parameters for the modified glass failure prediction for heat treated glass is not in common use. The modified glass failure prediction for heat treated glass uses two surface flaw parameters to characterize the surface strength of window glass lites and the residual compressive surface stress acts as the location parameter. Since, the surface flaw parameters are a function of residual compressive surface stress, it is important to select a representative residual compressive surface stress of the sample. In the past, the minimum, mean, or the maximum

measured residual compressive surface stress was used to represent the sample. The work herein presents the robust repeatable statistical method, the maximum likelihood estimator, to estimate the surface flaw parameters. Rather than using the minimum, mean, or the maximum measured residual compressive surface stress as a representative value, a method is introduced to estimate the residual compressive surface stress that best represent the sample. Six heat-treated sample sets consisting of two new heat-strengthened glass and four fully tempered glass (two new and two weathered in-service) are used to show the working principle of the maximum likelihood estimator method. This study reports the 3-sec surface surface flaw parameter for the six sample estimated using the maximum likelihood estimator method and the residual compressive surface stress that best represents each sample. Load resistance charts for similar sized annealed and heat-treated samples are compared and presented in this study to understand the affect of RCSS on load resistance and weathering of heat-treated glass. The analytical procedure in the ASTM E1300-16 uses the surface flaw for annealed glass in the modified glass failure prediction model to design heat-treated glass. Hence, load resistance of weathered in-service fully tempered samples are compared to the ASTM E1300-16 load resistance charts and presented in this study. Results suggests, ASTM E1300-16 overestimated the strength for weathered in-service heat-treated samples. However, the weathered in-service samples were exposed to an extreme event prior to their removal, their load resistances were expected to be lower than regular in-service conditions.

3.1 Introduction

Heat-treated (HT) glass, comprising of heat-strengthened (HS) and fully-tempered (FT), is a popular facade and cladding material, especially for ceramic enamel frit or spandrel glass that experiences high thermal stress [4]. Heat treatment in glass is achieved by reheating annealed (AN) flat glass to temperatures near its melting point followed by rapidly cooling the surface to impart a residual compressive surface stress (RCSS). Because of the large RCSS, FT glass breaks into tiny fragments when glass breaks thus making it suitable for safety glass, therefore achieving popularity in the facade industry. The increased load resistance (LR) of the glass and the post breakage characteristics makes it a popular construction material and allows designers to design larger openings with HT glass with reduced thickness as compared to AN glass, resulting in reduced glass weight and easier installation process [44]. In the United States, ASTM E1300-16 [11] is used by designers and engineers to determine the LR of a HT glass. However, the analytical method and the LR charts provided in ASTM E1300-16 [11] to design a HT glass component, uses the surface flaw parameters for AN glass.

The analytical method provided in ASTM E1300-16 [11] uses the glass failure prediction model (GFPM) [17], a probabilistic method based on the well known three-parameter Weibull distribution for brittle material. The two surface flaw parameters m_s and k_s , takes into account the number, size and direction of microscopic flaws, are analogous to the scale

and shape parameter respectively, while the RCSS of the HT glass, is analogous to the location parameter in a three-parameter Weibull distribution, acts as the shift parameter. The surface flaw parameters are impractical to measure instead they are estimated from destructive testing of similar dimension glass, while the RCSS is selected by the researcher as a representative RCSS value from the measured RCSS data for the sample. After a value of RCSS is chosen, shape and scale parameters estimation based on the researchers interpretation of the normalized failure data. The method to select a RCSS value followed by estimating surface flaw parameters based on the researchers interpretation introduces undesirable variations especially when others attempt to recreate/reproduce flaw parameters. To remove the variations, a well known objective and a repeatable procedure, the maximum likelihood estimator (MLE) method tailored to the GFPM for AN glass was put forward by Goswami et al. [31], and the same method is extended herein for HT glass samples. Goswami et al. [32] put forward a method to estimate a representative RCSS of a HT sample with holes, rather than manually selecting a RCSS value and the same method will be extended for HT monolithic (MO) glass.

A HT glass is categorized into two types depending on the rate of cooling, i.e. the RCSS imparted in the glass, a HS ($24 \text{ MPa (3500 psi)} < \text{RCSS} < 52 \text{ MPa (7500 psi)}$) or a FT ($\text{RCSS} > 69 \text{ MPa (10000 psi)}$) glass [8]. To date, 6 HT monolithic (MO) glass samples, 2 HS and 4 FT samples, monotonically loaded to failure have been reported in published and unpublished literature. In this work, the 6 samples are used to show the working principle of the MLE to estimate surface flaw parameters and a representative RCSS of

a HT sample. A design example is put forward to compare the LR of a glass calculated using the analytical method provided in ASTM E1300-16 [11], the surface flaw parameters estimated historically, and the surface flaw parameters estimated using MLE.

3.2 Background

3.2.1 Glass failure prediction model for annealed glass

Glass, a brittle material, fails suddenly at a stress much lower than the yield stress, rather than demonstrating apparent deformation before fracture like steel. The maximum allowable stress method used to design a ductile material cannot be used with a high degree of confidence to design glass, as the yield stress for glass is never achieved. Hence, an inclusive method encompassing all factors that affects the LR of glass is required. This spurred extensive research in the early 1900s to understand the factors that affect the strength of glass and a method to encompass them effectively. Weibull [64] proposed the Weibull distribution to predict the strength of brittle materials, hence the distribution is appropriate to predict the strength of glass. Weibull expresses the cumulative probability distribution function (CDF) for a two-parameter Weibull distribution, P_{2P} , as

$$P_{2P} = 1 - e^{(-\lambda \cdot x^\beta)} \quad (3.1)$$

where, λ denotes a parameter related to the shape parameter, β denotes the scale parameter, and x denotes the random variable. The terms in the power of the exponent is known as the material function. Although, the Weibull distribution was showed to predict the strength of glass, it does not address all the factors that affect the strength of glass. Therefore, a different material function was desired.

Glass fails predominantly because of flaws inherently present on the glass surface, known as Griffith flaws, due to the manufacturing process and handling of glass [33]. Stress concentrates at the tip of these Griffith flaws leading to high magnitudes of stress when glass is subjected to a load leading to change in the flaw depth and/or radius that causes the glass to fail. Hence, the shape and the size of flaws present on the surface of the glass needs to be addressed while calculating the LR of glass [33]. A glass plate subjected to a biaxial stress produces unequal principal stresses, as a result a flaw oriented perpendicular to the direction of the resultant stress will experience larger stresses, compared to a flaw oriented in a different direction. Thus, the orientation of the flaw also needs to be addressed [17]. The shape and size of the flaw are taken into account by two surface flaw parameters m_s and k_s , while the orientation of the flaw is addressed by a biaxial stress correction factor, c . Beason and Morgan [17] further showed that as the area of glass increases the probability to find a flaw that may initiate fracture increases, and vice versa. Hence, the area effect needs to be addressed. Beason and Morgan [17] advanced a material function, the GFPM, B_s , for glass plates based on the work of Brown [21] that included all the factors that effects

the LR of glass, expressed as

$$P_b = 1 - \exp(-B_s) \quad (3.2)$$

$$B_s = k_s S_{m_s}(NM(GEO, BC, P), m_s) \quad (3.3)$$

where S_{m_s} denotes the equivalent area and the surface flaw parameters, k_s and m_s , are analogous to λ and β in Equation 3.1. The addition of all the new material factors in the material function creates a new distribution that no longer follows a classical two-parameter Weibull distribution. The equivalent area is calculated from the results of a numerical model (NM) and is a function of the plate geometry (GEO), boundary condition (BC), and the load applied (P). The numerical model is used to calculate the maximum and minimum principal stresses (σ_1 and σ_2 respectively) for each nodal area A. The biaxial correction factor (c) is calculated using the ratio of σ_1 and σ_2 for each nodal area. Thus, the expression for the equivalent area is given as,

$$S_{m_s}(NM(GEO, BC, P), m_s) = \sum_{j=1}^N [(c_j \cdot \sigma_{1,j})^{m_s} \cdot A_j] \quad (3.4)$$

where all variables remain same as defined before.

3.2.2 Glass failure prediction model for heat-treated glass

Weibull [65] proposed a CDF for a three-parameter Weibull distribution, P_{3P} expressed as,

$$P_{3P} = 1 - e^{(-\lambda \cdot (x-x_u)^\beta)} \quad (3.5)$$

where x_u denotes the location parameter and other variables remain same as defined previously. The location parameter, x_u , is a shift parameter where the value of function at or below x_u is zero, i.e. the probability of occurrence is zero [65]. Because HT glass is produced by reheating AN flat glass to near melting point temperatures followed by rapidly cooling the surface to impart a RCSS, the surface of a HT glass is in compression, i.e. the surface flaws are in compression. In order to initiate fracture, the surface flaws on glass must be in tension to allow for the flaw tip radius to sharpen and create a stress concentration sufficient to initiate fracture [44]. Thus, a load must be applied large enough to exceed the RCSS of the glass before the flaws are in tension. Hence, the RCSS of a HT specimen acts as a location parameter because the probability of breakage of a HT glass below the RCSS is zero. Norville et al. [50] and Morse and Norville [44] put forward a modified GFPM (MGFPM) by introducing the RCSS of HT specimen as the third parameter and mathematically presented the material function of the MGFPM as

$$B_s = k_s S_{m_s}(NM(GEO, BC, P), m_s, RCSS) \quad (3.6)$$

where RCSS is the residual compressive stress and is analogous to the location parameter in Equation 3.5, and all other variables are same as defined before. The equivalent area is expressed as

$$S_{m_s}(NM(GEO, BC, P), m_s, RCSS) = \sum_{j=1}^N [(c_j \cdot (\sigma_{1,j} - RCSS))^{m_s} \cdot A_j] \quad (3.7)$$

where all variables denote the same as defined before. For a particular nodal area, if the value of σ_1 is less than the RCSS, the flaws in the nodal area are not stressed, and hence the probability of breakage for the nodal area is zero [42]. The RCSS for AN glass is equal to zero and substituting the value of RCSS as zero in Equation 3.7 reverts to Equation 3.4

3.2.3 Surface flaw parameter estimation

The surface flaw parameter, m_s and k_s , takes into account the shape and size of the microscopic flaws present on the surface of the glass. Since, the flaws are microscopic in nature, it is impractical to measure them, instead they are estimated from normalized failure data obtained from carefully controlled destructive testing of glass [18], [2], [52]. Glass of similar dimension are loaded to appropriately sized test frame consistent with ASTM E997-15 [15] and dry glazed with neoprene gaskets that allows for in-plane slippage and rotation to reasonably replicate the boundary condition of an actual window glass. The test frame and the glass specimen together creates a chamber, known as the test chamber. To avoid edge

pull out due to large center of glass deflection, the neoprene gasket are typically inset approximately 3 mm (1/8 in.) from the edge of the specimen. After glazing a specimen to the test frame, a pressure difference is created between the test chamber and the atmosphere by evacuating the air from the test chamber using a series of valves. The careful evacuation of air allows the atmospheric pressure to push the specimen into the test chamber, thus ensuring a monotonically increasing uniform pressure until the specimen fractures. A pressure transducer is used to measure the vacuum pressure inside the test chamber. The vacuum pressure vs the time till fracture of the specimen generates the failure load-time history (LTH) and is recorded for each specimen.

Glass specimens of the same dimension, monotonically loaded at the same rate, fails at different load and time due to the brittle nature of glass. Hence, to compare the LR of glass, the temporal part of the LTH requires normalization. The methodology to normalize the temporal part of the LTH was put forward by Brown [21]. Brown [21] formulated an expression that relates the resistance of a flaw, k_f to the time dependent applied tensile stress, denoted as $\sigma(P(t))$, as

$$k_f = \int_0^{t_f} [\sigma(P(t))]^n dt \quad (3.8)$$

where t_f denotes the time to failure, and n denotes the static fatigue constant, equal to 16 [24], [25]. Bergers et al. [19] and Afolabi et al. [4] recognized for HT glass, a flaw does not offer any resistance until the time dependent tensile stress is greater than the RCSS of

the specimen. Thus, a modified expression to relate the resistance of a flaw, k_f for HT glass was put forward as

$$k_f = \int_0^{t_f} [\sigma(P(t)) - RCSS]^n dt \quad (3.9)$$

where all variables denote the same as defined before. The resistance of a flaw, k_f , is a constant; hence to fail the same flaw but for a different time duration, t_d , the magnitude of stress due to a particular load ($\sigma(EFL_{t_d})$) required is calculated by

$$\sigma(EFL_{t_d}) = \left[\frac{\int_0^{t_f} (\sigma(P(t)) - RCSS)^n dt}{t_d} \right]^{\frac{1}{n}} + RCSS \quad (3.10)$$

where all symbols denote the same as defined before. The magnitude of stress due to a particular load ($\sigma(EFL_{t_d})$), is termed as the equivalent failure stress (EFS) and the corresponding load is known as the equivalent failure load (EFL). The surface flaw parameters were estimated by comparing statistical parameters such as mean, standard deviation (stdev), and coefficient of variation (COV) of the sample EFLs to a theoretical fit using an iterative method described in detail by Beason [18]. For HT glass, a RCSS was selected by the researcher to best represent the sample, before theoretical fit were created using Equation 3.6 and Equation 3.7. However, this method induces inherent variability as the selection of RCSS and the surface flaw parameter that best describe the normalized failure data is based on the researchers interpretation rather than a statistical method. In the event when multiple surface flaw parameters produces almost identical statistical parameters, a clear set of rule to select the best set of surface flaw parameters does not appear in the published

literature.

3.3 Methodology to estimate surface flaw parameters using the maximum likelihood estimator method for heat treated glass

Maximum-likelihood estimation (MLE) is a common statistical tool used to estimate the parameters of an assumed distribution. The MLE method estimates parameters consistently, efficiently, and often used for different distributions as it is conceptually simple. The MLE method estimates a set of parameter by maximizing the likelihood function so the parameters estimated provides the highest value of the probability distribution function of the observed data. Pisano and Carfagni [53] used MLE to estimate the scale and shape parameter for failure data from a ring-on-ring test, while Goswami et al. [32] and Goswami et al. [31] extended the MLE method tailored to the GFPM to estimate surface flaw parameters for glass with holes and AN MO glass. The MLE method herein is extended to estimate the surface flaw parameters for the MGFPM.

The likelihood function for a distribution is defined as the product of the probability distribution function (PDF) for each random variable in the sample. For the three-parameter Weibull distribution, the PDF $f(x, \lambda, \beta, x_u)$ is obtained by differentiating the CDF, P_{3P} ,

denoted in Equation 3.5 with respect to the random variable x as

$$f(x, \lambda, \beta, x_u) = \frac{d}{dx}(P_{3P}) = \frac{d}{dx}(F(x, \lambda, \beta, x_u)) \quad (3.11)$$

where $(F(x, \lambda, \beta, x_u))$ is another notation for the CDF of the function. The likelihood function is mathematically expressed as

$$L(\lambda, \beta, x_u) = \prod_{i=1}^{n_{sam}} (f(x_i, \lambda, \beta, x_u)) \quad (3.12)$$

where n_{sam} denotes the number of independent random variables. The estimates are obtained by setting the partial derivatives of the natural log of the likelihood function with respect to the unknown variables λ , β and x_u to zero. Analytical solutions for the equations are not available, hence the solutions are solved using a root-finding algorithm. Murthy et al. [45] explained that the set of equations obtained from setting the partial derivatives of the natural log of the likelihood function with respect to λ , β and x_u to zero, may have more than one solution or none at all.

The MGFPM is based on three-parameter Weibull distribution but with a modified material function hence the MLE method can be used to estimate the surface flaw parameters. The CDF for the three-parameter MGFPM can be expressed by substituting Equation 3.7 and

Equation 3.6 to Equation 3.2 leading to

$$P_b = F(EFL, m_s, k_s, RCSS) = 1 - e^{-k_s \cdot S_{m_s}(NM(GEO, BC, EFL), m_s, RCSS)}$$

$$F(EFL, m_s, k_s, RCSS) = 1 - e^{-k_s \cdot (\sum_{j=1}^N [(c_j \cdot (\sigma_{1,j} - RCSS))^{m_s} \cdot A_j])}$$
(3.13)

where EFL denotes the equivalent failure load for a specimen in the sample and all other symbols denote the same as before.

3.3.1 Shape and scale parameter estimation

The shape and scale parameter is estimated by maximizing the likelihood function of the MGFPM expressed as

$$L(EFL, m_s, k_s, RCSS) = \prod_{i=1}^{N_{spec}} \left[k_s \cdot \frac{d}{d(EFL)} (S_{m_s}(NM(GEO, BC, EFL), m_s, RCSS)_i) \right. \\ \left. \cdot \exp(-k_s \cdot S_{m_s}(NM(GEO, BC, EFL), m_s, RCSS)_i) \right]$$
(3.14)

where all are same as previously defined. Since, it is computationally simpler to maximize a summation form compared to a product form, the product form of the likelihood function, Equation 3.14, is translated to a summation form by taking the natural logarithm expressed

in Eqn. 3.15 as

$$\begin{aligned} \ln(L(EFL, m_s, k_s, RCSS)) = & \sum_{i=1}^{N_{spec}} \left[\ln(k_s) - k_s \cdot S_{m_s}(NM(GEO, BC, EFL), m_s, RCSS)_i \right. \\ & \left. + \ln \left(\frac{d}{d(EFL)} (S_{m_s}(NM(GEO, BC, EFL), m_s, RCSS)_i) \right) \right] \end{aligned} \quad (3.15)$$

where all symbols are same as previously defined. The scale parameter, k_s , is estimated by maximizing the natural logarithm of the likelihood equation (Equation. 3.15) with respect to k_s leading to

$$k_s = \frac{N_{spec}}{\sum_{i=1}^{N_{spec}} S_{m_s}(NM(GEO, BC, EFL), m_s, RCSS)_i} \quad (3.16)$$

Similarly, the shape parameter, m_s , is estimated by maximizing the natural logarithm of the likelihood equation (Equation. 3.15) with respect to m_s and substituting Equation 3.16 leads to

$$\begin{aligned} \sum_{i=1}^{N_{spec}} \left[\frac{d}{dm_s} \ln \left(\frac{d}{d(EFL)} S_{m_s}(NM(GEO, BC, EFL), m_s, RCSS)_i \right) \right. \\ \left. - \frac{N_{spec}}{\sum_{i=1}^{N_{spec}} S_{m_s}(NM(GEO, BC, EFL), m_s, RCSS)_i} \right. \\ \left. \cdot \frac{d}{dm_s} S_{m_s}(NM(GEO, BC, EFL), m_s, RCSS)_i \right] = 0 \end{aligned} \quad (3.17)$$

Analytical solution for Equation 3.17 is not available, hence to estimate the shape parameter m_s , a root-finding algorithm is used. The value of m_s once estimated is substituted in Equation 3.16 to calculate the scale parameter k_s .

3.3.2 Estimation of the location parameter (RCSS)

The surface flaw parameters are dependent on the RCSS of the sample. For different value of RCSS, the MLE method estimates a unique set of parameters that produces the highest value of the probability distribution function of the observed data. Thus, it is important to estimate the RCSS value. Goswami et al. [32] in their work calculated the difference between the pb's calculated for each EFL in the sample using the estimated surface flaw parameters and the representative RCSS value (base RCSS) and the measured RCSS for each specimen as follows

$$pb_{diff} = e^{-k_s \cdot S_{m_s}(NM(GEO,BC,EFL),m_s,RCSS_{measured})} - e^{-k_s \cdot S_{m_s}(NM(GEO,BC,P),m_s,RCSS_{base})} \quad (3.18)$$

where, $RCSS_{measured}$ is the measured RCSS of the specimen, and $RCSS_{base}$ is the RCSS chosen as the representative RCSS value for the sample for which the surface flaw parameters m_s and k_s are estimated, and all other variables are same as defined before. The results showed that using the minimum or the maximum measured RCSS as the base RCSS overestimates or underestimates the average of the pb_{diff} , respectively while the mean tends to both overestimate and underestimate the pb, thereby somewhat neutralizing the effect. Hence, a base RCSS was estimated for which the average pb_{diff} is zero.

3.4 Sample set and Analysis

Historically published six sample sets consisting of two HS (referred to as H#) and four FT (referred to as F#) monotonically loaded to failure are collected for the current work. Each specimens were dry glazed and loaded to failure consistent to the procedure described in § 3.2.3. Before a specimen is dry glazed, the RCSS of the specimen is measured with a stress measuring device pertinent to the period, such as a Differential Stress Refractometer (DSR) during the 1990s, a Grazing Angle Surface Polarimeter (GASP) during the 1990s and recently, or a Scattered Light Polariscope in recent years (SCALP). Three samples, H1, F1, and F2 preceded the standard for measuring surface compression [9], hence RCSS was measured at three locations, one at the center of the specimen, and one along the short and the long dimension one inch from the edge. Each measurements for these three samples were reported in relevant literature. For the remaining three samples, H2, F3, and F4, the measurement conformed to the specifications listed in ASTM C1048-18 [8] and reported in relevant literature. Thickness for individual lites were measured and reported for each specimen in a sample.

Due to the brittle nature of glass, glass specimen monotonically loaded rarely fails at the location of single largest maximum tensile stress (SLMPTS), rather due to imperfections on the surface of the glass that causes stress concentrations, glass fracture initiates at different locations. Hence, the location of fracture for each specimen were recorded and reported.

The combination of high fracture load and breaking characteristics of FT glass makes it difficult to locate fracture origins, hence fracture origins for F3 and F4 were not determined. Instead, it was assume fracture originated at the location of SLMPTS [4].

The details for the six sample set including pertinent information regarding sample are listed in Table 3.1. The LTH for H1 and F2 were not reported, hence an idealized triangular

Table 3.1
Sample Description

Sample	# Specimens	Rectangular Dimension mm x mm (in. x in.)	Measured Thickness mm (in.)	RCSS measured	LTH
H1 ^{a,e}	20	1930 x 965 (76 x 38)	5.66 (0.223)	Yes ^f	No
H2 ^b	26	1930 x 965 (76 x 38)	5.61 (0.221)	Yes* ^f	Yes
F1 ^c	26	1680 x 1680 (66 x 66)	5.66 (0.223)	Yes ^g	Yes
F2 ^{a,e}	20	1930 x 965 (76 x 38)	5.64 (0.222)	Yes ^g	No
F3 ^d	14	1520 x 737 (60 x 29)	5.87 (0.231)	Yes ^{f,h}	Yes
F4 ^d	16	2360 x 838 (93 x 33)	5.72 (0.225)	Yes ^{f,h}	Yes

^a reported in [20]; ^b reported in [19], ^c reported in [50]

^d reported in [3]; ^e reported in [51]

* only mean RCSS of sample was reported in [19]

stress measuring device used: ^f GASP, ^g DSR, and ^h SCALP

load-time distribution was approximated using the reported failure load and failure time. The assumption of an idealized triangular load-time distribution in the event when LTH is not reported is explained in details in Goswami et al. [31]. Although, Bergers et al. [19] did not report the LTH and reported only the mean RCSS of sample, the recorded LTH, RCSS and thickness measured for individual specimen was available to the author. Sample F3 and F4 were weathered in-service FT samples. F3 and F4 were both removed approximately after 20 years in service. Individual specimen failure load, failure time, minimum measured RCSS, location of failure are provided in the the Appendix C .

3.4.1 Comparison of reported and recreated equivalent failure loads

Based on design standard guidelines, researchers have calculated and reported EFLs for either a 60-sec or a 3-sec load duration, referred to as EFL_{Hist} . EFLs were calculated by converting the LTH to stress time history (STH), using a numerical model at the location of failure. For sample F3, and F4 where location of failure were not determined, the single largest maximum principle tensile stress (SLMPTS) was used. Norville and Minor [52], Bove Jr [20], Bergers et al. [19], and Afolabi [3] used a finite difference method developed by Wang [63], while all calculations in this work uses a nonlinear FEA model developed by Yew et al. [67]. The STH for individual specimen was used to calculate EFS using Equation 3.10 and an equivalent EFL that produces a EFS at the location of fracture, and in the case where location of failure were not determined, at the location of SLMPTS. Stress calculation is a function of the boundary conditions, therefore necessitates the proper use of boundary condition. Since a glazing were typically inset approximately 3 mm (1/8 in.) from the edge of the specimen to avoid edge pullout, the whole area of glass is not stressed. Thus, for sample where boundary conditions were mentioned in literature, stress calculation were based on the reported boundary conditions else the full dimension of the glass sample is used. EFL_{Hist} calculation for H1, F1, and F2 used RCSS equal to zero MPa (psi), while H2, F3, and F4, used a measured minimum amongst the mean RCSS of the sample. The EFLs for each specimen in a sample were recreated, referred to as EFL_{Rec} , using similar parameters as used by researchers and compare to EFL_{Hist} . Parameters such

as load-duration, RCSS used, boundary condition used by Norville et al. [50], Bove Jr [20], Bergers et al [19], and Afolabi [3] for EFL_{Hist} calculation are summarized in Table 3.2 for convenience. H1 consisted of 20 specimen but fracture origin of two specimens were not

Table 3.2
Parameters historically used to calculate equivalent failure load and surface flaw parameter

Sample	EFL_{Hist} and EFL_{Rec}			RCSS used to estimate surface flaw parameter MPa (psi)
	Normalized time (sec)	RCSS used MPa (psi)	Boundary conditions mm x mm (in. x in.)	
H1	60	0 (0)	1930 x 965 (76 x 38)	54.1 (7850)
H2	3	42.8 (6217)	1920 x 953 (75.5 x 37.5)	42.8 (6217)
F1	60	0 (0)	1680 x 1680 (66 x 66)	69 (10000)
F2	60	0 (0)	1930 x 965 (76 x 38)	69 (10000)
F3	3	72.9 (10574)	1510 x 711(59.4 x 28)	72.9 (10574)
F4	3	75.8 (11000)	2360 x 813 (92.4 x 32)	75.8 (11000)

recorded by Bove Jr [20], hence EFL_{Hist} of 18 specimens were reported. Bove Jr [20] used the RCSS equal to zero to calculate the EFL_{Hist} and boundary condition used to calculate EFS was not mentioned. Thus, for the motive of comparison, EFL_{Rec} s were calculated using the full rectangular dimension of glass and RCSS equal to zero. The EFL_{Rec} for the 18 specimen lay between -1.7% to 5.5% of the EFL_{Hist} . A difference in the EFL_{Rec} and EFL_{Hist} for H1 was expected because of missing LTH and difference in mesh sizes used in the numerical model.

Bergers et al. [19] used RCSS equal to the minimum measured RCSS of the sample (42.8 MPa (6217 psi)) to calculate EFL_{Hist} . Although the boundary conditions used to calculate EFL_{Hist} for H2 was not mentioned, calculations suggest that the long and short dimension

were reduced by 12.7 mm (1/2 in.) to account for overhang and dry glazing. LTH for H2 although were not published by Bergers et al. [19], the data was available to the authors. Hence, for the motive of comparison, EFL_{Rec} values were calculated using a rectangular dimension of 1920 mm \times 953 mm (75 1/2 in. \times 37 1/2 in.) with RCSS of 42.8 MPa (6271 psi) and using the original LTH. The EFL_{Rec} for H2 mostly lay between -0.38% and 0.67% compared to the EFL_{Hist} , apart from specimen number 5 that showed a difference of 2.34%. A marginal difference was observed because of the different numerical models used to calculate the EFLs. Figure 3.1 presents the EFL_{Rec} and EFL_{Hist} for H1 and H2.

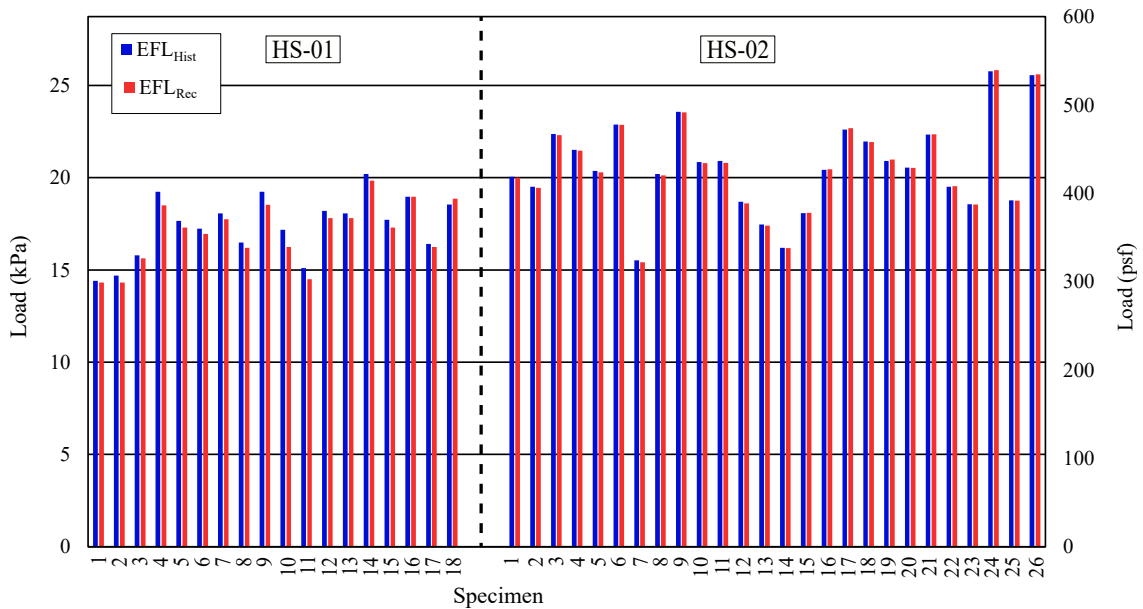


Figure 3.1: Comparison of EFL_{Hist} and EFL_{Rec} for H1 and H2

Norville et al. [50] used the RCSS equal to zero MPa (psi) while calculating EFL_{Hist} for F1. Boundary conditions to calculate EFL_{Hist} was not reported by Norville et al. [50]. Hence, while calculating the EFL_{Rec} values, the full rectangular dimension of the glass and RCSS equal to zero MPa (psi) was used. The LTH figures for individual specimen

was provided, and figures were digitized using a software and used for EFL_{Rec} calculation. The EFL_{Rec} for mostly between -4.10% and 5.44% compared to the EFL_{Hist} apart from three specimen (specimen no 4, 9 and 25) that showed a difference of more than 10%. Because, the EFLs are back calculated from EFSs, the EFS recreated were compared to the historically reported EFS. It was observed that the recreated EFS were within 5% of to the historically reported EFS values for the three specimens. The ability to recreate the EFS within 5% of the historically reported values, but a different EFL value points towards the inability of the numerical model to converge due to the square dimension of the plate. The calculation of stresses using either the FDM model developed by Wang [63] or the nonlinear FEA model developed by Yew et al. [67] for a square dimension for particular loads fails to converge thereby projecting incorrect stress values and thus incorrect EFLs. While calculating EFL_{Rec} , the authors faced similar convergence issues and discarded the load for which the solution did not converge. Thus, the authors believe the three specimen (specimen no 4, 9 and 25) that showed a difference of more than 10% between EFL_{Rec} and EFL_{Hist} was because of lack of convergence.

F2 consisted of 20 specimen but fracture origin of two specimens were not recorded by Bove Jr [20], hence EFL_{Hist} of 18 specimens were reported. Bove Jr [20] used the RCSS equal to zero MPa (psi) to calculate the EFL_{Hist} and the boundary condition used was not reported. Thus, the EFL_{Rec} s were calculated using the full rectangular dimension of the glass and a RCSS equal to zero MPa (psi). The EFL_{Rec} values for the 18 specimen lay

between -7.52% to 7.63% of the EFL_{Hist} . A difference in the EFL_{Rec} and EFL_{Hist} for FT-02 was expected because of reasons such as missing LTH, difference in mesh sizes used in the numerical model, and boundary condition.

Afolabi [3] used RCSS equal to the minimum measured RCSS of the sample (72.9 MPa (10574 psi)) to calculate EFL_{Hist} for F3 and a boundary condition that resulted in a rectangular dimension of 1510 mm \times 711 mm (59 $\frac{3}{8}$ in. \times 28 in.). The LTH for F3 were not published by Afolabi [3], but the data was available to the authors. Thus, EFL_{Rec} s were calculated using a rectangular dimension of 1510 mm \times 711 mm (59 $\frac{3}{8}$ in. \times 28 in.) with RCSS equal to 72.9 MPa (10574 psi) and using the original LTH. The EFL_{Rec} lay between -0.27% and 0.80% compared to the EFL_{Hist} . A small difference between EFL_{Rec} and EFL_{Hist} was observed due to the difference in numerical model.

Afolabi [3] used RCSS equal to the minimum measured RCSS of the sample (75.8 MPa (11000 psi)) to calculate EFL_{Hist} for F4 and a boundary condition that resulted in a rectangular dimension of 2360 mm \times 813 mm (92 $\frac{3}{8}$ in. \times 32 in.). However, on closer observation it was observed that Afolabi [3] used a rectangular dimension of 2360 mm \times 832 mm (92 $\frac{2}{5}$ in. \times 33 in.) for EFL_{Hist} calculation. Hence, EFL_{Rec} s were calculated using a rectangular dimension of 2360 mm \times 832 mm (92 $\frac{2}{5}$ in. \times 33 in.) with RCSS equal to 75.8 MPa (11000 psi) and using the original LTH. The EFL_{Rec} for F4 lay between -0.47% and 2.58% compared to the EFL_{Hist} . A small difference between EFL_{Rec} and EFL_{Hist} was observed due to the difference in numerical model. Figure 3.2 presents the EFL_{Rec} and

EFL_{Hist} for F1, F2, F3, and F4.

EFLs were recreated for the six samples using the same parameters as used by researchers

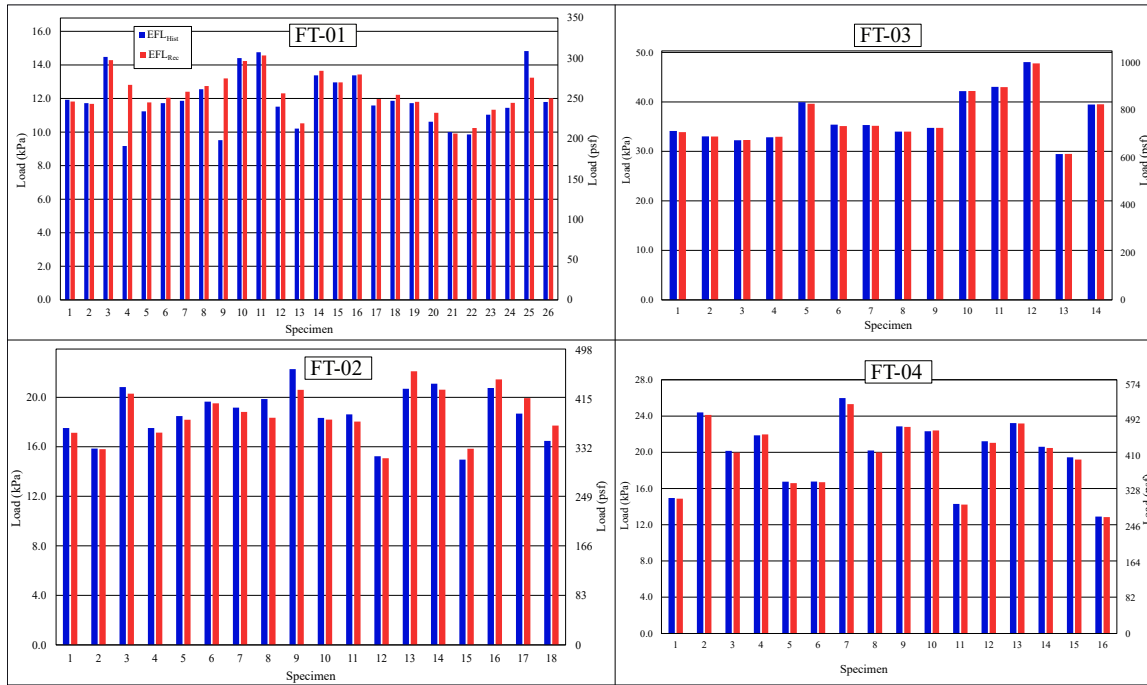


Figure 3.2: Comparison of EFL_{Hist} and EFL_{Rec} for FT-01, FT-02, FT-03 and FT-04

to calculate historically reported EFLs and compared. 92% (108 specimen) of the recreated EFL lay between -5% to 5% of the historically reported EFL, while only three specimens had a difference of more than 10%. The three specimens originated from sample F1, that had a square dimension, and a large difference was seen because of the inability of the numerical model to converge to a solution. The EFLs recreated for samples with recorded LTH, almost similar mesh size and proper documentation of boundary condition (H2, F3, and F4) showed less variability compared to other samples. The use of an idealized triangular load-time distribution when LTH is not reported or available, and location of boundary

condition do effect the calculation of EFL, but since 92% of the recreated EFL were between -5% to 5% of the historically reported EFL , the effect was deemed negligible.

3.4.2 3-sec equivalent failure load and surface flaw parameter estimation using MLE

Equivalent failure loads for each specimen in a sample are calculated for a reference time of 3-sec to be consistent with design codes using Equation 3.10. Afolabi et al. [4] in their work compared EFLs calculated for different value RCSS and RCSS equal to zero MPa (psi), and recommended to use the minimum measured RCSS for individual specimen in the EFL calculation. Hence, the work herein will use the minimum measured RCSS of individual specimen for all EFL calculation. To be consistent across all samples, the boundary conditions used to convert LTH to STH is assumed to be at the edges i.e. the full dimension of the plate is used for stress calculations.

To estimate a representative RCSS and corresponding surface flaw parameters for each sample, an iterative process was used so that the average of pb_{diff} calculated using Equation 3.18 is zero. An initial RCSS is chosen, usually the minimum measured RCSS. Corresponding surface flaw parameters, m_s and k_s , are estimated by solving Equation 3.17 and Equation 3.16, respectively. The average of pb_{diff} is calculated using the RCSS chosen and the measured RCSS for each EFL of a specimen in the sample. The process is repeated

until a value of RCSS is determined for which the corresponding surface flow parameters lead to the calculation of pb_{diff} to zero. Table 3.3 presents the representative RCSS of the sample and corresponding surface flow parameter for each sample. A graphical comparison

Table 3.3
3-sec surface flow parameters

Sample	RCSS MPa (psi)	3-sec Surface flow parameter	
		m_s	$\frac{k_s}{m^{(2 \cdot m_s - 2)} \cdot N^{-m_s}} \cdot (in. \cdot lb f^{-m_s})$
HS-01	64.3 (9317)	7.22	1.52E-18 (2.43E-31)
HS-02	42.5 (6160)	6.77	1.08E-18 (1.62E-30)
FT-01	76.7 (11119)	6.79	3.21E-18 (4.45E-30)
FT-02	68.4 (9921)	6.25	5.11E-17 (1.02E-27)
FT-03	82.4 (11943)	3.82	2.28E-12 (8.16E-18)
FT-04	84.7 (12278)	3.25	2.33E-11 (1.42E-15)

of the 3-sec EFL and the MLE estimated surface flow parameters is presented in Figure 3.3 (a) and Figure 3.3 (b) for HS and FT sample, respectively. For each sample, the EFLs are sorted in an ascending order ($i= 1$ to n) and assigned a median rank probability estimator, E_i according to Equation 3.19 [28] [45] [27]).

$$E_i = \frac{i - 0.3}{n_{sam} + 0.4} \quad (3.19)$$

Where, i = rank of the EFL of specimen, and n_{sam} is the number of specimen in the sample. The CDF for each sample is created using the MLE estimated surface flow parameters and RCSS listed in Table 3.3, in Equation.3.13 and the non-linear four-node quadrilateral finite-element model developed by Yew et al. [67] as the numerical model. The x-axis

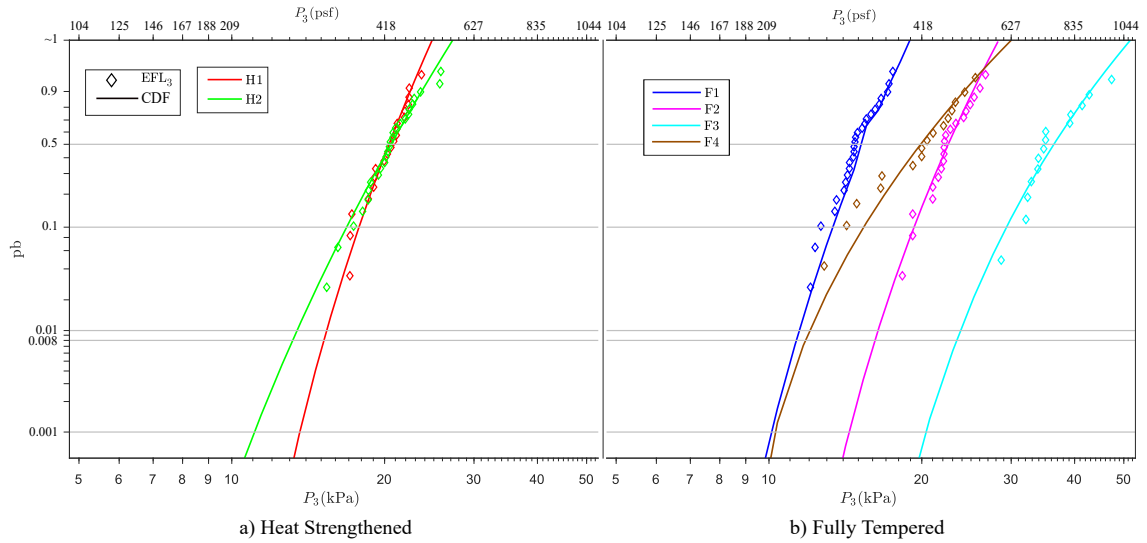


Figure 3.3: EFL_3 and CDF for HS and FT samples

on the graph represents the 3-sec uniform load, P_3 (log scale) and the y-axis represents the probability of breakage, p_b ($\ln(\ln(1/(1-(p_b \text{ or } E_i))))$ scale). In Figure 3.3 (a), both HT samples were of the same dimensions. Thus, the relative position of both the CDF were similar whereas the slopes were different. It was observed that the LR of H1 was stronger for p_b less than 0.1. According to the authors, the trend was observed due to the difference in measured RCSS between the two samples. The mean measured RCSS of H1 was 68.3 MPa (9909 psi) while the mean measured RCSS of H2 was 44.9 MPa (6514 psi). In Figure 3.3 (b), CDF of F3 was strongest, followed by the F2, F4, and F1. The trend was observed because among the four samples, F3 had the smallest area, followed by the F2 and F4, while F1 had the largest area. The CDF profile for F1 and F2 were observed to be similar, whereas CDF profile for F3 and F4 were observed to be similar. The authors does not have an explanation for the observed trend. Sample H1, H2, and F2 were of the were of the same dimensions and hence the CDF of the three samples were plotted together in Figure 3.4. It

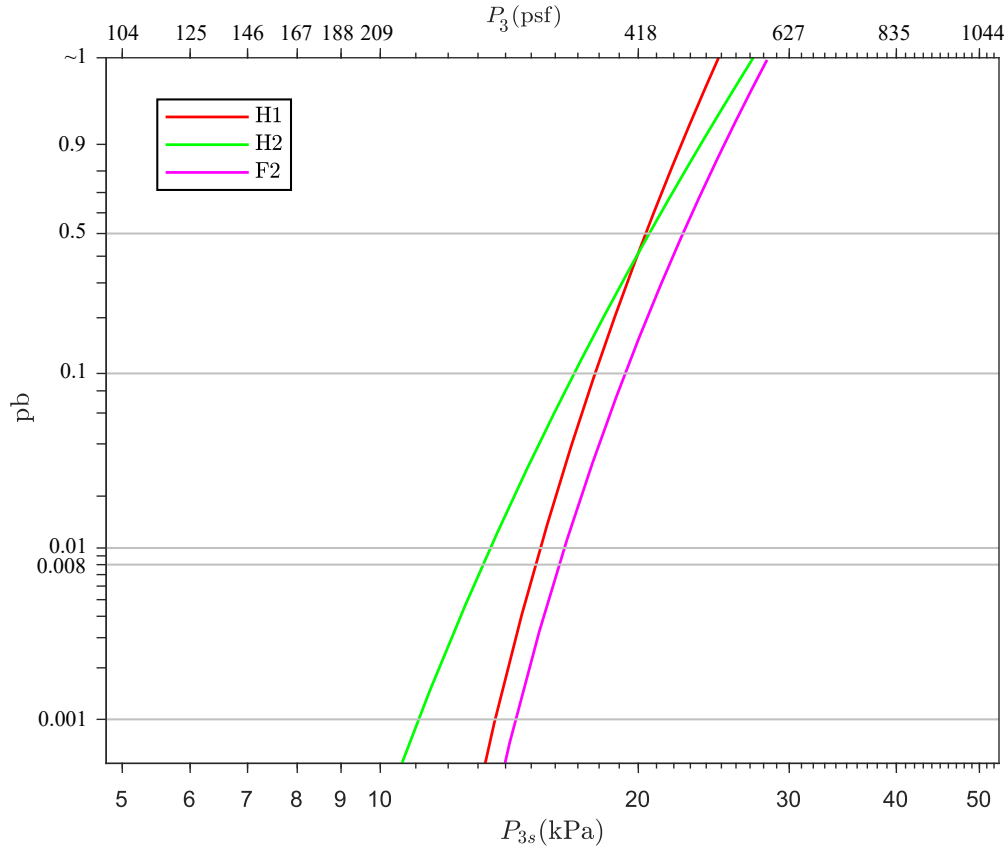


Figure 3.4: Comparison of H1, H1 and F2

was observed that the CDF profile of H1 and F2 were similar. Destructive testing of H1, F1 and F2 were performed by Bove Jr [20] and the authors believe either the similarity of experimental setup for the three samples or the relatively closeness of RCSS value of the sample is the reason behind the trend. The measured mean RCSS of F2 was 74.63 MPa (10821 psi), close to the mean measured RCSS of H1 was 68.3 MPa (9909 psi). ASTM E1300-16 [11] defines LR of a glass component as the ability to resist a uniform lateral load of 3-sec duration, resulting in a p_b equal to 0.008, while for overhead glazing, resulting in a p_b equal to 0.001 [1]. Therefore, load corresponding to 0.001 and 0.008 p_b are compared. The load corresponding to 0.001 and 0.008 p_b was lowest for H1, followed by H2, and F2

because the p_b correlated to the RCSS of the sample i.e. RCSS lowest H1, followed by H2, and F2, as expected.

3.5 Results and Discussion

ASTM E1300-16 [11] uses a multiplier, a glass type factor, of 2 and 4 to scale the LR of AN glass to design a HS and FT glass, respectively. However, the shift of LR due to RCSS is better explained by using the MGFPM rather than the glass type factors. ASTM E1300-16 [11] added the MGFPM to the analytical method in the appendix, but failed to explain the effect of RCSS to the LR. Therefore, to explain the effect of RCSS on the LR of a glass component, LR charts of glass of similar dimension but of different type i.e. AN, HS, FT, are compared in this section. To date, it is unknown if HT glass weathers similarly to AN glass, due to the presence of RCSS [4]. The work herein contains two weathered in-service FT glass, hence LR of the two weathered in-service FT samples are compared to the LR of the weathered in-service AN glass to explain the effect of RCSS on the weathering process. A rectangular glass component is designed as per ASTM E1300-16 [11] and using MLE estimated surface flaw parameters and results are compared for different p_b .

3.5.1 Effect of RCSS on the strength of glass

Goswami et al. [31] collected and estimated surface flaw parameters for new and weathered in-service AN glass samples loaded to failure. New AN sample, N02 in Goswami et al. [31] had the same dimension as H1, H2, and F2 (1930 mm x 975 mm (76in.x 38in.)). Since H1, H2, and F2 were new HT glass, the LR comparison of new AN glass to new HS and FT glass is provided here. Similarly, N07 in Goswami et al. [31] had the same dimension as F1, and as F1 was new FT glass, LR comparison of F1 and N07 is also presented. Samples F3 and F4 were weathered in-service FT samples, and hence LR was compared to the weathered in-service AN samples of similar sizes collected in Goswami et al. [31]. The nominal dimension of F3 was 1520 mm x 737 mm (60in.x 29in.) while the nominal dimension of W2 listed in Goswami et al. [31] was 1520 mm x 724 mm (60¹/₂ in. x 28 ¹/₂ in.). Although, the dimensions of W2 and F3 were not exactly the same, the sizes were comparable. The nominal dimension of F4 and W14 in Goswami et al. [31] was 2360 mm x 838 mm (93in. x 33in.) and a comparison of the two LRs are also presented. Surface flaw parameters listed in Table 3.3 for HT glass and surface flaw parameters estimated using MLE by Goswami et al. [31] for AN glass were used to create CDF for corresponding glass types and presented in Figure 3.5. Figure 3.5 (a), (b), (c), and (d) presents the CDF of different glass types for F2, F1, F3, and F4 dimension, respectively. In all the four figure, the slope of the CDF for new HT samples are much steeper compared to the CDF of the new AN glass suggesting towards a complex transformation of the LR from AN glass to

HT glass rather than a simple step up function. Furthermore, due to addition of the RCSS, there appears to be a curvature to the LR of HS and FT glass, prominent in F3 and F4 (Figure 3.5 (c) and Figure 3.5 (d)). Load corresponding to 0.001 and 0.008 are estimated for the same glass dimensions but different glass types and listed in Table 3.4. The ratio of the load corresponding to 0.001 and 0.008 p_b for HT to AN glass, are calculated for all the dimensions and presented in Table 3.4. Figure 3.6 presents the representative RCSS of the sample to the ratio of load corresponding to 0.008 p_b for new AN, HS, and FT glass types have a aspect ratio, ratio of the long to short dimension, equal to 2 i.e. H1, H2, F2, and F3. As W02 was weathered in-service sample, a adjustment factor of 1.67 was used to accommodate the strength reduction of 40% due to weathering. Figure 3.6 shows that as RCSS increases, the LR increases, implying that the glass type parameters used in ASTM E1300-16 [11] fails to adequately quantify the strength of HT glass. A same trend can be expected from different aspect ratios, but due to limited sample, trends cannot be plotted. Hence, quantifying the LR of HT glass by scaling up the AN LR using the glass type factors does not sufficiently adjust the LR, instead, the MGFPM should be used to calculate the LR of HT glass.

3.5.2 Effect of RCSS on weathering of HT glass

Two weathered in-service FT glass samples, F3 and F4, were monotonically loaded to failure, and similar sized AN weathered in-service samples (W02 and W14 in Goswami et al.

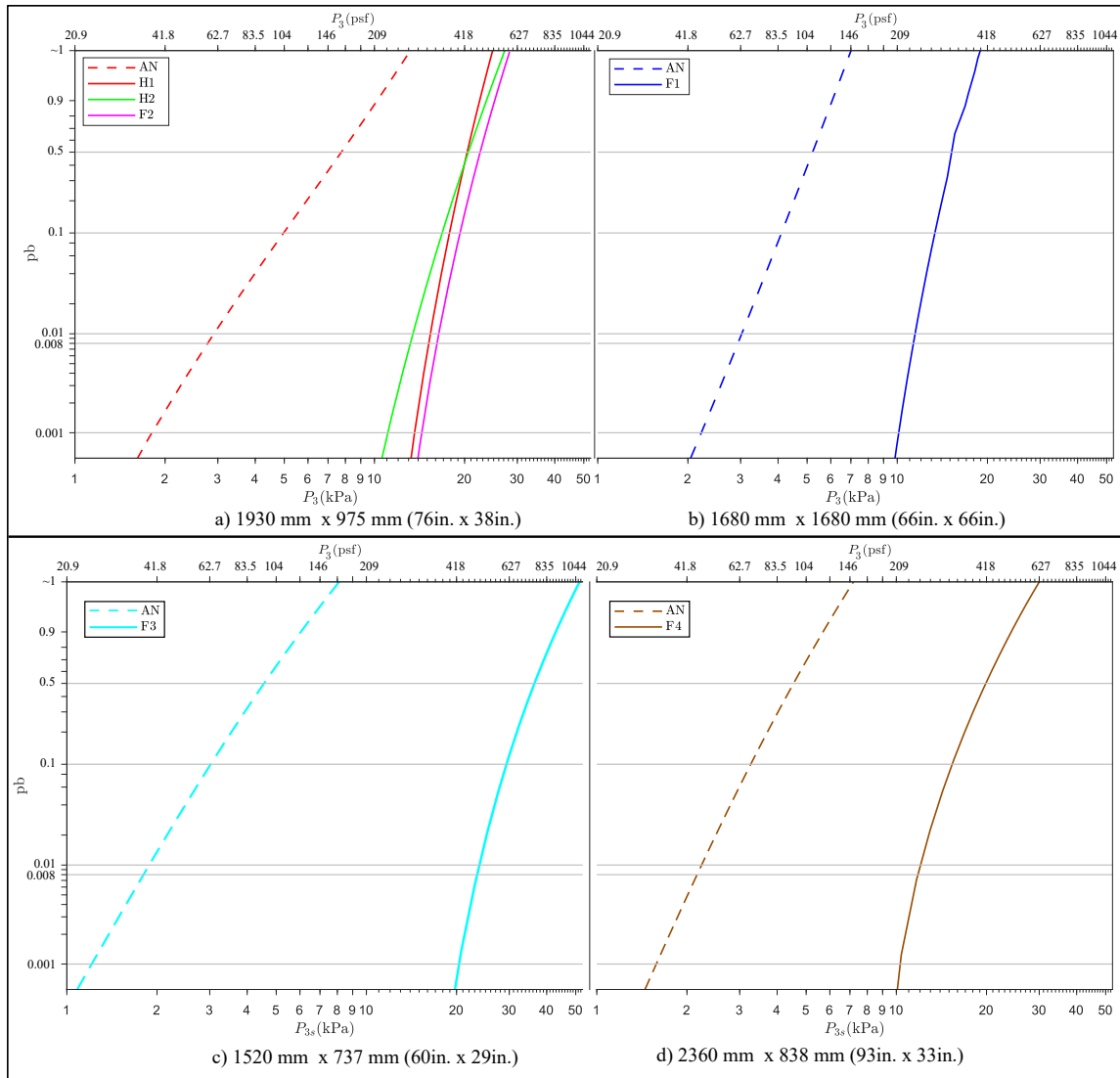


Figure 3.5: Comparison of LR for different type of glass of same dimension

[31]) were tested by different researchers and described in details in Goswami et al. [31]. Sample F3 served as an exterior sloped glazing, and thus weathered in-service predominantly due to environmental condition. Sample W02 in Goswami et al. [31] was 6mm (1/2in.) larger on each side compared to F3, and was reported to be storm damaged. Sample W14 and F4 originated from the same building and the samples were separated from a IG unit. The lite facing the exterior consisted of the W14, a 6mm (1/4 in.) MO AN glass, and

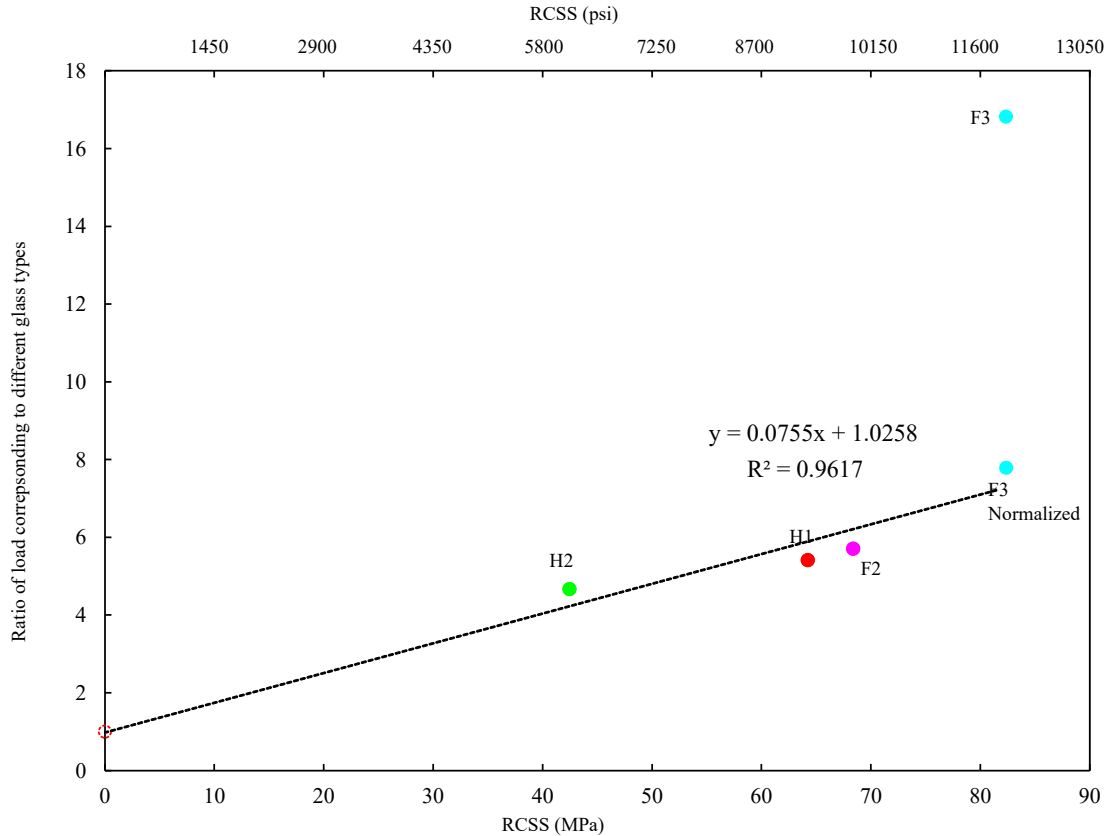


Figure 3.6: Load ratio vs RCSS of sample for glass sample with aspect ratio equal to 2

the lite facing the interior consisted of the F4. Thus, the W14 predominantly weathered in-service due to environmental conditions, whereas F4 predominantly weathered in-service from abrasion from cleaning the glass. The CDF for individual samples are created using surface flaw parameters listed in Table 3.3 for F3 and F4 and surface flaw parameters estimated using MLE by Goswami et al. [31] for W02 and W14 glass. In an effort to understand the effect of RCSS on weathering, surface flaw parameters for W02 and W14 were used with the RCSS of F3 and F4 (Table 3.3), respectively and CDFs were plotted together. Figure 3.7 presents the CDF for both glass dimensions for AN and FT glass. The

Table 3.4Load corresponding to different p_b for different glass types but similar dimension

Dimension	Sample	RCSS MPa (psi)	Load - kPa (psf)		Ratio	
			pb = 0.001	pb = 0.008	pb = 0.001	pb = 0.008
1930 mm x 965 mm (76in. x 38in.)	N02	0	1.81 (37.7)	2.77 (57.9)	1	1
	H2	42.5 (6160)	10.9 (227)	12.9 (270)	6.03	4.66
	H1	64.3 (9317)	13.5 (281)	15.0 (313)	7.45	5.41
	H2	68.4 (9921)	14.0 (293)	15.8 (330)	7.78	5.70
1680 mm x 1680 mm (66in. x 66in.)	N07	0	2.22 (46.4)	2.94 (61.5)	1	1
	F1	76.7 (11119)	10.1 (211)	11.3 (236)	4.55	3.84
1520 mm x 737 mm (60in. x 29in.)	W02	0	1.21 (25.2)	1.80 (37.6)	1	1
	F3	82.4 (11943)	20.4 (425)	23.4 (489)	16.8	13.0
2360 mm x 838 mm (93in. x 33 in.)	W14	0	1.58 (33.0)	2.16 (45.1)	1	1
	F4	84.7 (12278)	10.3 (215)	11.8 (246)	6.50	5.46

dash line represents the CDF for the weathered in-service AN sample, the solid line represents the CDF for the weathered in-service FT sample, and the dash-dot line represents the CDF created using the surface flaw parameters for W02 and W14 while using the RCSS of the F3 and F4 sample, respectively. Surface flaw parameters from W02 closely estimated the load corresponding to 0.001 and 0.008 p_b for F3 (a difference of 4.67% and 2.11%, respectively), whereas surface flaw parameters from W14 overestimated by 36.8% and by 36.5% at 0.001 and 0.008 p_b , respectively. The ability to closely estimate the LR for F3 at 0.001 and 0.008 p_b using W03 surface flaw parameters, point towards AN and FT samples weather in a similar manner. However, the inability to closely estimate the LR for F4 using W14 surface flaw parameters suggests, weathering conditions and other unknown variable may contribute towards a difference in LR.

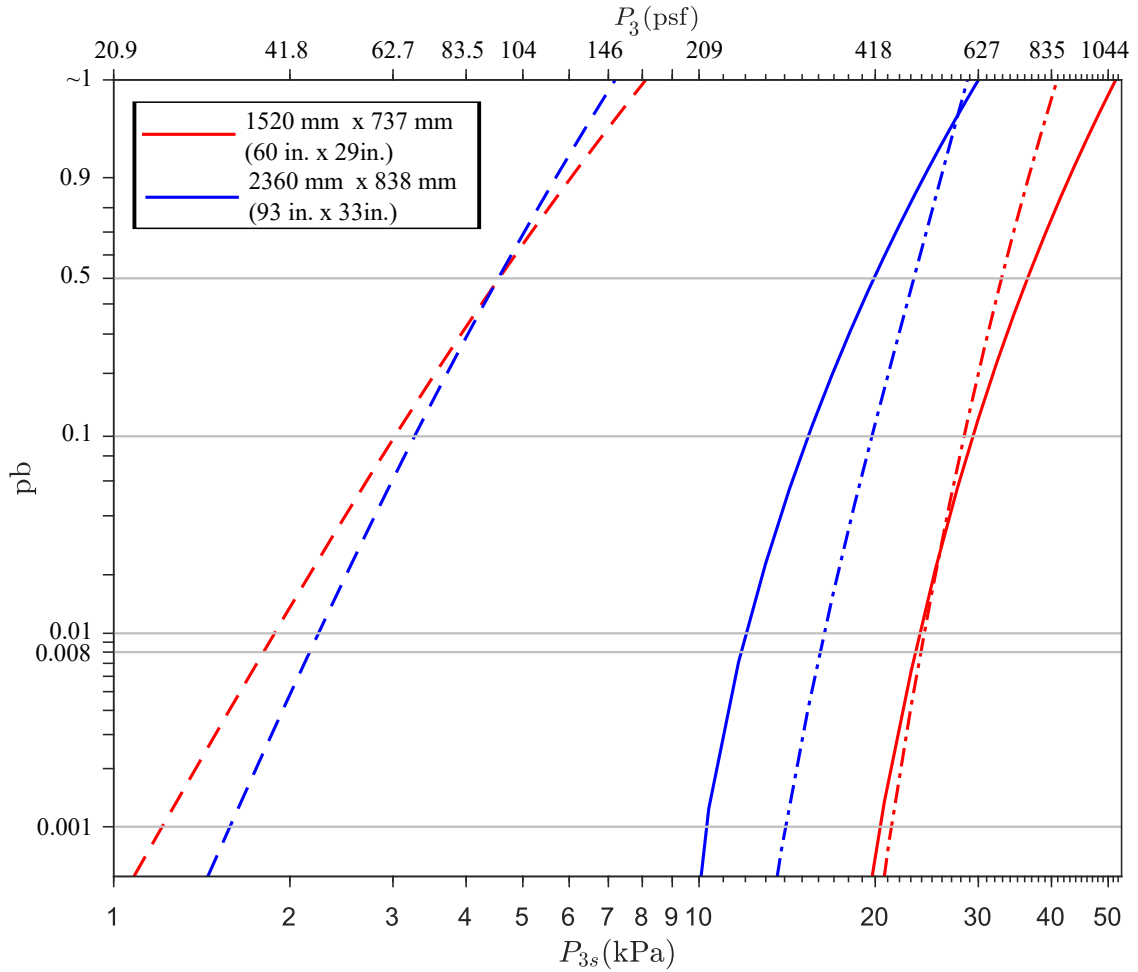


Figure 3.7: LR of weathered in-service AN and weathered in-service FT of similar dimension

3.5.3 Design example

The LR for a HT sample in ASTM E1300-16 [11] is calculated using the surface flaw parameters for weathered in-service sample, m_s equal to 7 and k_s equal to $2.68 \times 10^{-53} \text{ N}^{-7} \text{ m}^{12}$ ($1.368 \times 10^{-29} \text{ in.}^{12} \text{ lbf}^{-7}$) for a RCSS, usually 24 MPa (3500 psi) for HS glass and 69 MPa (10000 psi) for FT glass. A RCSS of 24 MPa (3500 psi) for HS glass and 69

MPa (10000 psi) for FT glass is used for design because, those values are the minimum requirement for the glass to be recognized as HS or FT glass [8]. Hence, using the lower-most value of RCSS acts as a safety factor while designing because HT glass usually has a higher RCSS than the prescribed lower value. The availability of the RCSS (measured or representative) for the sample used in this work allows us to compare the CDF created using the RCSS and different surface flaw parameters.

Four different dimensions are used to create CDF using the surface flaw parameters listed in Table 3.3 and plotted in Figure 3.8. The four dimensions chosen were the dimensions of H1, F1, F3 and F4 with their representative RCSS as listed in Table 3.3 and presented in Figure 3.8 (a), (b), (c), and (d), respectively. The solid line in each figure represents the CDF created using the surface flaw parameters estimated from the destructive testing of the sample, while the dotted lines represents the CDF created using the surface flaw parameter from different samples, but for the current dimension and RCSS. Thus, in Figure 3.8 (a), the solid line represents the CDF created using the surface flaw parameter estimated from H1 listed in Table 3.3 for a dimension of 1930mm x 975mm (76in. x 38 in.) and a RCSS of 64.3 MPa (9317 psi), while the green dotted line represents the CDF created using the surface flaw parameter estimated from H2 listed in Table 3.3, for the 1930mm x 975mm (76in. x 38 in.) dimension and 64.3 MPa (9317 psi) RCSS and so on. The black dotted line represents the CDF created using the ASTM E1300-16 [11] surface flaw parameters for the dimensions listed in each figure. At a 0.008 pb, the CDF created using the ASTM E1300-16 [11] surface flaw parameters for new HS and FT glass underestimates

the strength by 4.60% and 8.43% (Figure 3.8 (a) and Figure 3.8 (b)), respectively. For weathered in-service FT glass, the CDF created using the ASTM E1300-16 [11] surface flaw parameters overestimates the strength at 0.008 pb by 21.0% and 30.4%, respectively (Figure 3.8 (c) and Figure 3.8 (d)).

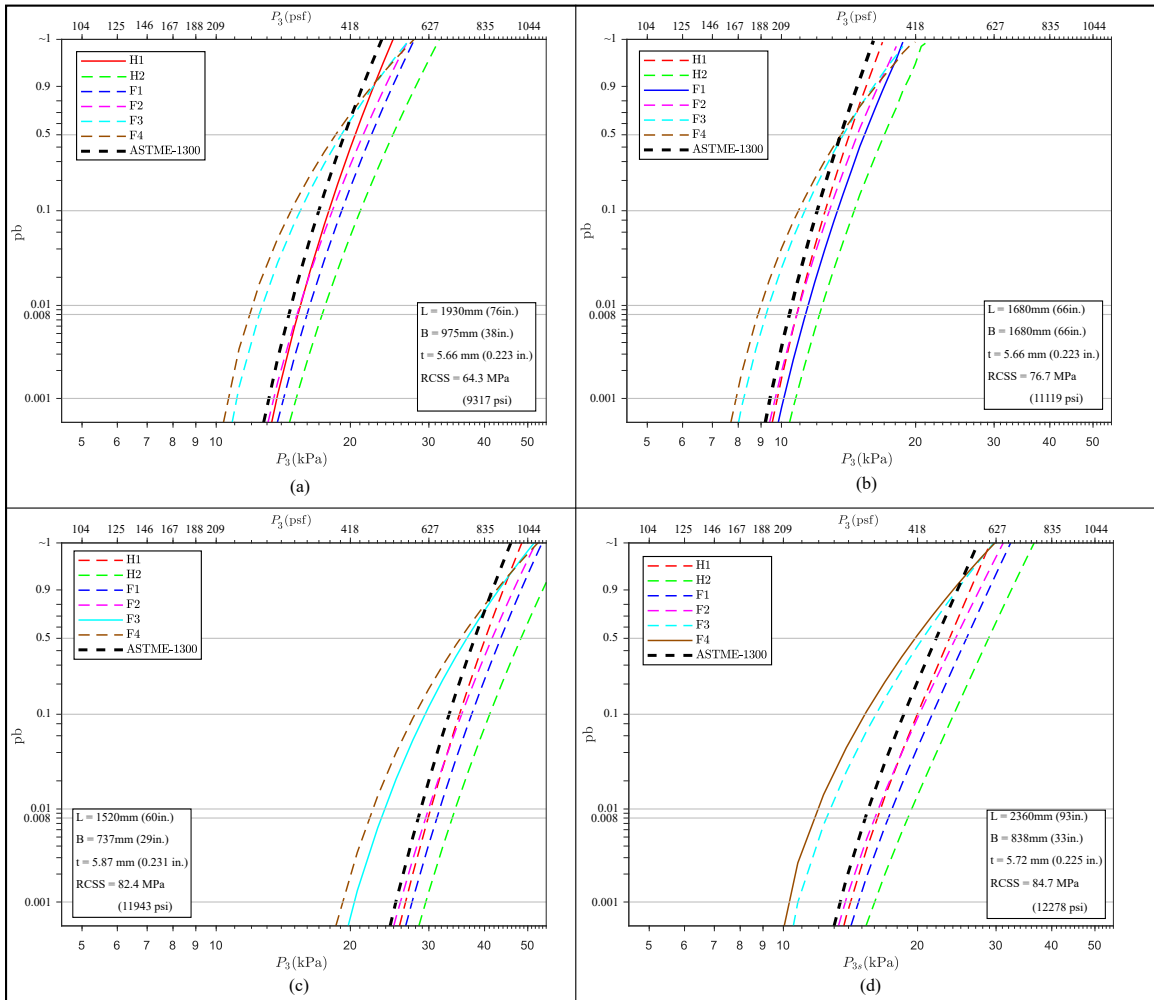


Figure 3.8: Design CDF for different dimension

A similar comparison is also provided from a designer perspective for the weathered in-service sample i.e. F3 and F4. While designing a glass component, the measured RCSS

of specimen is usually not available to the designer, hence a HT is usually designed using the minimum RCSS for the glass to be recognized as a HS or FT glass i.e. 24 MPa (3500 psi) and 69 MPa (10000 psi), respectively. Thus the CDF for F3 and F4 are created using the surface flaw parameters used in ASTM E1300-16 [11] and a RCSS of 69 MPa (10000 psi) and presented with the solid black line in Figure 3.9(a) and Fig 3.9(b), respectively. The figure also plots the CDF created for F3 and F4 using the MLE estimated surface flaw parameters and the representative RCSS from Table 3.3. The solid line in each figure represents the CDF created using the surface flaw parameters estimated from the destructive testing of the sample listed in Table 3.3, while the dotted lines represents the CDF created using the surface flaw parameter from the other weathered in-service sample. The black dotted line represents the CDF created using the surface flaw parameters used in ASTM E1300-16 [11] for the same dimensions but using the representative RCSS. At a 0.008 pb, the CDF created using the [11] surface flaw parameters and the minimum RCSS (69 MPa (10000 psi)) underestimates the strength by 3.32% and 1.06% for F3 and F4, respectively. Both F3 and F4 had a larger RCSS than 69 MPa (10000 psi), and it is conceivable to have either of the F3 or F4 with RCSS of 69 MPa (10000 psi). For specimen with RCSS of 69 MPa (10000 psi), the ASTM E1300-16 [11] surface flaw parameters will overestimate the LR, thereby not meeting the requirements of LR (strength) stated in the standard. However, both the historical weathered in-service FT sample sets were exposed to an extreme event prior to their removal, their load resistances were expected to be lower than regular in-service conditions. The 3-sec surface flaw parameter estimated from F4 i.e., $m_s = 3.25$ and

$k_s = 2.33 \times 10^{-11} (1.43 \times 10^{-15}) m^{(2 \cdot m_s - 2)} \cdot N^{-m_s} (in. (2 \cdot m_s - 2)) \cdot lb f^{-m_s}$ can be used for a conservative design of fully tempered weathered in-service glass.

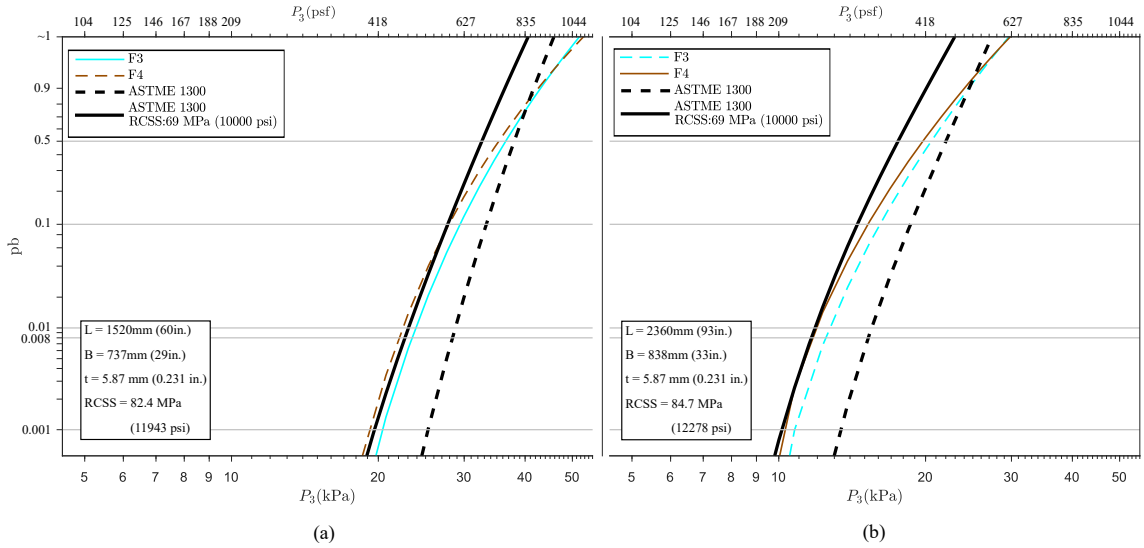


Figure 3.9: Design CDF for weathered FT glass

Figure 3.10 presents the relation between different value of RCSS to the ratio of load corresponding to $0.008 p_b$ for weathered in-service HT to AN glass, for 2360 mm x 838 mm x 5.72 mm (93in. x 33in. x 0.225 in.) dimension. The load corresponding to $0.008 p_b$ for HT is calculated using $m_s = 3.25$ and $k_s = 2.33 \times 10^{-11} (1.43 \times 10^{-15}) m^{(2 \cdot m_s - 2)} \cdot N^{-m_s} (in. (2 \cdot m_s - 2)) \cdot lb f^{-m_s}$ while for AN glass, the surface flaw parameters for W14 estimated using MLE by Goswami et al. [31] was used. Figure 3.10 also presents the relation between different value of RCSS to the ratio of load corresponding to $0.008 p_b$ for new HT to AN glass presented in Figure 3.6. According to the data, the trend for load ratio corresponding to $0.008 p_b$ for new HT to AN glass was higher than that of weathered in-service HT to AN glass. The results of this study show that as the RCSS of the samples increases, the

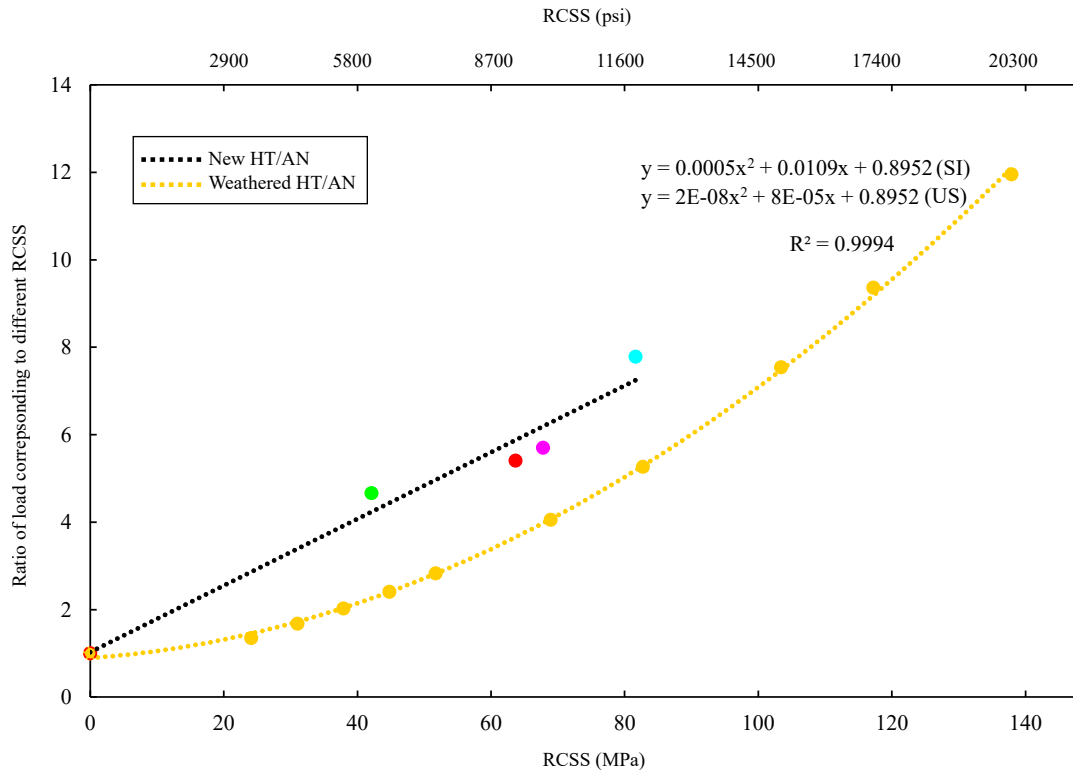


Figure 3.10: Relation between LR for HT and AN to RCSS for weathered samples

LR ratio for weathered in-service HT to AN glass at a 0.008 p_b increases in a polynomial order, expressed as

$$\left(\frac{Load_{HT}}{Load_{AN}}\right)_{0.008} = 5 \cdot 10^{-3} \cdot (RCSS(in MPa))^2 + 0.0109 \cdot (RCSS(in MPa)) + 0.8952$$

$$\left(\frac{Load_{HT}}{Load_{AN}}\right)_{0.008} = 2 \cdot 10^{-8} \cdot (RCSS(in psi))^2 + 8 \cdot 10^{-5} \cdot (RCSS(in psi)) + 0.8952 \quad (3.20)$$

3.6 Conclusion

Equations to estimate the surface flaw parameters using the maximum likelihood estimator (MLE) method for the modified glass failure prediction model (MGFPM) for heat treated samples was put forward. Failure data for two heat-strengthened and four fully-tempered samples were used to illustrate the MLE method to estimate the surface flaw parameters. Because, the surface flaw parameters in the MGFPM is dependent on the RCSS of the sample, a method was put forward to estimate a representative RCSS of the sample. Surface flaw parameters corresponding to the representative RCSS for each sample were estimated and presented. Two sample amongst the four fully tempered samples were weathered in-service samples, and thus load resistance from the two samples were compared to the load resistance calculated using ASTM E1300-16 surface flaw parameters. It was observed that the ASTM E1300-16 overestimated the strength for weathered in-service HT samples. As the weathered in-service HT samples were exposed to an extreme event prior to their removal, the ASTM E1300-16 was expected to overestimate the strength. Experimental data suggest that as the value of RCSS increase, the ratio of load for HT to AN corresponding to $0.008 p_b$ increases in a polynomial order.

Chapter 4

Estimation of Flaw Parameters for Holes in Glass using Maximum Likelihood Estimator

Currently, a widely accepted, objective, and repeatable procedure for determining the flaw parameters used in the glass failure prediction model does not exist. Historically flaw parameters were primarily based on statistical measures and the researchers' interpretation of experimental data. This paper advances a procedure to calculate the flaw parameters used in the two-parameter form of the glass failure prediction model for holes based on the well known maximum likelihood estimator method based on destructive testing. Additionally, the paper presents a three-parameter form of the glass failure prediction model

for holes to incorporate the residual compressive surface stress for heat-treated glass into the load resistance. The paper also advances a procedure to calculate the flaw parameters for the three-parameter form of the glass failure prediction model based on the maximum likelihood estimator method. The work herein uses failure test data from a set of historical four-point bending tests of glass beams with a hole located at the geometric center to illustrate the procedure to determine flaw parameters. Because the flaw parameters for the three-parameter glass failure prediction model are a function of the residual compressive surface stress, a method is presented to choose the residual compressive surface stress value to base the other two parameters upon. An example design scenario provides insight into the variations between the two- and three-parameter glass failure prediction models and the effect the residual compressive surface stress has on the load resistance.

4.1 Introduction

To increase facade transparency, engineers and architects increasingly use point-supported glass (PSG). Point-supported glass uses a bolt or similar hardware passing through one or more holes in the glass component as a typical support, rather than supported along the edges. Currently, the well known standard ASTM E1300-16 [11] provides a procedure to determine the load resistance (LR) of a glass component used in facades. However, the procedure contained in ASTM E1300-16 [11] is limited to rectangular glass infill panels, known as lites, continuously simply supported along two or more edges. Thus ASTM

E1300-16 [11] does not address PSG. Consequently, engineers often use a maximum stress procedure to design a PSG consistent with other commonly used construction materials (e.g. steel). However, glass a brittle material, does not have a yield stress or a well defined ultimate stress. As such, attempting to use a maximum stress design method often requires selecting a very low maximum stress; potentially without high confidence that the glass component strength is safe or adequate.

As glass does not have a well defined ultimate stress, the primary failure mechanism must be different than other commonly used building materials. The primary failure mechanism is generally accepted to be caused by stress concentrations resulting from randomly-distributed flaws on the glass surface that are intrinsic to the manufacture of float glass, and can be induced during handling or cutting of glass [33]. Thus, to reliably calculate the LR of glass components, the procedure must address the presence of surface flaws [18]. As the location, shape, size and orientation of the surface flaw initiating fracture are not known, a probabilistic method based on destructive testing can provide a reliable method to estimate the LR of glass components ([18], [2], [39], [47]).

ASTM E1300-16 [11] uses a probabilistic method known as the glass failure prediction model (GFPM) developed by Beason [18], based on a Weibull distribution. However it does not address the flaws present on the unsupported edges or the interior edge of holes resulting from the means used to cut the glass. Yew et. al. [68], Schultz et. al. [55], and Goswami and Morse [29] advanced extensions to the GFPM to include the effects of

the flaws present on the unsupported edges and/or the interior edge of holes. However, an extension of GFPM to design PSG requires flaw parameters for holes, typically based on destructive testing. Historical estimations of flaw parameters were based on interpretation of data ([18], [2], [4], [47], [55], [29]), rather than an objective and a repeatable procedure, introducing undesirable variations in the published records of flaw parameters.

This article advances the application of the well-known maximum likelihood estimator, (MLE) method tailored to the extended GFPM for holes put forward by Schultz et. al. [55] and Yew et. al. [68] to objectively estimate the flaw parameters for holes based on published destructive testing data by Cervenka [22]. Additionally, the work presents a modified GFPM for holes for heat-treated (HT) glass using a three-parameter distribution. The three-parameter distribution uses the measured residual compressive surface stress of the specimens as the shift parameter and utilizes MLE to estimate the other two flaw parameters. The extended GFPM for holes uses the MLE estimated hole parameters to calculate load and stress corresponding to different probabilities of breakages and compared them to the previous reported results. An example illustrates the LR calculation of a PSG component using the MLE estimated hole parameters and compared to the maximum allowable-stress mentioned in Table X7.1 in ASTM E1300 [11]. The current method will allow objective and repeatable estimates of flaw parameters for holes required to extend the GFPM to design PSG

4.2 Glass failure prediction model

4.2.1 Glass failure prediction model for window glass

Glass fails at a tensile stress well below its theoretical material strength due to stress concentrations occurring at the tip of microscopic flaws present on the glass surface [33]. Brown [21] determined the cumulative effect of damage to a particular flaw is constant. Hence, the rate of damage of the flaw is a function of the tensile stress magnitude at the flaw, denoted as $\sigma(P(t))$ (a function of loading time-history $P(t)$), the time required for fracture to occur, denoted as t_f , and the static fatigue constant denoted as n , equal to 16 [24] [25]. Thus Brown [21] expressed the magnitude of stress due to a particular load denoted as P_{t_d} , required to fail the same flaw for a different load and duration (t_d) as

$$\tilde{\sigma}(P_{t_d}) = \left[\frac{\int_0^{t_f} \sigma(P(t))^n dt}{t_d} \right]^{\frac{1}{n}} \quad (4.1)$$

Destructive testing of glass specimens results in varying failure load time-histories (TH), generally with varying magnitudes of load at fracture. Equation 4.1 uses the corresponding stress time-history ($\sigma(P(t))$) to normalize the temporal component of failure to a desired time, t_d , e.g. 3 sec or 60 sec resulting in an equivalent failure stress (EFS_{t_d}) and corresponding equivalent failure load (EFL_{t_d}).

The well-known Weibull distribution describes the strength of brittle materials, thus it is appropriate to describe the strength of glass [64]. Weibull [64] expressed the two-parameter cumulative probability distribution function (CDF) for a Weibull distribution [64], denoted as P_{2P} as

$$P_{2P} = 1 - \exp\left(-\lambda \cdot x^\beta\right) \quad (4.2)$$

where, x denotes the value of the random variable, λ and β denotes the shape and scale parameter, respectively. The term inside the exponent denotes the material risk function. Beason [18] showed as the area of glass increases, the probability for a critical flaw to initiate fracture increases; thus, an alternate material risk function to include the effect of area is desirable. The addition of the area factor to the material risk function creates a new distribution which does not follow a classical two-parameter Weibull distribution.

The GFPM advanced by Beason [18] includes all factors known to affect the LR of glass and expressed the corresponding CDF as

$$P_b = 1 - \exp(-B_s) \quad (4.3)$$

where, B_s represents the material risk function for glass, expressed as

$$B_s = k_s \cdot S_{m_s}(NM(GEO, BC, P), m_s) \quad (4.4)$$

where S_{m_s} denotes the equivalent area, and k_s and m_s (analogous to λ and β) denote the

surface flaw parameters. The equivalent area uses the plate geometry (GEO), boundary conditions (BC), and a load (P) in a numerical model to calculate the maximum and minimum principal stresses (σ_1 and σ_2 respectively) for each nodal area A. A biaxial correction factor (c), calculated using σ_1 and σ_2 for each nodal area, takes into account the orientation of the stress. Hence, the expression for the equivalent area is given as,

$$S_{m_s}(NM(GEO, BC, P), m_s) = \sum_{j=1}^N [(c_j \cdot \sigma_{1,j})^{m_s} \cdot A_j] \quad (4.5)$$

where ‘j’ denotes the nodal area, N denotes the number of nodes, and all other variables remain the same as defined previously. Estimation of surface flaw parameters (k_s and m_s) uses failure time-history data from destructive tests of multiple specimens with the same geometry subjected to monotonically increasing load. Due to the brittle nature of glass and the fact that location and orientation of the critical surface flaw to initiate fracture is not known, the time, magnitude of the load when fracture occurs, and the fracture location are not known until failure. Consequentially, Equation 4.1 normalizes the failure load time-histories to a common duration, t_d , commonly taken as 3 sec or 60 sec. In past publications, researchers [2], [39], [47] estimated surface flaw parameters by comparing statistical parameters such as mean, standard deviation (stdev), and coefficient of variation (cov) of the sample EFL’s to a theoretical fit using an iterative method described in detail by Beason [18]. However, the method to compare statistical parameters includes inherent variability in choosing the best surface flaw parameters as the basis of the method lies on the researchers interpretation of the data. As the criteria for selecting the best set of surface

flaw parameters does not appear in the published literature ambiguity arises in the event multiple surface flaw parameter sets produce almost the same statistical parameters (i.e. mean, stdev, cov).

4.2.2 Glass failure prediction model for heat treated glass

Heat-treated glass is annealed (AN) glass heated to near the softening point and then rapidly quenched to impart a residual compressive surface stress (RCSS). Residual compressive surface stress can vary due to tempered oven conditions including, position in oven, order, condition of quenching jet, resulting in different magnitudes in each specimen of a batch. The critical surface flaw must be in tension for the flaw tip radius to sharpen and create a stress concentration sufficient to initiate fracture [44]. Thus, an applied load must be large enough to produce a tensile stress that exceeds the RCSS before fracture can occur thereby shifting the LR proportional to the magnitude of the RCSS. Norville et al. [50] and Morse and Norville [42] advanced a modification to the GPFM material risk function to include RCSS for HT glass based on a three-parameter Weibull distribution which includes the addition of a location (shift) parameter expressed as

$$B_{s,3P} = k_s \cdot S_{m_s}(NM(GEO, BC, P), m_s, RCSS) \quad (4.6)$$

$$S_{m_s}(NM(GEO, BC, P), m_s, RCSS) = \sum_{j=1}^N (c_j \cdot (\sigma_{1,j} - RCSS))^{m_s} \cdot A_j \quad (4.7)$$

where all variables remain the same as defined previously. Afolabi et al. [4] and Natividad et al. [47] estimated the surface flaw parameters for HT glass by assuming the RCSS as the minimum measured RCSS of the sample using the method defined in ASTM C1048-18 [8] and comparing statistical parameters (i.e. mean, stdev, cov) to sample EFL. Afolabi et al. [4] modified the EFL calculations for HT specimen from Equation 4.1 to integrate the location parameter (i.e. RCSS) to be consistent with the modification to the GFPM by Norville et al. [50] and Morse and Norville [42] as

$$\tilde{\sigma}(P_{t_d}) = \left[\frac{\int_0^{t_f} (\sigma(P(t)) - RCSS_i)^{16} dt}{t_d} \right]^{\frac{1}{16}} + RCSS_i \quad (4.8)$$

where all variables remain the same as defined previously. Afolabi et al. [4] used the minimum measured RCSS of individual specimens in the calculation of the EFS for HT samples. Equation 4.6, put forward by Norville et al [50] and Morse and Norville [42], is termed as the three-parameter GFPM ($GFPM_{3P}$). The RCSS in the equation is analogous to the location parameter in a three-parameter Weibull distribution.

4.2.3 Glass failure prediction model for edges and holes in tension

Walker and Muir [62], while investigating louvre glass recognized the edges and the surface were stressed to the same magnitude. Since flaws exist on the surface, the edge faces, and the edge-lines, each with different geometries and distributions, Walker and Muir [62]

extended the GFPM to include the effect of both edges in addition to the surface to calculate the LR of louvre glass expressed as

$$B_l = B_s + B_e \quad (4.9)$$

In Equation 4.9, B_l denotes the risk function for the louvre glass, and B_s and B_e denote the risk functions for the surface and edges, respectively. The surface risk function, although reformatted, is essentially the same as advanced by Beason [18] and remains a function of specimen surface area. Whereas, the additional edge risk function is a function of the edge length, as the thickness of the edge is small compared to the length. Using algebraic manipulation, the risk functions, B_s and B_e can be transformed to a similar format as the GFPM in Equation 4.4. Here, the median failure stress of a surface element of unit area, σ_{os} , and median failure stress of edge element of unit length, σ_{oe} , in Equation 8 in Walker and Muir [62] formatted as k_s and k_e , respectively [61].

Goswami and Morse [29] showed that the flaws along the edge are a combination of flaws on the edge-face and the two edge-lines (the interface between the edge-face and the surface), by putting one edge-line in tension and other unstressed using a novel four-point bending test of a glass specimen. To address the flaws along the edge-line, Goswami and Morse [29] propose the following modified risk function for edge-lines utilizing a similar

approach as Walker and Muir [62]

$$B_{el} = k_{el} \cdot S_{m_{el}}(NM(GEO, BC, P), m_{el}) \quad (4.10)$$

where, k_{el} and m_{el} denote edge-line flaw parameters, and $S_{m_{el}}$ denotes the equivalent length expressed as

$$S_{m_{el}}(NM(GEO, BC, P), m_{el}) = \sum_{j=1}^N (\sigma_{1,j})^{m_{el}} L_j \quad (4.11)$$

$\sigma_{1,j}$ denotes MPTS for the j^{th} length element, N denotes the number of nodes, and L_j denotes the j^{th} nodal length. The risk function excludes the biaxial correction factor, denoted as c_j because the stresses induced in an edge-line is typically uniaxial in nature. Schultz et al. [55] used a similar risk function to calculate the LR of glass specimen with a hole, referred here in as $GFPM_{2H}$, where $\sigma_{1,j}$ denotes the MPTS for the length element j along the edge of the hole. Walker and Muir [62], Schultz et al. [55], and Goswami and Morse [29] also estimated the GFPM flaw parameters by comparing statistical parameters (i.e. mean, stdev, COV) to the sample EFL's.

4.3 Procedure to estimate flaw parameters for glass failure prediction model for holes

Historically, flaw parameters were estimated based on the researchers' interpretation of the data, thereby inducing inherent variability in choosing flaw parameter [18], [2], [4], [47], [55], [29]. Because the criteria to select the best set of flaw parameters were not provided, ambiguity exists when others attempt to recreate the flaw parameters from the historical data as different sets of flaw parameters appear to fit one or more of the three statistical measures well. Hence, it is desirable to have a transparent, consistent, and repeatable method to estimate flaw parameters tailored to the GFPM. Different estimation methods exist that provide a clear, repeatable procedure to estimate distribution parameters for commonly used distributions, (e.g. Normal, Log-normal, Weibull, Gumble, etc.) The maximum likelihood estimation (MLE) method is often used as it works for most distribution types and is conceptually simple. Because the GFPM is based on a Weibull distribution with a modified material risk function, it should be possible to apply the MLE method to estimate the flaw parameters of the GFPM. Pisano and Carfangi [53] showed the MLE method can be applied to the GFPM for ring-on-ring test data, suggesting it can be applied to failure data for other geometric and loading conditions. The current section advanced the application of the MLE method to the $GFPM_{2H}$ and introduces a three parameter GFPM for holes ($GFPM_{3H}$) to address heat-treated glass.

4.3.1 Application of maximum likelihood estimator to glass with holes

ASTM C1239-13 [10] provides a procedure for the computational technique, MLE method, to estimate the scale and shape parameters for a two-parameter Weibull distribution. The MLE method estimates the scale and shape parameters by maximizing a likelihood function so the parameters provide the highest value of the joint probability distribution function of the observed data. The likelihood function is defined as the product of the two-parameter Weibull probability distribution function (PDF) for each random variable in the sample. The PDF denoted as $f(x, \lambda, \beta)$ of a two-parameter Weibull distribution is obtained by differentiating with respect to the random variable x in the CDF denoted as $F(x, \lambda, \beta)$ which is equal to P_{2P} (Equation 4.2) and expressed as

$$f(x, \lambda, \beta) = \frac{d}{dx}F(x, \lambda, \beta) = \frac{d}{dx}(P_{2P}) \quad (4.12)$$

where all variables remain the same as defined previously and assumed to be independent.

Thus, the likelihood function $L(\lambda, \beta)$ becomes

$$L(\lambda, \beta) = \prod_{i=1}^{n_{sam}} f(x_i, \lambda, \beta) \quad (4.13)$$

where n_{sam} denotes the number of values of the independent random variable. The estimates are obtained by solving the set of equations resulting from setting the partial derivatives of the natural log of the likelihood function with respect to the unknown variables (λ and β) to zero. The equations resulting from the partial derivatives are solved numerically using a root finding algorithm because analytical solutions do not exist. Similar to a two-parameter Weibull distribution, the PDF and the likelihood function can be defined for a GFPM for holes as follows.

The expression for the $GFPM_{2H}$ or the CDF for holes, referred as the probability of breakage for glass with holes, after substituting Equation 4.10 into Equation 4.3 results in

$$P_b = F(EFL, K_H, m_H) = 1 - \exp\{-k_H \cdot S_{m_H}(NM(GEO, BC, EFL), m_H)\} \quad (4.14)$$

where, k_H and m_H denote hole flaw parameters, S_{m_H} denotes the equivalent hole length and all other variables remaining same as defined previously. The expression for the equivalent hole length, S_{m_H} becomes

$$S_{m_H}(NM(GEO, BC, EFL), m_H) = \sum_{j=1}^N (\sigma_{1,j})^{m_H} \cdot L_j \quad (4.15)$$

where all variables remain the same as defined before. In the two-parameter Weibull distribution, the random variable x is not a function of any other variable. Whereas in the $GFPM_{2H}$ the random variable $\sigma_{1,j}$ is a function of the location of the element around the

hole. Thus, the introduction of γ_j converts the random variable $\sigma_{1,j}$ in the $GFPM_{2H}$ to an independent variable (independent of the location). The term γ_j denotes the ratio between the elemental stress for the j^{th} length element ($\sigma_{1,j}$) to the EFS of the specimen (σ_{EFS}). Thus the $GFPM_{2H}$ becomes analogous to the two-parameter Weibull distribution i.e. a function of m_H, k_H and the random variable σ_{EFS} . Thus, the equivalent hole length becomes

$$S_{m_H}(NM(GEO, BC, EFL), m_H) = (\sigma_{EFS})^{m_H} \sum_{j=1}^N (\gamma_j)^{m_H} \cdot L_j \quad (4.16)$$

The MLE method estimates the flaw parameters by maximizing the likelihood function based on the PDF (Equation 4.17b) of the distribution. The product form of the likelihood function is denoted as $L(k_H, m_H)$ and is expressed as Equation 4.17c. The equation can be translated to a summation by taking the natural logarithm as expressed in Equation 4.17d,

simplifying the derivation.

$$f(EFL, k_H, m_H) = \frac{d}{d(EFL)} F(EFL, k_H, m_H) \quad (4.17a)$$

$$= k_H \frac{d}{d(EFL)} \cdot (S_{m_H}(NM(GEO, BC, EFL), m_H)) \cdot \exp(-k_H \cdot S_{m_H}(NM(GEO, BC, EFL), m_s)) \quad (4.17b)$$

$$L(k_H, m_H) = \prod_{i=1}^{n_{sam}} \left\{ k_H \cdot \frac{d}{d(EFL)} \cdot (S_{m_H}(NM(GEO, BC, EFL), m_H)_i) \exp\{-k_H \cdot (S_{m_H}(NM(GEO, BC, EFL), m_H)_i)\} \right\} \quad (4.17c)$$

$$\ln\{L(k_H, m_H)\} = \sum_{i=1}^{n_{sam}} \left[\ln(k_H) + \ln\left(\frac{d}{d(EFL)} \cdot (S_{m_H}(NM(GEO, BC, EFL), m_H)_i)\right) - k_H \cdot (S_{m_H}(NM(GEO, BC, EFL), m_H)_i) \right] \quad (4.17d)$$

where, n_{sam} denotes the number of independent random variable values, (i.e., the number of specimens loaded to failure). The scale parameter k_H , is estimated by equating the term obtained from differentiating the natural logarithm of the likelihood equation (Equation 4.17d) with respect to k_H , to zero. Because, $S_{m_H}(NM(GEO, BC, EFL), m_H)$ is not a function of k_H , rearranging the terms the scale parameter k_H becomes

$$\frac{d}{dk_H} \ln\{L(k_H, m_H)\} = \sum_{i=1}^{n_{sam}} \left[\frac{1}{k_H} - (S_{m_H}(NM(GEO, BC, EFL), m_H)_i) \right] = 0 \quad (4.18a)$$

$$k_H = \frac{n_{sam}}{\sum_{i=1}^{n_{sam}} [(S_{EFS,i})^{m_H} \cdot \sum_{j=1}^N \{(\gamma_{j,i})^{m_H} \cdot L_{j,i}\}]} \quad (4.18b)$$

The shape parameter, m_H is estimated by equating the term obtained from differentiating the natural logarithm of the likelihood equation, Equation 4.17d with respect to m_H to zero, resulting in

$$\begin{aligned} \frac{d}{dm_H} \ln\{L(k_H, m_H)\} = \sum_{i=1}^{n_{sam}} \left[\frac{d}{dm_H} \ln\left(\frac{d}{d(EFL)} \cdot (S_{m_H}(NM(GEO, BC, EFL), m_H)_i) \right. \right. \\ \left. \left. - k_H \cdot \frac{d}{dm_H} (S_{m_H}(NM(GEO, BC, EFL), m_H)_i) \right] = 0 \end{aligned} \quad (4.19)$$

Partial differentiation of the terms with respect to m_H results in

$$\begin{aligned} \frac{d}{dm_H} S_{m_H}(NM(GEO, BC, EFL), m_H) = (\sigma_{EFS})^{m_H} \cdot \left[\ln(\sigma_{EFS}) \cdot \left\{ \sum_{j=1}^N (\gamma_j)^{m_H} \cdot L_j \right\} \right. \\ \left. + \sum_{j=1}^N (\gamma_j)^{m_H} \cdot \ln(\gamma_j) \cdot L_j \right] \end{aligned} \quad (4.20a)$$

$$\begin{aligned} \frac{d}{dm_H} \ln\left(\frac{d}{d(EFL)} \cdot (S_{m_H}(NM(GEO, BC, EFL), m_H)_i)\right) = \frac{1}{m_H} + \ln(\sigma_{EFS}) \\ + \frac{d}{dm_H} \ln \left\{ \sum_{j=1}^N (\gamma_j)^{m_H} \cdot L_j \right\} \end{aligned} \quad (4.20b)$$

Rearranging the equation obtained from substituting the value of k_H from Equation 4.18b and the partial differentiation terms from Equation 4.20a and Equation 4.20b into Equation 4.19 produces an equation that has only one unknown variable, i.e. the parameter m_H

$$\frac{1}{m_H} + \frac{1}{n_{sam}} \sum_{i=1}^{n_{sam}} \ln(\sigma_{break,i}) + \frac{d}{dm_H} \ln \left\{ \sum_{j=1}^N (\gamma_j)^{m_H} \cdot L_j \right\} - \frac{A}{B} = 0 \quad (4.21)$$

where

$$A = \sum_{i=1}^{n_{sam}} (\sigma_{break,i})^{m_H} \cdot \left[\ln(\sigma_{break,i}) \cdot \left\{ \sum_{j=1}^N (\gamma_j)^{m_H} \cdot L_j \right\} + \sum_{j=1}^N (\gamma_j)^{m_H} \cdot \ln(\gamma_j) \cdot L_j \right]$$

$$B = \sum_{i=1}^{n_{sam}} [(\sigma_{break,i})^{m_H} \cdot \sum_{j=1}^N \{(\gamma_j)^{m_H} \cdot L_j\}]$$

Equation 4.21 is solved using a root finding algorithm because an analytical solution is not available. The scale parameter, k_H is calculated after substituting the value of m_H into Equation 4.18b.

4.3.2 Glass failure prediction model and parameter estimation for heat-treated glass with holes

While the $GFPM_{2H}$ adequately predicts the load resistance for heat-treated glass components with a hole [55], it does not address changes due to RCSS. The authors advance a modification to the GPFM material risk function for holes and edge-lines (Equation 4.10) to include RCSS for HT glass with holes. The modification is consistent with Norville et al. [50], and Morse and Norville [42], to include RCSS as the location parameter expressed

as

$$B_{el,3p} = k_H \cdot S_{m_H}(NM(GEO, BC, EFL), m_H, RCSS) \quad (4.22)$$

where,

$$S_{m_H}(NM(GEO, BC, EFL), m_H, RCSS) = \sum_{j=1}^N (\sigma_{1,j} - RCSS)^{m_H} \cdot L_j \quad (4.23)$$

where, all the variables remain the same as previously defined. Because the distribution has three parameters, (i.e. the two hole flow parameters, k_s and m_s , and the location parameter), the risk function is referred to as three-parameter GFPM for holes ($GFPM_{3H}$). As inter-dependency of the three parameters exist, multiple sets of parameters are obtained while using MLE to determine flow parameters for a single sample set. Thus, to have a unique set of hole parameters, the parameters are estimated based on predetermined value of location parameter (i.e. measured value of RCSS). Hole parameters for the $GFPM_{3H}$ are estimated using the MLE by defining the natural logarithm of the likelihood function expressed as

$$\ln\{L(k_H, m_H)\} = \sum_{i=1}^{n_{sam}} \left[\ln \left(\frac{d}{d(EFL)} (S_{m_H}(NM(GEO, BC, EFL), m_H, RCSS)) \right) - k_H \cdot S_{m_H}(NM(GEO, BC, EFL), m_H, RCSS) \right] \quad (4.24)$$

The scale and the shape parameters resulting from solving the partial differentiation of the natural logarithm of the likelihood equation, Equation 4.24, with respect to the scale and shape parameter, yielding

$$k_H = \frac{n_{sam}}{\sum_{i=1}^{n_{sam}} \left[\sum_{j=1}^N \{(\sigma_{EFL,i} \cdot \gamma_j - RCSS)^{m_H} \cdot L_j\} \right]} \quad (4.25)$$

and

$$\frac{1}{m_H} + \frac{1}{n_{sam}} \sum_{i=1}^{n_{sam}} \left\{ \frac{A}{B} \right\} - \left\{ \frac{C}{D} \right\} = 0 \quad (4.26)$$

where

$$\begin{aligned} A &= \sum_{j=1}^N (\sigma_{EFL,i} \cdot \gamma_{j,i} - RCSS)^{m_H-1} \cdot \ln(\sigma_{EFL,i} \cdot \gamma_{j,i} - RCSS) \cdot \gamma_{j,i} \cdot L_{j,i} \\ B &= \sum_{j=1}^N (\sigma_{EFL,i} \cdot \gamma_{j,i} - RCSS)^{m_H-1} \cdot \gamma_{j,i} \cdot L_{j,i} \\ C &= \sum_{i=1}^n \left\{ \sum_{j=1}^N (\sigma_{EFL,i} \cdot \gamma_{j,i} - RCSS)^{m_H} \cdot \ln(\sigma_{EFL,i} \cdot \gamma_{j,i} - RCSS) \cdot L_{j,i} \right\} \\ D &= \sum_{i=1}^n \left\{ \sum_{j=1}^N (\sigma_{EFL,i} \cdot \gamma_{j,i} - RCSS)^{m_H} \cdot L_{j,i} \right\} \end{aligned}$$

Similar to Equation 4.21, the only term unknown in Equation 4.26 is m_H , that can be computed numerically. The scale parameter k_H can be subsequently calculated by substituting the value of m_H obtained solving Equation 4.26 in equation 4.25.

4.4 Estimation of glass failure prediction model parameters for holes

4.4.1 Experimental failure data for glass specimen with a hole

Cervenka [22], using a four-point bending test, monotonically loaded to failure, ten fully tempered (FT) monolithic glass specimens with a water-jet cut hole (Figure 4.1). The nominal specimen size was 400 mm × 200 mm × 12.5 mm with a 36.4 mm diameter hole located at the center. The measured dimensions and RCSS value of each specimen is repeated in Table 4.1 for convenience of the reader.

Table 4.1
Measured specimen data

Specimen	Thickness, (t) (mm)	Width, (b) (mm)	Hole diameter, (d) (mm)	RCSS (MPa)
4H1	12.4	205	36.3	104
4H2	12.5	203	36.3	130
4H3	12.6	204	36.3	122
4H4	12.6	204	36.3	138
4H5	12.5	203	36.3	130
4H6	12.6	204	36.3	116
4H7	12.3	204	36.3	116
4H8	12.6	204	36.3	130
4H9	12.3	202	36.3	104
4H10	12.3	204	36.3	122

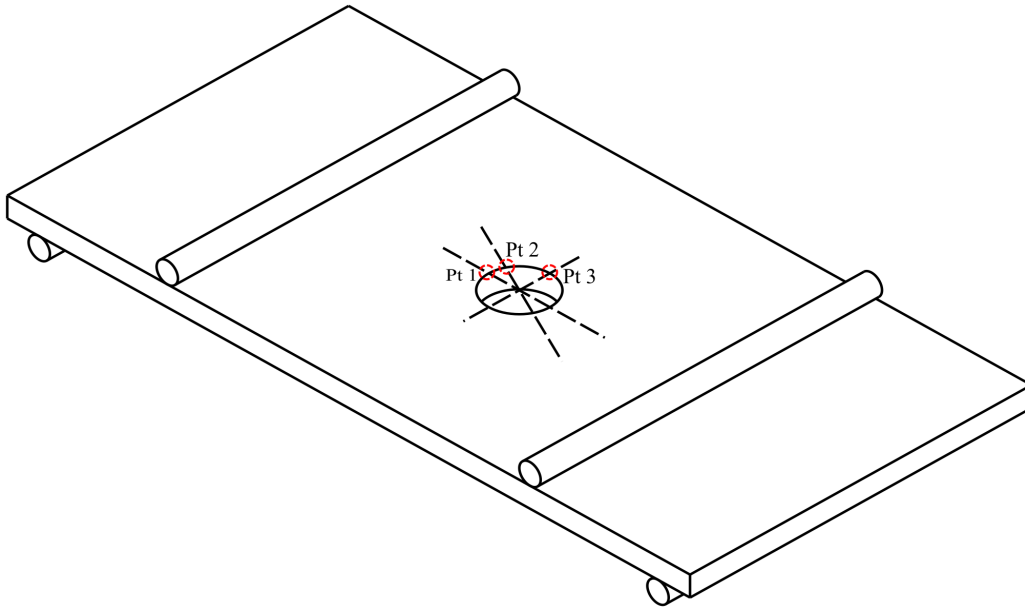


Figure 4.1: Specimen with holes

4.4.2 Equivalent failure loads for glass specimens with a hole

Before the specimen test data from Cervenka [22] can be used to estimate the $GFPM_{2H}$ and $GFPM_{3H}$ parameters, they must be normalized using Equations 4.1 or 4.8 (depending on specimen heat-treatment) to a common load duration as the glass specimens failed at different load duration and magnitude combinations. Calculation of stress associated with each load recorded in the time-history, $\sigma(P(t))_i$, with a finite element model (FEM) adjusted to the measured dimensions of each specimen, results in a large number of simulations (~ 2000). To reduce the time and effort required to perform the normalization of the failure data, several simplifying assumptions and models were employed. Due to the

fulminate nature of fully tempered specimen failure, it is difficult to determine the location of fracture, thus it is assumed fracture initiates at the location of maximum principal tensile stress. The maximum principal tensile stress (MPTS) is located near the edge-line of the hole (identified in Figure 4.1 as point 3) due to the specimen geometry and the presence of the hole at the center that causes a stress concentration [35]. Additionally, because the water-jet cutting process creates flaws at the edge-line of the hole, presumably with a different distribution and severity than those present on the surface [29], coupled with the polished parameter edges, the likelihood that fracture will initiate at or near the location of maximum principal stress increases. Based on the stated assumptions, the stress at the presumed location of fracture is estimated using the well known Euler–Bernoulli equation for beams with a stress concentration factor. Cervenka [22] determined a 1.59 stress concentration factor adequately agrees with the stresses calculated from Euler–Bernoulli beam equation to the FEM results from models that were calibrated with strain gauge measurements recorded near the hole. The authors then used Equation 4.1 to convert the recorded failure load TH to an EFL_{3s} for the $GFPM_{2H}$, denoted as 2P. While the authors used Equation 4.8, with measured RCSS for each specimen to convert the recorded failure load TH to an EFL_{3s} for the $GFMP_{3H}$ denoted as 3P. Table 4.2 lists the test load magnitude and time to failure for each specimen with the failure stress, EFS_{3s} and EFL_{3s} for both 2P and 3P. Table 4.2 is arranged in an ascending order according to the RCSS of the specimen, and in case of equal RCSS amongst specimen, in ascending order according to calculated EFL_{3s} . An additional set of notations (letters) were added to facilitate easy referencing in figures.

Table 4.2
Failure load and stress and EFS and EFL for specimens

Specimen	Recorded Data		Peak Failure stress (MPa)	2P		3P	
	Failure load (kN)	Failure time (sec)		EFS_{3s} (MPa)	EFL_{3s} (kN)	EFS_{3s} (MPa)	EFL_{3s} (kN)
A (4H9)	10.8	159	155	160	11.2	153	10.7
B (4H1)	13.4	120	189	203	14.4	191	13.6
C (4H7)	13.9	153	198	203	14.3	196	13.8
D (4H6)	14.3	159	194	204	15.0	194	14.3
E (4H3)	13.7	136	188	194	14.1	186	13.5
F (4H10)	14.2	168	203	217	15.2	204	14.3
G (4H2)	13.6	123	189	203	14.7	189	13.6
H (4H5)	14.2	124	196	201	14.5	193	14.0
I (4H8)	14.1	176	194	201	14.6	192	14.0
J (4H4)	13.2	136	182	192	14.0	181	13.2

4.4.3 Estimation of two parameter glass failure prediction model parameters for holes

The calculation for EFL_{3s} is based on the single largest MPTS located at point 3 in Figure 4.1. Whereas, estimation of hole parameters using Equation 4.14 requires MPTS ($\tilde{\sigma}(P)_{max,j}$) for each length element, ‘j’ along the hole edge-line. Stresses around the hole is calculated using the FEM advanced by Schultz et al. [55]. Additionally, Schultz et al. [55] showed all MPTS along the edge-line vary linearly with the applied load for a beam in 4-point bending. Figure 4.2 shows the variation of the ratio of the stresses, γ_j corresponding to each length element, ‘j’ to the single largest MPTS or EFS_{3s} for a specimen. Equation 4.21 and Equation 4.18b uses the 2P EFL_{3s} ’s to estimate the scale and shape parameter resulting in $m_H = 20.2$ and $k_H = 1.23 \times 10^{-48} mm^{2 \cdot m_H - 1} \cdot N^{-m_H}$. Table 4.3 lists the 2P

EFL_{3s} 's mean, stdev and cov, the $2P EFL_{3s}$ hole parameters reported in Schultz et al. [55] denoted as $2P_{schultz}$, the hole parameters estimated using the MLE method denoted as $2P_H$ and their corresponding mean, stdev and cov.

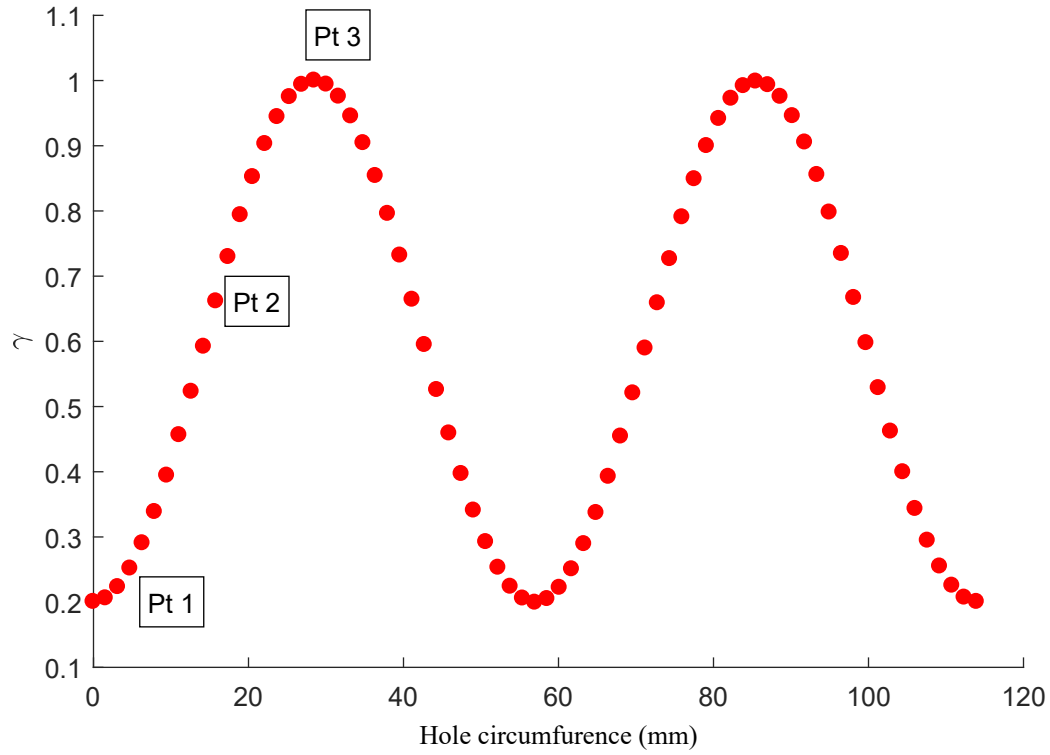


Figure 4.2: Variation of γ around the hole

Table 4.3
2 parameter hole estimates and statistical measures

	m_H	k_H $mm^{(2m_H-1)}N^{-m_H}$	Mean (kN)	Std. Dev (kN)	cov
$2P EFL_{3s}$	-	-	14.2	1.13	7.98
$2P_{schultz}$	15.25	5.06 E-37	13.9	1.10	7.97
$2P_H$	20.2	1.23 E-48	14.0	0.86	6.1

The MLE method estimates parameters that are closer to the mean of the $2P EFL_{3s}$ compared to the parameters estimated by Schultz et al. [55] (1.41 % versus 2.11 %), whereas

the stdev and the cov parameters estimated by Schultz et al. [55] are closer to the EFL_{3s} (2.65% and 0.13% versus to 23.9% and 23.6 %), respectively. A graph (Figure 4.3) of the two $GFPM_{2H}$ provides an insightful means to compare them to the EFL_{3s} 's because a numerical comparison of the estimated m_H and k_H values is not meaningful. EFL_{3s} from Table 4.2 are ranked in ascending order ($i = 1$ to n_{sam}) and median rank probability estimators, E_i , are assigned to each EFL_{3s} according to Equation 4.27 [28]; [27].

$$E_i = \frac{i - 0.3}{n_{sam} + 0.4} \quad (4.27)$$

where, i = rank of the EFL of specimen, and n_{sam} denotes the number of specimen in the sample. Figure 4.3 plots the $2P_H$, and $2P_{schultz}$ with the ranked $2P EFL_{3s}$. The 3-sec uniform load, (P_{3s}) on the x-axis and the probability of breakage, p_b , or median rank probability on the y-axis ($\ln(\ln(1/(1-p_b)))$ scale).

The median rank estimator for the lowest $2P EFL_{3s}$ (specimen 4H-9) is found to be an outlier according to ASTM E178-21 [14], but ASTM E178-21 [14] also mentions an outlier can be due to the inherent variability in the data and should be retained and processed if found to be true. Because there was no report of preexisting damage or issues during the load test for specimen 4H-9, the $2P EFL_{3s}$ data for 4H-9 is considered to be a valid observation and retained in the sample. ASTM E1300-16 [11] defines the load resistance as a 3-sec uniform lateral load corresponding to a p_b equal to 0.008. Additionally, AAMA GDSG-1-87[1] recommends a load resistance corresponding to a p_b equal to 0.001 for

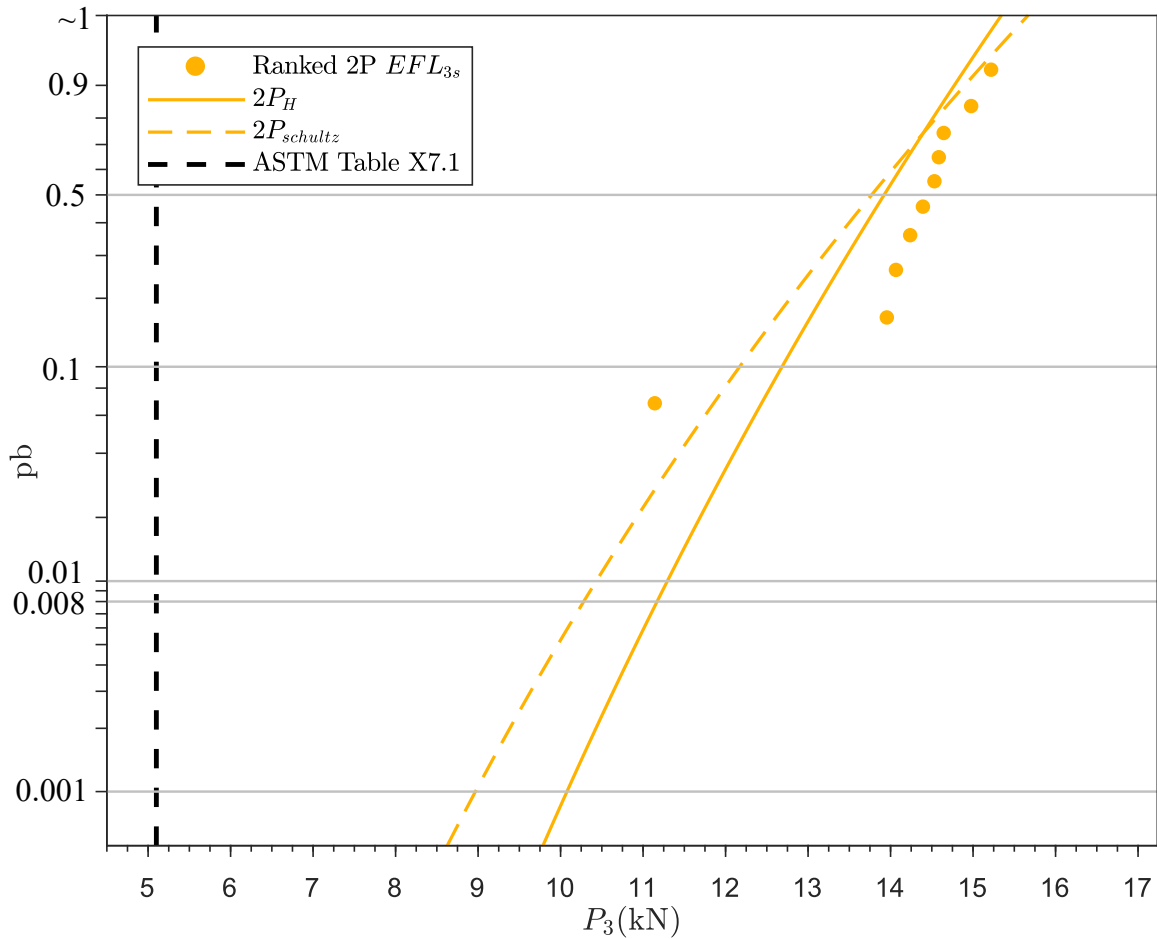


Figure 4.3: Cumulative distribution fit of a 2P GFPM for holes vs EFL_{3s}

overhead sloped glazing. Therefore, variations of the estimated load resistances at these pb's are used for comparisons. The difference between the P_{3s} of the two CDF's at a pb equal to 0.008 and 0.001 is 0.9 kN or 8.74%, and 1.13 kN or 12.6 %, respectively. The result suggests the parameters estimated using the MLE method are not as strongly affected by the lowest EFL.

Although, ASTM E1300-16 [11] is not intended for designing PSG or glass with a hole, engineers often design PSG by limiting the stresses around the hole to the allowable stress

mentioned in Table X7.1 [11]. Table X7.1 in ASTM E1300-16 [11] provides an approximate maximum allowable edge-stress to design non-rectangular glass shapes and/or alternate edge support conditions where the edge stress is significant such that the p_b for the design is less than or equal to 0.008 for a 3-s load duration. The process of cutting a hole in glass creates a special edge, likely with a different distribution of flaws than a scored edge resulting from cutting the glass to the desired geometry. It is assumed the heat-treatment process likely reduces the severity of the flaws on the hole edge-line to a similar extent as the cut edges of the specimen. Furthermore, the specimen edges and the hole edge were polished prior to heat-treatment, thus the fully tempered maximum allowable stress for polished edges is a reasonable value to use to calculate a corresponding load resistance for comparison to those from the GFPMs. Thus, for the specimen geometry, the maximum allowable stress around the hole should be limited to 73.0 MPa which corresponds to a 5.1 kN load resistance, represented in the Figure 4.3 with a dashed black line. The load corresponding to the maximum allowable stress in ASTM E1300-16 [11] is 5.18 kN smaller than $2P_{schultz}$ and 6.07 kN smaller than $2P_H$. The large difference suggest the hole edge is stronger than a regular edge, possibly due to a significantly larger RCSS around the hole.

4.4.4 Estimation of three parameter glass failure prediction model parameters for holes

The 3P EFL_{3s} from Table 4.2 are used to estimate the hole parameters for $GFPM_{3H}$ in Equation 4.22 using the same γ_j as for the $GFPM_{2H}$ parameter estimation. The determination of the $GFPM_{3H}$ parameters requires the selection of a representative RCSS value for the entire sample set. Since the sample exceeds the minimum RCSS value (69 MPa) for a fully tempered glass (ASTM C1048-18 [8]), 69 MPa could be used for the location parameter value. However, as 69 MPa is significantly lower than the minimum, mean or maximum of the measured sample RCSS's, using 69 MPa would shift the basis of the flaw parameter fit. Consequently, using the flaw parameters based on the lower 69 MPa value with the measured RCSS values of the sample would produce larger load resistances than were actually measured, indicating the selection of a representative RCSS value for the entire sample set must be related to the measured RCSS values of the specimens.

While devices are available to measure the RCSS at or near edges and holes, they are not commonly used for architectural and structural glass components. Furthermore, as the RCSS rapidly changes near edges, measurements at edges are often not as repeatable as those measured at locations away from the edges ([40], [49]). Unlike edges, the RCSS is typically larger at the interface between a hole and the surface plane [49]. Coupled with the multiple factors that affect the RCSS near holes (hole diameter, distance to the nearest edge

or corner, glass thickness, among others) it is reasonable to use a RCSS value measured at a location away from the hole and edges, (i.e. somewhere in the middle of the glass surface). Because RCSS typically varies for each specimen of a batch in addition to variation across the surface of each specimen [8], the representative value for the sample RCSS should be based on a statistical measure such as the minimum, mean, or maximum of the measured sample RCSS's. However, considering the assumed 69 MPa example discussed previously, simply taking the minimum measured RCSS value will likely result in larger predicted load resistances than is appropriate. To explore the effect of $GFPM_{3H}$ hole parameters based on the various statistical measures on the predicted load resistance, three sets of hole parameters are estimated by solving Equation 4.26 and Equation 4.25 based on the minimum, mean and maximum measured sample RCSS denoted as $3P_{H,\overline{RCSS}}$, $3P_{H,\overline{RCSS}}$, and $3P_{H,\widehat{RCSS}}$, respectively. Table 4.4 lists the 3P EFL_{3s} 's mean, stdev, and cov and the 3P hole parameters estimated using the MLE method for each RCSS statistical measure (minimum, mean, or maximum) with their the corresponding $GFPM_{3H}$ mean, stdev and the cov for each.

Table 4.4
3 parameter hole estimates and statistical measures

	m_H	$\frac{k_{el}}{mm^{(2m_H-1)} N^{-m_H}}$	Base RCSS (MPa)	Mean (kN)	Std. Dev (kN)	cov
$3P EFL_{3s}$	-	-	-	13.5	1.05	7.75
$3P_{H,\overline{RCSS}}$	9.42	3.04E-20	104	13.1	0.73	5.54
$3P_{H,\overline{RCSS}}$	7.24	2.46E-15	121	13.1	0.73	5.59
$3P_{H,\widehat{RCSS}}$	4.94	1.66E-10	138	13.1	0.76	5.80

ip

The three parameters estimated for the $GFPM_{3H}$ have minimum differences between the mean, stdev, and cov indicating the parameters are not strongly influenced by the RCSS magnitude. Figure 4.4 shows the three $3P_H$ distribution with the $2P_H$ distribution and their corresponding ranked ELF'_{3s} with 3-sec uniform load, (P_{3s}) on the x-axis and the probability of breakage P_b , or median rank probability on the y-axis ($\ln(\ln(1/(1-P_b)))$ scale). Figure 4.3 also shows the load resistance (5.1 kN) based on the E1300 maximum allowable stress of 73.0 MPa around the hole for the specimen geometry with a dashed black line. Figure 4.4 shows the ranked $3P$ ELF_{3s} shifted to the left and $P3P_H$'s have a more pronounced curvature compared to the ranked $2P$ ELF_{3s} and $2P_H$, respectively, due to the inclusion of the location parameter. The percent difference between the three $P3P_H$ evaluated for pb's between 0.008 and 0.001 is less than 4%, thus it is unclear which $P3P_H$ parameter set best represents the sample data.

The negligible difference between pb's from the three $3P_H$ parameter sets at design level pb's requires further analysis to determine which of the three $3P_H$ parameter sets best represents the sample set data. Each set of hole parameters are based on a single representative RCSS that are based on the measured specimen RCSS's (min, mean, max). Therefore, a comparison between the pb's calculated using the base RCSS versus the measured RCSS for each specimen for the corresponding EFL_{3s} may provide a useful measure to determine a base RCSS to best represent the sample set. The authors used Equation 4.28 to calculate the difference between pb's for each of the individual EFL_{3s} 's calculated for each of the three hole parameters and corresponding measured RCSS and base RCSS.

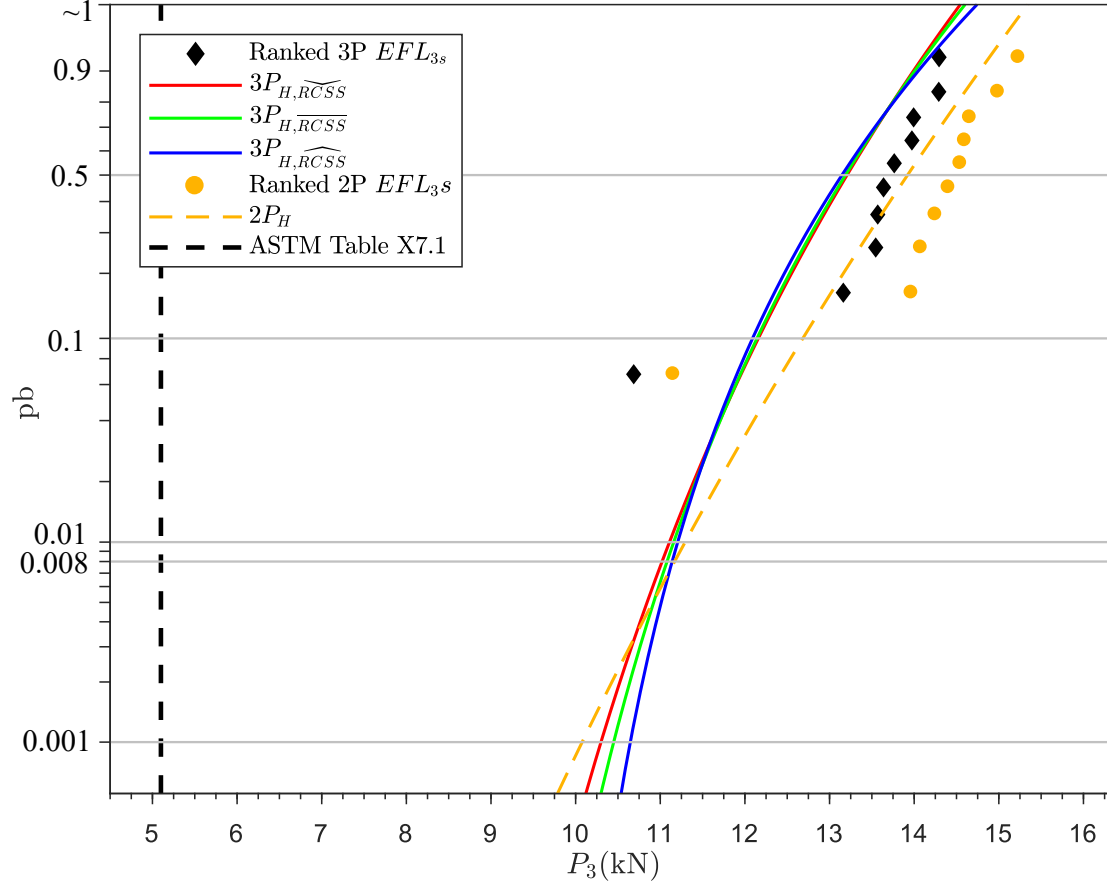


Figure 4.4: Cumulative distribution fit for $P3P_H$ vs EFL_{3s}

$$pb_{diff} = e^{-k_H \sum_{j=1}^N (\tilde{\sigma}(P)_{max,j} - RCSS_{measured})^{m_H} \cdot L_j} - e^{-k_H \sum_{j=1}^N (\tilde{\sigma}(P)_{max,j} - RCSS_{base})^{m_H} \cdot L_j} \quad (4.28)$$

where, k_H and m_H denotes hole parameters from Table 4.4, $RCSS_{measured}$ denotes the measured RCSS (Table 4.1), $RCSS_{base}$ denotes the base RCSS for the hole parameters (Table 4.4), and $\tilde{\sigma}(P)_{max,j}$ denotes the corresponding stress for individual EFL_{3s} . Figure 4.5 shows the pb_{diff} where the red, green, and blue bars represent the difference in pb using the $3P_{H,RCSS}$, $3P_{H,RCSS}$, and $3P_{H,RCSS}$ hole parameters, respectively. Figure 4.5 also shows

the average pb_{diff} with a horizontal line for each base RCSS. A positive average pb_{diff} using the $3P_{H,\overline{RCSS}}$ hole parameters suggests the fit with the minimum RCSS overestimates the pb. Similarly, a negative pb_{diff} using $3P_{H,\widehat{RCSS}}$ hole parameters indicates the fit with the maximum RCSS underestimates the pb. The $3P_{H,\overline{RCSS}}$ tends to both overestimate and underestimate the pb, thus neutralizing the effect to an extent. The average of pb_{diff} using $3P_{H,\overline{RCSS}}$ indicates the fit using mean RCSS overestimates the pb a little. Thus, hole parameters based on a RCSS that will have an average pb_{diff} near about equal to zero will likely best represent the failure data. An iterative root finding algorithm is used to converge on a base RCSS equal to 126 MPa with an average pb_{diff} nearly equal to zero. Figure 4.5 presents the difference in pb using RCSS equal to 126 MPa as the black bars. The corresponding hole parameters m_H and k_H were estimated as 6.65 and $4.60 \times 10^{-14} \text{ mm}^{(2m_H-1)} N^{-m_H}$, respectively, for the base RCSS 126 MPa.

The effects of using the estimated $2P_H$ and $3P_H$ hole parameters on the predicted load resistance for a PSG is explored with an example. A FT PSG of similar geometry to Cerevanka's experiment [22], (i.e. a rectangular specimen of 400 mm \times 200 mm \times 12.5 mm with a 36.4 mm diameter hole at the center) is used to create LR's as a function of pb. One of the essential parameters to design FT PSG is the RCSS of the glass, which is usually not known in advance. Thus, fully tempered glass is commonly designed assuming the RCSS of the glass as 69 MPa, as per ASTM C1048-18 [8]. Because, a location parameter is not associated with the $GFPM_{2H}$, the PSG LR calculated using Equation 4.10 with the estimated $2P_H$ parameters does not change with RCSS (Figure 4.3). Hence, to take into

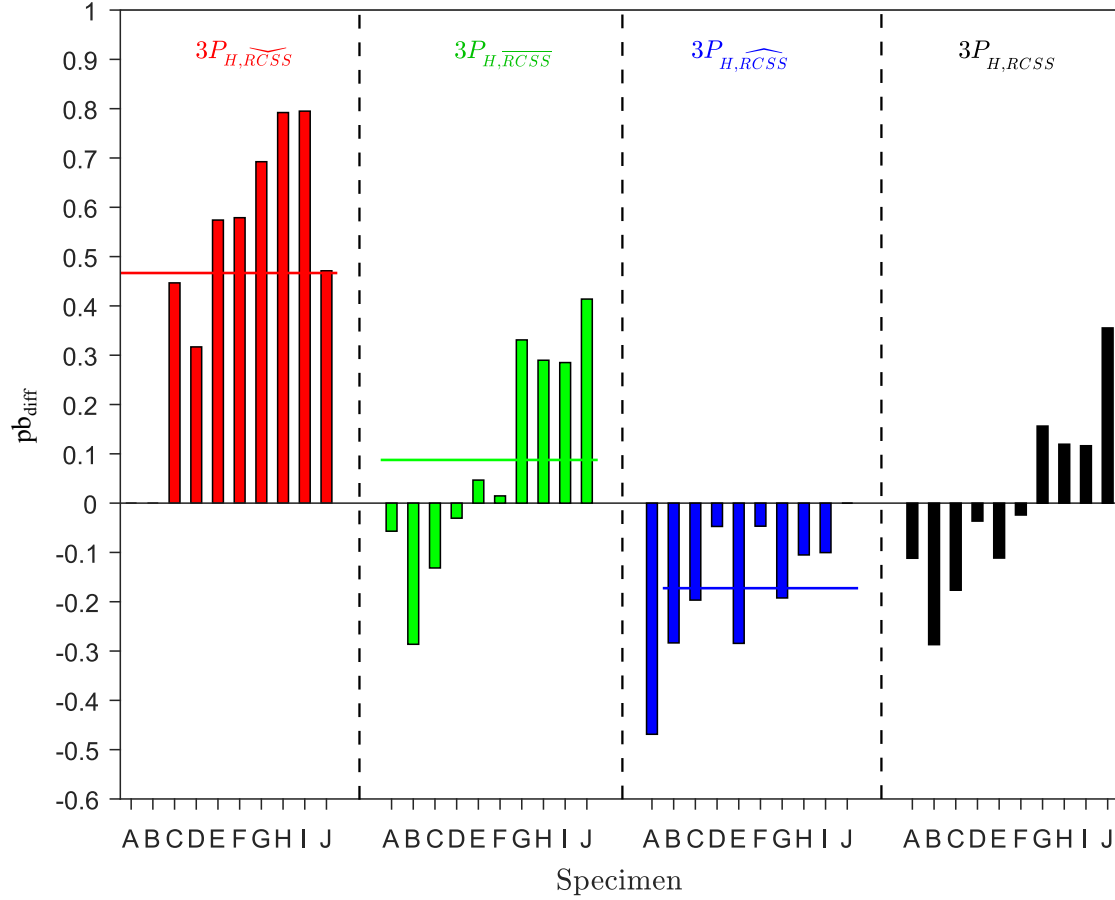


Figure 4.5: Difference in pb calculated using hole parameters with estimated RCSS and measured RCSS

account the RCSS of the specimen during designing of FT PSG with $GFPM_{2H}$, a pseudo $GFPM_{3H}$ is introduced as

$$P_b = 1 - e^{(-k_H \sum_{j=1}^N (\tilde{\sigma}(P)_{max,j} - RCSS_{net})^{m_H} \cdot L_j)} \quad (4.29)$$

where, $RCSS_{net} = RCSS_{base} - RCSS_{design}$. As a base RCSS value is not associated with the $GFPM_{2H}$, any value of RCSS can be chosen for the $RCSS_{base}$. However, as with the $3P_H$'s, the RCSS base should be related to the sample set, thus 126 MPa is used for $RCSS_{base}$. The

$GFPM_{3H}$ (Equation 4.22) uses the estimated $3P_H$ parameters with different design RCSS values to determine LR as a function of pb. Figure 4.6 shows the LR's as a function of pb for the pseudo $GFPM_{3H}$ (golden lines) and $GFPM_{3H}$ (black lines) for various RCSS's which shift as RCSS increases. The load corresponding to the maximum allowable stress in Table X7.1 in ASTM E1300-16 [11] for the particular glass specimen is denoted as red dash lines. The load corresponding to the maximum allowable stress in Table X7.1 in ASTM E1300-16 [11] to the 69 MPa LR is less than the load corresponding to the maximum allowable stress for this particular geometry, loading condition. and boundary condition. The slope for both the pseudo $GFPM_{3H}$ and the $GFPM_{3H}$ did not change with RCSS, but they did shift equally with RCSS. Even though the pseudo $GFPM_{2H}$ and the $GFPM_{3H}$ intersected near a pb equal to 0.008, a different intersection point will likely occur with more number of specimens or for other sample sets depending on hole pattern, loading geometry, and loading condition.

4.5 Conclusion

A modified glass failure prediction model for heat-treated, (heat-strengthened and fully tempered), glass with holes was introduced to address the effect of RCSS on the load resistance. Equations to estimate hole parameters using the maximum likelihood estimator (MLE) method were presented for both the two-parameter ($GFPM_{2H}$) and the three-parameter ($GFPM_{3H}$) glass failure prediction model for glass with holes. Failure data from

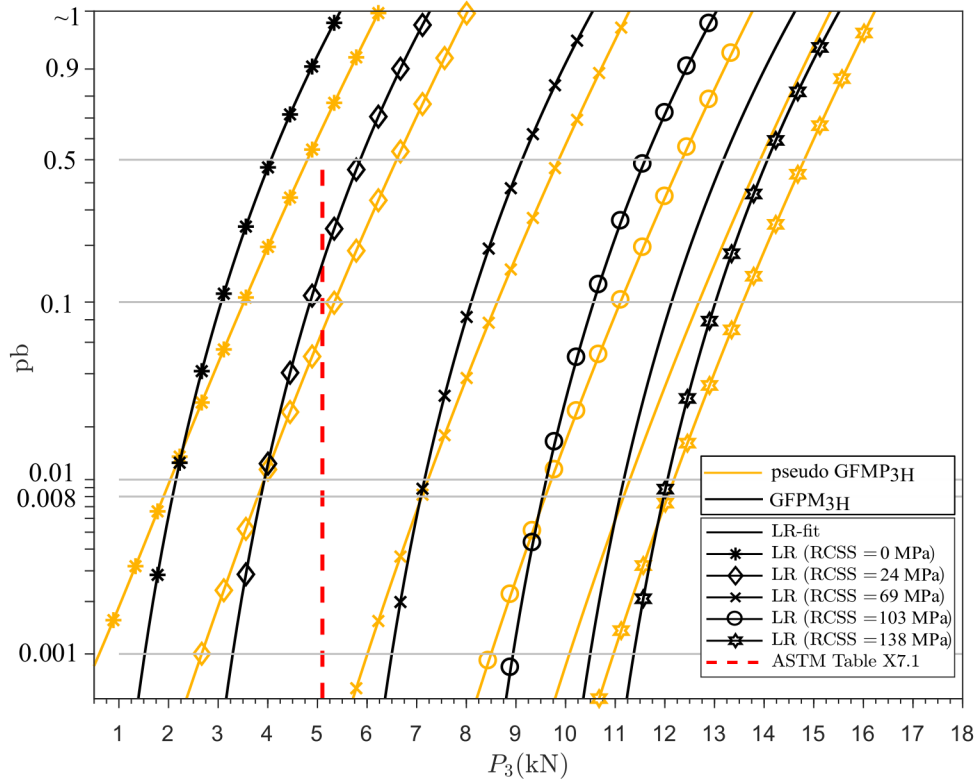


Figure 4.6: Load Resistance chart for test specimen

testing conducted by Cervenka [22] on ten fully tempered monolithic glass specimens with a water-jet cut hole monotonically loaded to failure using a four-point bending test was used to illustrate the MLE method to estimate $GFPM_{2H}$ and $GFPM_{3H}$ hole parameters. As hole parameters in $GFPM_{3H}$ are dependent on the location parameter (i.e. the RCSS value), multiple sets of hole parameters can be estimated. Difference in probability of breakages calculated using the base RCSS and measured RCSS for hole parameters based on the the minimum, mean and maximum measured RCSS for the sample suggested the pb's were mostly overestimated. Thus, a root finding algorithm was used to converge on a RCSS value, equal to 126 MPa, to provide nearly a zero average difference in pb's. The set of

hole parameters m_H and k_H equal to 6.65 and $4.60 \times 10^{-14} \text{ mm}^{(2m_H-1)} N^{-m_H}$, corresponding to base RCSS 126 MPa is selected to best describe the failure data for the specimen geometry, loading and boundary condition, and the hole location. For designing a fully-tempered glass with holes, either $GFPM_{2H}$ and $GFPM_{3H}$ can be used. To use $GFPM_{2H}$ to design a fully tempered glass for a desired RCSS it is necessary to include the RCSS of the sample using a pseudo $GFPM_{3H}$. The use of MLE to estimate GFPM flaw parameters can be extended to other geometries, boundary conditions including edges, surfaces and specialized surface treatments of beams and plates. With this method it is possible to objectively and repeatably estimate flaw parameters for holes that are required to extend the GFPM to design PSG.

Chapter 5

Conclusion

Three journal articles are presented to show the working of the robust, consistent, and repeatable method to estimate flaw parameters for different GFPM. In Chapter 2, multiple destructive uniform load test data, simply supported on all 4-edges performed on in-service and new AN monolithic glass were collected and presented [18] [2] [39] [34], [58], [34]. A minimum criteria of required data from the experimental records was established by replicating equivalent failure loads and comparing them to the published values. As the published records of some of these test data are not complete, strategies for using incomplete data sets were advanced. The MLE method was extended to estimate the GFPM surface flaw parameters and compared to load resistance predictions based on historically published surface flaw parameters. For each sample collected, the MLE method was used to estimate 3-sec surface flaw parameters. Results from several design examples suggest

the current GFPM surface flaw parameters used in ASTM E1300, the primary standard in the United States to determine the required thickness for simply-supported glass plates used for infill windows panels, overestimated the strength. However, as some of the historical sample sets included specimens exposed to an extreme event prior to their removal, their load resistances were expected to be lower than regular in-service conditions.

In Chapter 3, multiple destructive uniform load test data, simply supported on all 4-edges performed on in-service and new HT monolithic glass were collected and presented [52] [20] [46] [3]. Equivalent failure loads for each specimen were replicated and compared to the published values, that established a minimum criteria of required data from the collected experimental records and strategies laid down previously for incomplete data set were implemented. Equations to estimate the surface flaw parameters using the MLE method for the MGFPFPM for HT samples were put forward. As the surface flaw parameters in the MGFPFPM is dependent on the RCSS of the sample, a method was put forward to estimate a representative RCSS of the sample. The data sets collected were used to illustrate the working principle of MLE method to estimate the surface flaw parameters and the representative RCSS for each sample. Load resistance charts for HT glass and similar sized AN glass were compared to better understand the effect of RCSS on load resistance, and weathering of HT glass. Results suggest that ASTM E1300-16 overestimates the strength for weathered HT samples when the sample RCSS was used. However, as some of the historical sample sets included specimens exposed to an extreme event prior to their removal, their load resistances were expected to be lower than regular in-service conditions. Results

also suggests, for in-service glass as the value of RCSS increase, the ratio of load for HT to AN corresponding to $0.008 p_b$ increases in a polynomial order.

In chapter 4, the MLE method was applied to the two-parameter GFPM for holes to estimate the flaw parameters. A 4-point bending test on 10-FT glass samples with a hole in the center loaded to fracture was used as the experimental data. A three-parameter GFPM for holes was advanced consistent with the modified GFPM by Norville et al. [50] and Morse and Norville [44] to address the effect of RCSS on the load resistance. The MLE method was extended to estimate the flaw parameters for the three-parameter GFPM for holes. As the flaw parameters are dependent on the RCSS chosen to represent the sample, a method was introduced to select a representative RCSS rather than using the minimum, mean, or maximum RCSS of the sample as a representative value. Flaw parameters m_H and k_H equal to 6.65 and $4.60 \times 10^{-14} \text{ mm}^{(2m_H-1)} \text{ N}^{-m_H}$, corresponding to a representative base RCSS 126 MPa best described the failure data for the specimen geometry, loading and boundary condition, and the hole location. To design a FT glass with holes, it was shown either the two-parameter to the three-parameter can be used. a pseudo 3-parameter GFPM was so an alternate RCSS can be used based on the 2-parameter values.

Based on the observations, and result presented in Chapters 2 through Chapter 4. the following future works are recommended.

1. Full scale test for point supported glass and check the load resistance for the point

- supported glass using the surface flaw parameters for Chapter 4 to the experimental data.
2. Check if the surface flaw parameter are independent of aspect ratio and surface area. If dependency exist, explore the material function to more accurately account for surface area and aspect ratio
 3. Apply the MLE method to estimate surface flaw parameters for laminated glass and check if the laminated glass weathers the same as AN monolithic glass.
 4. Conduct experimental test for different glass sizes, different hole sizes, different tools to cut the hole, different thickness, to understand the affect of each on the load resistance of point supported glass, independently.
 5. Verify static fatigue constant equal to 16 does not change with heat-treatment of glass.
 6. Goswami [29] has extend the GFPM to incorporate the flaws on the edge-line of a glass. Extend the MLE method to estimate flaw parameters for the flaw parameters for edge-line of glass.
 7. Veer and Rodichev [60] and Goswami [30] has suggested the strength of a edge-line is better described by a bi-linear Weibull distribution. Extend the MLE method to estimate bi-linear Weibull distribution flaw parameters.

References

- [1] AAMA GDSG-1-87. Design Guide for Sloped Glazing and Skylights, an FGIA publication, 1987.
- [2] Jean J. Abiassi. *The strength of weathered window glass using surface characteristics*. PhD thesis, Texas Tech University, Lubbock, TX, 1981.
- [3] Bolaji A Afolabi. *A Study of Weathered Tempered Glass*. PhD thesis, Texas Tech University, Lubbock, TX, 2017.
- [4] Afolabi, Bolaji and Norville, H Scott and Morse, Stephen M. Experimental study of weathered tempered glass plates from the Northeastern United States. *Journal of Architectural Engineering*, 22(3):04016010, 2016.
- [5] ASCE 7 16. *Minimum Design Loads and Associated Criteria for Buildings and Other Structures*. American Society of Civil Engineers, asce/sei 7-16 edition, 2017.
- [6] ASCE 7-93. *Minimum Design Loads for Buildings and Other Structures*. American Society of Civil Engineers, ansi/asce 7-93 edition, 1994.

- [7] ASCE 7-95. *Minimum Design Loads for Buildings and Other Structures*. American Society of Civil Engineers, ansi/asce 7-95 edition, 1996.
- [8] ASTM C1048-18. Standard Specification for Heat-Strengthened and Fully Tempered Flat Glass. *ASTM International, West Conshohocken*, 2018.
- [9] ASTM C1048-97. Standard specification for heat-treated flat glass-kind hs, kind ft coated and uncoated glass. *ASTM International, West Conshohocken,PA*, 1997.
- [10] ASTM C1239-13. Standard Practice for Reporting Uniaxial Strength Data and Estimating Weibull Distribution Parameters for Advanced Ceramics. *ASTM International, West Conshohocken*, 2018.
- [11] ASTM E1300-16. Standard practice for determining load resistance of glass in buildings. *ASTM International, West Conshohocken*, 2016.
- [12] ASTM E1300-89. Standard practice for determining the minimum thickness of annealed glass required to resist a specific load. *ASTM International, West Conshohocken, PA, 2012*, 1989.
- [13] ASTM E1300-94. Standard practice for determining the minimum thickness and type of glass required to resist a specified load. *ASTM International, West Conshohocken*, 1994.
- [14] ASTM E178-21. Standard Practice for Dealing With Outlying Observations. *ASTM International, West Conshohocken, PA*, 2021.

- [15] ASTM E997-15. Standard test method for evaluating glass breakage probability under the influence of uniform static loads by proof load testing. *ASTM International, West Conshohocken, PA*, 2021.
- [16] TC Baker and FW Preston. Fatigue of glass under static loads. *Journal of Applied Physics*, 17(3):170–178, 1946.
- [17] W. L. Beason and J. R. Morgan. Glass failure prediction model. *Journal of Structural Engineering*, 110(2):197–212, 1984.
- [18] William L Beason. *A failure prediction model for window glass*. PhD thesis, Texas Tech University, Lubbock, TX, 1980.
- [19] Matt Bergers, Kayla Natividad, Stephen M Morse, and H Scott Norville. Full scale tests of heat strengthened glass with ceramic frit. *Glass Structures & Engineering*, 1(1):261–276, 2016.
- [20] Paul Mark Bove Jr. *Failure prediction for heat treated window glass*. Texas Tech University, 1995.
- [21] William G. Brown. *A practicable formulation for the strength of glass and its special application to large plates*. National Research Council Canada, 1974.
- [22] Jan Cervenka. Investigation of strength of glass plates with hole subjected to out-of-plane bending. *MS thesis*, 2016.

- [23] RJ Charles. Dynamic fatigue of glass. *Journal of Applied Physics*, 29(12):1657–1662, 1958.
- [24] RJ Charles. Static fatigue of glass. i. *Journal of Applied Physics*, 29(11):1549–1553, 1958.
- [25] RJ Charles. Static fatigue of glass. ii. *Journal of Applied Physics*, 29(11):1554–1560, 1958.
- [26] Matteo Ciccotti. Stress-corrosion mechanisms in silicate glasses. *Journal of physics D: Applied physics*, 42(21):214006, 2009.
- [27] Kyriaki Corinna Datsiou and Mauro Overend. Weibull parameter estimation and goodness-of-fit for glass strength data. *Structural Safety*, 73:29–41, 2018.
- [28] JC Fothergill. Estimating the cumulative probability of failure data points to be plotted on weibull and other probability paper. *IEEE Transactions on Electrical Insulation*, 25(3):489–492, 1990.
- [29] N Goswami and SM Morse. Edge-line strength of glass beams. In *GlassCon Global 2018*, pages 325–333, 2018.
- [30] Nabhajit Goswami and Stephen M Morse. Lower tail fit of the weibull distribution for edge-line glass strength for structural use of glass. In *Conference Proceedings, Glass Processing Days*, 2019.

- [31] Nabhajit Goswami, Joshua A. Schultz, Kui Zhang, R.Andrew. Schwartz, Daniel M. Dowden, and Stephen M Morse. Estimation of surface flaw parameters for annealed glass using maximum likelihood estimator. Unpublished.
- [32] Nabhajit Goswami, Joshua A. Schultz, Kui Zhang, R.Andrew. Schwartz, Daniel M. Dowden, and Stephen M Morse. Estimation of flaw parameters for holes in glass using maximum likelihood estimator. *Glass Structures & Engineering, Under Review*, 2022.
- [33] AA Griffith. The phenomena of flow and rupture in solids: *Phil. Trans. Roy. Soc. Lond. Ser. A*, 221:163–98, 1920.
- [34] Sheng Y. Hsu. *Comparison of window glass sample strength estimates: full scale versus concentric rings*. PhD thesis, Texas Tech University, Lubbock, TX, 1987.
- [35] Charles E. Inglis. Stresses in a plate due to the presence of cracks and sharp corners. *Transactions of the institute of naval architects*, 55(219-241):193–198, 1913.
- [36] S Johar. *Dynamic Fatigue of Flat Glass, Phase II*. Ontario Research Foundation, 1981.
- [37] S Johar. *Dynamic Fatigue of Flat Glass, Phase III*. Ontario Research Foundation, 1982.
- [38] DC Kanabolo and H Scott Norville. The strength of new window glass plates using

- surface characteristics. *Glass Research and Testing Laboratory, Texas Tech University, Lubbock, Tex*, 1985.
- [39] Diboro Celestine Kanabolo. *The strength of new window glass using surface characteristics*. PhD thesis, Texas Tech University, Lubbock, TX, 1984.
- [40] Wilfried Laufs and Gerhard Sedlacek. Stress distribution in thermally tempered glass panes near the edges, corners and holes. part 1. temperature distributions during the tempering process of glass panes. *Glass science and technology (Frankfurt)*, 72(1):7–14, 1999.
- [41] Terry A Michalske and Stephen W Freiman. A molecular mechanism for stress corrosion in vitreous silica. *Journal of the American Ceramic Society*, 66(4):284–288, 1983.
- [42] S Morse and H Norville. An analytical method for determining window glass strength. *Glass Performance Days*, pages 17–20, 2011.
- [43] SM Morse. New provisions in ASTM E1300-16: A comparison of the basic and new analytical procedures for determining the load resistance of window glass. In *Vol. 2 of Proc., Façade Tectonics 2018 World Congress*, edited by D. Noble, K. Kensek, and M. Elder, pages 529–541, 2018.
- [44] Stephen M Morse and H Scott Norville. Design methodology for determining the load resistance of heat-treated window glass. *Journal of architectural engineering*, 18(1):42–51, 2012.

- [45] DN Prabhakar Murthy, Min Xie, and Renyan Jiang. *Weibull models*, volume 505. John Wiley & Sons, 2004.
- [46] Kayla Natividad, Stephen M Morse, and H Scott Norville. Fracture origins and maximum principal stresses in rectangular glass lites. *Journal of Architectural Engineering*, 22(2):04015014, 2016.
- [47] Kayla Natividad, Stephen M Morse, and H Scott Norville. Tests of heat-treated glass with full-coverage ceramic frit. *Journal of Architectural Engineering*, 23(3):04017010, 2017.
- [48] Jens Henrik Nielsen. *Tempered Glass: bolted connections and related problems*. Technical University of Denmark, 2009.
- [49] Jens Henrik Nielsen, John Forbes Olesen, Peter Noe Poulsen, and Henrik Stang. Simulation of residual stresses at holes in tempered glass: a parametric study. *Materials and structures*, 43(7):947–961, 2010.
- [50] H Scott Norville, Paul M Bove, and Darrel L Sheridan. *The strength of new thermally tempered window glass lites*. Glass Research and Testing Laboratory, Department of Civil Engineering, 1991.
- [51] H Scott Norville, Paul M Bove, Darrel L Sheridan, and Stacey L Lawrence. Strength of new heat treated window glass lites and laminated glass units. *Journal of Structural Engineering*, 119(3):891–901, 1993.

- [52] H Scott Norville and Joseph E Minor. Strength of weathered window glass. *American Ceramic Society Bulletin*, 64(11):1467–1470, 1985.
- [53] Gabriele Pisano and Gianni Royer Carfagni. The statistical interpretation of the strength of float glass for structural applications. *Construction and Building Materials*, 98:741–756, 2015.
- [54] FW Preston. The mechanical properties of glass. *Journal of Applied Physics*, 13(10):623–634, 1942.
- [55] Joshua Schultz, John Knowles, and Stephen Morse. Glass failure prediction model for out-of-plane bending of waterjet-drilled holes. In *IABSE Symposium Report*, volume 109, pages 2354–2361. International Association for Bridge and Structural Engineering, 2017.
- [56] Errol B Shand. Breaking stress of glass determined from dimensions of fracture mirrors. *Journal of the American Ceramic Society*, 42(10):474–477, 1959.
- [57] Errol B Shand. Correlation of strength of glass with fracture flaws of measured size. *Journal of the American Ceramic Society*, 44(9):451–455, 1961.
- [58] June W Sligar. *Evaluation of weathered window glass strength*. PhD thesis, Texas Tech University, Lubbock, TX, 1989.
- [59] Brent Vander Werf. Compression/modeling with glass. *University of Arizona*, 16, 2014.

- [60] FA Veer and Yu M Rodichev. The structural strength of glass: hidden damage. *Strength of materials*, 43(3):302–315, 2011.
- [61] George R Walker. Discussion of “glass failure prediction model” by w. lynn beason and james r. morgan (february, 1984). *Journal of Structural Engineering*, 111(9):2059–2060, 1985.
- [62] GR Walker and LH Muir. Investigation of the bending strength of glass louvre blades. In *Ninth Australasian Conference on the Mechanics of Structures and Materials, ACMSM 9.*, pages 122–126, 1984.
- [63] Bob Yaoting Wang. *Nonlinear analysis of rectangular glass plates by finite difference method*. PhD thesis, Texas Tech University, Lubbock, TX, 1981.
- [64] Waloddi Weibull. A statistical theory of the strength of materials. *Ing. Vet. Ak. Handl.*, 1939.
- [65] Waloddi Weibull et al. A statistical distribution function of wide applicability. *Journal of applied mechanics*, 18(3):293–297, 1951.
- [66] SM Wiederhorn. Influence of water vapor on crack propagation in soda-lime glass. *Journal of the American Ceramic Society*, 50(8):407–414, 1967.
- [67] Guo Zheng Yew, H Scott Norville, and Stephen M Morse. Nonlinear finite-element analysis of laminated glass using the four-node reissner-mindlin formulation and assumed transverse shear strain fields. *Journal of Engineering Mechanics*,

145(7):04019042, 2019.

- [68] Guo Zheng Yew, HS Norville, and SM Morse. Load resistance of rectangular point-supported glass subjected to applied uniform loading. In *GlassCon Global 2018*, pages 477–483, 2018.

Appendix A

Failure Data and Load resistance table for annealed monolithic glass

Table A.1W01 - Loading time history, failure location, EFL_{60} and EFL_3

Spec. No.	Time History		Reported EFL_{60} kPa (psf)	Failure location		EFL_{60} Recreated kPa (psf)	EFL_3 kPa (psf)
	Failure Pressure kPa (psf)	Failure Time (sec)		to long dimension mm (in.)	to short dimension mm (in.)		
1	10.8 (225)	64	9.05 (189)	216 (8.50)	358 (14.1)	8.79 (184)	11.2 (234)
2	10.4 (217)	50	8.33 (174)	249 (9.80)	478 (18.8)	8.22 (172)	10.7 (223)
3	10.3 (216)	40	8.28 (173)	224 (8.80)	262 (10.3)	8.07 (168)	10.4 (217)
4	15.8 (330)	62	12.8 (268)	442 (17.4)	457 (18.0)	12.5 (261)	16.9 (353)
5	9.05 (189)	37	7.09 (148)	307 (12.1)	396 (15.6)	6.98 (146)	9.05 (189)
6	8.14 (170)	35	6.61 (138)	434 (17.1)	427 (16.8)	6.30 (132)	8.07 (169)
7	11.2 (233)	50	9.38 (196)	434 (17.1)	592 (23.3)	9.06 (189)	11.3 (235)
8	12.9 (269)	60	10.5 (219)	330 (13.0)	549 (23.4)	10.6 (221)	13.2 (275)
9	9.58 (200)	27	7.52 (157)	320 (12.6)	452 (17.8)	7.22 (151)	9.30 (194)
10	8.00 (167)	22	6.32 (132)	127 (5.00)	414 (16.3)	6.19 (129)	7.60 (159)
11	9.67 (202)	40	8.04 (168)	295 (11.6)	554 (21.8)	7.70 (161)	9.62 (201)
12	7.71 (161)	34	6.32 (132)	417 (16.4)	244 (9.60)	6.02 (126)	7.60 (159)
13	11.2 (233)	47	9.43 (197)	102 (4.00)	279 (11.0)	9.04 (189)	11.2 (234)
14	9.91 (207)	42	8.47 (177)	401 (15.8)	236 (9.30)	7.80 (163)	10.0 (208)
15	9.05 (189)	38	7.33 (153)	406 (16.0)	191 (7.50)	7.17 (150)	8.97 (187)
16	6.61 (138)	27	5.36 (112)	191 (7.50)	300 (11.8)	5.14 (107)	6.38 (133)
17	9.38 (196)	38	7.52 (157)	305 (12.0)	432 (17.0)	7.25 (151)	9.41 (197)
18	8.95 (187)	35	7.47 (156)	632 (24.9)	343 (13.5)	7.20 (150)	8.77 (183)
19	6.89 (144)	26	5.36 (112)	338 (13.3)	368 (14.5)	5.26 (110)	6.66 (139)
20	11.4 (238)	44	9.67 (202)	579 (22.8)	279 (11.0)	9.13 (191)	11.4 (238)

Table A.2
W02 - Loading time history, failure location, EFL_{60} and EFL_3

Spec. No.	Time History		Reported	Failure location		EFL_{60}	EFL_3
	Failure Pressure kPa (psf)	Failure Time (sec)	EFL_{60} kPa (psf)	to long dimension mm (in.)	to short dimension mm (in.)	Recreated kPa (psf)	
1	4.55 (95.0)	34	3.64 (76.0)	838 (33.0)	318 (12.5)	3.54 (74.0)	4.49 (93.7)
2	5.31 (111)	42	4.4 (92.0)	343 (13.5)	292 (11.5)	4.22 (88.1)	5.33 (111)
3	6.89 (144)	57	5.75 (120)	1130 (44.5)	343 (13.5)	5.49 (115)	7.20 (150)
4*	9.43 (197)	42	4.21 (88.0)	648 (25.5)	229 (9.00)	7.29 (152)	9.59 (200)
5	4.60 (96.0)	50	3.93 (82.0)	610 (24.0)	279 (11.0)	3.69 (77.1)	4.68 (97.7)
6	5.12 (107)	31	4.02 (84.0)	724 (28.5)	394 (15.5)	3.93 (82.2)	5.03 (105)
7	5.03 (105)	43	4.12 (86.0)	978 (38.5)	216 (8.50)	4.00 (83.6)	5.05 (105)
8	5.22 (109)	49	4.55 (95.0)	1290 (50.8)	211 (8.30)	4.23 (88.4)	5.26 (110)
9	4.55 (95.0)	30	3.64 (76.0)	897 (35.3)	572 (22.5)	3.55 (74.2)	4.43 (92.4)
10	6.03 (128)	23	4.98 (104)	660 (26.0)	318 (12.5)	4.55 (95.0)	5.87 (123)
11	3.73 (78.0)	28	2.97 (62.0)	787 (31.0)	559 (22.0)	2.92 (60.9)	3.61 (75.4)
12	3.16 (66.0)	25	2.54 (53.0)	1000 (39.5)	300 (11.8)	2.45 (51.2)	3.03 (63.3)
13	6.22 (130)	51	5.03 (105)	1130 (44.5)	343 (13.5)	4.94 (103)	6.41 (134)
14	3.64 (76.0)	36	2.97 (62.0)	826 (32.5)	203 (8.00)	2.89 (60.3)	3.59 (74.9)
15	3.88 (81.0)	43	3.45 (72.0)	1000 (39.5)	508 (20.0)	3.12 (65.1)	3.87 (80.9)
16	3.11 (65.0)	21	2.39 (50.0)	965 (38.0)	318 (12.5)	2.38 (49.7)	2.95 (61.6)
17	3.64 (76.0)	18	2.82 (59.0)	495 (19.5)	381 (15.0)	2.74 (57.2)	3.41 (71.2)
18	4.21 (88.0)	45	3.59 (75.0)	762 (30.0)	241 (9.50)	3.38 (70.5)	4.24 (88.5)
19	4.60 (96.0)	29	3.64 (76.0)	813 (32.0)	325 (12.8)	3.53 (73.8)	4.48 (93.5)
20	3.59 (75.0)	35	2.97 (62.0)	724 (28.5)	305 (12.0)	2.83 (59.1)	3.54 (73.9)

* Specimen removed from parameter estimation

Table A.3W03 - Loading time history, failure location, EFL_{60} and EFL_3

Spec. No.	Time History		Reported EFL_{60} kPa (psf)	Failure location		EFL_{60} Recreated kPa (psf)	EFL_3 kPa (psf)
	Failure Pressure kPa (psf)	Failure Time (sec)		to long dimension mm (in.)	to short dimension mm (in.)		
1	13.6 (284)	75	11.8 (247)	432 (17.0)	165 (6.50)	11.3 (237)	14.2 (297)
2	14.9 (311)	80	12.4 (260)	495 (19.5)	38.1 (1.50)	12.5 (260)	15.6 (327)
3	11.7 (245)	63	9.67 (202)	178 (7.00)	114 (4.50)	9.56 (200)	12.2 (256)
4	16.8 (350)	92	14.2 (296)	508 (20.0)	387 (15.3)	14.2 (297)	17.7 (369)
5	19.9 (416)	90	16.1 (336)	508 (20.0)	38.1 (1.50)	16.8 (351)	21.1 (441)
6	13.5 (282)	78	11.1 (231)	267 (10.5)	292 (11.5)	11.1 (232)	14.5 (303)
7	17.6 (367)	97	14.5 (303)	197 (7.75)	222 (8.75)	14.1 (295)	20.9 (436)
8	19.8 (413)	109	17.1 (358)	502 (19.8)	25.4 (1.00)	17.0 (355)	21.1 (441)
9	14.6 (304)	81	12.4 (258)	19.1 (0.75)	413 (16.3)	12.2 (256)	15.2 (318)
10	17.6 (367)	93	14.7 (306)	508 (20.0)	381 (15.0)	14.9 (311)	18.6 (389)
11	10.5 (220)	60	9.05 (189)	19.1 (0.75)	394 (15.5)	8.65 (181)	10.8 (225)
12	8.10 (170)	44	6.51 (136)	311 (12.3)	241 (9.50)	6.24 (130)	8.42 (176)
13	11.2 (233)	59	9.05 (189)	305 (12.0)	305 (12.0)	9.08 (190)	11.5 (241)
14	10.6 (222)	60	8.95 (187)	25.4 (1.00)	0.00 (0.00)	8.75 (183)	10.9 (227)
15	11.3 (235)	63	9.19 (192)	38.1 (1.50)	394 (15.5)	9.23 (193)	11.6 (243)
16	10.7 (223)	60	8.71 (182)	267 (10.5)	114 (4.50)	8.71 (182)	11.1 (231)
17	14.2 (297)	81	12.1 (253)	6.35 (0.25)	38.1 (1.50)	11.9 (249)	14.9 (312)
18	8.80 (183)	49	7.37 (154)	318 (12.5)	318 (12.5)	7.12 (149)	8.85 (185)
19	13.2 (276)	73	11.2 (234)	438 (17.3)	140 (5.50)	11.0 (230)	13.7 (286)
20	12.7 (266)	70	10.8 (226)	63.5 (2.50)	140 (5.50)	10.6 (221)	13.2 (275)
21	10.2 (213)	55	8.28 (173)	508 (20.0)	375 (14.8)	8.32 (174)	10.4 (217)
22	8.10 (170)	37	6.7 (140)	267 (10.5)	318 (12.5)	6.53 (136)	8.03 (168)

Table A.4W04 - Loading time history, failure location, EFL_{60} and EFL_3

Spec. No.	Time History		Reported EFL_{60} kPa (psf)	Failure location		EFL_{60} Recreated kPa (psf)	EFL_3 kPa (psf)
	Failure Pressure kPa (psf)	Failure Time (sec)		to long dimension mm (in.)	to short dimension mm (in.)		
1	11.5 (240)	64	9.58 (200)	527 (20.8)	197 (7.75)	9.36 (196)	12.0 (250)
2	8.00 (167)	44	6.56 (137)	232 (9.12)	286 (11.3)	6.47 (135)	7.98 (167)
3	8.19 (171)	47	6.75 (141)	724 (28.5)	248 (9.75)	6.64 (139)	8.22 (172)
4	6.08 (127)	38	5.31 (111)	76.2 (3.00)	352 (13.9)	4.92 (103)	5.99 (125)
5	8.67 (181)	49	7.18 (150)	559 (22.0)	127 (5.00)	7.00 (146)	8.76 (183)
6	7.18 (150)	39	5.79 (121)	362 (14.3)	159 (6.25)	5.73 (120)	7.12 (149)
7	7.52 (157)	41	6.22 (130)	476 (18.8)	203 (8.00)	6.02 (126)	7.48 (156)
8	9.29 (194)	56	7.71 (161)	432 (17.0)	92.0 (3.62)	7.59 (159)	9.47 (198)
9	8.04 (168)	50	6.61 (138)	343 (13.5)	114 (4.50)	6.53 (136)	8.13 (170)
10	8.47 (177)	44	6.89 (144)	343 (13.5)	152 (6.00)	6.78 (142)	8.50 (178)
11	8.95 (187)	47	7.37 (154)	356 (14.0)	203 (8.00)	7.19 (150)	9.04 (189)
12	4.84 (101)	26	3.93 (82.0)	572 (22.5)	235 (9.25)	3.80 (79.4)	4.65 (97.0)
13	7.66 (160)	44	6.42 (134)	343 (13.5)	203 (8.00)	6.15 (129)	7.67 (160)
14	8.62 (180)	51	7.04 (147)	495 (19.5)	191 (7.50)	6.98 (146)	8.75 (183)
15	6.32 (132)	32	5.22 (109)	400 (15.8)	133 (5.25)	5.00 (105)	6.17 (129)
16	5.79 (121)	37	4.74 (99.0)	921 (36.3)	0.00 (0.00)	4.70 (98.2)	5.68 (119)
17	9.53 (199)	57	7.85 (164)	718 (28.3)	235 (9.25)	7.79 (163)	9.74 (203)
18	8.43 (176)	49	7.18 (150)	572 (22.5)	127 (5.00)	6.82 (142)	8.51 (178)
19	8.76 (183)	45	7.18 (150)	381 (15.0)	165 (6.5)	7.02 (147)	8.81 (184)
20	6.32 (132)	33	5.17 (108)	635 (25.0)	203 (8.00)	5.00 (105)	6.18 (129)
21	3.64 (76.0)	21	2.97 (62.0)	6.35 (0.25)	318 (12.5)	2.86 (59.7)	3.44 (71.9)
22	5.94 (124)	35	4.69 (98.0)	654 (25.8)	133 (5.25)	4.74 (98.9)	5.83 (122)
23	4.36 (91)	26	3.50 (73.0)	114 (4.50)	362 (14.3)	3.41 (71.3)	4.19 (87.4)
24	7.80 (163)	44	6.27 (131)	381 (15.0)	254 (10.0)	6.29 (131)	7.80 (163)
25	8.76 (183)	47	6.89 (144)	457 (18.0)	184 (7.25)	7.05 (147)	8.84 (185)
26	9.86 (206)	53	7.85 (164)	495 (19.5)	152 (6.00)	7.97 (166)	10.1 (210)
27	5.65 (118)	29	4.55 (95.0)	921 (36.3)	381 (15.0)	4.52 (94.4)	5.46 (114)
28	8.67 (181)	47	6.89 (144)	178 (7.00)	146 (5.75)	6.99 (146)	8.73 (182)
29	8.76 (183)	50	7.23 (151)	787 (31.0)	102 (4.00)	7.16 (149)	8.82 (184)
30	10.5 (220)	61	8.62 (180)	711 (28.0)	203 (8.00)	8.57 (179)	10.9 (228)
31	7.85 (164)	42	6.56 (137)	533 (21.0)	159 (6.25)	6.28 (131)	7.84 (164)
32	5.22 (109)	29	4.36 (91.0)	12.7 (0.50)	368 (14.5)	4.18 (87.3)	5.04 (105)
33	6.61 (138)	39	5.36 (112)	229 (9.00)	216 (8.50)	5.30 (111)	6.54 (137)
34	10.2 (212)	56	8.47 (177)	756 (29.8)	279 (11.0)	8.34 (174)	10.3 (215)
35	7.37 (154)	42	5.99 (125)	546 (21.5)	241 (9.50)	5.93 (124)	7.34 (153)
36	8.33 (174)	46	6.70 (140)	203 (8.00)	229 (9.00)	6.73 (140)	8.36 (175)
37	6.13 (128)	35	5.12 (107)	159 (6.25)	216 (8.50)	4.90 (102)	6.01 (126)

W04 (Cont.) - Loading time history, failure location, EFL_{60} and EFL_3

Spec. No.	Time History		Reported EFL_{60} kPa (psf)	Failure location		EFL_{60} Recreated kPa (psf)	EFL_3 kPa (psf)
	Failure Pressure kPa (psf)	Failure Time (sec)		to long dimension mm (in.)	to short dimension mm (in.)		
38	9.15 (191)	48	7.66 (160)	165 (6.50)	76.2 (3.00)	7.45 (156)	9.18 (192)
39	5.79 (121)	32	4.74 (99.0)	279 (11.0)	222 (8.75)	4.60 (96.0)	5.65 (118)
40	7.52 (157)	42	5.99 (125)	495 (19.5)	254 (10.0)	6.05 (126)	7.49 (156)
41	5.70 (119)	31	4.60 (96.0)	565 (22.3)	235 (9.25)	4.52 (94.3)	5.54 (116)
42	4.40 (92.0)	615	4.36 (91.0)	921 (36.3)	44.5 (1.75)	4.27 (98.2)	5.14 (107)
43	6.94 (145)	902	7.09 (148)	660 (26.0)	292 (11.5)	6.93 (145)	8.56 (179)
44	4.12 (86.0)	500	4.12 (86.0)	50.8 (2.00)	0.00 (0.00)	3.94 (82.3)	4.75 (99.2)
45	7.09 (148)	952	7.33 (153)	514 (20.3)	197 (7.75)	7.13 (149)	8.95 (187)
46	6.75 (141)	908	6.75 (141)	622 (24.5)	229 (9.00)	6.76 (141)	8.45 (176)
47	7.85 (164)	1074	8.00(167)	0.00 (0.00)	368 (14.5)	7.89 (165)	9.57 (200)
48	9.05 (189)	1247	9.43 (197)	495 (19.5)	203 (8.00)	9.34 (195)	11.9 (249)
49	7.04 (147)	952	7.23 (151)	679 (26.5)	152 (6.00)	7.08 (148)	8.91 (186)
50	7.95 (166)	1067	8.19 (171)	356 (14.0)	330 (13.0)	8.04 (168)	9.96 (208)
51	8.47 (177)	1190	8.57 (179)	940 (37.0)	25.4 (1.00)	8.57 (179)	10.4 (216)
52	7.85 (164)	1120	7.85 (164)	19.1 (0.75)	0.00 (0.00)	7.91 (165)	9.56 (200)
53	7.95 (166)	1109	8.28 (173)	572 (22.5)	108 (4.25)	8.09 (169)	10.2 (212)
54	8.62 (180)	1135	8.95 (187)	419 (16.5)	191 (7.50)	8.82 (184)	11.2 (234)
55	9.05 (189)	1286	9.53 (199)	438 (17.3)	216 (8.50)	9.35 (195)	11.9 (249)
56	7.71 (161)	1069	7.95 (166)	368 (14.5)	248 (9.75)	7.82 (163)	9.80 (205)
57	5.84 (122)	833	5.94 (124)	476 (18.8)	267 (10.5)	5.80 (121)	7.15 (149)
58	5.79 (121)	789	5.84 (122)	559 (22.0)	279 (11.0)	5.73 (120)	7.05 (147)
59	6.13 (128)	822	6.08 (127)	483 (19.0)	260 (10.3)	6.08 (127)	7.52 (157)
60	7.33 (153)	1027	7.52 (157)	425 (16.8)	203 (8.00)	7.41 (155)	9.32 (195)
61	5.12 (107)	665	5.03 (105)	648 (25.5)	146 (5.75)	5.01 (105)	6.18 (129)
62	6.70 (140)	925	6.89 (144)	610 (24.0)	254 (10.0)	6.71 (140)	8.35 (174)
63	5.51 (115)	771	5.65 (118)	286 (11.3)	279 (11.0)	5.43 (113)	6.67 (139)
64	4.74 (99.0)	628	4.74 (99.0)	876 (34.5)	241 (9.50)	4.61 (96.4)	5.67 (118)
65	6.22 (130)	796	5.99 (125)	318 (12.5)	286 (11.3)	6.16 (129)	7.59 (159)
66	8.28 (173)	1097	8.62 (180)	0.00 (0.00)	375 (14.8)	8.34 (174)	10.1 (211)
67	5.22 (109)	701	5.31 (111)	610 (24.0)	114 (4.50)	5.12 (107)	6.31 (132)
68	7.95 (166)	1080	8.19 (171)	699 (27.5)	229 (9.00)	8.07 (169)	10.2 (212)
69	4.55 (95.0)	633	4.55 (95.0)	533 (21.0)	184 (7.25)	4.43 (92.5)	5.44 (114)
70	4.69 (98.0)	661	4.84 (101)	521 (20.5)	114 (4.50)	4.58 (95.7)	5.62 (117)
71	5.22 (109)	734	5.22 (109)	565 (22.3)	197 (7.75)	5.14 (107)	6.35 (133)
72	4.26 (89.0)	591	4.21 (88.0)	445 (17.5)	203 (8.00)	4.13 (86.2)	5.06 (106)
73	8.67 (181)	1081	8.33 (174)	57.0 (2.25)	31.8 (1.25)	8.76 (183)	10.8 (225)
74	6.42 (134)	1182	6.27 (131)	800 (31.5)	184 (7.25)	6.53 (136)	8.10 (169)

W04 (Cont.) - Loading time history, failure location, EFL_{60} and EFL_3

Spec. No.	Time History		Reported EFL_{60} kPa (psf)	Failure location		EFL_{60} Recreated kPa (psf)	EFL_3 kPa (psf)
	Failure Pressure kPa (psf)	Failure Time (sec)		to long dimension mm (in.)	to short dimension mm (in.)		
75	5.60 (117)	722	5.65 (118)	514 (20.3)	165 (6.50)	5.51 (115)	6.82 (142)
76	4.98 (104)	592	4.50 (94.0)	413 (16.3)	140 (5.50)	4.83 (101)	5.94 (124)
77	4.36 (91.0)	577	4.07 (85.0)	330 (13.0)	159 (6.25)	4.21 (88.0)	5.17 (108)
78	5.84 (122)	662	5.12 (107)	330 (13.0)	241 (9.50)	5.71 (119)	7.06 (148)
79	9.58 (200)	1297	9.53 (199)	521 (20.5)	235 (9.25)	9.91 (207)	12.6 (264)
80	9.43 (197)	1	6.13 (128)	38.1 (1.50)	0.00 (0.00)	6.10 (127)	7.36 (154)
81	8.62 (180)	1	5.79 (121)	394 (15.5)	216 (8.50)	5.28 (110)	6.52 (136)
82	9.24 (193)	2	6.46 (135)	457 (18.0)	267 (10.5)	5.98 (125)	7.38 (154)
83	7.80 (163)	1	4.98 (104)	343 (13.5)	191 (7.50)	4.80 (100)	5.92 (124)
84	9.05 (189)	1	5.94 (124)	445 (17.5)	178 (7.00)	5.51 (115)	6.83 (143)
85	9.38 (196)	2	6.27 (131)	495 (19.5)	178 (7.00)	5.98 (125)	7.44 (155)
86	11.0 (229)	4	8.19 (171)	584 (23.0)	165 (6.50)	7.22 (151)	9.10 (190)
87	10.5 (220)	1	6.42 (134)	559 (22.0)	171 (6.75)	6.31 (132)	7.87 (164)
88	11.1 (232)	1	7.04 (147)	432 (17.0)	102 (4.00)	6.72 (140)	8.35 (174)
89	8.14 (170)	1	4.88 (102)	584 (23.0)	178 (7.00)	4.98 (104)	6.16 (129)
90	8.57 (179)	1	5.36 (112)	432 (17.0)	127 (5.00)	5.27 (110)	6.50 (136)
91*	12.8 (268)	1	3.45 (72.0)	356 (14.0)	0.00 (0.00)	5.12 (107)	7.72 (161)
92	8.76 (183)	1	5.36 (112)	368 (14.5)	152 (6.00)	5.35 (112)	6.62 (138)
93	11.9 (248)	1	7.95 (166)	737 (29.0)	254 (10.0)	7.26 (152)	8.98 (188)
94	11.3 (235)	1	7.09 (148)	457 (18.0)	229 (9.00)	6.76 (141)	8.43 (176)
95	6.08 (127)	2	4.21 (88.0)	597 (23.5)	152 (6.00)	3.99 (83.3)	4.89 (102)
96	6.85 (143)	3	4.98 (104)	292 (11.5)	152 (6.00)	4.58 (95.6)	5.64 (118)
97	8.19 (171)	2	5.70 (119)	737 (29.0)	248 (9.75)	5.36 (112)	6.58 (137)
98	7.57 (158)	1	4.55 (95.0)	356 (14.0)	203 (8.00)	4.67 (97.5)	5.75 (120)
99	10.6 (222)	1	6.42 (134)	279 (11.0)	210 (8.25)	6.35 (133)	7.93 (166)
100	10.2 (212)	1	6.32 (132)	38.1 (1.50)	25.0 (1.00)	6.44 (135)	7.84 (164)
101	13.8 (289)	1	8.14 (170)	178 (7.00)	146 (5.75)	8.10 (169)	10.2 (213)
102	6.56 (137)	1	3.78 (79.0)	495 (19.5)	184 (7.25)	4.09 (85.5)	5.02 (105)
103	11.8 (246)	1	7.09 (148)	438 (17.3)	159 (6.25)	6.98 (146)	8.75 (183)
104	8.62 (180)	1	5.17 (108)	394 (15.5)	229 (9.00)	5.29 (111)	6.53 (136)
105	14.3 (298)	1	8.62 (180)	241 (9.50)	210 (8.25)	8.22 (172)	10.4 (218)
106	14.9 (311)	1	9.38 (196)	813 (32.0)	178 (7.00)	8.86 (185)	11.1 (233)
107	13.9 (291)	1	8.43 (176)	237 (10.8)	222 (8.75)	8.11 (169)	10.3 (214)
108	15.0 (314)	2	9.53 (199)	457 (18.0)	229 (9.00)	9.23 (193)	11.7 (245)
109	9.10 (190)	1	5.70 (119)	0.00 (0.00)	279 (11.0)	5.73 (120)	6.99 (146)
110	15.5 (323)	2	10.8 (225)	229 (9.00)	279 (11.0)	9.78 (204)	12.2 (255)
111	9.91 (207)	1	6.22 (130)	229 (9.00)	178 (7.00)	5.95 (124)	7.41 (155)

* Specimen removed from parameter estimation

Table A.5W05 - Loading time history, failure location, EFL_{60} and EFL_3

Spec. No.	Time History		Reported EFL_{60} kPa (psf)	Failure location		EFL_{60} Recreated kPa (psf)	EFL_3 kPa (psf)
	Failure Pressure kPa (psf)	Failure Time (sec)		to long dimension mm (in.)	to short dimension mm (in.)		
1	10.1 (212)	30.1	8.14 (170)	740 (29.1)	9.82 (205)	8.12 (170)	9.82 (205)
2	7.38 (154)	21.2	5.79 (121)	749 (29.5)	6.99 (146)	5.79 (121)	6.99 (146)
3	4.34 (90.7)	13.6	3.31 (69.1)	1210 (47.8)	4.00 (83.6)	3.31 (69.2)	4.00 (83.6)
4	3.79 (79.2)	11.2	2.90 (60.5)	1110 (43.5)	3.45 (72.1)	2.86 (59.7)	3.45 (72.1)
5	8.48 (177)	28.2	6.76 (141)	616 (24.3)	8.18 (171)	6.76 (141)	8.18 (171)
6	5.65 (118)	15.2	4.34 (90.7)	521 (20.5)	5.24 (110)	4.34 (90.6)	5.24 (110)
7	5.79 (121)	14.4	4.41 (92.2)	610 (24.0)	5.35 (112)	4.43 (92.6)	5.35 (112)
8	7.17 (150)	25.1	5.65 (118)	552 (21.8)	6.86 (143)	5.68 (119)	6.86 (143)
9	7.45 (156)	25.4	5.86 (122)	152 (6.00)	7.14 (149)	5.88 (123)	7.14 (149)
10	8.83 (184)	30.9	7.10 (148)	857 (33.8)	8.56 (179)	7.09 (148)	8.56 (179)
11	10.0 (209)	34.2	8.07 (168)	1300 (51.0)	9.77 (204)	8.05 (168)	9.77 (204)
12	6.07 (127)	18.4	4.76 (99.4)	914 (36.0)	5.70 (119)	4.72 (98.6)	5.70 (119)
13	9.72 (203)	32.3	7.86 (164)	864 (34.0)	9.46 (197)	7.83 (164)	9.46 (197)
14	12.1 (252)	42.7	9.86 (206)	406 (16.0)	12.0 (250)	9.83 (205)	12.0 (250)
15	6.00 (125)	17.6	4.69 (97.9)	1220 (48.0)	5.61 (117)	4.65 (97.0)	5.61 (117)
16	9.45 (197)	33.2	7.65 (160)	1160 (45.5)	9.21 (192)	7.60 (159)	9.21 (192)
17	10.3 (216)	35.5	8.34 (174)	330 (13.0)	10.1 (212)	8.34 (174)	10.1 (212)
18	10.0 (209)	36	8.07 (168)	419 (16.5)	9.80 (205)	8.07 (168)	9.80 (205)
19	8.14 (170)	28.7	6.48 (135)	432 (17.0)	7.86 (164)	6.48 (135)	7.86 (164)
20	8.34 (174)	29.4	6.69 (140)	1250 (49.0)	8.07 (169)	6.66 (139)	8.07 (169)
21	8.48 (177)	30.1	6.76 (141)	305 (12.0)	8.22 (172)	6.78 (142)	8.22 (172)
22	5.79 (121)	20.9	4.55 (95.0)	1320 (52.0)	5.48 (114)	4.53 (94.7)	5.48 (114)
23	8.34 (174)	27	6.62 (138)	959 (37.8)	8.02 (168)	6.64 (139)	8.02 (168)
24	7.93 (166)	26.9	6.34 (132)	305 (12.0)	7.63 (159)	6.30 (132)	7.63 (159)
25	7.38 (154)	20.7	5.79 (121)	1370 (54.0)	6.98 (146)	5.76 (120)	6.98 (146)
26	7.45 (156)	25.7	5.93 (124)	445 (17.5)	7.14 (149)	5.90 (123)	7.14 (149)
27	7.03 (147)	26	5.58 (117)	508 (20.0)	6.75 (141)	5.58 (117)	6.75 (141)
28	13.3 (278)	48.5	11.0 (229)	76.2 (3.00)	13.3 (278)	11.0 (229)	13.3 (278)
29	11.2 (235)	39.7	9.17 (192)	648 (25.5)	11.1 (231)	9.15 (191)	11.1 (231)
30	5.58 (117)	17.9	4.34 (90.7)	1440 (56.5)	5.23 (109)	4.33 (90.5)	5.23 (109)
31	9.65 (202)	35.1	8.00 (167)	343 (13.5)	9.45 (197)	7.79 (163)	9.45 (197)
32	8.83 (184)	28.1	7.03 (147)	1320 (52.0)	8.51 (178)	7.02 (147)	8.51 (178)
33	9.45 (197)	32.9	7.58 (158)	464 (18.3)	9.21 (192)	7.59 (158)	9.21 (192)
34	9.38 (196)	33	7.58 (158)	400 (15.8)	9.14 (191)	7.54 (157)	9.14 (191)
35	7.03 (147)	25.3	5.58 (117)	572 (22.5)	6.74 (141)	5.57 (116)	6.74 (141)
36	8.55 (179)	30.4	6.83 (143)	1350 (53.0)	8.29 (173)	6.83 (143)	8.29 (173)

W05 (Cont.) - Loading time history, failure location, EFL_{60} and EFL_3

Spec. No.	Time History		Reported EFL_{60} kPa (psf)	Failure location		EFL_{60} Recreated kPa (psf)	EFL_3 kPa (psf)
	Failure Pressure kPa (psf)	Failure Time (sec)		to long dimension mm (in.)	to short dimension mm (in.)		
37	6.83 (143)	24.6	5.38 (112)	279 (11.0)	6.53 (136)	5.40 (113)	6.53 (136)
38	5.72 (120)	19.7	4.48 (93.6)	1000 (39.5)	5.40 (113)	4.47 (93.4)	5.40 (113)
39	8.48 (177)	30.1	6.83 (143)	686 (27.0)	8.21 (172)	6.80 (142)	8.21 (172)
40	6.55 (137)	23.4	5.17 (108)	279 (11.0)	6.24 (130)	5.16 (108)	6.24 (130)
41	11.9 (249)	41.9	9.72 (203)	610 (24.0)	11.8 (247)	9.73 (203)	11.8 (247)
42	8.34 (174)	30.2	6.69 (140)	311 (12.3)	8.08 (169)	6.68 (139)	8.08 (169)
43	8.62 (180)	29.3	6.89 (144)	927 (36.5)	8.33 (174)	6.90 (144)	8.33 (174)
44	9.72 (203)	32.8	7.79 (163)	254 (10.0)	9.47 (198)	7.81 (163)	9.47 (198)
45	7.58 (158)	24.7	6.00 (125)	508 (20.0)	7.25 (152)	5.99 (125)	7.25 (152)
46	6.00 (125)	19.9	4.69 (97.9)	1300 (51.0)	5.66 (118)	4.68 (97.8)	5.66 (118)
47	6.89 (144)	23.7	5.45 (114)	406 (16.0)	6.58 (137)	5.44 (114)	6.58 (137)
48	5.45 (114)	19	4.27 (89.3)	914 (36.0)	5.12 (107)	4.25 (88.7)	5.12 (107)
49	5.45 (114)	19.8	4.27 (89.3)	1020 (40.0)	5.14 (107)	4.26 (88.9)	5.14 (107)
50	5.38 (112)	18.7	4.21 (97.8)	1020 (40.0)	5.05 (106)	4.19 (87.5)	5.05 (106)
51	6.00 (125)	21.1	4.69 (98.0)	1020 (40.0)	5.68 (119)	4.71 (98.3)	5.68 (119)
52	7.58 (158)	26.1	6.00 (125)	400 (15.8)	7.28 (152)	6.01 (126)	7.28 (152)
53	7.38 (154)	26.8	5.86 (122)	1380 (54.5)	7.09 (148)	5.86 (122)	7.09 (148)
54	8.34 (174)	29.2	6.69 (140)	381 (15.0)	8.07 (168)	6.66 (139)	8.07 (168)
55	7.93 (166)	27.3	6.27 (131)	1400 (55.0)	7.63 (159)	6.30 (132)	7.63 (159)
56	6.21 (130)	20.9	4.83 (101)	1440 (56.5)	5.87 (123)	4.86 (101)	5.87 (123)
57	7.72 (161)	28.2	6.14 (128)	622 (24.5)	7.45 (156)	6.16 (129)	7.45 (156)
58	7.17 (150)	25.1	5.65 (118)	470 (18.5)	6.87 (143)	5.67 (118)	6.87 (143)
59	8.48 (177)	30.2	6.83 (143)	1020 (40.0)	8.21 (172)	6.80 (142)	8.21 (172)
60	9.86 (206)	34	7.93 (166)	432 (17.0)	9.63 (201)	7.93 (166)	9.63 (201)
61	9.58 (200)	34.3	7.79 (163)	343 (13.5)	9.37 (196)	7.72 (161)	9.37 (196)
62	6.14 (128)	21.9	4.83 (101)	927 (36.5)	5.82 (122)	4.83 (101)	5.82 (122)
63	7.79 (163)	27.6	6.21 (130)	673 (26.5)	7.50 (157)	6.21 (130)	7.50 (157)
64	10.1 (212)	36.4	8.20 (171)	660 (26.0)	9.94 (208)	8.21 (171)	9.94 (208)
65	8.48 (177)	31.7	6.96 (145)	1230 (48.5)	8.24 (172)	6.80 (142)	8.24 (172)
66	7.72 (161)	28.9	6.14 (128)	330 (13.0)	7.46 (156)	6.17 (129)	7.46 (156)
67	8.27 (173)	28.5	6.62 (138)	864 (34.0)	7.98 (167)	6.62 (138)	7.98 (167)
68	8.83 (184)	31.5	7.10 (148)	591 (23.3)	8.57 (179)	7.08 (148)	8.57 (179)
69	7.24 (151)	27.5	5.79 (121)	686 (27.0)	6.97 (146)	5.77 (121)	6.97 (146)
70	6.34 (132)	23.9	5.03 (105)	356 (14.0)	6.05 (126)	5.01 (105)	6.05 (126)
71	7.03 (147)	24.6	5.58 (117)	775 (30.5)	6.72 (140)	5.57 (116)	6.72 (140)
72	8.83 (184)	30.5	7.10 (148)	1080 (42.5)	8.55 (179)	7.07 (148)	8.55 (179)

W05(Cont.) - Loading time history, failure location, EFL_{60} and EFL_3

Spec. No.	Time History		Reported EFL_{60} kPa (psf)	Failure location		EFL_{60} Recreated kPa (psf)	EFL_3 kPa (psf)
	Failure Pressure kPa (psf)	Failure Time (sec)		to long dimension mm (in.)	to short dimension mm (in.)		
73	10.0 (209)	25	7.93 (166)	267 (10.5)	9.57 (200)	7.89 (165)	9.57 (200)
74	8.76 (183)	31.8	7.03 (147)	921 (36.3)	8.51 (178)	7.05 (147)	8.51 (178)
75	15.9 (333)	53.9	13.2 (276)	533 (21.0)	16.1 (335)	13.2 (275)	16.1 (335)
76	8.96 (187)	28.1	7.17 (150)	1040 (41.0)	8.64 (181)	7.15 (149)	8.64 (181)
77	11.3 (236)	40.8	9.24 (193)	273 (10.8)	11.2 (234)	9.19 (192)	11.2 (234)
78	10.1 (210)	34.0	8.14 (170)	229 (9.00)	9.83 (205)	8.10 (169)	9.83 (205)
79	8.62 (180)	29.4	6.89 (144)	1320 (52.0)	8.34 (174)	6.87 (144)	8.34 (174)
80	7.93 (166)	29.3	6.34 (132)	381 (15.0)	7.67 (160)	6.33 (132)	7.67 (160)
81	8.20 (171)	28.3	6.55 (137)	279 (11.0)	7.92 (165)	6.53 (136)	7.92 (165)
82	10.7 (223)	38	8.69 (181)	737 (29.0)	10.5 (219)	8.69 (181)	10.5 (219)

Table A.6W06 - Loading time history, failure location, EFL_{60} and EFL_3

Spec. No.	Time History		Reported EFL_{60} kPa (psf)	Failure location		EFL_{60} Recreated kPa (psf)	EFL_3 kPa (psf)
	Failure Pressure kPa (psf)	Failure Time (sec)		to long dimension mm (in.)	to short dimension mm (in.)		
1	19.8 (413)	59.6	16.5 (346)	806 (31.8)	114 (4.5)	16.2 (338)	19.6 (410)
2	10.3 (215)	29.6	8.21 (171)	489 (19.3)	203 (8.0)	8.03 (168)	9.73 (203)
3	15.2 (318)	43.4	12.5 (261)	838 (33.0)	191 (7.5)	12.2 (255)	14.8 (309)
4	18.2 (380)	54.6	15.1 (315)	737 (29.0)	140 (5.5)	14.8 (309)	17.9 (375)
5	20.8 (435)	60.8	17.2 (359)	473 (18.6)	241 (9.5)	16.9 (353)	20.8 (434)
6	18.6 (389)	65.4	15.7 (327)	851 (33.5)	219 (8.62)	15.3 (320)	18.6 (388)
7	15.5 (324)	55.5	12.9 (269)	851 (33.5)	241 (9.5)	12.6 (264)	15.3 (319)
8	18.3 (382)	62.3	15.3 (320)	851 (33.5)	222 (8.75)	15.0 (313)	18.2 (379)
9	20.1 (419)	67.5	16.8 (350)	654 (25.8)	184 (7.25)	16.5 (344)	20.1 (420)
10	16.2 (338)	55.5	13.4 (281)	508 (20.0)	108 (4.25)	13.2 (275)	16.0 (334)
11	20.8 (433)	71.9	17.4 (363)	483 (19.0)	229 (9.0)	17.1 (356)	20.9 (437)
12	19.4 (406)	66.4	16.2 (338)	508 (20.0)	191 (7.5)	15.9 (333)	19.5 (407)
13	17.0 (356)	58.1	14.2 (297)	737 (29.0)	146 (5.75)	13.9 (290)	16.8 (352)
14	13.4 (281)	47.4	11.0 (230)	495 (19.5)	210 (8.25)	10.8 (226)	13.1 (274)
15	10.3 (215)	36.3	8.27 (173)	483 (19.0)	206 (8.12)	8.14 (170)	9.86 (206)
16	11.7 (245)	40.8	9.58 (200)	714 (28.1)	146 (5.75)	9.37 (196)	11.3 (237)
17	15.7 (327)	56.0	13.0 (271)	686 (27.0)	213 (8.38)	12.7 (266)	15.4 (323)
18	14.5 (304)	50.1	12.0 (251)	432 (17.0)	133 (5.25)	11.7 (245)	14.3 (298)
19	15.6 (325)	53.3	12.9 (269)	686 (27.0)	235 (9.25)	12.6 (264)	15.3 (320)
20	28.3 (590)	98.0	24.2 (505)	178 (7.00)	95 (3.75)	23.7 (496)	29.1 (607)
21	9.86 (206)	33.6	7.93 (166)	483 (19.0)	210 (8.25)	7.77 (162)	9.41 (197)
22	14.8 (310)	53.1	12.3 (258)	743 (29.3)	197 (7.8)	12.0 (251)	14.6 (304)
23	16.3 (341)	57.9	13.5 (282)	425 (16.8)	152 (6.0)	13.3 (278)	16.2 (338)
24	15.9 (333)	54.9	13.2 (275)	622 (24.5)	248 (9.8)	12.9 (270)	15.7 (328)
25	16.1 (336)	50.3	13.2 (276)	813 (32.0)	222 (8.8)	13.0 (271)	15.7 (329)
26	11.7 (245)	41.8	9.52 (199)	483 (19.0)	191 (7.5)	9.4 (195)	11.4 (237)
27	24.3 (507)	85.5	20.5 (429)	432 (17.0)	191 (7.5)	20.1 (420)	24.8 (519)
28	19.7 (412)	69.7	16.5 (346)	635 (25.0)	248 (9.8)	16.2 (339)	19.8 (413)
29	11.8 (246)	40.5	9.58 (200)	483 (19.0)	235 (9.3)	9.4 (196)	11.4 (238)
30	16.5 (346)	56.6	13.7 (285)	140 (5.50)	50.8 (2.0)	13.4 (280)	16.4 (342)
31	26.0 (543)	91.2	22.2 (464)	425 (16.8)	102 (4.0)	21.7 (453)	26.6 (557)
32	21.7 (454)	78.1	18.3 (383)	533 (21.0)	152 (6.0)	18.0 (376)	22.0 (459)
33	18.4 (384)	63.5	15.4 (321)	635 (25.0)	210 (8.3)	15.1 (315)	18.3 (383)
34	11.6 (242)	41.0	9.45 (197)	483 (19.0)	235 (9.3)	9.24 (193)	11.2 (234)
35	12.9 (269)	45.7	10.6 (222)	775 (30.5)	146 (5.8)	10.4 (217)	12.5 (262)
36	16.5 (346)	57.2	13.7 (287)	381 (15.0)	146 (5.8)	13.4 (281)	16.4 (342)

W06 (Cont.) - Loading time history, failure location, EFL_{60} and EFL_3

Spec. No.	Time History		Reported EFL_{60} kPa (psf)	Failure location		EFL_{60} Recreated kPa (psf)	EFL_3 kPa (psf)
	Failure Pressure kPa (psf)	Failure Time (sec)		to long dimension mm (in.)	to short dimension mm (in.)		
37	17.3 (361)	61.5	14.3 (300)	381 (15.0)	203 (8.0)	14.1 (294)	17.2 (360)
38	11.3 (236)	40.2	9.17 (192)	279 (11.0)	159 (6.3)	9.01 (188)	10.9 (228)
39	17.9 (374)	62.1	15.0 (312)	635 (25.0)	203 (8.0)	14.7 (306)	17.8 (373)
40	16.3 (341)	58.1	13.6 (284)	635 (25.0)	178 (7.0)	13.3 (278)	16.2 (338)
41	11.2 (235)	38.6	9.17 (192)	667 (26.3)	210 (8.3)	8.95 (187)	10.8 (226)
42	14.5 (304)	50.5	12.0 (251)	660 (26.0)	152 (6.0)	11.8 (246)	14.3 (298)
43	18.3 (382)	62.7	15.3 (320)	635 (25.0)	197 (7.8)	15.0 (312)	18.2 (380)
44	10.8 (225)	37.7	8.69 (181)	483 (19.0)	165 (6.5)	8.54 (178)	10.3 (216)
45	20.3 (425)	71.6	17.2 (359)	635 (25.0)	159 (6.3)	16.8 (350)	20.4 (427)
46	19.4 (406)	69.2	16.3 (340)	781 (30.8)	203 (8.0)	16.0 (335)	19.5 (407)
47	17.1 (357)	60.4	14.3 (298)	724 (28.5)	184 (7.3)	14.0 (292)	17.0 (354)
48	14.1 (295)	49.3	11.7 (243)	433 (17.1)	26.7 (1.1)	11.4 (237)	13.9 (290)
49	9.65 (202)	34.1	7.79 (163)	483 (19.0)	222 (8.8)	7.62 (159)	9.23 (193)
50	11.4 (238)	39.5	9.24 (193)	483 (19.0)	184 (7.3)	9.05 (189)	11.0 (229)
51	20.4 (426)	70.2	17.0 (356)	406 (16.0)	210 (8.3)	16.7 (349)	20.6 (429)
52	17.6 (367)	60.3	14.7 (307)	699 (27.5)	121 (4.8)	14.4 (300)	17.4 (364)
53	25.1 (524)	88.7	21.4 (448)	864 (34.0)	121 (4.8)	21.0 (438)	25.6 (535)

Table A.7
W07 - Loading time history, failure location, EFL_{60} and EFL_3

Spec. No.	Time History		Reported EFL_{60} kPa (psf)	Failure location		EFL_{60} Recreated kPa (psf)	EFL_3 kPa (psf)
	Failure Pressure kPa (psf)	Failure Time (sec)		to long dimension mm (in.)	to short dimension mm (in.)		
1	14.3 (298)	41.8	11.7 (243)	619 (24.4)	210 (8.25)	11.4 (238)	13.8 (289)
2	15.2 (318)	44.3	12.4 (259)	483 (19.0)	108 (4.25)	12.2 (255)	14.8 (310)
3	17.3 (361)	49.9	14.2 (297)	470 (18.5)	222 (8.75)	13.9 (291)	17.0 (355)
4	20.8 (433)	60.2	17.2 (360)	483 (19.0)	121 (4.75)	16.9 (353)	20.6 (431)
5	23.6 (492)	93.9	20.2 (422)	521 (20.5)	171 (6.75)	19.7 (412)	24.2 (506)
6	12.4 (259)	43.4	10.1 (212)	483 (19.0)	171 (6.75)	9.93 (207)	12.1 (252)
7	16.8 (350)	58.3	13.9 (289)	591 (23.3)	241 (9.50)	13.6 (285)	16.6 (347)
8	21.9 (456)	76.3	18.4 (384)	699 (27.5)	235 (9.25)	18.1 (378)	22.1 (461)
9	20.3 (425)	71.6	17.1 (357)	676 (26.6)	102 (4.00)	16.8 (351)	20.4 (427)
10	15.0 (314)	52.7	12.4 (259)	641 (25.3)	178 (7.00)	12.2 (254)	14.8 (309)
11	10.6 (222)	37.1	8.62 (180)	483 (19.0)	238 (9.37)	8.42 (176)	10.2 (213)
12	12.4 (259)	42.8	10.1 (212)	673 (26.5)	191 (7.50)	9.94 (208)	12.0 (251)
13	17.7 (370)	63.9	14.9 (311)	711 (28.0)	152 (6.00)	14.5 (304)	17.6 (369)
14	27.0 (564)	95.5	23.3 (487)	57.2 (2.25)	8.89 (0.35)	22.8 (477)	27.5 (575)
15	24.5 (511)	85.6	20.8 (435)	114 (4.50)	102 (4.00)	20.4 (425)	25.0 (521)
16	10.8 (226)	36.2	8.76 (183)	705 (27.8)	191 (7.50)	8.59 (179)	10.4 (217)
17	15.0 (314)	53.5	12.4 (259)	432 (17.0)	178(7.0)	12.2 (254)	14.8 (309)
18	22.8 (475)	81.5	19.2 (402)	102 (4.00)	133 (5.25)	18.9 (394)	23.1 (483)
19	17.8 (372)	61.4	14.8 (310)	368 (14.5)	121 (4.75)	14.5 (303)	17.7 (370)
20	13.0 (272)	44	10.7 (223)	724 (28.5)	121 (4.75)	10.5 (219)	12.7 (264)
21	21.6 (451)	75.3	18.1 (379)	445 (17.5)	171 (6.75)	17.8 (371)	21.8 (456)
22	17.9 (373)	63.5	15.0 (312)	851 (33.5)	216 (8.50)	14.7 (306)	17.8 (371)
23	16.3 (340)	56.6	13.5 (282)	660 (26.0)	222 (8.75)	13.2 (277)	16.1 (336)
24	13.1 (274)	46.7	10.8 (225)	813 (32.0)	248 (9.75)	10.6 (221)	12.8 (267)
25	16.8 (350)	58.9	13.9 (291)	381 (15.0)	146 (5.75)	13.6 (285)	16.6 (347)
26	13.5 (282)	43.3	11.0 (230)	394 (15.5)	203 (8.00)	10.8 (225)	13.1 (274)
27	13.4 (281)	46.5	11.1 (232)	838 (33.0)	229 (9.00)	10.8 (226)	13.1 (274)
28	26.1 (546)	95.7	22.4 (468)	178 (7.00)	69.9 (2.75)	21.9 (457)	26.9 (561)
29	11.4 (239)	38	9.24 (193)	483 (19.0)	219 (8.63)	9.08 (190)	11.0 (230)
30	10.5 (219)	15	8.07 (168)	41.2 (1.62)	12.7 (0.50)	7.88 (165)	9.51 (199)
31	20.1 (420)	73.2	16.9 (353)	216 (8.50)	76.2 (3.00)	16.6 (346)	20.3 (424)
32	23.0 (481)	81	19.5 (408)	800 (31.5)	229 (9.00)	19.1 (400)	23.4 (488)
33	23.0 (481)	81	19.6 (409)	69.9 (2.75)	19.2 (0.80)	19.2 (401)	23.3 (486)
34	24.1 (503)	84	20.5 (428)	381 (15.0)	102 (4.00)	20.0 (418)	24.5 (512)

W07 (Cont.) - Loading time history, failure location, EFL_{60} and EFL_3

Spec. No.	Time History		Reported	Failure location		EFL_{60}	EFL_3 kPa (psf)
	Failure Pressure kPa (psf)	Failure Time (sec)	EFL_{60} kPa (psf)	to long dimension mm (in.)	to short dimension mm (in.)	Recreated kPa (psf)	
35	11.8 (246)	41.4	9.65 (202)	483 (19.0)	235 (9.25)	9.40 (196)	11.4 (238)
36	12.5 (262)	43.2	10.3 (215)	686 (27.0)	140 (5.50)	10.1 (210)	12.2 (254)
37	16.8 (350)	59.2	13.9 (289)	381 (15.0)	178 (7.00)	13.6 (285)	16.6 (348)
38	22.8 (477)	80.8	19.4 (405)	597 (23.5)	248 (9.75)	18.9 (395)	23.2 (485)
39	13.9 (289)	49	11.4 (239)	692 (27.3)	184 (7.25)	11.2 (234)	13.6 (283)
40	11.1 (232)	41.5	9.10 (190)	483 (19.0)	159 (6.25)	8.87 (185)	10.7 (224)

Table A.8W08 - Loading time history, failure location, EFL_{60} and EFL_3

Spec. No.	Time History		Reported EFL_{60} kPa (psf)	Failure location		EFL_{60} Recreated kPa (psf)	EFL_3 kPa (psf)
	Failure Pressure kPa (psf)	Failure Time (sec)		to long dimension mm (in.)	to short dimension mm (in.)		
1	20.5 (428)	61.0	17.1 (357)	0.00 (0.00)	102 (4.00)	16.8 (350)	20.3 (424)
2	22.1 (461)	63.9	18.4 (384)	660 (26.0)	241 (9.50)	18.0 (377)	22.0 (460)
3	9.79 (204)	27.8	7.79 (163)	483 (19.0)	229 (9.00)	7.62 (159)	9.24 (193)
4	12.5 (261)	35.9	10.1 (210)	572 (22.5)	191 (7.50)	9.87 (206)	12.0 (250)
5	9.52 (199)	26.5	7.58 (158)	591 (23.3)	241 (9.50)	7.40 (154)	8.95 (187)
6	10.8 (226)	39.7	8.82 (184)	794 (31.3)	127 (5.00)	8.65 (181)	10.4 (218)
7	11.2 (235)	39.4	9.17 (192)	762 (30.0)	229 (9.00)	8.97 (187)	10.8 (226)
8	16.3 (341)	56.5	13.6 (284)	864 (34.0)	95.3 (3.75)	13.3 (278)	16.1 (337)
9	16.1 (337)	55.8	13.4 (281)	578 (22.8)	165 (6.50)	13.1 (274)	15.9 (333)
10	20.5 (429)	73.3	17.3 (361)	572 (22.5)	108 (4.25)	17.0 (354)	20.7 (432)
11	6.55 (137)	23.4	5.17 (108)	533 (21.0)	229 (9.00)	5.06 (106)	6.11 (128)
12	9.99 (209)	34.5	8.07 (168)	711 (28.0)	191 (7.50)	7.91 (165)	9.56 (200)
13	11.0 (230)	38.8	8.96 (187)	660 (26.0)	140 (5.50)	8.79 (184)	10.6 (222)
14	19.6 (409)	68.2	16.5 (344)	495 (19.5)	184 (7.25)	16.1 (335)	19.7 (411)
15	9.52 (199)	32.3	7.58 (158)	622 (24.5)	140 (5.50)	7.50 (157)	9.06 (189)
16	13.4 (281)	46.4	11.0 (230)	495 (19.5)	171 (6.75)	10.8 (226)	13.1 (274)
17	11.2 (235)	38.5	9.17 (192)	768 (30.3)	127 (5.00)	8.96 (187)	10.8 (226)
18	17.7 (370)	60.0	14.8 (308)	610 (24.0)	248 (9.75)	14.4 (302)	17.6 (368)
19	11.8 (246)	41.0	9.58 (200)	489 (19.3)	248 (9.75)	9.40 (196)	11.4 (238)
20	13.0 (271)	45.0	10.6 (222)	737 (29.0)	197 (7.75)	10.4 (218)	12.6 (263)
21	11.2 (235)	40.3	9.17 (192)	762 (30.0)	146 (5.75)	8.98 (188)	10.9 (227)
22	11.0 (230)	38.8	8.96 (187)	654 (25.8)	235 (9.25)	8.79 (184)	10.6 (222)
23	20.4 (426)	71.3	17.1 (357)	533 (21.0)	210 (8.25)	16.8 (351)	20.5 (429)
24	10.7 (223)	36.5	8.68 (181)	813 (32.0)	146 (5.75)	8.49 (177)	10.3 (214)
25	16.7 (348)	59.3	13.9 (289)	845 (33.3)	121 (4.75)	13.6 (285)	16.5 (345)
26	14.3 (300)	49.7	11.8 (246)	546 (21.5)	241 (9.50)	11.6 (242)	14.1 (294)
27	12.0 (251)	42.4	9.79 (204)	686 (27.0)	251 (9.87)	9.61 (201)	11.6 (243)
28	11.9 (248)	41.8	9.65 (202)	635 (25.0)	184 (7.25)	9.49 (198)	11.5 (240)
29	11.1 (232)	39.6	9.03 (189)	540 (21.3)	114 (4.50)	8.85 (185)	10.7 (224)
30	15.4 (323)	57.1	12.8 (268)	610 (24.0)	241 (9.50)	12.6 (263)	15.3 (319)
31	16.1 (337)	58.5	13.4 (279)	629 (24.8)	114 (4.50)	13.2 (275)	16.0 (334)
32	16.8 (350)	60.1	13.9 (291)	559 (22.0)	222 (8.75)	13.7 (285)	16.6 (348)
33	8.89 (186)	31.1	7.17 (150)	483 (19.0)	207 (8.13)	6.98 (146)	8.45 (176)
34	15.3 (320)	53.4	12.5 (262)	432 (17.0)	222 (8.75)	12.4 (258)	15.1 (315)
35	13.2 (275)	45.7	10.8 (225)	241 (9.50)	159 (6.25)	10.6 (221)	12.8 (268)
36	11.5 (240)	38.3	9.31 (194)	381 (15.0)	229 (9.00)	9.13 (191)	11.1 (232)
37	11.5 (240)	41.7	9.37 (196)	730 (28.8)	184 (7.25)	9.22 (193)	11.1 (233)

W08 (Cont.) - Loading time history, failure location, EFL_{60} and EFL_3

Spec. No.	Time History		Reported EFL_{60} kPa (psf)	Failure location		EFL_{60} Recreated kPa (psf)	EFL_3 kPa (psf)
	Failure Pressure kPa (psf)	Failure Time (sec)		to long dimension mm (in.)	to short dimension mm (in.)		
38	11.9 (249)	40.8	9.72 (203)	578 (22.8)	171 (6.75)	9.52 (199)	11.5 (241)
39	15.5 (324)	55.0	12.9 (269)	483 (19.0)	127 (5.00)	12.6 (263)	15.3 (320)
40	16.9 (353)	60.1	14.0 (292)	305 (12.0)	140 (5.50)	13.8 (288)	16.8 (350)
41	9.31 (194)	32.4	7.45 (156)	483 (19.0)	248 (9.75)	7.32 (153)	8.87 (185)
42	12.5 (261)	43.6	10.2 (213)	533 (21.0)	235 (9.25)	9.99 (209)	12.1 (253)
43	13.2 (276)	44.3	10.8 (226)	711 (28.0)	197 (7.75)	10.6 (222)	12.9 (269)
44	16.2 (338)	55.6	13.4 (281)	635 (25.0)	146 (5.75)	13.2 (275)	16.0 (334)
45	16.5 (344)	56.5	13.6 (284)	254 (10.0)	197 (7.75)	13.4 (279)	16.3 (341)
46	12.5 (261)	43.5	10.2 (213)	845 (33.3)	229 (9.00)	10.0 (209)	12.1 (253)
47	10.2 (213)	35.2	8.21 (171)	368 (14.5)	222 (8.75)	8.06 (168)	9.78 (204)
48	12.2 (255)	40.3	10.0 (209)	813 (32.0)	178 (7.00)	9.75 (204)	11.8 (246)
49	11.7 (243)	40.2	9.45 (197)	273 (10.8)	222 (8.75)	9.28 (194)	11.3 (235)
50	17.3 (361)	59.0	14.4 (301)	749 (29.5)	229 (9.00)	14.1 (295)	17.1 (358)
51	13.2 (276)	45.1	10.8 (226)	514 (20.3)	203 (8.00)	10.6 (222)	12.9 (269)
52	13.4 (279)	46.7	11.0 (230)	724 (28.5)	102 (4.00)	10.8 (225)	13.0 (272)
53	10.1 (212)	35.3	8.21 (171)	787 (31.0)	203 (8.00)	8.04 (168)	9.70(203)
54	6.96 (145)	22.7	5.52 (115)	635 (25.0)	197 (7.75)	5.37 (112)	6.48 (135)
55	12.3 (256)	43.0	10.0 (209)	483 (19.0)	165 (6.50)	9.82 (205)	11.9 (249)
56	13.0 (272)	44.9	10.7 (223)	495 (19.5)	127 (5.00)	10.5 (218)	12.7 (265)
57	4.34 (91)	15.5	3.31 (69)	140 (5.5)	121 (4.75)	3.26 (68.2)	3.95 (82.4)
58	14.1 (295)	50.3	11.7 (245)	857 (33.8)	82.5 (3.25)	11.5 (239)	13.8 (289)
59	9.65 (202)	34.4	7.79 (163)	660 (26.0)	235 (9.25)	7.63 (159)	9.23 (193)
60	14.1 (295)	50.3	11.7 (243)	394 (15.5)	165 (6.50)	11.4 (238)	13.9 (290)
61	13.4 (279)	46.8	11.0 (229)	552 (21.8)	171 (6.75)	10.8 (225)	13.1 (273)
62	18.1 (379)	63.4	15.1 (315)	356 (14.0)	203 (8.00)	14.8 (309)	18.1 (379)
63	14.3 (298)	49.4	11.8 (246)	813 (32.0)	241 (9.50)	11.5 (241)	14.0 (292)
64	9.52 (199)	33.9	7.65 (160)	660 (26.0)	184 (7.25)	7.52 (157)	9.09 (190)
65	14.8 (310)	54.8	12.3 (256)	76.2 (3.00)	50.8 (2.00)	12.0 (251)	14.6 (305)
66	16.8 (351)	48.2	13.8 (288)	718 (28.3)	184 (7.25)	13.6 (283)	16.4 (344)

Table A.9W09 - Loading time history, failure location, EFL_{60} and EFL_3

Spec. No.	Time History		Reported EFL_{60} kPa (psf)	Failure location		EFL_{60} Recreated kPa (psf)	EFL_3 kPa (psf)
	Failure Pressure kPa (psf)	Failure Time (sec)		to long dimension mm (in.)	to short dimension mm (in.)		
1	7.13 (149)	59	-	692 (27.3)	241 (9.5)	5.74 (120)	7.13 (149)
2	8.32 (174)	55	-	367 (14.4)	273 (10.8)	6.65 (139)	8.29 (173)
3	7.87 (164)	40	-	718 (28.3)	273 (10.8)	6.14 (128)	7.66 (160)
4	7.30 (152)	49	-	718 (28.3)	321 (12.6)	5.78 (121)	7.21 (151)
5	8.12 (170)	59	-	621 (24.4)	298 (11.8)	6.50 (136)	8.15 (170)
6	8.07 (169)	76	-	629 (24.8)	276 (10.9)	6.59 (138)	8.26 (173)
7	7.79 (163)	72	-	705 (27.8)	248 (9.75)	6.34 (132)	7.93 (166)
8	7.17 (150)	68	-	533 (21.0)	318 (12.5)	5.82 (122)	7.26 (152)
9	8.51 (178)	89	-	102 (4.00)	6.35 (0.25)	7.12 (149)	8.68 (181)
10	8.61 (180)	87	-	483 (19.0)	241 (9.50)	7.10 (148)	8.91 (186)
11	7.65 (160)	67	-	540 (21.3)	286 (11.3)	6.20 (129)	7.75 (162)
12	6.27 (131)	64	-	616 (24.3)	267 (10.5)	5.09 (106)	6.29 (131)
13	8.07 (169)	83	-	521 (20.5)	286 (11.3)	6.63 (139)	8.32 (174)
14	7.87 (164)	56	-	648 (25.5)	222 (8.75)	6.30 (132)	7.85 (164)
15	9.80 (205)	107	-	565 (22.3)	238 (9.38)	8.18 (171)	10.4 (216)
16	6.67 (139)	61	-	584 (23.0)	295 (11.6)	5.38 (112)	6.68 (140)
17	9.92 (207)	87	-	464 (18.3)	298 (11.8)	8.13 (170)	10.3 (216)
18	5.29 (110)	37	-	514 (20.3)	324 (12.8)	4.15 (86.6)	5.10 (106)
19	4.65 (97.1)	43	-	743 (29.3)	318 (12.5)	3.69 (77.2)	4.52 (94.5)
20	7.49 (157)	73	-	425 (16.8)	254 (10.0)	6.12 (128)	7.62 (159)
21	9.61 (201)	119	-	476 (18.8)	311 (12.3)	8.07 (169)	10.3 (215)
22	9.07 (190)	89	-	679 (26.8)	178 (7.00)	7.50 (157)	9.39 (196)
23	8.18 (171)	82	-	114 (4.5)	6.35 (0.25)	6.80 (142)	8.30 (173)

Table A.10
W10 - Loading time history, failure location, EFL_{60} and EFL_3

Spec. No.	Time History		Reported EFL_{60} kPa (psf)	Failure location		EFL_{60} Recreated kPa (psf)	EFL_3 kPa (psf)
	Failure Pressure kPa (psf)	Failure Time (sec)		to long dimension mm (in.)	to short dimension mm (in.)		
1	7.57 (158)	71	-	533 (21.0)	305 (12.0)	5.97 (125)	7.96 (166)
2	7.11 (149)	62	-	318 (12.5)	305 (12.0)	5.61 (117)	7.28 (152)
3	7.95 (166)	65	-	216 (8.50)	343 (13.5)	6.44 (135)	8.00 (167)
4	10.9 (227)	100	-	241 (9.50)	267 (10.5)	8.91 (186)	11.6 (242)
5	6.66 (139)	67	-	25.4 (1.00)	25.4 (1.00)	5.43 (113)	6.69 (140)
6	4.65 (97.1)	49	-	102 (4.00)	0.00 (0.00)	3.72 (77.6)	4.57 (95.5)
7	5.31 (111)	51	-	0.00 (0.00)	0.00 (0.00)	4.26 (88.9)	5.23 (109)
8	2.96 (61.9)	27	-	381 (15.0)	241 (9.50)	2.27 (47.5)	2.80 (58.4)
9	7.13 (149)	67	-	400 (15.8)	330 (13.0)	5.62 (117)	7.41 (155)
10	6.94 (145)	62	-	241 (9.50)	12.7 (0.50)	5.29 (111)	7.42 (155)
11	11.1 (232)	106	-	88.9 (3.50)	19.1 (0.75)	9.30 (194)	11.7 (244)
12	9.49 (198)	82	-	76.2 (3.00)	0.00 (0.00)	7.81 (163)	9.71 (203)

Table A.11W11 - Loading time history, failure location, EFL_{60} and EFL_3

Spec. No.	Time History		Reported EFL_{60} kPa (psf)	Failure location		EFL_{60} Recreated kPa (psf)	EFL_3 kPa (psf)
	Failure Pressure kPa (psf)	Failure Time (sec)		to long dimension mm (in.)	to short dimension mm (in.)		
1	10.7 (224)	86	-	356 (14.0)	318 (12.5)	8.55 (179)	11.7 (244)
2	11.0 (230)	123	-	419 (16.5)	356 (14.0)	9.04 (189)	12.7 (265)
3	9.69 (203)	91	-	267 (10.5)	222 (8.75)	7.92 (166)	10.2 (213)
4	9.64 (201)	49	-	127 (5.00)	254 (10.0)	7.61 (159)	9.52 (199)
5	11.8 (246)	84	-	50.8 (2.00)	19.1 (0.75)	9.70 (203)	12.1 (253)
6	12.6 (263)	77	-	352 (13.9)	368 (14.5)	9.80 (205)	13.8 (288)
7	10.7 (223)	61	-	356 (14.0)	279 (11.0)	8.30 (173)	11.1 (232)
8	11.0 (229)	81	-	38.1 (1.50)	12.7 (0.50)	9.03 (189)	11.2 (234)
9	6.42 (134)	61	-	25.4 (1.0)	63.5 (2.50)	5.19 (108)	6.42 (134)
10	12.9 (270)	125	-	31.8 (1.25)	50.8 (2.00)	11.0 (229)	13.7 (286)
11	5.61 (117)	42	-	216 (8.50)	216 (8.50)	4.37 (91.2)	5.50 (115)

Table A.12W12 - Loading time history, failure location, EFL_{60} and EFL_3

Spec. No.	Time History		Reported EFL_{60} kPa (psf)	Failure location		EFL_{60} Recreated kPa (psf)	EFL_3 kPa (psf)
	Failure Pressure kPa (psf)	Failure Time (sec)		to long dimension mm (in.)	to short dimension mm (in.)		
1	5.94 (124)	49	-	50.8 (2.00)	50.8 (2.00)	4.70 (98.1)	5.87 (123)
2	6.85 (143)	65	-	171 (6.75)	121 (4.75)	5.53 (115)	6.92 (145)
3	5.33 (111)	62	-	343 (13.5)	292 (11.5)	3.81 (79.7)	6.11 (128)
4	6.03 (126)	61	-	12.7 (0.50)	0.00 (0.00)	4.88 (102)	6.03 (126)
5	5.69 (119)	71	-	102 (4.00)	76.2 (3.00)	4.65 (97.1)	5.76 (120)
6	6.33 (132)	68	-	76.2 (3.00)	12.7 (0.50)	5.06 (106)	6.51 (136)
7	3.81 (79.6)	39	-	50.8 (2.00)	12.7 (0.50)	2.96 (61.8)	3.70 (77.4)
8	5.69 (119)	70	-	394 (15.5)	267 (10.5)	4.16 (86.9)	6.73 (141)
9	7.40 (155)	75	-	394 (15.5)	235 (9.25)	5.52 (115)	8.64 (181)
10	7.58 (158)	93	-	63.5 (2.50)	105 (4.13)	6.32 (132)	7.80 (163)
11	5.07 (106)	54	-	95.3 (3.75)	3.18 (0.13)	3.89 (81.3)	5.20 (109)
12	6.18 (129)	66	-	0.00 (0.00)	38.1 (1.50)	5.01 (105)	6.22 (130)
13	4.77 (99.6)	39	-	12.7 (0.50)	0.00 (0.00)	3.73 (78.0)	4.62 (96.5)
14	7.27 (152)	72	-	76.2 (3.00)	57.2 (2.25)	5.94 (124)	7.36 (154)
15	7.80 (163)	67	-	79.9 (2.75)	82.6 (3.25)	6.36 (133)	7.84 (164)
16	5.31 (111)	51	-	25.4 (1.00)	12.7 (0.5)	4.24 (88.5)	5.25 (110)
17	7.17 (150)	74	-	152 (6.0)0	248 (9.75)	5.66 (118)	7.62 (159)
18	9.44 (197)	97	-	31.8 (1.25)	44.5 (1.75)	7.85 (164)	9.80 (205)
19	10.8 (226)	85	-	203 (8.0)0	102 (4.00)	8.85 (185)	11.3 (236)
20	8.44 (176)	77	-	159 (6.25)	127 (5.00)	6.87 (143)	8.68 (181)
21	5.76 (120)	44	-	50.8 (2.00)	0.00 (0.00)	4.51 (94.2)	5.64 (118)
22	6.60 (138)	55	-	146 (5.75)	146 (5.75)	5.21 (109)	6.63 (138)
23	5.77 (121)	46	-	292 (11.5)	159 (6.25)	4.34 (90.7)	5.83 (122)
24	8.17 (171)	43	-	159 (6.25)	203 (8.00)	6.15 (128)	8.16 (171)
25	4.29 (89.6)	36	-	406 (16.0)	260 (10.3)	2.90 (61.6)	4.47 (93.4)
26	4.81 (101)	43	-	140 (5.50)	203 (8.00)	3.71 (77.6)	4.74 (99.0)
27	7.56 (158)	74	-	368 (14.5)	171 (6.75)	5.87 (123)	8.15 (170)
28	5.69 (119)	46	-	152 (6.00)	159 (6.25)	4.41 (92.0)	5.65 (118)

Table A.13
W13 - Loading time history, failure location, EFL_{60} and EFL_3

Spec. No.	Time History		Reported EFL_{60} kPa (psf)	Failure location		EFL_{60} Recreated kPa (psf)	EFL_3 kPa (psf)
	Failure Pressure kPa (psf)	Failure Time (sec)		to long dimension mm (in.)	to short dimension mm (in.)		
1	3.79 (79.2)	27	-	267 (10.5)	121(4.75)	2.83 (59.2)	3.59 (75.0)
2	9.24 (193)	53	-	50.8 (2.00)	0.00 (0.00)	7.31 (153)	9.21 (192)
3	7.25 (152)	44	-	203 (8.00)	102 (4.00)	5.69 (119)	7.12 (149)
4	8.47 (177)	43	-	69.9 (2.75)	165 (6.50)	6.72 (140)	8.24 (172)
5	5.54 (116)	30	-	82.6 (3.25)	12.7 (0.50)	4.11 (85.9)	5.32 (111)
6	3.88 (81.1)	33	-	127 (5.00)	178 (7.00)	2.98 (62.2)	3.73 (77.8)
7	4.76 (100)	19	-	146 (5.75)	108 (4.25)	3.54 (73.9)	4.39 (91.6)
8	5.00 (105)	32	-	6.35 (0.25)	0.00 (0.00)	3.86 (80.7)	4.78 (99.8)
9	10.7 (224)	59	-	127 (5.00)	57.2 (2.25)	8.71 (182)	10.6 (222)
10	4.77 (100)	37	-	121(4.75)	88. 9 (3.50)	3.71 (77.6)	4.60 (96.2)
11	7.60 (159)	63	-	273 (10.8)	279 (11.0)	5.67 (119)	8.26 (173)
12	6.85 (143)	49	-	63.5 (2.50)	12.7 (0.50)	5.37 (112)	6.81 (142)
13	9.56 (200)	68	-	88.9 (3.50)	63.5 (2.50)	7.81 (163)	9.61 (201)
14	5.00 (104)	51	-	330 (13.0)	191 (7.50)	3.73 (78.0)	5.18 (108)
15	12.9(268)	87	-	82.6 (3.25)	0.00 (0.00)	9.92 (207)	15.6 (326)
16	9.29 (194)	57	-	76.2 (3.00)	229 (9.00)	7.37 (154)	9.35 (195)
17	5.13 (107)	35	-	203 (8.00)	165 (6.50)	3.87 (80.7)	4.98 (104)
18	7.75 (162)	40	-	273 (10.8)	140 (5.50)	5.80 (121)	7.69 (161)
19	9.88 (206)	70	-	69.9 (2.75)	0.00 (0.00)	7.82 (163)	10.3 (216)
20	6.88 (144)	36	-	0.00 (0.00)	31.8 (1.25)	5.35 (112)	6.62 (138)
21	8.13(170)	41	-	165 (6.50)	114 (4.50)	6.36 (133)	7.93 (166)

Table A.14
W14 - Loading time history, failure location, EFL_{60} and EFL_3

Spec. No.	Time History		Reported EFL_{60} kPa (psf)	Failure location		EFL_{60} Recreated kPa (psf)	EFL_3 kPa (psf)
	Failure Pressure kPa (psf)	Failure Time (sec)		to long dimension mm (in.)	to short dimension mm (in.)		
1	2.50 (52.2)	58.6	-	919 (36.2)	322 (12.7)	-	2.33 (48.8)
2	3.36 (70.1)	59.7	-	872 (34.3)	335 (13.2)	-	3.23 (67.4)
3	3.74 (78.2)	53.4	-	894 (35.2)	344 (13.6)	-	3.48 (72.7)
4	3.75 (78.3)	65	-	1040 (40.9)	338 (13.3)	-	3.59 (74.9)
5	4.04 (84.4)	51.3	-	1160 (45.7)	259 (10.2)	-	3.84 (80.2)
6	5.66 (118)	56.5	-	732 (28.8)	237 (9.3)	-	5.72 (120)
7	4.30 (89.9)	49.4	-	1100 (43.2)	386 (15.2)	-	4.14 (86.5)
8	4.30 (89.9)	46.8	-	843 (33.2)	259 (10.2)	-	4.15 (86.6)
9	4.47 (93.4)	56.2	-	487 (19.2)	237 (9.3)	-	4.25 (88.9)
10	4.67 (97.6)	73.6	-	1050 (41.2)	360 (14.2)	-	4.44 (92.7)
11	4.93 (103)	64.4	-	1020 (40.2)	259 (10.2)	-	4.69 (98.0)
12	4.98 (104)	54.8	-	889 (35.0)	383 (15.1)	-	4.74 (99.0)
13	4.75 (99.1)	54.4	-	1010 (39.7)	290 (11.4)	-	4.88 (102)
14	5.01 (105)	69.7	-	1160 (45.7)	360 (14.2)	-	4.85 (101)
15	5.58 (116)	55.3	-	178 (7.00)	178 (7.00)	-	5.39 (113)
16	5.72 (119)	65.8	-	973 (38.3)	246 (9.69)	-	5.43 (113)
17	5.66 (118)	56.5	-	922 (36.3)	262 (10.3)	-	5.74 (120)
18	6.25 (130)	67.9	-	1160 (45.8)	233 (9.19)	-	6.11 (128)

Table A.15
N01 - Loading time history, failure location, EFL_{60} and EFL_3

Spec. No.	Time History		Reported	Failure location		EFL_{60}	EFL_3
	Failure Pressure kPa (psf)	Failure Time (sec)	EFL_{60} kPa (psf)	to long dimension mm (in.)	to short dimension mm (in.)	Recreated kPa (psf)	
1	23.6 (492)	51	20.3 (424)	305 (12.0)	451 (17.8)	19.2 (402)	23.9 (499)
2	17.3 (361)	37	14.0 (293)	368 (14.5)	508 (20.0)	13.5 (283)	17.0 (355)
3	24.6 (513)	52	21.1 (440)	127 (5.00)	445 (17.5)	20.1 (419)	24.9 (521)
4	29.6 (618)	64	24.8 (519)	76.2 (3.00)	88.9 (3.50)	24.4 (511)	30.3 (632)
5	22.1 (461)	48	18.8 (392)	337 (13.3)	95.3 (3.75)	17.8 (372)	22.2 (463)
6	30.0 (626)	62	25.7 (536)	368 (14.5)	381 (15.0)	24.9 (519)	30.9 (645)
7	18.3 (382)	38	15.0 (313)	368 (14.5)	508 (20.0)	14.3 (300)	18.0 (377)
8	19.5 (407)	42	16.5 (344)	95.3 (3.75)	286 (11.3)	15.0 (312)	19.3 (404)
9	26.1 (546)	60	22.7 (474)	0.00 (0.00)	25.4 (1.00)	21.5 (449)	26.6 (555)
10	33.9 (708)	63	28.2 (590)	140 (5.50)	394 (15.5)	27.0 (565)	34.5 (721)
11	31.5 (657)	87	26.8 (559)	191 (7.50)	406 (16.0)	25.6 (536)	32.7 (683)
12	21.9 (458)	47	18.8 (392)	25.4 (1.00)	508 (20.0)	17.7 (370)	21.9 (458)
13	21.2 (443)	46	18.0 (375)	394 (15.5)	508 (20.0)	17.2 (358)	21.2 (443)
14	23.3 (487)	51	19.3 (404)	25.4 (1.00)	508 (20.0)	19.0 (396)	23.5 (490)
15	25.1 (524)	53	21.0 (438)	406 (16.0)	508 (20.0)	20.5 (429)	25.3 (528)
16	23.3 (487)	49	19.6 (409)	406 (16.0)	0.00 (0.00)	19.0 (396)	23.4 (488)
17	23.7 (495)	51	18.5 (387)	0.00 (0.00)	419 (16.5)	16.9 (352)	24.1 (503)
18	21.8 (455)	46	17.1 (357)	6.35 (0.25)	0.00 (0.00)	17.6 (368)	21.8 (454)
19	22.4 (467)	47	18.4 (385)	25.4 (1.00)	0.00 (0.00)	18.1 (377)	22.4 (467)
20	27.8 (580)	59	23.5 (490)	394 (15.5)	0.00 (0.00)	22.9 (478)	28.2 (589)
21*	28.4 (592)	59	24.2 (506)	286 (11.3)	0.00 (0.00)	18.2 (380)	31.8 (664)
22	21.1 (441)	50	18.1 (378)	406 (16.0)	0.00 (0.00)	17.2 (359)	21.2 (443)
23	24.1 (504)	68	20.4 (427)	406 (16.0)	0.00 (0.00)	20.1 (420)	24.7 (517)

* Specimen removed from parameter estimation

Table A.16N02 - Loading time history, failure location, EFL_{60} and EFL_3

Spec. No.	Time History		Reported EFL_{60} kPa (psf)	Failure location		EFL_{60} Recreated kPa (psf)	EFL_3 kPa (psf)
	Failure Pressure kPa (psf)	Failure Time (sec)		to long dimension mm (in.)	to short dimension mm (in.)		
1	6.94 (145)	41.4	5.17 (108)	851 (33.5)	387 (15.3)	5.06 (106)	7.34 (153)
2	6.56 (137)	37.7	4.88 (102)	705 (27.8)	330 (13.0)	4.82 (101)	6.75 (141)
3	6.46 (135)	39.5	4.93 (103)	886 (34.9)	305 (12.0)	4.82 (101)	6.64 (139)
4	5.46 (114)	28.7	4.07 (85.0)	184 (7.25)	149 (5.88)	4.26 (89.1)	5.29 (110)
5	7.18 (150)	52.9	5.84 (122)	241 (9.50)	203 (8.00)	5.86 (122)	7.27 (152)
6	6.75 (141)	45.6	6.13 (128)	159 (6.25)	152 (6.00)	5.47 (114)	6.75 (141)
7	7.23 (151)	52.0	5.70 (119)	495 (19.5)	254 (10.0)	5.66 (118)	7.52 (157)
8	7.37 (154)	52.3	5.46 (114)	762 (30.0)	368 (14.5)	5.53 (115)	8.03 (168)
9	6.94 (145)	52.6	5.46 (114)	457 (18.0)	305 (12.0)	5.38 (112)	7.32 (153)
10	8.04 (168)	56.3	5.89 (123)	813 (32.0)	365 (14.4)	6.07 (127)	8.86 (185)
11	7.66 (160)	51.0	5.84 (122)	435 (17.1)	298 (11.8)	5.92 (124)	8.03 (168)
12	6.56 (137)	45.1	4.88 (102)	591 (23.3)	406 (16.0)	4.78 (100)	7.09 (148)
13	7.85 (164)	57.3	5.89 (123)	743(29.3)	359 (14.1)	5.96 (124)	8.63 (180)
14	6.94 (145)	47.7	5.27 (110)	927 (36.5)	432 (17.0)	5.09 (106)	7.57 (158)
15	6.56 (137)	44.8	5.03 (105)	616 (24.3)	311 (12.3)	4.95 (103)	6.84 (143)
16	5.84 (122)	42.1	4.31 (90.0)	956 (37.6)	425 (16.8)	4.27 (89.3)	6.18 (129)
17	7.04 (147)	52.8	5.27 (110)	715 (28.1)	356 (14.0)	5.31 (111)	7.62 (159)
18	5.94 (124)	43.9	4.26 (89.0)	600 (23.6)	416 (16.4)	4.33 (90.5)	6.37 (133)
19	6.32 (132)	44.4	4.84 (101)	771 (30.4)	324 (12.8)	4.75 (99.2)	6.61 (138)
20	4.55 (95.0)	30.5	3.11 (65.0)	568 (22.4)	365 (14.4)	3.29 (68.8)	4.55 (95.1)
21	9.29 (194)	3.14	6.61 (138)	63.5 (2.50)	0.00 (0.00)	6.25 (131)	7.71 (161)
22	8.28 (173)	6.57	4.88 (102)	927 (36.5)	324 (12.8)	5.00 (104)	6.98 (146)
23	10.1 (210)	3.96	5.22 (109)	851 (33.5)	381 (15.0)	5.37 (112)	7.83 (164)
24	9.53 (199)	5.03	5.65 (118)	622 (24.5)	273 (10.8)	5.78 (121)	7.86 (164)
25	9.77 (204)	3.75	5.41 (113)	349 (13.8)	324 (12.8)	5.74 (120)	7.79 (163)
26	9.19 (192)	3.81	5.94 (124)	406 (16.0)	152 (6.00)	6.06 (127)	7.63 (159)
27	8.81 (184)	3.10	5.94 (124)	203 (8.00)	114 (4.50)	5.94 (124)	7.32 (153)
28	9.53 (199)	3.11	5.99 (125)	394 (15.5)	152 (6.00)	6.21 (130)	7.79 (163)
29	8.00 (167)	2.81	5.31 (111)	178 (7.00)	165(6.50)	5.35 (112)	6.60 (138)
30	8.95 (187)	3.31	4.88 (102)	864 (34.0)	318 (12.5)	5.03 (105)	6.98 (146)
31	8.47 (177)	4.19	4.26 (89.0)	591 (23.3)	470 (18.5)	4.33 (90.5)	6.53 (136)
32	8.57 (179)	6.14	5.79 (121)	76.2 (3.00)	0.00 (0.00)	6.01 (125)	7.43 (155)
33	9.53 (199)	5.70	6.56 (137)	267 (10.5)	152 (6.00)	6.71 (140)	8.25 (172)

N02 (Cont.) - Loading time history, failure location, EFL_{60} and EFL_3

Spec. No.	Time History		Reported EFL_{60} kPa (psf)	Failure location		EFL_{60} Recreated kPa (psf)	EFL_3 kPa (psf)
	Failure Pressure kPa (psf)	Failure Time (sec)		to long dimension mm (in.)	to short dimension mm (in.)		
34	9.05 (189)	8.21	6.89 (144)	12.7 (0.50)	31.8 (1.25)	6.54 (137)	8.04 (168)
35	12.9 (269)	3.86	8.81 (184)	254 (10.0)	165 (6.50)	8.79 (184)	10.82 (226)
36	2.87 (60.0)	1.60	1.92 (40.0)	787 (31.0)	318 (12.5)	1.68 (35.1)	2.17 (45.2)
37	11.7 (245)	7.64	8.62 (180)	0.00 (0.00)	69.9 (2.75)	8.35 (174)	10.3 (216)
38	9.29 (194)	8.26	6.42 (134)	102 (4.00)	0.00 (0.00)	6.53 (136)	8.20 (171)
39	7.95 (166)	131	6.32 (132)	864 (34.0)	292 (11.5)	6.73 (141)	9.32 (195)
40	1.58 (33.0)	230	1.44 (30.0)	394 (15.5)	318 (12.5)	1.43 (29.9)	1.79 (37.5)
41	5.79 (121)	1020	6.13 (128)	724 (28.5)	406 (16.0)	6.29 (131)	9.55 (199)
42	7.09 (148)	1160	7.85 (164)	470 (18.5)	330 (13.0)	7.64 (160)	10.9 (228)
43	6.75 (141)	980	6.80 (142)	229 (9.0)	140 (5.50)	6.78 (142)	8.33 (174)
44	6.13 (128)	862	6.32 (132)	927 (36.5)	406 (16.0)	6.51 (136)	9.85 (206)
45	8.00 (167)	1130	9.10 (190)	787 (31.0)	368 (14.5)	8.83 (184)	13.4 (279)
46	6.32 (132)	1120	6.61 (138)	610 (24.0)	203 (8.00)	6.57 (137)	8.63 (180)
47	4.69 (98.0)	979	4.88 (102)	864 (34.0)	406 (16.0)	4.99 (104)	7.31 (153)
48	6.22 (130)	969	7.52 (157)	705 (27.8)	422 (16.6)	6.78 (142)	10.6 (221)
49	5.03 (105)	1140	5.27 (110)	464 (18.3)	298 (11.8)	5.28 (110)	7.16 (150)
50	7.09 (148)	1270	7.76 (162)	673 (26.5)	273 (10.8)	7.61 (159)	10.4 (218)
51	5.75 (120)	1230	6.13 (128)	692 (27.3)	318 (12.5)	6.20 (130)	8.72 (182)
52	6.61 (138)	1500	6.94 (145)	88.9 (3.50)	63.5 (2.50)	6.88 (144)	8.56 (179)
53	5.60 (117)	1200	5.99 (125)	908 (35.8)	413 (16.3)	6.19 (129)	9.37 (196)

Table A.17N03 - Loading time history, failure location, EFL_{60} and EFL_3

Spec. No.	Time History		Reported EFL_{60} kPa (psf)	Failure location		EFL_{60} Recreated kPa (psf)	EFL_3 kPa (psf)
	Failure Pressure kPa (psf)	Failure Time (sec)		to long dimension mm (in.)	to short dimension mm (in.)		
1	9.29 (194)	44.2	7.47 (156)	318 (12.5)	699 (27.5)	7.46 (156)	9.30 (194)
2	6.94 (145)	32.7	5.51 (115)	908 (35.8)	438 (17.3)	5.12 (107)	6.97 (146)
3	15.4 (321)	74.3	11.4 (239)	413 (16.3)	279 (11.0)	12.2 (256)	17.0 (355)
4	13.0 (271)	62	9.91 (207)	864 (34.0)	311 (12.3)	10.1 (210)	14.2 (297)
5	11.5 (240)	55.9	9.38 (196)	88.9 (3.50)	76.2 (3.00)	9.39 (196)	11.7 (244)
6	11.7 (245)	57	9.29 (194)	362 (14.3)	114 (4.50)	9.57 (200)	12.0 (250)
7	12.8 (268)	61.4	10.5 (220)	47.8 (1.88)	6.35 (0.25)	10.6 (222)	13.1 (273)
8	11.8 (246)	56.5	9.05 (189)	775 (30.5)	305 (12.0)	9.07 (189)	12.7 (265)
9	11.9 (249)	58	9.82 (205)	19.1 (0.75)	6.35 (0.25)	9.85 (206)	12.1 (253)
10	12.2 (255)	57.9	10.0 (209)	38.1 (1.50)	6.35 (0.25)	10.1 (211)	12.4 (259)
11*	13.5 (281)	64.4	8.09 (169)	31.8 (1.25)	25.4 (1.00)	11.2 (234)	13.8 (288)
12	10.8 (225)	51.7	8.24 (172)	1010 (39.8)	508 (20.0)	8.18 (171)	11.5 (241)
13	11.8 (246)	56.6	8.95 (187)	362 (14.3)	368 (14.5)	8.96 (187)	12.9 (270)
14	12.7 (266)	62.7	10.5 (220)	25.4 (1.00)	6.35 (0.25)	10.6 (221)	13.0 (272)
15	8.43 (176)	40.5	6.37 (133)	1120 (44.0)	254 (10.0)	6.45 (135)	8.56 (179)
16	8.19 (171)	39.6	6.27 (131)	394 (15.5)	267 (10.5)	6.32 (132)	8.26 (172)
17	12.2 (255)	58.8	10.1 (210)	25.4 (1.00)	19.1 (0.75)	10.1 (211)	12.4 (259)
18	8.57(179)	40.3	6.27 (131)	1060 (41.8)	483 (19.0)	6.38 (133)	8.87 (185)
19	8.95(187)	43	6.80 (142)	1080 (42.5)	343 (13.5)	6.71 (140)	9.34 (195)

* Specimen removed from parameter estimation

Table A.18N04 - Loading time history, failure location, EFL_{60} and EFL_3

Spec. No.	Time History		Reported EFL_{60} kPa (psf)	Failure location		EFL_{60} Recreated kPa (psf)	EFL_3 kPa (psf)
	Failure Pressure kPa (psf)	Failure Time (sec)		to long dimension mm (in.)	to short dimension mm (in.)		
1*	6.85 (143)	78.6	2.87 (60.0)	127 (5.00)	140 (5.50)	5.77 (121)	7.10 (148)
2	6.27 (131)	72.2	5.17 (108)	737 (29.0)	165 (6.50)	5.14 (107)	6.62 (138)
3	5.65 (118)	37.4	4.79 (100)	165 (6.50)	229 (9.00)	4.52 (94.4)	5.57 (116)
4	6.56 (137)	71.1	5.22 (109)	673 (26.5)	334 (13.1)	5.22 (109)	7.15 (149)
5	6.75 (141)	62.8	5.36 (112)	527 (20.8)	305 (12.0)	5.38 (112)	7.16 (150)
6	4.36 (91.0)	43.7	3.59 (75.0)	686 (27.0)	140 (5.50)	3.45 (72.0)	4.39 (91.7)
7	5.79 (121)	76.2	4.79 (100)	483 (19.0)	318 (12.5)	4.71 (98.5)	6.24 (130)
8	5.36 (112)	48.5	4.31 (90.0)	552 (21.8)	213 (8.38)	4.26 (89.1)	5.46 (114)
9	5.12 (107)	56.1	3.97 (83.0)	1090 (43.0)	362 (14.3)	3.95 (82.6)	5.48 (115)
10	5.46 (114)	59.6	4.55 (95.0)	165 (6.50)	197 (7.75)	4.52 (94.4)	5.55 (116)
11	2.97 (62.0)	29.4	2.35 (49.0)	965 (38.0)	400 (15.8)	2.16 (45.2)	2.95 (61.6)
12	3.73 (78.0)	44.9	3.02 (63.0)	165 (6.50)	197 (7.75)	3.01 (62.9)	3.74 (78.0)
13	4.55 (95.0)	53	3.40 (71.0)	1050 (41.5)	419 (16.5)	3.45 (72.1)	4.89 (102)
14	4.98 (104)	60.3	4.07 85.0)(1099 (43.3)	286 (11.3)	3.94 (82.3)	5.27 (110)
15	3.78 (79.0)	50.1	2.63 (55.0)	654 (25.8)	229 (9.00)	3.00 (62.7)	3.87 (80.9)
16	5.75 (120)	74	4.69 (98.0)	953 (37.5)	229 (9.00)	4.68 (97.7)	6.13 (128)

* Specimen removed from parameter estimation

Table A.19
N05 - Loading time history, failure location, EFL_{60} and EFL_3

Spec. No.	Time History		Reported EFL_{60} kPa (psf)	Failure location		EFL_{60} Recreated kPa (psf)	EFL_3 kPa (psf)
	Failure Pressure kPa (psf)	Failure Time (sec)		to long dimension mm (in.)	to short dimension mm (in.)		
1	8.00 (167)	47.1	6.37 (133)	165 (6.50)	191 (7.50)	6.52 (136)	8.00 (167)
2	8.62 (180)	75.3	7.23 (151)	165 (6.50)	184 (7.25)	7.26 (152)	8.90 (186)
3	8.33 (174)	75.4	6.85 (143)	241 (9.50)	279 (11.0)	6.91 (144)	8.76 (183)
4	6.94 (145)	61.0	5.70 (119)	191 (7.50)	178 (7.00)	5.76 (120)	7.07 (148)
5	9.24 (193)	74.5	7.76 (162)	254 (10.0)	140 (5.50)	7.78 (163)	9.54 (199)
6	9.24 (193)	79.7	7.80 (163)	152 (6.00)	216 (8.50)	7.82 (163)	9.58 (200)
7	7.04 (147)	61.0	5.55 (116)	140 (5.50)	12.7 (0.50)	5.64 (118)	7.38 (154)
8	7.52 (157)	65.2	6.22 (130)	152 (6.00)	203 (8.00)	6.27 (131)	7.69 (161)
9	7.23 (151)	62.4	5.99 (125)	203 (8.00)	121 (4.75)	6.00 (125)	7.38 (154)
10	7.47 (156)	66.2	6.03 (126)	178 (7.00)	260 (10.3)	6.22 (130)	7.67 (160)
11	4.55 (95.0)	38.2	3.59 (75.0)	114 (4.50)	38.1 (1.50)	3.59 (74.9)	4.52 (94.4)
12	8.57 (179)	72.5	7.18 (150)	178 (7.00)	152 (6.00)	7.21 (151)	8.82 (184)
13	8.04 (168)	31.4	6.37 (133)	222 (8.75)	146 (5.75)	6.38 (133)	7.83 (164)
14	6.56 (137)	52.8	5.36 (112)	57.2 (2.25)	6.35 (0.25)	5.37 (112)	6.63 (138)
15	7.47 (156)	66.9	6.18 (129)	171 (6.75)	152 (6.00)	6.24 (130)	7.65 (160)
16	6.42 (134)	55.7	5.17 (108)	502 (19.8)	235 (9.25)	5.09 (106)	6.68 (140)
17	5.84 (122)	49.1	4.74 (99.0)	6.35 (0.25)	82.6 (3.25)	4.73 (98.7)	5.90 (123)
18	7.80 (163)	67.0	6.42 (134)	88.9 (3.50)	69.9 (2.75)	6.46 (135)	8.06 (168)
19	6.22 (130)	52.2	5.08 (106)	197 (7.75)	197 (7.75)	5.10 (107)	6.28 (131)

Table A.20
N06 - Loading time history, failure location, EFL_{60} and EFL_3

Spec. No.	Time History		Reported EFL_{60} kPa (psf)	Failure location		EFL_{60} Recreated kPa (psf)	EFL_3 kPa (psf)
	Failure Pressure kPa (psf)	Failure Time (sec)		to long dimension mm (in.)	to short dimension mm (in.)		
1	10.5 (219)	51.2	7.71 (161)	19.1 (0.75)	95.3 (3.75)	8.46 (177)	10.7 (222)
2	12.4 (259)	60.5	9.67 (202)	19.1 (0.75)	12.7 (0.50)	10.2 (214)	12.7 (264)
3	12.7 (266)	62.8	10.1 (210)	279 (11.0)	171 (6.75)	10.5 (220)	13.0 (272)
4	13.6 (284)	66.0	10.7 (223)	203 (8.00)	235 (9.25)	11.2 (235)	14.0 (293)
5	14.9 (311)	72.1	12.6 (263)	286 (11.3)	178 (7.00)	12.4 (259)	15.5 (323)
6	14.2 (297)	68.4	11.5 (240)	241 (9.50)	127 (5.00)	11.9 (249)	14.6 (305)
7	11.2 (233)	54.1	8.09 (169)	210 (8.25)	476 (18.8)	8.84 (185)	11.6 (242)
8	10.3 (216)	49.4	7.80 (163)	57.2 (2.25)	22.4 (0.88)	8.39 (175)	10.4 (218)
9	14.4 (301)	70.0	11.4 (237)	229 (9.00)	330 (13.0)	11.8 (246)	15.2 (317)
10	14.2 (297)	69.6	11.2 (233)	229 (9.00)	226 (8.88)	11.7 (245)	14.8 (310)
11	15.8 (330)	77.1	12.9 (269)	12.7 (0.50)	12.7 (0.50)	13.3 (278)	16.4 (342)
12	13.2 (275)	64.0	10.4 (217)	102 (4.00)	171 (6.75)	10.9 (228)	13.5 (282)
13	16.9 (353)	82.9	14.1 (295)	127 (5.00)	121 (4.75)	14.3 (299)	17.6 (367)
14	13.2 (275)	63.5	10.4 (217)	102 (4.00)	165 (6.50)	10.9 (228)	13.5 (282)
15	15.7 (327)	74.7	12.7 (266)	203 (8.00)	260 (10.3)	13.0 (272)	16.4 (342)
16	15.7 (328)	77.5	12.8 (267)	216 (8.50)	207 (8.13)	13.1 (274)	16.4 (343)
17	14.2 (297)	70.0	11.3 (236)	50.8 (2.00)	31.8 (1.25)	11.8 (247)	14.7 (307)
18	10.3 (216)	48.8	7.71 (161)	184 (7.25)	267 (10.5)	8.41 (176)	10.4 (217)

Table A.21
 N07 - Loading time history, failure location, EFL_{60} and EFL_3

Spec. No.	Time History		Reported EFL_{60} kPa (psf)	Failure location		EFL_{60} Recreated kPa (psf)	EFL_3 kPa (psf)
	Failure Pressure kPa (psf)	Failure Time (sec)		to long dimension mm (in.)	to short dimension mm (in.)		
1	4.74 (99.0)	55.4	3.88 (81.0)	203 (8.00)	368 (14.5)	3.87 (80.9)	4.83 (101)
2	4.69 (98.0)	58.9	3.78 (79.0)	419 (16.5)	248 (9.75)	3.80 (79.4)	4.85 (101)
3	5.36 (112)	64.1	4.50 (94.0)	184 (7.25)	260 (10.3)	4.47 (93.3)	5.48 (115)
4	6.42 (134)	69.9	5.36 (112)	229 (9.00)	178 (7.00)	5.38 (112)	6.60 (138)
5	5.17 (108)	59.1	4.31 (90.0)	203 (8.00)	152 (6.00)	4.30 (89.7)	5.25 (110)
6	5.51 (115)	63.1	4.55 (95.0)	53.9 (2.12)	22.1 (0.87)	4.57 (95.4)	5.63 (118)
7	4.69 (98.0)	52.5	3.78 (79.0)	102 (4.00)	495 (19.5)	3.79 (79.1)	4.79 (100)
8	3.45 (72.0)	38.3	2.68 (56.0)	95.3 (3.75)	11.4 (0.45)	2.74 (57.2)	3.42 (71.3)
9	5.65 (118)	61.5	4.69 (98.0)	318 (12.50)	146 (5.75)	4.69 (98.1)	5.76 (120)
10	5.22 (109)	59.3	4.17 (87.0)	318 (12.50)	324 (12.8)	4.18 (87.3)	5.46 (114)
11	5.51 (115)	61.9	4.60 (96.0)	219 (8.62)	136 (5.37)	4.59 (95.9)	5.60 (117)
12	4.50 (94.0)	50.5	3.59 (75.0)	241 (9.50)	216 (8.50)	3.68 (76.9)	4.53 (94.6)

Table A.22
N08 - Loading time history, failure location, EFL_{60} and EFL_3

Spec. No.	Time History		Reported EFL_{60} kPa (psf)	Failure location		EFL_{60} Recreated kPa (psf)	EFL_3 kPa (psf)
	Failure Pressure kPa (psf)	Failure Time (sec)		to long dimension mm (in.)	to short dimension mm (in.)		
1	3.73 (78.0)	46.4	3.11 (65.0)	248 (9.75)	241 (9.50)	3.04 (63.5)	3.74 (78.1)
2	2.97 (62.0)	35.1	2.25 (47.0)	6.35 (0.25)	12.7 (0.50)	2.37 (49.5)	2.91 (60.8)
3	2.39 (50.0)	32.0	2.06 (43.0)	6.35 (0.25)	76.2 (3.00)	1.90 (39.6)	2.34 (48.8)
4	3.11 (65.0)	36.8	2.59 (54.0)	3.05 (0.12)	88.9 (3.50)	2.48 (51.8)	3.07 (64.1)
5	2.49 (52.0)	30.7	2.01 (42.0)	6.35 (0.25)	76.2 (3.00)	1.97 (41.1)	2.42 (50.6)
6	3.02 (63.0)	40.3	2.54 (53.0)	44.5 (1.75)	12.7 (0.50)	2.43 (50.7)	2.99 (62.4)
7	3.11 (65.0)	38.0	2.63 (55.0)	28.7 (1.13)	12.7 (0.50)	2.50 (52.2)	3.07 (64.1)
8	3.11 (65.0)	41.6	2.59 (54.0)	413 (16.3)	175 (6.88)	2.51 (52.4)	3.09 (64.6)
9	3.88 (81.0)	47.7	3.26 (68.0)	181 (7.12)	283 (11.1)	3.17 (66.2)	3.88 (81.1)
10	3.11 (65.0)	39.5	2.63 (55.0)	241 (9.50)	273 (10.8)	2.50 (52.3)	3.08 (64.3)
11	2.97 (62.0)	38.3	2.54 (53.0)	381 (15.0)	279 (11.0)	2.35 (49.1)	2.95 (61.5)
12	3.88 (81.0)	50.2	3.21 (67.0)	292 (11.5)	254 (10.0)	3.15 (65.9)	3.92 (81.8)
13	3.64 (76.0)	44.6	2.97 (62.0)	394 (15.5)	292 (11.5)	2.89 (60.3)	3.67 (76.7)
14	3.64 (76.0)	43.4	3.06 (64.0)	7.62 (0.30)	69.9 (2.75)	2.94 (61.5)	3.63 (75.7)
15	4.12 (86.0)	48.8	3.35 (70.0)	254 (10.0)	197 (7.75)	3.38 (70.5)	4.13 (86.2)

Table A.23N09 - Loading time history, failure location, EFL_{60} and EFL_3

Spec. No.	Time History		Reported EFL_{60} kPa (psf)	Failure location		EFL_{60} Recreated kPa (psf)	EFL_3 kPa (psf)
	Failure Pressure kPa (psf)	Failure Time (sec)		to long dimension mm (in.)	to short dimension mm (in.)		
1	4.48 (93.6)	29.5	-	0.00 (0.00)	61.0 (2.40)	-	4.35 (90.8)
2	5.86 (122)	38.6	-	0.00 (0.00)	81.3 (3.20)	-	5.80 (121)
3	5.52 (115)	36.4	-	274 (10.8)	191 (7.50)	-	5.43 (113)
4	5.17 (108)	34.1	-	231 (9.10)	155 (6.10)	-	5.05 (105)
5	7.93 (166)	52.3	-	38.1 (1.50)	0.00 (0.00)	-	8.03 (168)
6	7.24 (151)	47.7	-	251 (9.90)	343 (13.5)	-	7.43 (155)
7	6.89 (144)	45.5	-	264 (10.4)	333 (13.1)	-	7.04 (147)
8	6.89 (144)	45.5	-	150 (5.90)	0.00 (0.00)	-	7.57 (158)
9	7.24 (151)	47.7	-	76.2 (3.00)	15.2 (0.60)	-	7.27 (152)
10	6.21 (130)	40.9	-	208 (8.20)	188 (7.40)	-	6.14 (128)
11	4.48 (93.6)	29.5	-	99.1 (3.90)	178 (7.00)	-	4.35 (90.9)
12	6.21 (130)	40.9	-	447 (17.6)	394 (15.5)	-	6.39 (133)
13	4.48 (93.6)	29.5	-	0.00 (0.00)	76.2 (3.00)	-	4.35 (90.8)
14	6.41 (134)	42.3	-	206 (8.10)	409 (16.1)	-	6.47 (135)
15	4.00 (83.5)	26.4	-	0.00 (0.00)	91.4 (3.60)	-	3.85 (80.5)
16	5.52 (115)	36.4	-	0.00 (0.00)	63.5 (2.50)	-	5.43 (113)
17	4.48 (93.6)	29.5	-	234 (9.20)	40.6 (1.60)	-	4.45 (92.9)
18	5.72 (120)	37.7	-	307 (12.1)	366 (14.4)	-	5.74 (120)
19	4.48 (93.6)	29.5	-	0.00 (0.00)	71.1 (2.80)	-	4.35 (90.8)
20	5.52 (115)	36.4	-	0.00 (0.00)	55.9 (2.20)	-	5.43 (113)
21	5.31 (111)	35.0	-	155 (6.10)	130 (5.10)	-	5.20 (109)
22	4.96 (104)	32.7	-	226 (8.90)	213 (8.40)	-	4.84 (101)
23	3.72 (77.8)	24.5	-	0.00 (0.00)	35.6 (1.40)	-	3.56 (74.4)
24	5.24 (109)	34.5	-	508 (20.0)	218 (8.60)	-	5.20 (109)
25	4.69 (97.9)	30.9	-	218 (8.60)	267 (10.5)	-	4.56 (95.3)
26	5.52 (115)	36.4	-	50.8 (2.00)	12.7 (0.50)	-	5.43 (113)
27	4.62 (96.5)	30.5	-	246 (9.70)	401 (15.8)	-	4.52 (94.4)
28	6.07 (127)	40.0	-	318 (12.5)	244 (9.60)	-	6.06 (127)
29	4.69 (97.9)	30.9	-	269 (10.6)	130 (5.10)	-	4.56 (95.2)
30	5.86 (122)	38.6	-	163(6.40)	353 (13.9)	-	5.81 (121)
31	4.83 (101)	31.8	-	551 (21.7)	511 (20.1)	-	4.88 (102)
32	7.45 (156)	4.90	-	264 (10.4)	239 (9.40)	-	6.29 (131)
33	7.24 (151)	4.80	-	279 (11.0)	254 (10.0)	-	6.09 (127)
34	7.93 (166)	5.20	-	277 (10.9)	381 (15.0)	-	6.61 (138)
35	7.45 (156)	4.90	-	180 (7.10)	201 (7.90)	-	6.40 (134)
36	7.10 (148)	4.70	-	315 (12.4)	155 (6.10)	-	6.06 (126)
37	8.62 (180)	5.70	-	257 (10.1)	155 (6.10)	-	7.46 (156)

N09 (Cont.) - Loading time history, failure location, EFL_{60} and EFL_3

Spec. No.	Time History		Reported EFL_{60} kPa (psf)	Failure location		EFL_{60} Recreated kPa (psf)	EFL_3 kPa (psf)
	Failure Pressure kPa (psf)	Failure Time (sec)		to long dimension mm (in.)	to short dimension mm (in.)		
38	6.55 (137)	4.30	-	114 (4.50)	38.1 (1.50)	-	5.50 (115)
39	7.79 (163)	5.10	-	175 (6.90)	137 (5.40)	-	6.73 (141)
40	6.55 (137)	4.30	-	132 (5.20)	130 (5.10)	-	5.58 (117)
41	6.89 (144)	4.50	-	147 (5.80)	150 (5.90)	-	5.92 (124)
42	7.93 (166)	5.20	-	0.00 (0.00)	86.4 (3.40)	-	6.77 (141)
43	7.24 (151)	4.80	-	231 (9.10)	216 (8.50)	-	6.17 (129)
44	4.14 (86.4)	2.70	-	0.00 (0.00)	30.5 (1.20)	-	3.40 (71.1)
45	5.17 (108)	3.40	-	0.00 (0.00)	91.4 (3.60)	-	4.29 (89.5)
46	7.24 (151)	4.80	-	0.00 (0.00)	61.0 (2.40)	-	6.17 (129)
47	8.00 (167)	5.30	-	439 (17.3)	155 (6.10)	-	6.79 (142)
48	3.45 (72.0)	2.30	-	38.1 (1.50)	0.00 (0.00)	-	2.80 (58.5)
49	7.10 (148)	4.70	-	25.4 (1.00)	0.00 (0.00)	-	6.05 (126)
50	5.86 (122)	3.90	-	533 (21.0)	396 (15.6)	-	4.68 (97.7)
51	4.55 (95.0)	3.00	-	178 (7.00)	142 (5.60)	-	3.79 (79.1)
52	4.69 (97.9)	3.10	-	88.9 (3.50)	0.00 (0.00)	-	3.87 (80.7)
53	5.17 (108)	3.40	-	226 (8.90)	218 (8.60)	-	4.32 (90.3)
54	6.96 (145)	4.60	-	297 (11.7)	201 (7.90)	-	5.90 (123)
55	6.34 (132)	4.20	-	318 (12.5)	155 (6.10)	-	5.38 (112)
56	4.48 (93.6)	3.00	-	251 (9.90)	178 (7.00)	-	3.73 (77.9)
57	6.55 (137)	4.30	-	211 (8.30)	320 (12.6)	-	5.49 (115)
58	2.90 (60.5)	1.90	-	224 (8.80)	594 (23.4)	-	2.24 (46.8)
59	4.83 (101)	3.20	-	328 (12.9)	267 (10.5)	-	3.96 (82.7)
60	6.07 (127)	4.00	-	168 (6.60)	191 (7.50)	-	5.16 (108)
61	8.41 (176)	0.60	-	0.00 (0.00)	48.3 (1.90)	-	6.14 (128)
62	8.96 (187)	0.60	-	152 (6.00)	178 (7.00)	-	6.74 (141)
63	6.00 (125)	0.40	-	145 (5.70)	152 (6.00)	-	4.38 (91.6)
64	5.65 (118)	0.40	-	117 (4.60)	394 (15.5)	-	3.97 (83.0)
65	6.07 (127)	0.40	-	211 (8.30)	274 (10.8)	-	4.32 (90.2)
66	7.58 (158)	0.50	-	155 (6.10)	155 (6.10)	-	5.66 (118)
67	7.93 (166)	0.50	-	114 (4.50)	0.00 (0.00)	-	5.43 (113)
68	8.41 (176)	0.60	-	63.5 (2.50)	0.00 (0.00)	-	6.14 (128)
69	7.10 (148)	0.50	-	203 (8.00)	279 (11.0)	-	5.07 (106)
70	7.03 (147)	0.50	-	396 (15.6)	91.4 (3.60)	-	4.95 (103)
71	7.38 (154)	0.50	-	0.00 (0.00)	99.1 (3.90)	-	5.21 (109)
72	4.83 (101)	0.30	-	63.5 (2.50)	0.00 (0.00)	-	3.42 (71.4)
73	5.45 (114)	0.40	-	0.00 (0.00)	25.4 (1.00)	-	3.90 (81.4)
74	6.34 (132)	0.40	-	0.00 (0.00)	38.1 (1.50)	-	4.57 (95.5)

N09 (Cont.) - Loading time history, failure location, EFL_{60} and EFL_3

Spec. No.	Time History		Reported EFL_{60} kPa (psf)	Failure location		EFL_{60} Recreated kPa (psf)	EFL_3 kPa (psf)
	Failure Pressure kPa (psf)	Failure Time (sec)		to long dimension mm (in.)	to short dimension mm (in.)		
75	4.83 (101)	0.30	-	251 (9.90)	264 (10.4)	-	3.40 (71.0)
76	7.24 (151)	0.50	-	302 (11.9)	257 (10.1)	-	5.09 (106)
77	7.79 (163)	0.50	-	455 (17.9)	249 (9.80)	-	5.31 (111)
78	8.14 (170)	0.50	-	638 (25.1)	343 (13.5)	-	5.35 (112)
79	6.96 (145)	0.50	-	218 (8.60)	348 (13.7)	-	4.88 (102)
80	7.58 (158)	0.50	-	180 (7.10)	163 (6.40)	-	5.65 (118)
81	6.76 (141)	0.40	-	432 (17.0)	262 (10.3)	-	4.58 (95.7)
82	7.38 (154)	0.50	-	152 (6.00)	112 (4.40)	-	5.42 (113)
83	6.89 (144)	0.50	-	264 (10.4)	130 (5.10)	-	5.06 (106)
84	7.45 (156)	0.50	-	117 (4.60)	229 (9.00)	-	5.46 (114)
85	5.45 (114)	0.40	-	218 (8.60)	282 (11.1)	-	3.86 (80.5)
86	5.79 (121)	0.40	-	229 (9.00)	142 (5.60)	-	4.23 (88.4)
87	3.65 (76.3)	0.20	-	284 (11.2)	2.54 (0.10)	-	1.55 (32.5)
88	4.48 (93.6)	0.30	-	279 (11.0)	198 (7.80)	-	3.19 (66.5)
89	5.38 (112)	0.40	-	206 (8.10)	239 (9.40)	-	3.86 (80.5)
90	5.38 (112)	0.40	-	0.00 (0.00)	117 (4.60)	-	3.66 (76.3)
91	3.10 (64.8)	1250	-	107 (4.20)	78.7 (3.10)	-	3.95 (82.4)
92	3.93 (82.1)	1583	-	10.2 (0.40)	102 (4.00)	-	5.16 (108)
93	2.96 (61.9)	1229	-	76.2 (3.00)	69.9 (2.75)	-	3.75 (78.3)
94	4.69 (97.9)	2000	-	12.7 (0.50)	66.0 (2.60)	-	6.11 (128)
95	3.38 (70.6)	1400	-	91.4 (3.60)	40.6 (1.60)	-	4.33 (90.4)
96	2.69 (56.2)	1114	-	50.8 (2.00)	0.00 (0.00)	-	3.35 (70.0)
97	2.55 (53.3)	1028	-	1220 (48.0)	762 (30.0)	-	3.70 (77.2)
98	2.83 (59.0)	2050	-	104 (4.10)	66.0 (2.60)	-	3.74 (78.0)
99	3.24 (67.7)	1424	-	0.00 (0.00)	81.3 (3.20)	-	4.13 (86.3)
100	3.45 (72.0)	1250	-	409 (16.1)	218 (8.60)	-	4.44 (92.7)
101	4.69 (97.9)	2061	-	269 (10.6)	231 (9.10)	-	6.19 (129)
102	4.34 (90.7)	1615	-	91.4 (3.60)	142 (5.60)	-	5.61 (117)
103	3.17 (66.2)	1150	-	38.1 (1.50)	38.1 (1.50)	-	3.97 (82.9)
104	1.93 (40.3)	757	-	0.00 (0.00)	50.8 (2.00)	-	2.34 (49.0)
105	2.48 (51.8)	900	-	50.8 (2.00)	0.00 (0.00)	-	3.05 (63.6)
106	4.83 (101)	2059	-	1060 (41.6)	620 (24.4)	-	7.56 (158)
107	4.21 (87.8)	1605	-	262 (10.3)	218 (8.60)	-	5.39 (113)
108	2.34 (49.0)	919	-	460 (18.1)	282 (11.1)	-	2.98 (62.2)
109	3.24 (67.7)	1270	-	76.2 (3.00)	38.1 (1.50)	-	4.09 (85.5)
110	3.93 (82.1)	1541	-	5.08 (0.20)	127 (5.00)	-	5.38 (112)
111	3.86 (80.6)	1697	-	249 (9.80)	193 (7.60)	-	4.90 (102)

N09 (Cont.) - Loading time history, failure location, EFL_{60} and EFL_3

Spec. No.	Time History		Reported EFL_{60} kPa (psf)	Failure location		EFL_{60} Recreated kPa (psf)	EFL_3 kPa (psf)
	Failure Pressure kPa (psf)	Failure Time (sec)		to long dimension mm (in.)	to short dimension mm (in.)		
112	5.48 (114)	227	-	78.7 (3.10)	0.00 (0.00)	-	6.15 (129)
113	4.96 (104)	200	-	168 (6.60)	41.4 (1.63)	-	5.74 (120)
114	4.48 (93.6)	176	-	0.00 (0.00)	76.2 (3.00)	-	4.93 (103)
115	3.03 (63.4)	126	-	0.00 (0.00)	50.8 (2.00)	-	3.25 (67.9)
116	3.03 (63.4)	122	-	0.00 (0.00)	130 (5.10)	-	3.32 (69.3)
117	4.90 (102)	209	-	0.00 (0.00)	114 (4.50)	-	5.62 (117)
118	4.41 (92.2)	200	-	193 (7.60)	244 (9.60)	-	4.86 (102)
119	3.93 (82.1)	121	-	6.35 (0.25)	122 (4.80)	-	4.30 (89.8)
120	4.41 (92.2)	178	-	78.7 (3.10)	0.00 (0.00)	-	4.86 (101)
121	4.69 (97.9)	194	-	295 (11.6)	244 (9.60)	-	5.24 (109)
122	3.24 (67.7)	121	-	45.7 (1.80)	71.1 (2.80)	-	3.47 (72.5)
123	2.48 (51.8)	100	-	0.00 (0.00)	127 (5.00)	-	2.66 (55.5)
124	5.45 (114)	219	-	5.08 (0.20)	97.5 (3.80)	-	6.18 (129)
125	4.34 (90.7)	170	-	130 (5.10)	193 (7.60)	-	4.74 (99.1)
126	3.45 (72.0)	135	-	30.5 (1.20)	38.1 (1.50)	-	3.72 (77.6)
127	3.17 (66.2)	131	-	107 (4.20)	71.1 (2.80)	-	3.43 (71.7)
128	6.21 (130)	250	-	12.7 (0.50)	71.1 (2.80)	-	7.00 (146)
129	2.76 (57.6)	111	-	127 (5.00)	50.8 (2.00)	-	2.96 (61.9)
130	5.10 (107)	206	-	165 (6.50)	38.1 (1.50)	-	5.95 (124)
131	3.72 (77.8)	146	-	282 (11.1)	231 (9.10)	-	4.03 (84.2)
132	4.69 (97.9)	194	-	345 (13.6)	193 (7.60)	-	5.22 (109)
133	4.83 (101)	20.6	-	53.3 (2.10)	104 (4.10)	-	4.57 (95.4)
134	5.79 (121)	25.5	-	5.08 (0.20)	40.6 (1.60)	-	5.56 (116)
135	6.62 (138)	29.1	-	320 (12.6)	206 (8.10)	-	6.43 (134)
136	5.52 (115)	23.5	-	0.00 (0.00)	38.1 (1.50)	-	5.27 (110)
137	6.55 (137)	27.9	-	180 (7.10)	130 (5.10)	-	6.32 (132)
138	5.17 (108)	24.2	-	55.9 (2.20)	0.00 (0.00)	-	4.95 (103)
139	6.34 (132)	26.3	-	472 (18.6)	295 (11.6)	-	6.18 (129)
140	6.21 (130)	25.7	-	12.7 (0.50)	122 (4.80)	-	6.00 (125)
141	6.21 (130)	23.7	-	76.2 (3.00)	0.00 (0.00)	-	5.93 (124)
142	5.52 (115)	21.6	-	396 (15.6)	198 (7.80)	-	5.24 (109)
143	4.76 (99.4)	19.2	-	168 (6.60)	53.3 (2.10)	-	4.48 (93.6)
144	4.41 (92.2)	17.8	-	50.8 (2.00)	0.00 (0.00)	-	4.13 (86.3)
145	5.17 (108)	19.7	-	0.00 (0.00)	50.8 (2.00)	-	4.88 (102)
146	5.79 (121)	23.3	-	333 (13.1)	244 (9.60)	-	5.54 (116)
147	4.83 (101)	19.4	-	117 (4.60)	27.9 (1.10)	-	4.55 (95.0)
148	3.45 (72.0)	13.9	-	0.00 (0.00)	50.8 (2.00)	-	3.17 (66.3)

N09 (Cont.) - Loading time history, failure location, EFL_{60} and EFL_3

Spec. No.	Time History		Reported EFL_{60} kPa (psf)	Failure location		EFL_{60} Recreated kPa (psf)	EFL_3 kPa (psf)
	Failure Pressure kPa (psf)	Failure Time (sec)		to long dimension mm (in.)	to short dimension mm (in.)		
149	5.10 (107)	20.6	-	307 (12.1)	231 (9.10)	-	4.83 (101)
150	3.52 (73.4)	14.2	-	50.8 (2.00)	71.1 (2.80)	-	3.24 (67.7)
151	6.89 (144)	28.6	-	38.1 (1.50)	30.5 (1.20)	-	6.67 (139)
152	5.93 (124)	23.9	-	117 (4.60)	45.7 (1.80)	-	5.68 (119)
153	6.62 (138)	27.4	-	168 (6.60)	142 (5.60)	-	6.38 (133)
154	5.38 (112)	22.3	-	208 (8.20)	63.5 (2.50)	-	5.13 (107)
155	8.96 (187)	5.00	-	188 (7.40)	198 (7.80)	-	7.70 (161)
156	5.52 (115)	3.10	-	12.7 (0.50)	142 (5.60)	-	4.40 (91.8)
157	7.24 (151)	4.40	-	193 (7.60)	244 (9.60)	-	6.14 (128)
158	5.24 (109)	3.20	-	218 (8.60)	262 (10.3)	-	4.34 (90.7)
159	5.10 (107)	2.10	-	0.00 (0.00)	44.5 (1.75)	-	4.11 (85.9)
160	4.76 (99.4)	1.90	-	396 (15.6)	396 (15.6)	-	3.58 (74.7)
161	4.00 (83.5)	1.50	-	0.00 (0.00)	130 (5.10)	-	3.06 (64.0)
162	8.20 (171)	3.10	-	40.6 (1.60)	53.3 (2.10)	-	6.81 (142)
163	5.58 (117)	2.10	-	434 (17.1)	371 (14.6)	-	4.24 (88.5)
164	5.58 (117)	1.90	-	173 (6.80)	231 (9.10)	-	4.52 (94.3)
165	5.65 (118)	3.00	-	300 (11.8)	206 (8.10)	-	4.67 (97.5)
166	8.14 (170)	2.90	-	244 (9.60)	206 (8.10)	-	6.67 (139)
167	5.24 (109)	1.90	-	180 (7.10)	224 (8.80)	-	4.24 (88.5)
168	6.34 (132)	2.60	-	76.2 (3.00)	0.00 (0.00)	-	5.19 (108)
169	5.38 (112)	2.10	-	130 (5.10)	249 (9.80)	-	4.35 (90.9)
170	5.79(121)	2.20	-	12.7 (0.50)	142 (5.60)	-	4.47 (93.3)
171	5.58 (117)	1.80	-	114 (4.50)	38.1 (1.50)	-	4.39 (91.7)
172	5.79 (121)	2.20	-	117 (4.60)	244 (9.60)	-	4.69 (97.9)
173	6.76 (141)	2.50	-	88.9 (3.50)	0.00 (0.00)	-	5.47 (114)
174	4.83 (101)	1.80	-	81.3 (3.20)	38.1 (1.50)	-	3.85 (80.4)
175	5.79 (121)	2.30	-	109 (4.30)	231 (9.10)	-	4.69 (98.0)
176	5.24 (109)	2.00	-	127 (5.00)	63.5 (2.50)	-	4.18 (87.2)
177	4.76 (99.4)	1.90	-	0.00 (0.00)	76.2 (3.00)	-	3.81 (79.6)
178	8.41 (176)	3.60	-	269 (10.6)	231 (9.10)	-	6.93 (145)
179	4.55 (95.0)	0.20	-	25.4 (1.00)	88.9 (3.50)	-	3.07 (64.2)
180	6.07 (127)	0.20	-	127 (5.00)	0.00 (0.00)	-	3.92 (81.8)
181	8.83 (184)	0.30	-	625 (24.6)	269 (10.6)	-	5.59 (117)
182	7.72 (161)	0.20	-	193 (7.60)	244 (9.60)	-	5.28 (110)
183	5.58 (117)	0.20	-	38.1 (1.50)	40.6 (1.60)	-	3.78 (79.0)
184	4.83 (101)	0.10	-	130 (5.10)	53.3 (2.10)	-	3.08 (64.4)
185	6.76 (141)	0.10	-	485 (19.1)	384 (15.1)	-	3.79 (79.1)

N09 (Cont.) - Loading time history, failure location, EFL_{60} and EFL_3

Spec. No.	Time History		Reported EFL_{60} kPa (psf)	Failure location		EFL_{60} Recreated kPa (psf)	EFL_3 kPa (psf)
	Failure Pressure kPa (psf)	Failure Time (sec)		to long dimension mm (in.)	to short dimension mm (in.)		
186	5.52 (115)	0.30	-	5.08 (0.20)	130 (5.10)	-	3.64 (76.0)
187	5.38 (112)	0.30	-	325 (12.8)	269 (10.6)	-	3.68 (76.9)
188	4.83 (101)	0.20	-	63.5 (2.50)	38.1 (1.50)	-	3.27 (68.4)
189	5.79 (121)	0.20	-	50.8 (2.00)	0.00 (0.00)	-	3.94 (82.2)
190	4.83 (101)	0.20	-	38.1 (1.50)	38.1 (1.50)	-	3.26 (68.1)
191	9.24 (193)	0.40	-	173 (6.80)	244 (9.60)	-	6.61 (138)
192	7.86 (164)	0.40	-	168 (6.60)	231 (9.10)	-	5.70 (119)
193	6.07 (127)	0.10	-	0.00 (0.00)	58.4 (2.30)	-	4.07 (84.9)
194	6.00 (125)	0.10	-	0.00 (0.00)	50.8 (2.00)	-	4.03 (84.1)
195	5.17 (108)	0.10	-	152 (6.00)	63.5 (2.50)	-	3.36 (70.2)
196	8.41 (176)	0.30	-	180 (7.10)	257 (10.1)	-	5.95 (124)
197	5.58 (117)	0.30	-	12.7 (0.50)	55.9 (2.20)	-	3.89 (81.2)

Table A.24

W01: 60-sec cumulative distribution table : reported vs recreated
 (Data related to Figure 2.5)

Load kPa (psf)	p_b Historical	p_b Recreated
0.00 (0.0)	0.00E+00	0.00E+00
0.72 (15.0)	8.60E-07	1.11E-06
1.44 (30.0)	5.51E-05	6.93E-05
2.15 (45.0)	6.06E-04	7.51E-04
2.87 (60.0)	3.19E-03	3.91E-03
3.59 (75.0)	1.11E-02	1.35E-02
4.31 (90.0)	2.96E-02	3.57E-02
5.03 (105)	6.55E-02	7.83E-02
5.75 (120)	1.25E-01	1.48E-01
6.46 (135)	2.14E-01	2.50E-01
7.18 (150)	3.30E-01	3.79E-01
7.90 (165)	4.66E-01	5.25E-01
8.62 (180)	6.09E-01	6.71E-01
9.34 (195)	7.40E-01	7.97E-01
10.1 (210)	8.47E-01	8.91E-01
10.8 (225)	9.21E-01	9.50E-01
11.5 (240)	9.65E-01	9.81E-01
12.2 (255)	9.87E-01	9.94E-01
12.9 (270)	9.96E-01	9.99E-01
13.6 (285)	9.99E-01	1.00E+00
14.4 (300)	1.00E+00	1.00E+00

Table A.25

W02: 60-sec cumulative distribution table : reported vs recreated
 (Data related to Figure 2.5)

Load kPa (psf)	p_b Historical	p_b Recreated
0.00 (0.0)	0.00E+00	0.00E+00
0.36 (7.50)	7.99E-07	3.15E-06
0.72 (15.0)	5.07E-05	1.45E-04
1.08 (22.5)	5.62E-04	1.34E-03
1.44 (30.0)	3.02E-03	6.32E-03
1.80 (37.5)	1.09E-02	2.05E-02
2.15 (45.0)	3.00E-02	5.22E-02
2.51 (52.5)	6.88E-02	1.11E-01
2.87 (60.0)	1.36E-01	2.05E-01
3.23 (67.5)	2.39E-01	3.35E-01
3.59 (75.0)	3.75E-01	4.90E-01
3.95 (82.5)	5.32E-01	6.51E-01
4.31 (90.0)	6.89E-01	7.91E-01
4.67 (97.5)	8.21E-01	8.94E-01
5.03 (105)	9.14E-01	9.56E-01
5.39 (113)	9.66E-01	9.85E-01
5.75 (120)	9.89E-01	9.96E-01
6.10 (128)	9.98E-01	9.99E-01
6.46 (135)	1.00E+00	1.00E+00
6.82 (143)	1.00E+00	1.00E+00
7.18 (150)	1.00E+00	1.00E+00

Table A.26

W03: 60-sec cumulative distribution table : reported vs recreated
(Data related to Figure 2.5)

Load kPa (psf)	p_b Historical	p_b Recreated
0.00 (0.0)	0.00E+00	0.00E+00
1.08 (22.5)	7.97E-06	9.80E-06
2.15 (45.0)	4.33E-04	4.47E-04
3.23 (67.5)	3.80E-03	3.56E-03
4.31 (90.0)	1.58E-02	1.40E-02
5.39 (113)	4.45E-02	3.77E-02
6.46 (135)	9.79E-02	8.07E-02
7.54 (158)	1.82E-01	1.48E-01
8.62 (180)	2.98E-01	2.40E-01
9.70 (203)	4.38E-01	3.55E-01
10.8 (225)	5.88E-01	4.84E-01
11.9 (248)	7.29E-01	6.17E-01
12.9 (270)	8.44E-01	7.39E-01
14.0 (293)	9.23E-01	8.40E-01
15.1 (315)	9.68E-01	9.12E-01
16.2 (338)	9.89E-01	9.58E-01
17.2 (360)	9.97E-01	9.83E-01
18.3 (383)	9.99E-01	9.94E-01
19.4 (405)	1.00E+00	9.98E-01
20.5 (428)	1.00E+00	1.00E+00
21.5 (450)	1.00E+00	1.00E+00

Table A.27

W04: 60-sec cumulative distribution table : reported vs recreated
 (Data related to Figure 2.5)

Load kPa (psf)	p_b Historical	p_b Recreated
0.00 (0.0)	0.00E+00	0.00E+00
0.67 (14.0)	1.16E-05	9.57E-06
1.34 (28.0)	3.68E-04	3.28E-04
2.01 (42.0)	2.75E-03	2.56E-03
2.68 (56.0)	1.13E-02	1.08E-02
3.35 (70.0)	3.29E-02	3.23E-02
4.02 (84.0)	7.69E-02	7.67E-02
4.69 (98.0)	1.52E-01	1.54E-01
5.36 (112)	2.64E-01	2.70E-01
6.03 (126)	4.07E-01	4.19E-01
6.70 (140)	5.67E-01	5.83E-01
7.37 (154)	7.19E-01	7.38E-01
8.04 (168)	8.42E-01	8.59E-01
8.71 (182)	9.25E-01	9.37E-01
9.38 (196)	9.70E-01	9.77E-01
10.1 (210)	9.91E-01	9.94E-01
10.7 (224)	9.98E-01	9.99E-01
11.4 (238)	1.00E+00	1.00E+00
12.1 (252)	1.00E+00	1.00E+00
12.7 (266)	1.00E+00	1.00E+00
13.4 (280)	1.00E+00	1.00E+00

Table A.28

W05: 60-sec cumulative distribution table : reported vs recreated
 (Data related to Figure 2.5)

Load kPa (psf)	p_b Historical	p_b Recreated
0.00 (0.0)	0.00E+00	0.00E+00
0.67 (14.0)	3.16E-05	9.84E-05
1.34 (28.0)	6.58E-04	1.50E-03
2.01 (42.0)	3.88E-03	7.37E-03
2.68 (56.0)	1.36E-02	2.26E-02
3.35 (70.0)	3.58E-02	5.36E-02
4.02 (84.0)	7.77E-02	1.07E-01
4.69 (98.0)	1.47E-01	1.86E-01
5.36 (112)	2.48E-01	2.94E-01
6.03 (126)	3.79E-01	4.24E-01
6.70 (140)	5.29E-01	5.66E-01
7.37 (154)	6.80E-01	7.02E-01
8.04 (168)	8.11E-01	8.17E-01
8.71 (182)	9.05E-01	9.02E-01
9.38 (196)	9.61E-01	9.55E-01
10.1 (210)	9.87E-01	9.82E-01
10.7 (224)	9.97E-01	9.94E-01
11.4 (238)	9.99E-01	9.99E-01
12.1 (252)	1.00E+00	1.00E+00
12.7 (266)	1.00E+00	1.00E+00
13.4 (280)	1.00E+00	1.00E+00

Table A.29

W06: 60-sec cumulative distribution table : reported vs recreated
 (Data related to Figure 2.5)

Load kPa (psf)	p_b Historical	p_b Recreated
0.00 (0.0)	0.00E+00	0.00E+00
1.44 (30.0)	4.78E-05	8.07E-05
2.87 (60.0)	9.17E-04	1.35E-03
4.31 (90.0)	5.14E-03	6.97E-03
5.75 (120)	1.74E-02	2.22E-02
7.18 (150)	4.41E-02	5.38E-02
8.62 (180)	9.29E-02	1.09E-01
10.1 (210)	1.70E-01	1.93E-01
11.5 (240)	2.78E-01	3.06E-01
12.9 (270)	4.13E-01	4.42E-01
14.4 (300)	5.62E-01	5.87E-01
15.8 (330)	7.05E-01	7.23E-01
17.2 (360)	8.25E-01	8.35E-01
18.7 (390)	9.10E-01	9.15E-01
20.1 (420)	9.61E-01	9.62E-01
21.5 (450)	9.86E-01	9.86E-01
23.0 (480)	9.96E-01	9.96E-01
24.4 (510)	9.99E-01	9.99E-01
25.9 (540)	1.00E+00	1.00E+00
27.3 (570)	1.00E+00	1.00E+00
28.7 (600)	1.00E+00	1.00E+00

Table A.30

W07: 60-sec cumulative distribution table : reported vs recreated
 (Data related to Figure 2.5)

Load kPa (psf)	p_b Historical	p_b Recreated
0.00 (0.00)	0.00E+00	0.00E+00
1.63 (34.0)	1.67E-04	1.84E-04
3.26 (68.0)	2.40E-03	2.63E-03
4.88 (102)	1.14E-02	1.24E-02
6.51 (136)	3.39E-02	3.67E-02
8.14 (170)	7.79E-02	8.37E-02
9.77 (204)	1.50E-01	1.60E-01
11.4 (238)	2.52E-01	2.68E-01
13.0 (272)	3.82E-01	4.03E-01
14.7 (306)	5.26E-01	5.50E-01
16.3 (340)	6.69E-01	6.92E-01
17.9 (374)	7.92E-01	8.12E-01
19.5 (408)	8.84E-01	8.99E-01
21.2 (442)	9.44E-01	9.53E-01
22.8 (476)	9.77E-01	9.82E-01
24.4 (510)	9.92E-01	9.94E-01
26.0 (544)	9.98E-01	9.98E-01
27.7 (578)	9.99E-01	1.00E+00
29.3 (612)	1.00E+00	1.00E+00
30.9 (646)	1.00E+00	1.00E+00
32.6 (680)	1.00E+00	1.00E+00

Table A.31

W08: 60-sec cumulative distribution table : reported vs recreated
 (Data related to Figure 2.5)

Load kPa (psf)	p_b Historical	p_b Recreated
0.00 (0.0)	0.00E+00	0.00E+00
0.96 (20.0)	3.23E-05	4.90E-05
1.92 (40.0)	5.62E-04	7.68E-04
2.87 (60.0)	2.99E-03	3.84E-03
3.83 (80.0)	9.73E-03	1.20E-02
4.79 (100)	2.42E-02	2.87E-02
5.75 (120)	5.05E-02	5.82E-02
6.70 (140)	9.29E-02	1.04E-01
7.66 (160)	1.55E-01	1.70E-01
8.62 (180)	2.38E-01	2.57E-01
9.58 (200)	3.42E-01	3.62E-01
10.5 (220)	4.60E-01	4.79E-01
11.5 (240)	5.84E-01	5.99E-01
12.4 (260)	7.02E-01	7.13E-01
13.4 (280)	8.04E-01	8.10E-01
14.4 (300)	8.83E-01	8.86E-01
15.3 (320)	9.38E-01	9.38E-01
16.3 (340)	9.71E-01	9.70E-01
17.2 (360)	9.88E-01	9.87E-01
18.2 (380)	9.96E-01	9.95E-01
19.2 (400)	9.99E-01	9.98E-01

Table A.32

W09: 60-sec cumulative distribution table : reported vs recreated
 (Data related to Figure 2.5)

Load kPa (psf)	p_b Historical	p_b Recreated
0.00 (0.0)	0.00E+00	0.00E+00
0.60 (12.5)	2.58E-07	1.32E-08
1.20 (25.0)	2.23E-05	2.76E-06
1.80 (37.5)	2.99E-04	6.17E-05
2.39 (50.0)	1.85E-03	5.49E-04
2.99 (62.5)	7.49E-03	2.93E-03
3.59 (75.0)	2.30E-02	1.12E-02
4.19 (87.5)	5.77E-02	3.42E-02
4.79 (100)	1.24E-01	8.65E-02
5.39 (113)	2.33E-01	1.87E-01
5.99 (125)	3.86E-01	3.49E-01
6.58 (138)	5.67E-01	5.59E-01
7.18 (150)	7.44E-01	7.68E-01
7.78 (163)	8.79E-01	9.15E-01
8.38 (175)	9.57E-01	9.81E-01
8.98 (188)	9.89E-01	9.98E-01
9.58 (200)	9.98E-01	1.00E+00
10.2 (213)	1.00E+00	1.00E+00
10.8 (225)	1.00E+00	1.00E+00
11.4 (238)	1.00E+00	1.00E+00
12.0 (250)	1.00E+00	1.00E+00

Table A.33

W10: 60-sec cumulative distribution table : reported vs recreated
(Data related to Figure 2.5)

Load kPa (psf)	p_b Historical	p_b Recreated
0.00 (0.0)	0.00E+00	0.00E+00
0.72 (15.0)	5.39E-05	1.87E-04
1.44 (30.0)	1.48E-03	3.46E-03
2.15 (45.0)	9.57E-03	1.80E-02
2.87 (60.0)	3.38E-02	5.45E-02
3.59 (75.0)	8.49E-02	1.22E-01
4.31 (90.0)	1.70E-01	2.22E-01
5.03 (105)	2.89E-01	3.49E-01
5.75 (120)	4.33E-01	4.90E-01
6.46 (135)	5.85E-01	6.30E-01
7.18 (150)	7.24E-01	7.52E-01
7.90 (165)	8.35E-01	8.48E-01
8.62 (180)	9.13E-01	9.15E-01
9.34 (195)	9.60E-01	9.57E-01
10.1 (210)	9.84E-01	9.81E-01
10.8 (225)	9.95E-01	9.92E-01
11.5 (240)	9.98E-01	9.97E-01
12.2 (255)	1.00E+00	9.99E-01
12.9 (270)	1.00E+00	1.00E+00
13.6 (285)	1.00E+00	1.00E+00
14.4 (300)	1.00E+00	1.00E+00

Table A.34

W11: 60-sec cumulative distribution table : reported vs recreated
 (Data related to Figure 2.5)

Load kPa (psf)	p_b Historical	p_b Recreated
0.00 (0.0)	0.00E+00	0.00E+00
0.72 (15.0)	1.29E-07	2.70E-08
1.44 (30.0)	1.63E-05	5.54E-06
2.15 (45.0)	2.56E-04	1.14E-04
2.87 (60.0)	1.68E-03	9.01E-04
3.59 (75.0)	6.78E-03	4.17E-03
4.31 (90.0)	2.01E-02	1.38E-02
5.03 (105)	4.83E-02	3.61E-02
5.75 (120)	9.91E-02	7.98E-02
6.46 (135)	1.79E-01	1.54E-01
7.18 (150)	2.91E-01	2.64E-01
7.90 (165)	4.30E-01	4.08E-01
8.62 (180)	5.82E-01	5.71E-01
9.34 (195)	7.27E-01	7.30E-01
10.1 (210)	8.46E-01	8.57E-01
10.8 (225)	9.26E-01	9.39E-01
11.5 (240)	9.72E-01	9.80E-01
12.2 (255)	9.91E-01	9.95E-01
12.9 (270)	9.98E-01	9.99E-01
13.6 (285)	1.00E+00	1.00E+00
14.4 (300)	1.00E+00	1.00E+00

Table A.35

W12: 60-sec cumulative distribution table : reported vs recreated
 (Data related to Figure 2.5)

Load kPa (psf)	p_b Historical	p_b Recreated
0.00 (0.0)	0.00E+00	0.00E+00
0.53 (11.0)	4.56E-05	6.39E-05
1.05 (22.0)	1.29E-03	1.57E-03
1.58 (33.0)	7.26E-03	8.25E-03
2.11 (44.0)	2.29E-02	2.49E-02
2.63 (55.0)	5.41E-02	5.66E-02
3.16 (66.0)	1.07E-01	1.09E-01
3.69 (77.0)	1.86E-01	1.85E-01
4.21 (88.0)	2.93E-01	2.86E-01
4.74 (99.0)	4.24E-01	4.09E-01
5.27 (110)	5.68E-01	5.44E-01
5.79 (121)	7.09E-01	6.78E-01
6.32 (132)	8.28E-01	7.96E-01
6.85 (143)	9.13E-01	8.87E-01
7.37 (154)	9.64E-01	9.46E-01
7.90 (165)	9.88E-01	9.79E-01
8.43 (176)	9.97E-01	9.93E-01
8.95 (187)	9.99E-01	9.98E-01
9.48 (198)	1.00E+00	1.00E+00
10.0 (209)	1.00E+00	1.00E+00
10.5 (220)	1.00E+00	1.00E+00

Table A.36

W13: 60-sec cumulative distribution table : reported vs recreated
 (Data related to Figure 2.5)

Load kPa (psf)	p_b Historical	p_b Recreated
0.00 (0.0)	0.00E+00	0.00E+00
0.72 (15.0)	9.85E-04	1.05E-03
1.44 (30.0)	1.01E-02	1.06E-02
2.15 (45.0)	3.50E-02	3.65E-02
2.87 (60.0)	8.21E-02	8.51E-02
3.59 (75.0)	1.56E-01	1.61E-01
4.31 (90.0)	2.58E-01	2.64E-01
5.03 (105)	3.82E-01	3.90E-01
5.75 (120)	5.20E-01	5.28E-01
6.46 (135)	6.56E-01	6.64E-01
7.18 (150)	7.75E-01	7.82E-01
7.90 (165)	8.69E-01	8.73E-01
8.62 (180)	9.32E-01	9.35E-01
9.34 (195)	9.69E-01	9.71E-01
10.1 (210)	9.88E-01	9.89E-01
10.8 (225)	9.96E-01	9.96E-01
11.5 (240)	9.99E-01	9.99E-01
12.2 (255)	1.00E+00	1.00E+00
12.9 (270)	1.00E+00	1.00E+00
13.6 (285)	1.00E+00	1.00E+00
14.4 (300)	1.00E+00	1.00E+00

Table A.37

N01: 60-sec cumulative distribution table : reported vs recreated
 (Data related to Figure 2.6)

Load kPa (psf)	p_b Historical	p_b Recreated
0.05 (1.0)	0.00E+00	0.00E+00
1.34 (28.0)	1.08E-08	2.89E-08
2.63 (55.0)	2.77E-06	4.74E-06
3.93 (82.0)	5.21E-05	7.05E-05
5.22 (109)	3.53E-04	4.12E-04
6.51 (136)	1.44E-03	1.51E-03
7.80 (163)	4.36E-03	4.19E-03
9.10 (190)	1.09E-02	9.75E-03
10.4 (217)	2.38E-02	2.01E-02
11.7 (244)	4.70E-02	3.77E-02
13.0 (271)	8.59E-02	6.59E-02
14.3 (298)	1.46E-01	1.08E-01
15.6 (325)	2.34E-01	1.69E-01
16.9 (352)	3.51E-01	2.51E-01
18.1 (379)	4.93E-01	3.54E-01
19.4 (406)	6.47E-01	4.75E-01
20.7 (433)	7.89E-01	6.06E-01
22.0 (460)	8.98E-01	7.33E-01
23.3 (487)	9.62E-01	8.41E-01
24.6 (514)	9.90E-01	9.20E-01
25.9 (541)	9.98E-01	9.67E-01
27.2 (568)	1.00E+00	9.90E-01
28.5 (595)	1.00E+00	9.98E-01
29.8 (622)	1.00E+00	1.00E+00
31.1 (649)	1.00E+00	1.00E+00

Table A.38

N02: 60-sec cumulative distribution table : reported vs recreated
 (Data related to Figure 2.6)

Load kPa (psf)	p_b Historical	p_b Recreated
0.05 (1.00)	6.66E-14	2.42E-14
0.48 (10.0)	7.92E-07	4.94E-07
0.91 (19.0)	5.48E-05	3.93E-05
1.34 (28.0)	5.71E-04	4.41E-04
1.77 (37.0)	2.71E-03	2.20E-03
2.20 (46.0)	8.46E-03	7.12E-03
2.63 (55.0)	2.05E-02	1.78E-02
3.06 (64.0)	4.22E-02	3.73E-02
3.50 (73.0)	7.67E-02	6.93E-02
3.93 (82.0)	1.27E-01	1.17E-01
4.36 (91.0)	1.96E-01	1.83E-01
4.79 (100)	2.82E-01	2.68E-01
5.22 (109)	3.85E-01	3.70E-01
5.65 (118)	4.99E-01	4.85E-01
6.08 (127)	6.15E-01	6.04E-01
6.51 (136)	7.26E-01	7.18E-01
6.94 (145)	8.21E-01	8.16E-01
7.37 (154)	8.94E-01	8.93E-01
7.80 (163)	9.45E-01	9.45E-01
8.24 (172)	9.75E-01	9.76E-01
8.67 (181)	9.90E-01	9.91E-01
9.10 (190)	9.97E-01	9.97E-01
9.53 (199)	9.99E-01	9.99E-01
9.96 (208)	1.00E+00	1.00E+00
10.4 (217)	1.00E+00	1.00E+00

Table A.39

N03: 60-sec cumulative distribution table : reported vs recreated
 (Data related to Figure 2.6)

Load kPa (psf)	p_b Historical	p_b Recreated
0.05 (1.00)	0.00E+00	0.00E+00
0.62 (13.0)	3.61E-10	2.82E-09
1.20 (25.0)	1.72E-07	7.44E-07
1.77 (37.0)	5.78E-06	1.79E-05
2.35 (49.0)	6.23E-05	1.54E-04
2.92 (61.0)	3.60E-04	7.55E-04
3.50 (73.0)	1.41E-03	2.61E-03
4.07 (85.0)	4.27E-03	7.12E-03
4.64 (97.0)	1.07E-02	1.64E-02
5.22 (109)	2.35E-02	3.34E-02
5.79 (121)	4.61E-02	6.16E-02
6.37 (133)	8.30E-02	1.05E-01
6.94 (145)	1.39E-01	1.66E-01
7.52 (157)	2.17E-01	2.48E-01
8.09 (169)	3.18E-01	3.49E-01
8.67 (181)	4.40E-01	4.65E-01
9.24 (193)	5.73E-01	5.88E-01
9.82 (205)	7.03E-01	7.08E-01
10.4 (217)	8.17E-01	8.12E-01
11.0 (229)	9.02E-01	8.92E-01
11.5 (241)	9.57E-01	9.46E-01
12.1 (253)	9.85E-01	9.77E-01
12.7 (265)	9.96E-01	9.92E-01
13.3 (277)	9.99E-01	9.98E-01
13.8 (289)	1.00E+00	1.00E+00

Table A.40

N04: 60-sec cumulative distribution table : reported vs recreated
 (Data related to Figure 2.6)

Load kPa (psf)	p_b Historical	p_b Recreated
0.05 (1.00)	4.02E-14	5.55E-16
0.34 (7.00)	1.97E-07	2.36E-08
0.62 (13.0)	1.82E-05	3.98E-06
0.91 (19.0)	2.28E-04	6.90E-05
1.20 (25.0)	1.23E-03	4.61E-04
1.48 (31.0)	4.22E-03	1.86E-03
1.77 (37.0)	1.11E-02	5.52E-03
2.06 (43.0)	2.44E-02	1.34E-02
2.35 (49.0)	4.73E-02	2.83E-02
2.63 (55.0)	8.32E-02	5.37E-02
2.92 (61.0)	1.35E-01	9.37E-02
3.21 (67.0)	2.06E-01	1.52E-01
3.50 (73.0)	2.97E-01	2.33E-01
3.78 (79.0)	4.05E-01	3.36E-01
4.07 (85.0)	5.25E-01	4.58E-01
4.36 (91.0)	6.47E-01	5.92E-01
4.64 (97.0)	7.61E-01	7.22E-01
4.93 (103)	8.55E-01	8.34E-01
5.22 (109)	9.23E-01	9.16E-01
5.51 (115)	9.66E-01	9.66E-01
5.79 (121)	9.87E-01	9.89E-01
6.08 (127)	9.96E-01	9.98E-01
6.37 (133)	9.99E-01	1.00E+00
6.66 (139)	1.00E+00	1.00E+00
6.94 (145)	1.00E+00	1.00E+00

Table A.41

N05: 60-sec cumulative distribution table : reported vs recreated
 (Data related to Figure 2.6)

Load kPa (psf)	p_b Historical	p_b Recreated
0.05 (1.00)	1.11E-16	1.11E-16
0.43 (9.00)	2.71E-08	2.41E-08
0.81 (17.0)	2.41E-06	2.08E-06
1.20 (25.0)	2.71E-05	2.30E-05
1.58 (33.0)	1.45E-04	1.21E-04
1.96 (41.0)	5.30E-04	4.41E-04
2.35 (49.0)	1.56E-03	1.28E-03
2.73 (57.0)	3.94E-03	3.23E-03
3.11 (65.0)	8.96E-03	7.29E-03
3.50 (73.0)	1.87E-02	1.52E-02
3.88 (81.0)	3.64E-02	2.94E-02
4.26 (89.0)	6.68E-02	5.38E-02
4.64 (97.0)	1.16E-01	9.33E-02
5.03 (105)	1.90E-01	1.54E-01
5.41 (113)	2.94E-01	2.40E-01
5.79 (121)	4.28E-01	3.56E-01
6.18 (129)	5.83E-01	4.96E-01
6.56 (137)	7.37E-01	6.47E-01
6.94 (145)	8.64E-01	7.88E-01
7.33 (153)	9.46E-01	8.96E-01
7.71 (161)	9.85E-01	9.61E-01
8.09 (169)	9.97E-01	9.90E-01
8.47 (177)	1.00E+00	9.98E-01
8.86 (185)	1.00E+00	1.00E+00
9.24 (193)	1.00E+00	1.00E+00

Table A.42

N06: 60-sec cumulative distribution table : reported vs recreated
 (Data related to Figure 2.6)

Load kPa (psf)	p_b Historical	p_b Recreated
0.05 (1.00)	0.00E+00	0.00E+00
0.71 (14.8)	1.23E-08	1.12E-09
1.37 (28.6)	1.77E-06	2.90E-07
2.03 (42.4)	2.42E-05	5.33E-06
2.69 (56.2)	1.38E-04	3.69E-05
3.35 (70.0)	5.10E-04	1.58E-04
4.01 (83.8)	1.47E-03	5.16E-04
4.67 (97.6)	3.60E-03	1.41E-03
5.33 (111)	7.88E-03	3.38E-03
5.99 (125)	1.58E-02	7.39E-03
6.66 (139)	2.96E-02	1.50E-02
7.32 (153)	5.25E-02	2.88E-02
7.98 (167)	8.83E-02	5.23E-02
8.64 (180)	1.42E-01	9.04E-02
9.30 (194)	2.17E-01	1.49E-01
9.96 (208)	3.18E-01	2.35E-01
10.6 (222)	4.41E-01	3.50E-01
11.3 (236)	5.80E-01	4.91E-01
11.9 (249)	7.18E-01	6.46E-01
12.6 (263)	8.38E-01	7.91E-01
13.3 (277)	9.23E-01	9.01E-01
13.9 (291)	9.72E-01	9.66E-01
14.6 (305)	9.93E-01	9.92E-01
15.2 (318)	9.99E-01	9.99E-01
15.9 (332)	1.00E+00	1.00E+00

Table A.43

N07: 60-sec cumulative distribution table : reported vs recreated
 (Data related to Figure 2.6)

Load kPa (psf)	p_b Historical	p_b Recreated
0.05 (1.00)	9.21E-15	3.22E-15
0.30 (6.20)	3.13E-08	1.61E-08
0.55 (11.4)	1.59E-06	8.91E-07
0.79 (16.6)	1.52E-05	9.00E-06
1.04 (21.8)	7.85E-05	4.82E-05
1.29 (27.0)	2.93E-04	1.86E-04
1.54 (32.2)	8.90E-04	5.81E-04
1.79 (37.4)	2.34E-03	1.57E-03
2.04 (42.6)	5.54E-03	3.80E-03
2.29 (47.8)	1.20E-02	8.42E-03
2.54 (53.0)	2.43E-02	1.73E-02
2.79 (58.2)	4.60E-02	3.35E-02
3.04 (63.4)	8.22E-02	6.13E-02
3.28 (68.6)	1.39E-01	1.06E-01
3.53 (73.8)	2.23E-01	1.75E-01
3.78 (79.0)	3.38E-01	2.72E-01
4.03 (84.2)	4.80E-01	4.00E-01
4.28 (89.4)	6.36E-01	5.50E-01
4.53 (94.6)	7.83E-01	7.05E-01
4.78 (99.8)	8.96E-01	8.39E-01
5.03 (105)	9.63E-01	9.31E-01
5.28 (110)	9.91E-01	9.79E-01
5.53 (115)	9.99E-01	9.96E-01
5.77 (121)	1.00E+00	1.00E+00
6.02 (126)	1.00E+00	1.00E+00

Table A.44

N08: 60-sec cumulative distribution table : reported vs recreated
 (Data related to Figure 2.6)

Load kPa (psf)	p_b Historical	p_b Recreated
0.05 (1.00)	2.19E-14	5.07E-13
0.21 (4.40)	1.67E-08	1.01E-07
0.37 (7.80)	1.13E-06	4.61E-06
0.54 (11.2)	1.22E-05	4.03E-05
0.70 (14.6)	6.50E-05	1.84E-04
0.86 (18.0)	2.40E-04	6.03E-04
1.02 (21.4)	7.17E-04	1.62E-03
1.19 (24.8)	1.86E-03	3.82E-03
1.35 (28.2)	4.36E-03	8.19E-03
1.51 (31.6)	9.48E-03	1.64E-02
1.68 (35.0)	1.94E-02	3.08E-02
1.84 (38.4)	3.75E-02	5.51E-02
2.00 (41.8)	6.90E-02	9.39E-02
2.16 (45.2)	1.21E-01	1.53E-01
2.33 (48.6)	2.01E-01	2.38E-01
2.49 (52.0)	3.16E-01	3.51E-01
2.65 (55.4)	4.65E-01	4.89E-01
2.82 (58.8)	6.34E-01	6.39E-01
2.98 (62.2)	7.94E-01	7.81E-01
3.14 (65.6)	9.12E-01	8.92E-01
3.30 (69.0)	9.75E-01	9.59E-01
3.47 (72.4)	9.96E-01	9.89E-01
3.63 (75.8)	1.00E+00	9.98E-01
3.79 (79.2)	1.00E+00	1.00E+00
3.95 (82.6)	1.00E+00	1.00E+00

Table A.45

W01: 3-sec cumulative distribution table
(Data related to Figure 2.7)

Load kPa (psf)	P_b
0.05 (1.00)	1.10E-13
0.86 (18.0)	1.85E-06
1.68 (35.0)	8.34E-05
2.49 (52.0)	7.69E-04
3.30 (69.0)	3.59E-03
4.12 (86.0)	1.14E-02
4.93 (103)	2.82E-02
5.75 (120)	5.87E-02
6.56 (137)	1.07E-01
7.37 (154)	1.77E-01
8.19 (171)	2.68E-01
9.00 (188)	3.77E-01
9.82 (205)	4.96E-01
10.6 (222)	6.18E-01
11.4 (239)	7.30E-01
12.3 (256)	8.24E-01
13.1 (273)	8.95E-01
13.9 (290)	9.44E-01
14.7 (307)	9.73E-01
15.5 (324)	9.89E-01
16.3 (341)	9.96E-01
17.1 (358)	9.99E-01
18.0 (375)	1.00E+00
18.8 (392)	1.00E+00
19.6 (409)	1.00E+00

Table A.46

W02: 3-sec cumulative distribution table
(Data related to Figure 2.7)

Load kPa (psf)	P_b
0.05 (1.00)	2.61E-11
0.43 (9.00)	3.89E-06
0.81 (17.0)	1.20E-04
1.20 (25.0)	9.44E-04
1.58 (33.0)	4.06E-03
1.96 (41.0)	1.24E-02
2.35 (49.0)	3.02E-02
2.73 (57.0)	6.25E-02
3.11 (65.0)	1.14E-01
3.50 (73.0)	1.89E-01
3.88 (81.0)	2.87E-01
4.26 (89.0)	4.04E-01
4.64 (97.0)	5.30E-01
5.03 (105)	6.55E-01
5.41 (113)	7.67E-01
5.79 (121)	8.56E-01
6.18 (129)	9.20E-01
6.56 (137)	9.60E-01
6.94 (145)	9.82E-01
7.33 (153)	9.93E-01
7.71 (161)	9.98E-01
8.09 (169)	9.99E-01
8.47 (177)	1.00E+00
8.86 (185)	1.00E+00
9.24 (193)	1.00E+00

Table A.47

W03: 3-sec cumulative distribution table
(Data related to Figure 2.7)

Load kPa (psf)	P_b
0.05 (1.00)	1.12E-13
1.29 (27.0)	1.17E-05
2.54 (53.0)	4.15E-04
3.78 (79.0)	2.88E-03
5.03 (105)	1.03E-02
6.27 (131)	2.62E-02
7.52 (157)	5.41E-02
8.76 (183)	9.70E-02
10.0 (209)	1.57E-01
11.3 (235)	2.35E-01
12.5 (261)	3.29E-01
13.7 (287)	4.35E-01
15.0 (313)	5.46E-01
16.2 (339)	6.56E-01
17.5 (365)	7.56E-01
18.7 (391)	8.39E-01
20.0 (417)	9.03E-01
21.2 (443)	9.47E-01
22.5 (469)	9.74E-01
23.7 (495)	9.89E-01
24.9 (521)	9.96E-01
26.2 (547)	9.99E-01
27.4 (573)	1.00E+00
28.7 (599)	1.00E+00
29.9 (625)	1.00E+00

Table A.48W04: 3-sec cumulative distribution table
(Data related to Figure 2.7)

Load kPa (psf)	P_b
0.05 (1.00)	4.87E-12
0.72 (15.0)	5.10E-06
1.39 (29.0)	1.48E-04
2.06 (43.0)	1.09E-03
2.73 (57.0)	4.50E-03
3.40 (71.0)	1.33E-02
4.07 (85.0)	3.18E-02
4.74 (99.0)	6.50E-02
5.41 (113)	1.18E-01
6.08 (127)	1.94E-01
6.75 (141)	2.93E-01
7.42 (155)	4.12E-01
8.09 (169)	5.39E-01
8.76 (183)	6.65E-01
9.43 (197)	7.75E-01
10.1 (211)	8.63E-01
10.8 (225)	9.25E-01
11.4 (239)	9.63E-01
12.1 (253)	9.84E-01
12.8 (267)	9.94E-01
13.5 (281)	9.98E-01
14.1 (295)	9.99E-01
14.8 (309)	1.00E+00
15.5 (323)	1.00E+00
16.1 (337)	1.00E+00

Table A.49

W05: 3-sec cumulative distribution table
(Data related to Figure 2.7)

Load kPa (psf)	P_b
0.05 (1.00)	1.51E-09
0.74 (15.4)	6.96E-05
1.43 (29.9)	9.30E-04
2.12 (44.3)	4.36E-03
2.81 (58.7)	1.31E-02
3.50 (73.2)	3.09E-02
4.19 (87.6)	6.15E-02
4.88 (102)	1.09E-01
5.58 (116)	1.76E-01
6.27 (131)	2.64E-01
6.96 (145)	3.69E-01
7.65 (160)	4.86E-01
8.34 (174)	6.06E-01
9.03 (189)	7.19E-01
9.72 (203)	8.16E-01
10.4 (217)	8.90E-01
11.1 (232)	9.41E-01
11.8 (246)	9.72E-01
12.5 (261)	9.88E-01
13.2 (275)	9.96E-01
13.9 (290)	9.99E-01
14.6 (304)	1.00E+00
15.2 (318)	1.00E+00
15.9 (333)	1.00E+00
16.6 (347)	1.00E+00

Table A.50W06: 3-sec cumulative distribution table
(Data related to Figure 2.7)

Load kPa (psf)	P_b
0.05 (1.00)	3.57E-11
1.33 (27.8)	2.67E-05
2.61 (54.5)	4.17E-04
3.89 (81.3)	2.12E-03
5.17 (108)	6.71E-03
6.45 (135)	1.64E-02
7.73 (162)	3.38E-02
9.01 (188)	6.18E-02
10.3 (215)	1.03E-01
11.6 (242)	1.60E-01
12.9 (269)	2.32E-01
14.1 (295)	3.19E-01
15.4 (322)	4.18E-01
16.7 (349)	5.23E-01
18.0 (376)	6.27E-01
19.3 (402)	7.24E-01
20.5 (429)	8.08E-01
21.8 (456)	8.75E-01
23.1 (483)	9.24E-01
24.4 (509)	9.57E-01
25.7 (536)	9.78E-01
26.9 (563)	9.90E-01
28.2 (590)	9.96E-01
29.5 (616)	9.98E-01
30.8 (643)	9.99E-01

Table A.51

W07: 3-sec cumulative distribution table
(Data related to Figure 2.7)

Load kPa (psf)	P_b
0.05 (1.00)	1.03E-10
1.26 (26.3)	3.14E-05
2.47 (51.7)	4.24E-04
3.69 (77.0)	1.98E-03
4.90 (102)	5.91E-03
6.11 (128)	1.38E-02
7.33 (153)	2.75E-02
8.54 (178)	4.88E-02
9.75 (204)	7.97E-02
11.0 (229)	1.22E-01
12.2 (254)	1.75E-01
13.4 (280)	2.41E-01
14.6 (305)	3.17E-01
15.8 (330)	4.02E-01
17.0 (356)	4.91E-01
18.2 (381)	5.81E-01
19.5 (406)	6.68E-01
20.7 (432)	7.46E-01
21.9 (457)	8.15E-01
23.1 (482)	8.71E-01
24.3 (508)	9.14E-01
25.5 (533)	9.46E-01
26.7 (559)	9.68E-01
28.0 (584)	9.82E-01
29.2 (609)	9.90E-01

Table A.52W08: 3-sec cumulative distribution table
(Data related to Figure 2.7)

Load kPa (psf)	P_b
0.05 (1.00)	1.62E-10
1.02 (21.3)	3.00E-05
1.99 (41.6)	4.26E-04
2.96 (61.8)	2.06E-03
3.93 (82.1)	6.33E-03
4.90 (102)	1.51E-02
5.87 (123)	3.06E-02
6.85 (143)	5.53E-02
7.82 (163)	9.14E-02
8.79 (184)	1.41E-01
9.76 (204)	2.05E-01
10.7 (224)	2.82E-01
11.7 (244)	3.72E-01
12.7 (265)	4.69E-01
13.6 (285)	5.69E-01
14.6 (305)	6.66E-01
15.6 (326)	7.54E-01
16.6 (346)	8.29E-01
17.5 (366)	8.88E-01
18.5 (386)	9.32E-01
19.5 (407)	9.61E-01
20.4 (427)	9.80E-01
21.4 (447)	9.90E-01
22.4 (467)	9.96E-01
23.4 (488)	9.98E-01

Table A.53W09: 3-sec cumulative distribution table
(Data related to Figure 2.7)

Load kPa (psf)	P_b
0.05 (1.00)	0.00E+00
0.50 (10.5)	9.64E-10
0.96 (20.1)	1.34E-07
1.42 (29.6)	2.61E-06
1.88 (39.2)	2.18E-05
2.33 (48.7)	1.13E-04
2.79 (58.3)	4.29E-04
3.25 (67.8)	1.32E-03
3.70 (77.4)	3.44E-03
4.16 (86.9)	7.96E-03
4.62 (96.5)	1.67E-02
5.07 (106)	3.21E-02
5.53 (116)	5.76E-02
5.99 (125)	9.71E-02
6.45 (135)	1.54E-01
6.90 (144)	2.32E-01
7.36 (154)	3.32E-01
7.82 (163)	4.48E-01
8.27 (173)	5.75E-01
8.73 (182)	6.99E-01
9.19 (192)	8.08E-01
9.64 (201)	8.92E-01
10.1 (211)	9.47E-01
10.6 (221)	9.78E-01
11.0 (230)	9.93E-01

Table A.54W10: 3-sec cumulative distribution table
(Data related to Figure 2.7)

Load kPa (psf)	P_b
0.05 (1.00)	3.02E-10
0.56 (11.8)	1.87E-05
1.08 (22.6)	3.36E-04
1.60 (33.3)	1.85E-03
2.11 (44.1)	6.10E-03
2.63 (54.9)	1.50E-02
3.14 (65.7)	3.05E-02
3.66 (76.4)	5.45E-02
4.18 (87.2)	8.82E-02
4.69 (98.0)	1.32E-01
5.21 (109)	1.86E-01
5.72 (120)	2.50E-01
6.24 (130)	3.21E-01
6.76 (141)	3.98E-01
7.27 (152)	4.78E-01
7.79 (163)	5.57E-01
8.30 (173)	6.33E-01
8.82 (184)	7.04E-01
9.34 (195)	7.68E-01
9.85 (206)	8.23E-01
10.4 (217)	8.69E-01
10.9 (227)	9.06E-01
11.4 (238)	9.35E-01
11.9 (249)	9.56E-01
12.4 (260)	9.72E-01

Table A.55

W11: 3-sec cumulative distribution table
(Data related to Figure 2.7)

Load kPa (psf)	P_b
0.05 (1.00)	0.00E+00
0.65 (13.7)	3.07E-09
1.26 (26.3)	4.83E-07
1.87 (39.0)	9.39E-06
2.47 (51.7)	7.38E-05
3.08 (64.3)	3.48E-04
3.69 (77.0)	1.18E-03
4.29 (89.7)	3.22E-03
4.90 (102)	7.44E-03
5.51 (115)	1.52E-02
6.11 (128)	2.83E-02
6.72 (140)	4.86E-02
7.33 (153)	7.85E-02
7.93 (166)	1.20E-01
8.54 (178)	1.75E-01
9.15 (191)	2.44E-01
9.75 (204)	3.26E-01
10.4 (216)	4.20E-01
11.0 (229)	5.21E-01
11.6 (242)	6.23E-01
12.2 (254)	7.20E-01
12.8 (267)	8.06E-01
13.4 (280)	8.75E-01
14.0 (292)	9.27E-01
14.6 (305)	9.61E-01

Table A.56W12: 3-sec cumulative distribution table
(Data related to Figure 2.7)

Load kPa (psf)	P_b
0.05 (1.00)	2.43E-11
0.55 (11.4)	2.14E-05
1.05 (21.9)	4.53E-04
1.55 (32.3)	2.33E-03
2.04 (42.7)	7.05E-03
2.54 (53.1)	1.63E-02
3.04 (63.5)	3.20E-02
3.54 (74.0)	5.64E-02
4.04 (84.4)	9.17E-02
4.54 (94.8)	1.40E-01
5.04 (105)	2.02E-01
5.54 (116)	2.79E-01
6.04 (126)	3.69E-01
6.54 (137)	4.69E-01
7.04 (147)	5.74E-01
7.53 (157)	6.76E-01
8.03 (168)	7.70E-01
8.53 (178)	8.48E-01
9.03 (189)	9.08E-01
9.53 (199)	9.50E-01
10.0 (209)	9.76E-01
10.5 (220)	9.90E-01
11.0 (230)	9.96E-01
11.5 (241)	9.99E-01
12.0 (251)	1.00E+00

Table A.57W13: 3-sec cumulative distribution table
(Data related to Figure 2.7)

Load kPa (psf)	P_b
0.05 (1.00)	7.26E-08
0.73 (15.3)	1.46E-03
1.42 (29.7)	9.70E-03
2.11 (44.0)	2.74E-02
2.79 (58.4)	5.64E-02
3.48 (72.7)	9.78E-02
4.17 (87.0)	1.52E-01
4.85 (101)	2.19E-01
5.54 (116)	2.96E-01
6.23 (130)	3.81E-01
6.91 (144)	4.70E-01
7.60 (159)	5.59E-01
8.29 (173)	6.45E-01
8.98 (187)	7.23E-01
9.66 (202)	7.92E-01
10.3 (216)	8.49E-01
11.0 (230)	8.95E-01
11.7 (245)	9.30E-01
12.4 (259)	9.56E-01
13.1 (274)	9.73E-01
13.8 (288)	9.84E-01
14.5 (302)	9.91E-01
15.2 (317)	9.95E-01
15.8 (331)	9.98E-01
16.5 (345)	9.99E-01

Table A.58W14: 3-sec cumulative distribution table
(Data related to Figure 2.7)

Load kPa (psf)	P_b
0.05 (1.00)	1.44E-14
0.32 (6.63)	1.18E-08
0.59 (12.3)	9.68E-07
0.86 (17.9)	1.42E-05
1.13 (23.5)	9.74E-05
1.40 (29.1)	4.30E-04
1.67 (34.8)	1.43E-03
1.94 (40.4)	3.89E-03
2.20 (46.0)	9.09E-03
2.47 (51.7)	1.89E-02
2.74 (57.3)	3.59E-02
3.01 (62.9)	6.29E-02
3.28 (68.6)	1.03E-01
3.55 (74.2)	1.59E-01
3.82 (79.8)	2.33E-01
4.09 (85.5)	3.23E-01
4.36 (91.1)	4.27E-01
4.63 (96.7)	5.39E-01
4.90 (102)	6.50E-01
5.17 (108)	7.53E-01
5.44 (114)	8.38E-01
5.71 (119)	9.04E-01
5.98 (125)	9.48E-01
6.25 (131)	9.75E-01
6.52 (136)	9.90E-01

Table A.59N01: 3-sec cumulative distribution table
(Data related to Figure 2.8)

Load kPa (psf)	P_b
0.05 (1.00)	0.00E+00
1.63 (34.0)	8.31E-08
3.21 (67.0)	9.12E-06
4.79 (100)	1.06E-04
6.37 (133)	5.29E-04
7.95 (166)	1.75E-03
9.53 (199)	4.52E-03
11.1 (232)	1.00E-02
12.7 (265)	1.99E-02
14.3 (298)	3.63E-02
15.8 (331)	6.22E-02
17.4 (364)	1.01E-01
19.0 (397)	1.55E-01
20.6 (430)	2.29E-01
22.2 (463)	3.22E-01
23.7 (496)	4.34E-01
25.3 (529)	5.57E-01
26.9 (562)	6.81E-01
28.5 (595)	7.94E-01
30.1 (628)	8.84E-01
31.6 (661)	9.44E-01
33.2 (694)	9.78E-01
34.8 (727)	9.93E-01
36.4 (760)	9.99E-01
38.0 (793)	1.00E+00

Table A.60N02: 3-sec cumulative distribution table
(Data related to Figure 2.8)

Load kPa (psf)	P_b
0.05 (1.00)	7.03E-14
0.62 (13.0)	2.09E-06
1.20 (25.0)	1.08E-04
1.77 (37.0)	9.04E-04
2.35 (49.0)	3.65E-03
2.92 (61.0)	1.02E-02
3.50 (73.0)	2.27E-02
4.07 (85.0)	4.37E-02
4.64 (97.0)	7.58E-02
5.22 (109)	1.21E-01
5.79 (121)	1.82E-01
6.37 (133)	2.59E-01
6.94 (145)	3.51E-01
7.52 (157)	4.55E-01
8.09 (169)	5.65E-01
8.67 (181)	6.73E-01
9.24 (193)	7.73E-01
9.82 (205)	8.55E-01
10.4 (217)	9.17E-01
11.0 (229)	9.58E-01
11.5 (241)	9.82E-01
12.1 (253)	9.93E-01
12.7 (265)	9.98E-01
13.3 (277)	1.00E+00
13.8 (289)	1.00E+00

Table A.61N03: 3-sec cumulative distribution table
(Data related to Figure 2.8)

Load kPa (psf)	P_b
0.05 (1.00)	0.00E+00
0.86 (18.0)	1.97E-08
1.68 (35.0)	4.05E-06
2.49 (52.0)	7.57E-05
3.30 (69.0)	5.28E-04
4.12 (86.0)	2.18E-03
4.93 (103)	6.53E-03
5.75 (120)	1.59E-02
6.56 (137)	3.33E-02
7.37 (154)	6.25E-02
8.19 (171)	1.07E-01
9.00 (188)	1.71E-01
9.82 (205)	2.56E-01
10.6 (222)	3.61E-01
11.4 (239)	4.81E-01
12.3 (256)	6.08E-01
13.1 (273)	7.29E-01
13.9 (290)	8.32E-01
14.7 (307)	9.09E-01
15.5 (324)	9.58E-01
16.3 (341)	9.84E-01
17.1 (358)	9.95E-01
18.0 (375)	9.99E-01
18.8 (392)	1.00E+00
19.6 (409)	1.00E+00

Table A.62N04: 3-sec cumulative distribution table
(Data related to Figure 2.8)

Load kPa (psf)	P_b
0.05 (1.00)	2.33E-15
0.43 (9.00)	1.57E-07
0.81 (17.0)	1.61E-05
1.20 (25.0)	1.96E-04
1.58 (33.0)	1.02E-03
1.96 (41.0)	3.42E-03
2.35 (49.0)	8.87E-03
2.73 (57.0)	1.94E-02
3.11 (65.0)	3.78E-02
3.50 (73.0)	6.74E-02
3.88 (81.0)	1.12E-01
4.26 (89.0)	1.75E-01
4.64 (97.0)	2.58E-01
5.03 (105)	3.63E-01
5.41 (113)	4.86E-01
5.79 (121)	6.17E-01
6.18 (129)	7.43E-01
6.56 (137)	8.49E-01
6.94 (145)	9.26E-01
7.33 (153)	9.71E-01
7.71 (161)	9.91E-01
8.09 (169)	9.98E-01
8.47 (177)	1.00E+00
8.86 (185)	1.00E+00
9.24 (193)	1.00E+00

Table A.63N05: 3-sec cumulative distribution table
(Data related to Figure 2.8)

Load kPa (psf)	P_b
0.05 (1.00)	0.00E+00
0.53 (11.0)	1.57E-08
1.01 (21.0)	1.28E-06
1.48 (31.0)	1.42E-05
1.96 (41.0)	7.80E-05
2.44 (51.0)	2.99E-04
2.92 (61.0)	9.21E-04
3.40 (71.0)	2.45E-03
3.88 (81.0)	5.83E-03
4.36 (91.0)	1.27E-02
4.84 (101)	2.58E-02
5.31 (111)	4.91E-02
5.79 (121)	8.81E-02
6.27 (131)	1.50E-01
6.75 (141)	2.40E-01
7.23 (151)	3.63E-01
7.71 (161)	5.13E-01
8.19 (171)	6.73E-01
8.67 (181)	8.17E-01
9.15 (191)	9.20E-01
9.62 (201)	9.75E-01
10.1 (211)	9.95E-01
10.6 (221)	9.99E-01
11.1 (231)	1.00E+00
11.5 (241)	1.00E+00

Table A.64
 N06 3-sec cumulative distribution table
 (Data related to Figure 2.8)

Load kPa (psf)	P_b
0.05 (1.00)	0.00E+00
0.86 (18.0)	1.11E-09
1.68 (35.0)	2.37E-07
2.49 (52.0)	3.91E-06
3.30 (69.0)	2.59E-05
4.12 (86.0)	1.10E-04
4.93 (103)	3.63E-04
5.75 (120)	1.01E-03
6.56 (137)	2.49E-03
7.37 (154)	5.61E-03
8.19 (171)	1.17E-02
9.00 (188)	2.31E-02
9.82 (205)	4.31E-02
10.6 (222)	7.65E-02
11.4 (239)	1.29E-01
12.3 (256)	2.08E-01
13.1 (273)	3.18E-01
13.9 (290)	4.57E-01
14.7 (307)	6.14E-01
15.5 (324)	7.66E-01
16.3 (341)	8.87E-01
17.1 (358)	9.59E-01
18.0 (375)	9.90E-01
18.8 (392)	9.99E-01
19.6 (409)	1.00E+00

Table A.65N07: 3-sec cumulative distribution table
(Data related to Figure 2.8)

Load kPa (psf)	P_b
0.05 (1.00)	1.11E-16
0.35 (7.40)	5.04E-09
0.66 (13.8)	3.12E-07
0.97 (20.2)	3.54E-06
1.27 (26.6)	2.13E-05
1.58 (33.0)	9.12E-05
1.89 (39.4)	3.14E-04
2.19 (45.8)	9.23E-04
2.50 (52.2)	2.40E-03
2.81 (58.6)	5.68E-03
3.11 (65.0)	1.24E-02
3.42 (71.4)	2.52E-02
3.73 (77.8)	4.82E-02
4.03 (84.2)	8.73E-02
4.34 (90.6)	1.50E-01
4.64 (97.0)	2.42E-01
4.95 (103)	3.68E-01
5.26 (110)	5.22E-01
5.56 (116)	6.86E-01
5.87 (123)	8.31E-01
6.18 (129)	9.31E-01
6.48 (135)	9.81E-01
6.79 (142)	9.97E-01
7.10 (148)	1.00E+00
7.40 (155)	1.00E+00

Table A.66N08: 3-sec cumulative distribution table
(Data related to Figure 2.8)

Load kPa (psf)	P_b
0.05 (1.00)	1.63E-13
0.25 (5.20)	8.94E-08
0.45 (9.40)	3.75E-06
0.65 (13.6)	3.13E-05
0.85 (17.8)	1.42E-04
1.05 (22.0)	4.69E-04
1.25 (26.2)	1.29E-03
1.46 (30.4)	3.12E-03
1.66 (34.6)	6.90E-03
1.86 (38.8)	1.42E-02
2.06 (43.0)	2.74E-02
2.26 (47.2)	5.02E-02
2.46 (51.4)	8.74E-02
2.66 (55.6)	1.45E-01
2.86 (59.8)	2.29E-01
3.06 (64.0)	3.42E-01
3.27 (68.2)	4.81E-01
3.47 (72.4)	6.34E-01
3.67 (76.6)	7.79E-01
3.87 (80.8)	8.91E-01
4.07 (85.0)	9.60E-01
4.27 (89.2)	9.90E-01
4.47 (93.4)	9.98E-01
4.67 (97.6)	1.00E+00
4.87 (102)	1.00E+00

Table A.67N09: 3-sec cumulative distribution table
(Data related to Figure 2.8)

Load kPa (psf)	P_b
0.05 (1.00)	4.73E-10
0.43 (9.00)	3.87E-05
0.81 (17.0)	4.78E-04
1.20 (25.0)	2.06E-03
1.58 (33.0)	5.97E-03
1.96 (41.0)	1.40E-02
2.35 (49.0)	2.84E-02
2.73 (57.0)	5.24E-02
3.11 (65.0)	8.94E-02
3.50 (73.0)	1.43E-01
3.88 (81.0)	2.14E-01
4.26 (89.0)	3.05E-01
4.64 (97.0)	4.13E-01
5.03 (105)	5.32E-01
5.41 (113)	6.51E-01
5.79 (121)	7.62E-01
6.18 (129)	8.53E-01
6.56 (137)	9.20E-01
6.94 (145)	9.62E-01
7.33 (153)	9.85E-01
7.71 (161)	9.95E-01
8.09 (169)	9.99E-01
8.47 (177)	1.00E+00
8.86 (185)	1.00E+00
9.24 (193)	1.00E+00

Appendix B

Failure Data and load resistance table for heat-treated monolithic glass

Table B.1
H1 - Loading time history, failure location, EFL_{60} , and EFL_3

Spec. No.	Time History		Thickness mm (in.)	Minimum Measured RCSS MPa (psi.)	Fracture Origin		Reported EFL_{60} kPa (psf)	Recracked EFL_{60} kPa (psf)	EFL_3 kPa (psf)
	Failure Pressure kPa (psf)	Failure Time (Sec)			to long dimension mm (in.)	to short dimension mm (in.)			
1	17.6 (367)	63.8	5.61 (0.221)	46.6 (6754)	31.8 (1.25)	1910 (75.0)	14.4 (301)	14.3 (299)	17.1 (357)
2	17.6 (367)	63.8	5.61 (0.221)	50.0 (7247)	927 (36.5)	31.8 (1.25)	14.7 (307)	14.3 (299)	17.1 (357)
3	19.1 (399)	69.3	5.64 (0.222)	57.7 (8370)	50.8 (2.00)	1880 (74.0)	15.8 (330)	15.6 (326)	18.6 (388)
4	22.8 (477)	82.8	5.64 (0.222)	68.4 (9923)	0.0 (0.00)	0.00 (0.00)	0.00 (0.00)	18.9 (395)	22.4 (467)
5	22.4 (468)	81.3	5.72 (0.225)	62.2 (9015)	889 (35.0)	1880 (74.0)	19.2 (402)	18.5 (386)	21.9 (458)
6	20.9 (436)	75.8	5.59 (0.220)	67.1 (9732)	769 (30.3)	1830 (72.0)	17.7 (369)	17.3 (361)	20.3 (423)
7	21.6 (452)	78.5	5.59 (0.220)	65.8 (9545)	0.00 (0.00)	0.00 (0.00)	0.00 (0.00)	17.9 (374)	21.2 (442)
8	20.5 (429)	74.5	5.66 (0.223)	62.2 (9015)	143 (5.63)	1840 (72.5)	17.2 (360)	16.9 (354)	20.0 (417)
9	21.4 (448)	77.8	5.66 (0.223)	64.6 (9364)	826 (32.5)	88.9 (3.50)	18.1 (377)	17.7 (371)	20.9 (436)
10	19.7 (412)	71.5	5.64 (0.222)	67.1 (9732)	826 (32.5)	1730 (68.0)	16.5 (344)	16.2 (338)	19.1 (400)
11	22.4 (468)	81.3	5.66 (0.223)	67.1 (9732)	82.5 (3.25)	1870 (73.5)	19.2 (402)	18.5 (387)	21.9 (457)
12	19.7 (410)	71.3	5.69 (0.224)	69.8 (10120)	838 (33.0)	1780 (70.0)	17.2 (359)	16.2 (339)	19.0 (397)
13	17.8 (372)	64.5	5.66 (0.223)	61.0 (8848)	965 (38.0)	1880 (74.0)	15.1 (315)	14.5 (303)	17.2 (360)
14	21.6 (451)	78.3	5.66 (0.223)	64.6 (9364)	44.4 (1.75)	0.00 (0.00)	18.2 (380)	17.8 (372)	21.1 (441)
15	21.6 (451)	78.3	5.69 (0.224)	67.1 (9732)	34.3 (1.35)	1920 (75.4)	18.1 (377)	17.8 (372)	21.1 (441)
16	24.1 (503)	87.3	5.66 (0.223)	67.1 (9732)	876 (34.5)	38.1 (1.50)	20.2 (422)	19.8 (414)	23.6 (494)
17	21.1 (440)	76.5	5.64 (0.222)	64.6 (9364)	889 (35.0)	1890 (74.5)	17.7 (370)	17.3 (361)	20.6 (430)
18	22.8 (477)	82.8	5.66 (0.223)	71.2(10323)	831 (32.7)	178 (7.00)	19.0 (396)	19.0 (396)	22.3 (465)
19	19.8 (413)	71.8	5.66 (0.223)	72.6(10533)	935 (36.8)	38.1 (1.50)	16.4 (343)	16.2 (339)	19.2 (401)
20	22.8 (475)	82.5	5.66 (0.223)	62.2 (9015)	935 (36.8)	50.8 (2.00)	18.5 (387)	18.9 (394)	22.3 (467)

Table B.2
H2 - Loading time history, failure location, and EFL_3

Spec. No.	Time History		Thickness mm (in.)	Minimum Measured RCSS MPa (psi.)	Fracture Origin		Reported EFL_3 kPa (psf)	Retreated EFL_3 kPa (psf)
	Failure Pressure kPa (psf)	Failure Time (Sec)			to long dimension mm (in.)	to short dimension mm (in.)		
1	20.7 (433)	25.2	5.64 (0.222)	44.4 (6435)	25.4 (1.00)	25.4 (1.00)	20.0 (419)	20.0 (418)
2	20.6 (430)	18.6	5.64 (0.222)	43.6 (6323)	108 (4.25)	44.5 (1.75)	19.5 (407)	19.4 (406)
3	23.4 (489)	20.9	5.66 (0.223)	42.1 (6105)	946 (37.23)	1890 (74.5)	22.4 (467)	22.3 (466)
4	22.6 (473)	24.4	5.70 (0.225)	45.2 (6549)	933 (36.8)	31.8 (1.25)	21.5 (449)	21.5 (448)
5	21.7 (454)	22.6	5.69 (0.224)	43.6 (6323)	916 (36.1)	4.76 (0.19)	20.4 (425)	20.3 (424)
6	23.0 (481)	36.8	5.69 (0.224)	42.1 (6105)	3.17 (0.13)	44.5 (1.75)	22.9 (478)	22.9 (478)
7	16.8 (350)	15.2	5.64 (0.222)	40.6 (5894)	959 (37.8)	1930 (76.0)	15.5 (324)	15.4 (321)
8	20.7 (433)	22.1	6.02 (0.237)	42.1 (6105)	959 (37.8)	1890 (74.4)	20.2 (422)	20.1 (420)
9	24.2 (506)	28.4	5.69 (0.224)	42.1 (6105)	38.1 (1.50)	1930 (75.9)	23.6 (492)	23.5 (492)
10	21.9 (458)	18.0	5.71 (0.225)	41.4 (5998)	964 (37.9)	1890 (74.4)	20.8 (435)	20.8 (434)
11	22.4 (468)	16.5	5.69 (0.224)	41.4 (5998)	962 (37.9)	1900 (74.6)	20.9 (437)	20.8 (434)
12	20.0 (418)	17.7	5.68 (0.224)	41.4 (5998)	962 (37.9)	1900 (74.9)	18.7 (390)	18.6 (388)
13	18.6 (388)	21.2	5.66 (0.223)	39.9 (5791)	50.8 (2.00)	1930 (75.9)	17.5 (365)	17.4 (363)
14	16.6 (347)	33.5	5.65 (0.223)	42.1 (6105)	9.52 (0.38)	82.6 (3.25)	16.2 (338)	16.2 (338)
15	17.7 (370)	55.2	5.66 (0.223)	42.8 (6213)	962 (37.9)	1890 (74.3)	18.1 (377)	18.1 (378)
16	19.9 (416)	57.6	5.69 (0.224)	45.2 (6549)	42.9 (1.69)	1930 (75.9)	20.4 (427)	20.5 (427)
17	20.7 (433)	92.4	5.65 (0.223)	42.1 (6105)	44.5 (1.75)	1930 (75.9)	22.6 (472)	22.7 (474)
18	21.7 (454)	107	5.66 (0.223)	42.1 (6105)	149 (5.88)	1770 (69.8)	22.0 (459)	21.9 (458)

H2(Cont.) - Loading time history, failure location, and EFL_3

Spec. No.	Time History		Thickness mm (in.)	Minimum Measured RCSS MPa (psi.)	Fracture Origin		Reported EFL_3 kPa (psf)	Recracked EFL_3 kPa (psf)
	Failure Pressure kPa (psf)	Failure Time (Sec)			to long dimension mm (in.)	to short dimension mm (in.)		
19	19.8 (414)	79.6	5.69 (0.224)	42.3 (6138) *	965 (38.0)	1910 (75.3)	20.9 (437)	21.0 (438)
20	21.1 (440)	44.0	5.89 (0.232)	43.6 (6323)	26.9 (1.06)	1920 (75.6)	20.5 (429)	20.5 (429)
21	22.0 (460)	67.5	5.69 (0.224)	43.6 (6323)	962 (37.9)	1890 (74.4)	22.3 (466)	22.4 (467)
22	19.0 (397)	73.2	5.66 (0.223)	39.9 (5791)	11.1 (0.44)	98.4 (3.88)	19.5 (407)	19.5 (408)
23	18.8 (392)	57.9	5.69 (0.224)	40.6 (5894)	102 (4.00)	114 (4.50)	18.6 (387)	18.5 (387)
24	25.3 (528)	110	5.66 (0.223)	45.2 (6549)	22.2 (0.88)	0.00 (0.00)	25.8 (538)	25.8 (539)
25	18.9 (396)	46.6	5.69 (0.224)	41.4 (5998)	876 (34.5)	1910 (75.0)	18.8 (392)	18.7 (391)
26	24.6 (513)	67.0	5.66 (0.223)	40.6 (5894)	93.7 (3.69)	1920 (75.6)	25.5 (534)	25.6 (535)

* Specimen RCSS not reported, mean RCSS calculated from the remaining specimen is used

Table B.3
F1 - Loading time history, failure location, EFL_{60} , and EFL_3

Spec. No.	Time History		Thickness mm (in.)	Minimum Measured RCSS MPa (psi.)	Fracture Origin		Reported EFL_{60} kPa (psf)	Retreated EFL_{60} kPa (psf)	EFL_3 kPa (psf)
	Failure Pressure kPa (psf)	Failure Time (Sec)			to long dimension mm (in.)	to short dimension mm (in.)			
1	15.9 (333)	28.0	5.71 (0.225)	86.7 (12582)	1610 (63.5)	50.8 (2.00)	11.9 (249)	11.8 (247)	14.9 (312)
2	14.3 (298)	42.5	5.54 (0.218)	70.7 (10252)	63.5 (2.50)	63.5 (2.50)	11.7 (245)	11.7 (244)	14.1 (294)
3	17.4 (363)	53.0	5.66 (0.223)	80.3 (11650)	88.9 (3.50)	76.2 (3.00)	14.5 (302)	14.3 (298)	17.1 (358)
4	15.7 (328)	49.0	5.49 (0.216)	77.1 (11184)	152 (6.00)	152 (6.00)	9.17 (192)	12.8 (268)	15.5 (323)
5	15.0 (314)	45.0	5.46 (0.215)	77.1 (11184)	165 (6.50)	165 (6.50)	11.2 (235)	11.8 (246)	14.3 (298)
6	14.8 (308)	44.5	5.69 (0.224)	73.9 (10718)	127 (5.00)	133 (5.25)	11.7 (245)	12.0 (252)	14.4 (301)
7	14.9 (311)	46.0	5.66 (0.223)	67.5 (9786)	114 (4.50)	152 (6.00)	11.9 (248)	12.4 (259)	14.7 (307)
8	15.6 (325)	47.0	5.66 (0.223)	83.5 (12116)	1590 (62.5)	155 (6.10)	12.5 (262)	12.7 (266)	15.3 (319)
9	16.6 (347)	49.0	5.66 (0.223)	77.1 (11184)	1500 (59.0)	356 (14.0)	9.51 (199)	13.2 (276)	16.6 (347)
10	17.6 (367)	46.0	5.69 (0.224)	73.9 (10718)	25.4 (1.00)	25.4 (1.00)	14.4 (301)	14.2 (297)	17.2 (360)
11	17.9 (374)	52.0	5.69 (0.224)	80.3 (11650)	102 (4.00)	1600 (63.0)	14.8 (308)	14.6 (304)	17.5 (366)
12	15.2 (318)	46.0	5.66 (0.223)	77.1 (11184)	152 (6.00)	1520 (60.0)	11.5 (240)	12.3 (257)	14.8 (309)
13	12.8 (266)	40.0	5.69 (0.224)	77.1 (11184)	1660 (65.4)	1630 (64.0)	10.2 (213)	10.5 (220)	12.7 (264)
14	16.5 (344)	50.0	5.69 (0.224)	77.1 (11184)	127 (5.00)	127 (5.00)	13.4 (279)	13.6 (285)	16.2 (338)
15	16.1 (336)	45.0	5.66 (0.223)	77.1 (11184)	1550 (61.0)	1500 (59.0)	13.0 (271)	13.0 (271)	15.5 (325)
16	16.8 (350)	45.0	5.69 (0.224)	70.7 (10252)	1450 (57.2)	1490 (58.5)	13.4 (279)	13.4 (280)	16.5 (345)
17	15.0 (314)	45.0	5.64 (0.222)	77.1 (11184)	1490 (58.5)	1408 (58.2)	11.6 (242)	12.0 (250)	14.7 (306)
18	15.0 (312)	45.0	5.64 (0.222)	77.1 (11184)	152 (6.00)	1490 (58.5)	11.9 (248)	12.2 (255)	14.7 (307)

F1 (cont.) - Loading time history, failure location, EFL_{60} , and EFL_3

Spec. No.	Time History		Thickness mm (in.)	Minimum Measured RCSS MPa (psi.)	Fracture Origin		Reported EFL_{60} kPa (psf)	Recracked EFL_{60} kPa (psf)	EFL_3 kPa (psf)
	Failure Pressure kPa (psf)	Failure Time (Sec)			to long dimension mm (in.)	to short dimension mm (in.)			
19	14.8 (310)	44.0	5.64 (0.222)	77.1 (11184)	1630 (64.0)	6.35 (0.25)	11.7 (245)	11.8 (246)	14.4 (301)
20	13.6 (284)	38.0	5.69 (0.224)	77.1 (11184)	76.2 (3.00)	1630 (64.1)	10.6 (222)	11.2 (233)	13.5 (282)
21	12.4 (259)	37.0	5.66 (0.223)	77.1 (11184)	76.2 (3.00)	1610 (63.5)	10.0 (209)	9.9 (207)	12.1 (252)
22	12.6 (264)	37.0	5.69 (0.224)	80.3 (11650)	133 (5.25)	1550 (61.2)	9.86 (206)	10.2 (214)	12.3 (257)
23	13.9 (291)	42.0	5.69 (0.224)	80.3 (11650)	203 (8.00)	1560 (61.5)	11.0 (230)	11.3 (237)	13.6 (284)
24	14.4 (301)	43.0	5.66 (0.223)	77.1 (11184)	1630 (64.0)	88.9 (3.50)	11.4 (239)	11.7 (245)	14.2 (296)
25	16.3 (340)	48.0	5.69 (0.224)	77.1 (11184)	88.9 (3.50)	1610 (63.5)	14.8 (310)	13.2 (277)	15.9 (332)
26	15.2 (317)	44.0	5.69 (0.224)	73.9 (10718)	1520 (60.0)	1440 (56.5)	11.8 (246)	12.0 (251)	14.8 (308)

Table B.4
F2 - Loading time history, failure location, EFL_{60} , and EFL_3

Spec. No.	Time History		Thickness mm (in.)	Minimum Measured RCSS MPa (psi.)	Fracture Origin		Reported		Retreated	
	Failure Pressure kPa (psf)	Failure Time (Sec)			to long dimension mm (in.)	to short dimension mm (in.)	EFL_{60} kPa (psf)	EFL_{60} kPa (psf)	EFL_3 kPa (psf)	
1	22.1 (461)	40.0	5.61 (0.221)	67.5 (9786)	216 (8.50)	787 (31.0)	17.5 (366)	17.1 (358)	21.0 (439)	
2	20.2 (422)	36.6	5.77 (0.227)	70.7 (10252)	50.8 (2.00)	914 (36.0)	15.9 (331)	15.8 (330)	19.2 (401)	
3	25.5 (533)	46.3	5.74 (0.226)	77.1 (11184)	1880 (74.0)	6.35 (0.25)	20.8 (435)	20.3 (424)	24.4 (511)	
4	22.1 (461)	40.0	5.66 (0.223)	73.9 (10718)	1900 (74.8)	82.6 (3.25)	17.5 (366)	17.1 (358)	21.0 (439)	
5	23.2 (484)	42.0	5.61 (0.221)	67.5 (9786)	1920 (75.5)	63.5 (2.50)	18.5 (386)	18.2 (380)	22.1 (462)	
6	24.4 (510)	44.3	5.64 (0.222)	67.5 (9786)	146 (5.75)	133 (5.25)	19.7 (410)	19.5 (408)	23.3 (488)	
7	23.8 (497)	43.1	5.64 (0.222)	64.3 (9320)	1930 (76.0)	50.8 (2.00)	19.2 (400)	18.8 (393)	22.8 (475)	
8	23.3 (487)	42.3	5.66 (0.223)	57.8 (8388)	1730 (68.0)	152 (6.00)	19.9 (415)	18.3 (383)	22.3 (465)	
9	26.3 (550)	47.8	5.59 (0.220)	64.3 (9320)	1920 (75.5)	889 (35.0)	22.3 (465)	20.6 (430)	25.4 (530)	
10	23.2 (484)	42.0	5.61 (0.221)	64.3 (9320)	102 (4.00)	50.8 (2.00)	18.3 (383)	18.2 (380)	22.1 (462)	
11	22.9 (478)	41.5	5.61 (0.221)	64.3 (9320)	38.1 (1.50)	63.5 (2.50)	18.6 (389)	18.0 (377)	21.9 (456)	
12	19.3 (403)	35.0	5.61 (0.221)	57.8 (8388)	50.8 (2.00)	965 (38.0)	15.2 (318)	15.1 (315)	18.3 (382)	
13	27.6 (577)	50.1	5.59 (0.220)	61.0 (8854)	1890 (74.5)	12.7 (0.50)	20.7 (432)	22.1 (462)	26.7 (558)	
14	26.0 (543)	47.1	5.66 (0.223)	77.1 (11184)	159 (6.25)	165 (6.50)	21.1 (441)	20.6 (431)	24.9 (520)	
15	23.1 (482)	41.9	5.64 (0.222)	64.3 (9320)	-	-	-	-	22.1 (461)	
16	23.2 (485)	42.1	5.61 (0.221)	77.1 (11184)	-	-	-	-	22.2 (463)	
17	20.2 (422)	36.6	5.69 (0.224)	70.7 (10252)	25.4 (1.00)	6.35 (0.25)	15.0 (312)	15.8 (331)	19.2 (401)	
18	27.1 (566)	49.1	5.61 (0.221)	73.9 (10718)	1770 (69.8)	787 (31.0)	20.8 (433)	21.4 (448)	26.0 (544)	
19	25.2 (527)	45.8	5.61 (0.221)	70.7 (10252)	1890 (74.5)	889 (35.0)	18.7 (390)	19.9 (416)	24.2 (505)	
20	22.6 (472)	41.0	5.66 (0.223)	73.9 (10718)	178 (7.00)	178 (7.00)	16.5 (344)	17.7 (370)	21.6 (450)	

Table B.5
F3 - Loading time history, failure location, and EFL_3

Spec. No.	Time History		Thickness mm (in.)	Minimum Measured RCSS MPa (psi.)	Fracture Origin		Reported EFL_3 kPa (psf)	Retacted EFL_3 kPa (psf)
	Failure Pressure kPa (psf)	Failure Time (Sec)			to long dimension mm (in.)	to short dimension mm (in.)		
1	34.0 (710)	54.8	5.87 (0.231)	77.6 (11248)	-	-	34.1 (713)	33.9 (708)
2	31.4 (657)	365	5.84 (0.230)	77.6 (11248)	-	-	33.0 (690)	33.0 (689)
3	32.3 (674)	46.9	5.84 (0.230)	87.9 (12747)	-	-	32.3 (674)	32.3 (675)
4	30.8 (644)	283	5.84 (0.230)	84.5 (12250)	-	-	32.9 (686)	32.9 (688)
5	38.1 (797)	89.8	5.87 (0.231)	86.3 (12517)	-	-	39.9 (834)	39.6 (827)
6	35.8 (747)	46.4	5.87 (0.231)	79.2 (11482)	-	-	35.4 (739)	35.1 (733)
7	33.7 (705)	210	5.89 (0.232)	80.9 (11732)	-	-	35.3 (738)	35.2 (735)
8	34.3 (716)	58.4	5.84 (0.230)	82.3 (11932)	-	-	34.0 (710)	34.0 (710)
9	34.8 (728)	29.0	5.84 (0.230)	72.9 (10574)	-	-	34.8 (726)	34.7 (726)
10	38.7 (807)	123	5.84 (0.230)	92.4 (13402)	-	-	42.2 (881)	42.2 (882)
11	41.1 (859)	78.8	5.89 (0.232)	86.3 (12517)	-	-	43.0 (899)	43.0 (898)
12	42.6 (889)	888	5.87 (0.231)	82.6 (11982)	-	-	48.0 (1000)	47.8 (998)
13	29.2 (609)	49.9	5.87 (0.231)	88.3 (12805)	-	-	29.5 (615)	29.5 (616)
14	36.8 (768)	259	5.89 (0.232)	84.5 (12250)	-	-	39.5 (824)	39.5 (825)

Table B.6
F4 - Loading time history, failure location, and EFL_3

Spec. No.	Time History		Thickness mm (in.)	Minimum Measured RCSS MPa (psi.)	Fracture Origin		Reported EFL_3 kPa (psf)	Recracked EFL_3 kPa (psf)
	Failure Pressure kPa (psf)	Failure Time (Sec)			to long dimension mm (in.)	to short dimension mm (in.)		
1	15.3 (319)	57.8	5.71 (0.225)	79.3 (11500)	-	-	15.0 (312)	14.9 (311)
2	19.9 (416)	418	5.71 (0.225)	86.2 (12500)	-	-	24.4 (510)	24.1 (504)
3	17.3 (360)	130	5.71 (0.225)	79.3 (11500)	-	-	20.2 (421)	20.0 (417)
4	21.7 (454)	76.0	5.71 (0.225)	79.3 (11500)	-	-	21.9 (457)	22.0 (459)
5	17.0 (355)	73.4	5.71 (0.225)	86.2 (12500)	-	-	16.7 (350)	16.6 (347)
6	17.3 (361)	119	5.71 (0.225)	75.8 (11000)	-	-	16.8 (350)	16.7 (349)
7	22.0 (460)	2546	5.71 (0.225)	90.3 (13100)	-	-	26.0 (543)	25.3 (529)
8	20.3 (423)	69.3	5.71 (0.225)	90.3 (13100)	-	-	20.2 (422)	20.0 (417)
9	21.8 (456)	90.2	5.71 (0.225)	90.3 (13100)	-	-	22.9 (477)	22.8 (476)
10	21.5 (449)	75.9	5.71 (0.225)	86.2 (12500)	-	-	22.3 (466)	22.4 (468)
11	14.6 (304)	65.8	5.71 (0.225)	79.3 (11500)	-	-	14.3 (298)	14.2 (297)
12	21.1 (441)	73.9	5.74 (0.226)	86.2 (12500)	-	-	21.2 (443)	21.0 (440)
13	22.0 (460)	97.5	5.71 (0.225)	86.2 (12500)	-	-	23.2 (485)	23.2 (484)
14	20.1 (421)	72.4	5.71 (0.225)	82.7 (12000)	-	-	20.6 (430)	20.5 (428)
15	19.8 (413)	64.7	5.74 (0.226)	90.3 (13100)	-	-	19.4 (406)	19.2 (401)
16	13.2 (275)	60.2	5.71 (0.225)	79.3 (11500)	-	-	12.9 (269)	12.8 (268)

Table B.7

H1: 3-sec cumulative distribution table
(Data related to Figure 3.3)

Load kPa (psf)	P_b
0.05 (1.00)	0.00E+00
1.09 (22.7)	0.00E+00
2.13 (44.5)	0.00E+00
3.17 (66.2)	0.00E+00
4.21 (87.9)	0.00E+00
5.25 (110)	0.00E+00
6.29 (131)	0.00E+00
7.33 (153)	0.00E+00
8.37 (175)	0.00E+00
9.41 (197)	3.43E-09
10.5 (218)	6.74E-07
11.5 (240)	1.61E-05
12.5 (262)	1.59E-04
13.6 (284)	9.47E-04
14.6 (305)	4.06E-03
15.7 (327)	1.37E-02
16.7 (349)	3.88E-02
17.7 (371)	9.50E-02
18.8 (392)	2.03E-01
19.8 (414)	3.78E-01
20.9 (436)	6.04E-01
21.9 (457)	8.18E-01
22.9 (479)	9.50E-01
24.0 (501)	9.93E-01
25.0 (523)	1.00E+00

Table B.8

H2: 3-sec cumulative distribution table
(Data related to Figure 3.3)

Load kPa (psf)	P_b
0.05 (1.00)	0.00E+00
1.19 (24.8)	0.00E+00
2.32 (48.5)	0.00E+00
3.46 (72.3)	0.00E+00
4.60 (96.0)	3.27E-13
5.74 (120)	8.18E-09
6.87 (144)	5.14E-07
8.01 (167)	8.44E-06
9.15 (191)	7.03E-05
10.3 (215)	3.75E-04
11.4 (239)	1.47E-03
12.6 (262)	4.62E-03
13.7 (286)	1.23E-02
14.8 (310)	2.88E-02
16.0 (334)	6.07E-02
17.1 (357)	1.16E-01
18.2 (381)	2.05E-01
19.4 (405)	3.30E-01
20.5 (429)	4.89E-01
21.7 (452)	6.61E-01
22.8 (476)	8.15E-01
23.9 (500)	9.22E-01
25.1 (524)	9.77E-01
26.2 (547)	9.96E-01
27.3 (571)	1.00E+00

Table B.9F1: 3-sec cumulative distribution table
(Data related to Figure 3.3)

Load kPa (psf)	P_b
6.51 (136)	4.29E-13
6.94 (145)	2.23E-09
7.37 (154)	9.00E-08
7.80 (163)	1.02E-06
8.24 (172)	6.37E-06
8.67 (181)	2.79E-05
9.10 (190)	9.70E-05
9.53 (199)	2.85E-04
9.96 (208)	7.34E-04
10.4 (217)	1.71E-03
10.8 (226)	3.65E-03
11.3 (235)	7.21E-03
11.7 (244)	1.36E-02
12.5 (262)	4.13E-02
13.0 (271)	6.74E-02
13.4 (280)	1.05E-01
14.3 (298)	2.30E-01
15.1 (316)	7.19E-01
16.0 (334)	6.67E-01
16.4 (343)	7.78E-01
17.3 (361)	9.35E-01
17.7 (370)	9.71E-01
18.1 (379)	9.89E-01
18.6 (388)	9.98E-01
19.0 (397)	1.00E+00

Table B.10F2: 3-sec cumulative distribution table
(Data related to Figure 3.3)

Load kPa (psf)	P_b
0.05 (1.00)	0.00E+00
1.22 (25.6)	0.00E+00
2.40 (50.1)	0.00E+00
3.57 (74.7)	0.00E+00
4.75 (99.2)	0.00E+00
5.93 (124)	0.00E+00
7.10 (148)	0.00E+00
8.28 (173)	0.00E+00
9.45 (197)	3.83E-12
10.6 (222)	1.53E-07
11.8 (247)	8.15E-06
13.0 (271)	1.08E-04
14.2 (296)	7.29E-04
15.3 (320)	3.27E-03
16.5 (345)	1.11E-02
17.7 (369)	3.10E-02
18.9 (394)	7.43E-02
20.0 (418)	1.56E-01
21.2 (443)	2.89E-01
22.4 (467)	4.72E-01
23.6 (492)	6.77E-01
24.7 (517)	8.50E-01
25.9 (541)	9.53E-01
27.1 (566)	9.91E-01
28.3 (590)	9.99E-01

Table B.11F3: 3-sec cumulative distribution table
(Data related to Figure 3.3)

Load kPa (psf)	P_b
0.05 (1.00)	0.00E+00
2.35 (49.0)	0.00E+00
4.64 (97.0)	0.00E+00
6.94 (145)	0.00E+00
9.24 (193)	0.00E+00
11.5 (241)	0.00E+00
13.8 (289)	0.00E+00
16.1 (337)	1.74E-06
18.4 (385)	1.53E-04
20.7 (433)	1.35E-03
23.0 (481)	6.38E-03
25.3 (529)	2.13E-02
27.6 (577)	5.52E-02
29.9 (625)	1.19E-01
32.2 (673)	2.22E-01
34.5 (721)	3.64E-01
36.8 (769)	5.31E-01
39.1 (817)	6.98E-01
41.4 (865)	8.36E-01
43.7 (913)	9.27E-01
46.0 (961)	9.75E-01
48.3 (1000)	9.93E-01
50.6 (1060)	9.99E-01
52.9 (1110)	1.00E+00
55.2 (1150)	1.00E+00

Table B.12F4: 3-sec cumulative distribution table
(Data related to Figure 3.3)

Load kPa (psf)	P_b
0.05 (1.00)	0.00E+00
1.34 (28.0)	0.00E+00
2.63 (55.0)	0.00E+00
3.93 (82.0)	0.00E+00
5.22 (109)	0.00E+00
6.51 (136)	0.00E+00
7.80 (163)	0.00E+00
9.10 (190)	3.52E-05
10.4 (217)	1.24E-03
11.7 (244)	7.12E-03
13.0 (271)	2.25E-02
14.3 (298)	5.46E-02
15.6 (325)	1.11E-01
16.9 (352)	1.95E-01
18.1 (379)	3.11E-01
19.4 (406)	4.49E-01
20.7 (433)	5.95E-01
22.0 (460)	7.33E-01
23.3 (487)	8.44E-01
24.6 (514)	9.22E-01
25.9 (541)	9.66E-01
27.2 (568)	9.88E-01
28.5 (595)	9.97E-01
29.8 (622)	9.99E-01
31.1 (649)	1.00E+00

Appendix C

Load resistance table for point supported glass

Table C.1
 Cumulative distribution table for 2P GFPM for holes
 (Data related to Figure 4.3)

Load (kN)	pb $2P_{Schultz}$	pb $2P_H$
0.00	0.00E+00	0.00E+00
0.83	0.00E+00	0.00E+00
1.66	6.99E-15	0.00E+00
2.50	3.38E-12	5.55E-16
3.33	2.71E-10	1.82E-13
4.16	8.16E-09	1.67E-11
4.99	1.32E-07	6.67E-10
5.82	1.38E-06	1.51E-08
6.65	1.06E-05	2.25E-07
7.49	6.38E-05	2.44E-06
8.32	3.18E-04	2.06E-05
9.15	1.36E-03	1.42E-04
9.98	5.11E-03	8.25E-04
10.8	1.72E-02	4.16E-03
11.6	5.24E-02	1.85E-02
12.5	1.43E-01	7.27E-02
13.3	3.38E-01	2.43E-01
14.1	6.46E-01	6.14E-01
15.0	9.17E-01	9.51E-01
15.8	9.97E-01	0.99988
16.6	1	1

Table C.2
 Cumulative distribution table for $P3P_H$ for holes
 (Data related to Figure 4.4 and Figure 4.5)

Load (kN)	pb $3P_{H,RCSS}$	pb $3P_{H,RCSS}$	pb $3P_{H,RCSS}$	pb $3P_{H,RCSS}$
5.16	0.00E+00	0.00E+00	0.00E+00	0.00E+00
7.83	6.66E-11	0.00E+00	0.00E+00	0.00E+00
8.27	2.04E-08	0.00E+00	0.00E+00	0.00E+00
8.72	7.38E-07	2.59E-10	0.00E+00	0.00E+00
9.16	1.01E-05	3.96E-07	0.00E+00	3.78E-08
9.61	7.98E-05	1.57E-05	2.19E-13	6.60E-06
10.1	4.37E-04	1.86E-04	1.10E-05	1.26E-04
10.5	1.86E-03	1.20E-03	4.40E-04	1.01E-03
10.9	6.51E-03	5.33E-03	3.83E-03	4.97E-03
11.4	1.97E-02	1.84E-02	1.77E-02	1.81E-02
11.8	5.25E-02	5.27E-02	5.70E-02	5.31E-02
12.3	1.25E-01	1.29E-01	1.44E-01	1.31E-01
12.7	2.62E-01	2.72E-01	2.97E-01	2.76E-01
13.2	4.78E-01	4.88E-01	5.11E-01	4.92E-01
13.6	7.31E-01	7.34E-01	7.36E-01	7.34E-01
14.1	9.21E-01	9.15E-01	9.02E-01	9.13E-01
14.5	9.91E-01	9.88E-01	9.79E-01	9.86E-01
14.9	0.99976	0.99943	0.99772	0.99923
15.4	1	1	0.99991	0.99999
15.8	1	1	1	1

Table C.3
 Cumulative distribution table for test specimen with RCSS = 126 MPa
 (Data related to Figure 4.6)

Load (kN)	pseudo $GFPM_{3H}$ (RCSS = 0 MPa)	$GFPM_{3H}$ (RCSS = 0 MPa)
0.09	4.68E-04	6.34E-12
0.36	6.88E-04	6.40E-08
0.71	1.18E-03	6.43E-06
1.07	2.08E-03	9.53E-05
1.42	3.69E-03	6.46E-04
1.78	6.58E-03	2.84E-03
2.14	1.17E-02	9.53E-03
2.49	2.07E-02	2.63E-02
2.85	3.63E-02	6.28E-02
3.20	6.26E-02	1.32E-01
3.56	1.06E-01	2.49E-01
3.91	1.74E-01	4.17E-01
4.27	2.77E-01	6.18E-01
4.63	4.19E-01	8.06E-01
4.98	5.93E-01	9.32E-01
5.34	7.70E-01	9.86E-01
5.69	9.08E-01	9.99E-01
6.05	9.78E-01	0.99994
6.41	9.98E-01	1
6.76	0.99993	1
7.03	1	1

Table C.4
 Cumulative distribution table for test specimen with RCSS = 126 MPa
 (Data related to Figure 4.6)

Load (kN)	pseudo $G_{FPM_{3H}}$ (RCSS = 24 MPa)	$G_{FPM_{3H}}$ (RCSS = 24 MPa)
0.36	1.04E-05	0.00E+00
0.71	2.05E-05	0.00E+00
1.07	4.15E-05	0.00E+00
1.42	8.51E-05	0.00E+00
1.78	1.74E-04	2.51E-12
2.14	3.55E-04	1.41E-07
2.49	7.12E-04	8.27E-06
2.85	1.41E-03	1.05E-04
3.20	2.74E-03	6.70E-04
3.56	5.22E-03	2.87E-03
3.91	9.79E-03	9.45E-03
4.27	1.80E-02	2.59E-02
4.63	3.25E-02	6.14E-02
4.98	5.75E-02	1.29E-01
5.34	9.92E-02	2.43E-01
5.69	1.66E-01	4.08E-01
6.05	2.67E-01	6.07E-01
6.41	4.09E-01	7.96E-01
6.76	5.84E-01	9.26E-01
7.12	7.65E-01	9.84E-01
7.47	9.06E-01	9.98E-01
7.83	9.78E-01	0.99992
8.18	9.98E-01	1
8.81	1	1

Table C.5

Cumulative distribution table for test specimen with RCSS = 126 MPa
(Data related to Figure 4.6)

Load (kN)	pseudo $GFPM_{3H}$ (RCSS = 69 MPa)	$GFPM_{3H}$ (RCSS = 69 MPa)
0.09	5.33E-11	0.00E+00
0.62	3.37E-10	0.00E+00
1.25	3.17E-09	0.00E+00
1.87	2.64E-08	0.00E+00
2.49	1.87E-07	0.00E+00
3.11	1.13E-06	0.00E+00
3.74	5.93E-06	0.00E+00
4.36	2.76E-05	0.00E+00
4.98	1.15E-04	1.04E-10
5.60	4.40E-04	4.98E-06
6.23	1.55E-03	2.93E-04
6.85	5.04E-03	3.76E-03
7.47	1.54E-02	2.39E-02
8.10	4.38E-02	9.94E-02
8.72	1.15E-01	2.95E-01
9.34	2.74E-01	6.22E-01
9.96	5.52E-01	9.06E-01
10.6	8.55E-01	9.94E-01
11.2	9.89E-01	0.99997
11.8	0.99996	1
12.0	1	1

Table C.6

Cumulative distribution table for test specimen with RCSS = 126 MPa
(Data related to Figure 4.6)

Load (kN)	pseudo $GFPM_{3H}$ (RCSS = 103 MPa)	$GFPM_{3H}$ (RCSS = 103 MPa)
0.71	1.11E-16	0.00E+00
1.42	2.50E-14	0.00E+00
2.14	1.77E-12	0.00E+00
2.85	6.03E-11	0.00E+00
3.56	1.22E-09	0.00E+00
4.27	1.67E-08	0.00E+00
4.98	1.70E-07	0.00E+00
5.69	1.37E-06	0.00E+00
6.41	9.02E-06	0.00E+00
7.12	5.07E-05	0.00E+00
7.83	2.49E-04	6.82E-07
8.54	1.09E-03	1.56E-04
9.25	4.30E-03	3.21E-03
9.96	1.55E-02	2.60E-02
10.7	5.10E-02	1.24E-01
11.4	1.51E-01	3.86E-01
12.1	3.84E-01	7.67E-01
12.8	7.41E-01	9.76E-01
13.5	9.72E-01	0.99982
14.2	0.99989	1
14.5	1	1

Table C.7

Cumulative distribution table for test specimen with RCSS = 126 MPa
(Data related to Figure 4.6)

Load (kN)	pseudo $GFPM_{3H}$ (RCSS = 126 MPa)	$GFPM_{3H}$ (RCSS = 126 MPa)
2.22	0.00E+00	0.00E+00
2.94	1.44E-14	0.00E+00
3.65	1.17E-12	0.00E+00
4.36	4.31E-11	0.00E+00
5.07	9.21E-10	0.00E+00
5.78	1.31E-08	0.00E+00
6.49	1.38E-07	0.00E+00
7.21	1.13E-06	0.00E+00
7.92	7.60E-06	0.00E+00
8.63	4.34E-05	0.00E+00
9.34	2.16E-04	4.74E-07
10.1	9.53E-04	1.26E-04
10.8	3.80E-03	2.74E-03
11.5	1.38E-02	2.28E-02
12.2	4.59E-02	1.11E-01
12.9	1.38E-01	3.55E-01
13.6	3.56E-01	7.34E-01
14.3	6.63E-01	9.54E-01
15.0	9.63E-01	1.00E+00
15.7	0.99977	1
16.5	1	1

Table C.8
 Cumulative distribution table for test specimen with RCSS = 126 MPa
 (Data related to Figure 4.6)

Load (kN)	pseudo $GFPM_{3H}$ (RCSS = 138 MPa)	$GFPM_{3H}$ (RCSS = 138 MPa)
3.20	1.11E-16	0.00E+00
3.83	1.48E-14	0.00E+00
4.45	7.19E-13	0.00E+00
5.07	1.87E-11	0.00E+00
5.69	3.11E-10	0.00E+00
6.32	3.66E-09	0.00E+00
6.94	3.29E-08	0.00E+00
7.56	2.39E-07	0.00E+00
8.18	1.45E-06	0.00E+00
8.81	7.62E-06	0.00E+00
9.43	3.53E-05	0.00E+00
10.1	1.46E-04	5.23E-08
10.7	5.54E-04	2.78E-05
11.3	1.93E-03	7.34E-04
11.9	6.24E-03	6.76E-03
12.5	1.88E-02	3.59E-02
13.2	5.30E-02	1.32E-01
13.8	1.38E-01	3.56E-01
14.4	3.20E-01	6.88E-01
15.0	6.16E-01	9.35E-01
15.7	8.99E-01	9.97E-01
16.28	9.95E-01	0.99999
16.99	1	1